University of Technology, Sydney

School of Civil and Environmental Engineering

Faculty of Engineering and Information Technology

Short and Long Term Performance of Concrete Structures Repaired/Strengthened with FRP

by

Muhammad Ikramul Kabir

Thesis submitted for fulfilment of

the requirements for the degree of

Doctor of Philosophy

April 2014

Certificate of authorship/originality

I certify that the work in this thesis has not previously been submitted for a degree nor has it been submitted as part of requirements for a degree except as fully acknowledged within the text.

I also certify that the thesis has been written by me. Any help that I have received in my research work and the preparation of the thesis itself has been acknowledged. In addition, I certify that all information sources and literature used are indicated in the thesis.

_____

Muhammad Ikramul Kabir

Date:

To my parents because of whom I have found my existence in the vivid and vibrant Earth

Acknowledgments

I would like to acknowledge the constant support of my supervisors Prof. Bijan Samali and Dr Rijun Shrestha over the last three and a half years as the completion of my research and the dissertation would have never been possible without their guidance. From the very beginning of the postgraduate study till now, I have been receiving advice from them not only on the planning for the research study and analysing the test results but also on my future career. As an international student, it was not so easy for me to adapt with a totally new environment initially, but Prof. Bijan always helped me to make a right decision and to endure all kind of challenges. I still recall most of the meetings I had with Prof. Bijan, where I always felt very comfortable to express my opinion regarding the research and discuss my personal issues. The kindness and co-operation of him would always be memorable throughout my life. I was very lucky that Dr Rijun's office was on the same floor as mine, which allowed me to meet him any time I required to. Specially, in the case of any new observation from my research, I could discuss it with him which certainly helped me in explaining the findings.

I would also like to give special thanks to Dr Kirk vessalas and Dr Jianchun Li, who were the panel members for my Master's assessment, for their inspirations which made it possible to upgrade my course of study from Masters by research to PhD.

As I had to spend a significant amount of time on the experimental work, I strongly believe that the supports from the staff of laboratory played a very important role in conducting my experimental study. Especially, I would like to mention Mr Mulugheta Hailu from Materials Testing Laboratory who taught me how to prepare the test set-up and operate testing machines. I received help from him whenever I faced any kind of difficulties during the testing. Although working in laboratories was always challenging, especially, in the phase of fabrication of specimens, the guidance of Mr Rami Haddad, Mr David Dicker and Mr Peter Brown from the Structures Laboratory and Mr Laurence Stonard from Engineering Workshop helped me to overcome those challenges.

My parents and my sister have certainly made an invaluable contribution to the completion of my research as I would have never been able to come overseas for post graduate studies without their support and encouragement. Many times during my PhD, I felt it is impossible to take it to the next stage but I was always motivated by my family to complete my research study.

I cannot but mention some of my colleagues and friends who have major contributions toward the successful completion of my dissertation. Firstly, I would like to thank Dr Amir Zad, with whom I shared the same office during the last three years, for his friendly attitude and co-operation. Secondly, I am very thankful to Mr Chij Shrestha who helped me to be familiar with the MATLAB curve fitting toolbox. Finally, I would also like to give special thanks to Dr Mahbube Subhani, Dr Aslan Sadeghi Hokmabadi and Dr Mohsen Askari who were not only my fellow researchers but also very good friends. As all four of us had been writing our dissertations almost at the same time during the last four months of my candidature, I believe that inspiring and encouraging one another worked certainly very well for the completion of our dissertations.

Finally, I would like to acknowledge the financial supports provided by Centre for Built Infrastructure Research (CBIR) of University of Technology, Sydney (UTS) for conducting my research. The IRS and CBIR scholarships offered by UTS provided me with extensive support to accomplish my PhD goal.

Muhammad Ikramul Kabir

April 2014

List of publications based on this thesis

Conference publications

1. **Kabir, M. I.**, Shrestha, R. & Samali, B. 2013, 'Experimental study on durability of CFRP-concrete bond subjected to temperature, humidity and outdoor environment' *Proceedings of the Fourth Asia-Pacific Conference on FRP in Structures (APFIS 2013)*, 11-13 December 2013, Melbourne, Australia
2. **Kabir, M. I.**, Shrestha, R. & Samali, B. 2012, 'Effects of temperature, relative humidity and outdoor environment on FRP-concrete bond' *Proceedings of the 22nd Australasian Conference on the Mechanics of Structures and Materials (ACMSM 22)*, 11-14 December 2012, University of Technology, Sydney, Australia.

Journal publications

3. **Kabir, M. I.**, Shrestha, R. & Samali, B. 2013, 'Experimental and analytical investigation on the repair of damaged concrete beams with CFRP' (submitted to *Australian Journal of Civil Engineering*)

Abstract

Fibre Reinforced Polymer (FRP) composites have lately become a popular choice for strengthening and/or repairing of reinforced concrete (RC) structures due to their advantageous properties such as high strength- to-weight ratio, high corrosion resistance and easy application process. As the performance of FRP bonded RC structures depends on the effective stress transfer between FRP and concrete, extensive research has been conducted on the FRP-concrete bond system under short term loads. However, studies on the long term performance of FRP-concrete bond subjected to environmental conditions are very limited.

Experimental studies on the long term performance of FRP strengthened structures to-date include the study of the effect of various environmental conditions using a variety of test set-ups such as pull-off, bending tests of beams and direct shear tests. However, the available studies based on various conditions and set-ups make it difficult to compare the findings. As the effectiveness of FRP-strengthening schemes, either used for flexural or shear strengthening, lies in the shear stress transfer between FRP and concrete, study of FRP-concrete bond subjected to different environmental conditions by direct shear tests were suggested by some of the researchers. Even sensitivity of this set-up to environmental conditions was also reported. Therefore, more research with similar test set-ups to create a large database of FRP-concrete bond behaviour under various environmental conditions can be of immense value. In addition, using very high temperature for accelerated ageing was found to be very common in available literatures. However, in reality structures may not be exposed to such high temperatures and using high temperature may lead to conservative prediction of long-term properties. Moreover, unavailability of test data for FRP-concrete bond subjected to natural ageing observed in the existing literatures necessitates the investigation on FRP-concrete behaviour under natural environment.

In regards to the short term performance of reinforced concrete beams strengthened and/or repaired with FRP, extensive research have been conducted to-date in terms of experimental and analytical study. Some of these studies have also proposed design guidelines. However, the equations for prediction of load carrying capacity of severely

damaged repaired beams, especially, considering the strain hardening after yielding are not recommended.

Considering the identified gaps in the previous research on long term performance of FRP-concrete bond system and the short term performance of RC beams strengthened and/or repaired with FRP, the research study presented in this dissertation has mainly focused on the experimental investigation of the long-term performance of carbon FRP and glass FRP-concrete bond under three separate environmental conditions, namely, temperature cycles, wet-dry cycles and outdoor environment up to 18 months. The secondary objective is to investigate the effectiveness of typical FRP-strengthening schemes, used for strengthening of reinforced concrete beams, in the repair of severely damaged beams.

The long term performance of two types of FRP (CFRP and GFRP)-concrete bond is studied by extensive experimental investigations using single shear tests (is referred to as pull-out tests). The maximum temperature of the temperature cycles is intentionally kept below the glass transition temperature of epoxy resin to avoid any over-degradation. In the wet-dry cycles, temperature close to ambient is maintained. Also, outdoor environmental exposure is applied to address the unavailability of test data of natural ageing of FRP-concrete bond system. Pull-out tests conducted after exposure durations are analysed based on the pull-out strength, failure modes and strain distributions along the bond length. In addition, material properties, namely, CFRP tensile strength and modulus of elasticity, and concrete compressive strength are determined to understand the effect of changing material properties on the pull-out strength by correlation of bond strength with failure modes. Curve fitting of shear stresses against slips of only CFRP-concrete bond is conducted to determine the fracture energy release rate and the effect of environmental conditions on it. In addition, interface laws are proposed for control and exposed conditions based on an existing model. Results obtained for long term performance of bond systems provide interesting findings due to imposed environmental conditions. Based on the observations, strength reduction factors for CFRP and GFRP-concrete bond are proposed.

The short term performance of FRP-repaired beams is investigated both experimentally and analytically. Three severely damaged beams, fabricated from conventional concrete (normal concrete with water, cement and aggregate) and non-conventional concrete

(concrete with additives such as fibres and rubbers) are repaired with CFRP for flexure. Anchorage provided by complete CFRP wrapping at two ends and mid-span is found to be effective for preventing the debonding of FRP at least partially. Analytical study is conducted to understand the effect of existing steel reinforcement on the response of repaired beams under flexure. Considering the strain hardening of steel after yielding, equations are also proposed for better prediction of load carrying capacity of the repaired beams and compared with experimental results.

Finally, all the major findings of the two areas of research are summarised and recommendations for future research are made.

List of abbreviations and acronyms

ACI	American Concrete Institute
AFRP	Aramid Fibre Reinforced Polymer
AS	Australian Standard
ASTM	American Society for Testing and Materials
CF	Carbon Fibre
CFRP	Carbon Fibre Reinforced Polymer
CFS	Carbon Fibre Sheet
CoV	Coefficient of Variation
CSS	Carbon Strand Sheet
CZM	Cohesive Zone Model
DIC	Digital Image Correlation
DMTA	Dynamic Mechanical Thermal Analysis
EG	E-Glass
ERR	Energy Release Rate
FA	Fly Ash
FRP	Fibre Reinforced Polymer
GFRP	Glass Fibre Reinforced Polymer
GRC	Glass Fibre Reinforced Cement
IRRH	Interface Region Relative Humidity
IRT	Infrared Thermography
LED	Light Emitting Diode
LEFM	Linear Elastic Fracture Mechanics
LVDT	Linear Variable Differential Transformer
MOE	Modulus of Elasticity
NLFM	Nonlinear Fracture Mechanics
PC	Portland cement
PP	Polypropylene
QIRT	Quantitative Infrared Thermography
RC	Reinforced Concrete
RH	Relative Humidity
RTC	Residual Thickness of Concrete

SBR	Styrene Butadiene Rubber
SCCB	Single Contoured Cantilever Beam
SG	Strain Gauge
TSF	Time Shift Factor
UV	Ultraviolet
VCCT	Virtual Crack Closure Technique

List of notations

A	A constant in the test condition for accelerated ageing with Arrhenius principle
A_f	Cross sectional area of FRP
a_f	Depth of equivalent rectangular stress block of FRP strengthened/repaired beam
$A_{f_{anchor}}$	Area of FRP anchor
A_s	Area of steel reinforcement
$A_{s_{bottom}}$	Area of bottom steel reinforcement
$A_{s_{top}}$	Area of top steel reinforcement
b	Width of beam
b_c	Width of a concrete member
b_f	Width of FRP plate or sheet
c	The depth of neutral axis of a beam / interface cohesion in a Mohr-Coulomb envelope
c_f	A regression constant for fracture energy
C_{th}	Threshold interface moisture content beyond which no further degradation occurs
d	Depth of bottom steel axis from the top of the beam
d'	Depth of top steel axis from the top of the beam
E_a	Activation energy
E_c	Elastic modulus of concrete
E_f	Tensile modulus of elasticity of FRP
Es	Tensile modulus of elasticity of steel
f_c'	Concrete compressive strength
f_{ctm}	Concrete surface tensile strength
f_f	Axial stress in FRP plate or sheet
f_{fu}	Ultimate tensile stress in FRP at rupture

$f_{s\,\mathrm{Re}s}$	Residual strength of steel
f_t	Tensile strength of concrete
f_u	Ultimate tensile stress of steel
f_y	Yield stress of steel
G_f	Fracture energy/fracture energy release rate
G_{Ic}	Fracture energy under mode I loading
G_{IIc}	Fracture energy under mode II loading
h	Height of beam
J	Energy release rate at a debonding tip
k	Reaction rate constant with respect to a temperature T
k_f	Geometrical factor related to FRP width and concrete width
L_e	Effective bond length
M_n	Nominal moment capacity of beam
P_f	Applied load in FRP
$P_{\max}$	Ultimate bond strength / ultimate load at bond failure
R	Universal gas constant
$s_{\max}$	Slip value at the maximum shear stress
T	Absolute temperature in Kelvin
t	Time
t_f	Thickness of FRP sheet or plate
T_g	Glass transition temperature (sometimes referred to as heat distortion temperature) of polymer
w_f	Width of FRP anchor
Y	Tensile strength retention value
β_L	Length factor of FRP-concrete bond
β_p	Width factor of FRP-concrete bond
δ or s	Slip between FRP and concrete
δ_f	Maximum slip of FRP-concrete bond

ε_f	Axial strain in FRP
ε_{f0}	Initial strain of concrete at the level of FRP reinforcement
$\varepsilon_{fe_{anchor}}$	Effective strain of FRP anchor
ε_{fu}	Ultimate tensile strain of FRP
ε_{s0}	Initial strain the steel reinforcement
ε_u	Ultimate tensile strain of steel
ε_y	Yield strain of steel
$\sigma(t)$ or $P(t)$	Composite strength after an exposure time *t*
σ_0 or P_0	Composite strength for unexposed condition
σ_∞	Composite strength after infinite exposure time
σ_{db}	Maximum axial stress of FRP at debonding failure
τ	Interface shear stress / a characteristic time dependent on temperature
$\tau_{\max}$	Maximum shear stress at failure of bond
ϕ	Friction angle in a Mohr-Coulomb envelope

Table of contents

List of tables

List of figures

CHAPTER 1

INTRODUCTION

1 Introduction

1.1 Preamble

The older reinforced concrete (RC) structures often become structurally deficient due to the demand for increased load carrying capacity, aggressive environmental conditions and extreme loading conditions such as earthquake and blast loading. As a result, strengthening of the deficient structural elements with suitable technique becomes essential.

Conventional strengthening techniques such as external post tensioning, bonding thin steel plates to the tension face of the member and concrete jacketing require complex anchorage details, and corrosion of steel plates can result in the deterioration of bond between steel and concrete. Additionally, such techniques impose additional load on the structure and are labour intensive.

Fibre Reinforced Polymer (FRP) composites possess a number of advantageous properties over conventionally used techniques and have been found to be effective in repair and/or strengthening of concrete structures. Saadatmanesh and Ehsani (1991), Chajes et al. (1994), Arduini and Nanni (1997), Norris and Saadatmanesh & Ehsani (1997) reported the effectiveness of FRP on the strengthening of RC beams by experimental investigation, whereas research conducted by An, Saadatmanesh & Ehsani (1991), Picard, Massicotte & Boucher (1995), Saadatmanesh and Malek (1998) and Rasheed and Pervaiz (2003) provided design guidelines and analytical models for beam strengthening with FRP.

The main advantages of using FRP over the other conventional techniques are its high strength-to-weight ratio and corrosion resistance. High strength-to-weight ratio makes site handling easier and reduces the labour cost, while high corrosion resistance ensures durability. Additionally, ease in cutting into different shapes is another advantage of FRP composites which leads to easy application process, especially, on curved surfaces. Compared to steel plates, FRP plates are stronger and lighter. Usually, FRP plates are at least two times stronger than steel plates and can be more than 10 times stronger,

whereas the weight of FRP plates is only 20% of that of steel (Teng 2002). Because of its high strength-to-weight ratio, it neither causes increase in cross-section size nor adds more load on the foundation.

Use of FRP composites in aerospace engineering and their superior properties are well known. Limited use of FRP in civil engineering is generally attributed to its high cost. However, the price of FRP composites has been coming down rapidly (Teng 2002). In spite of its high price, overall cost for strengthening with FRP is less compared to other techniques because it reduces the labour cost and loss due to interruptions to services. Therefore, the use of FRP for strengthening of structures has become a popular choice lately. FRP plate/sheet bonding and column wrapping/confinement are widely applied strengthening techniques. FRP laminates in the form of rigid plates or flexible sheets are externally bonded to the tension faces of the RC elements with structural adhesive such as epoxy resin or polyester resin for flexural strengthening and FRP wrapping is commonly used for shear strengthening.

Although using FRP composites have lately become a popular choice for strengthening and/or repairing of reinforced concrete (RC) structures, issues related to bonding of FRP to the concrete substrate still need to be resolved. In addition, the suitability of existing equations, recommended by design codes, for the repairing of damaged structural members requires to be assessed.

1.2 Problem identification

Based on an extensive literature review, two areas of research, namely, long term performance of FRP-concrete bond and repairing of severely damaged reinforced concrete members, have been identified as areas with limited information. The problems identified in these two areas are discussed in this section.

1.2.1 Long term performance of FRP-concrete bond

Despite the number of advantages that FRP composites possess, one of the major limitations of FRP composites is premature failure by debonding from concrete. Debonding, which is failure of FRP by peeling of FRP from concrete, limits the

effectiveness of FRP as the debonding strength is much lower than its rupture strength. To take into account the possibility of such premature failure in FRP repaired and/or strengthened structures, ACI 440.2R (2008) recommends the use of a bond reduction coefficient for the calculation of the effective strain of FRP reinforcement. The effective strain of FRP reinforcement should be calculated by multiplying the ultimate strain of specific FRP reinforcement with the bond reduction coefficient.

Although extensive research has been conducted on debonding phenomenon under short term load, limited work has been done on investigating the long term performance of FRP-concrete bond subjected to environmental conditions. Chajes et al. (1995), Toutanji & Gómez (1997), Myers et al. (2001) and Li et al. (2002) studied the long term performance of FRP strengthened concrete beams subjected to various environmental conditions such as freeze-thaw cycles, wet-dry cycles, combined environmental cycles, boiling water and UV radiation to investigate the degradation of ultimate strength and stiffness of beams. Homam et al. (2001), Dai et al. (2010), Benzarti et al. (2011) and Yun & Wu (2011) investigated FRP-concrete bond degradation under freeze-thaw cycles, temperature cycles, alkali solutions, moisture ingression, hydrothermal ageing with the help of various test set-ups such as pull-off, bend tests and single-lap-joint shear tests. Also, Tuakta & Büyüköztürk (2011b) studied the effect of moisture on FRP-concrete bond system by tri-layer fracture mechanics using peel and shear fracture tests. Research studies by Litherland et al. (1981) , Dejke & Tepfers (2001) and Phani & Bose (1987) dealt with proposing long term prediction models for FRP and FRP in concrete environment based on the accelerated ageing rate using high temperature.

From the previous research stated above (Chapter 2 provides a summary of previous research more extensively), it can be understood that various test set-ups and conditions used in the study of FRP-concrete bond under environmental exposures have posed difficulty in relation to comparison of research findings. As the effectiveness of FRP strengthening scheme, either used for flexural or shear strengthening, lies in the shear stress transfer between FRP and concrete, study of FRP-concrete bond, subjected to different environmental conditions, should be carried out by direct shear tests (Imani 2010). Benzarti et al. (2011) also reported that single-lap-joint shear test (direct shear or pull-out test) is more sensitive to environmental conditions and should be used for

adhesive bonded joint. Therefore, more research need to be conducted with similar test set-ups to create a large database of FRP-concrete bond behaviour under various environmental conditions. Regarding the common practice of using high temperature as an accelerating factor for any degradation mechanism to develop long term prediction models of FRP and FRP-concrete bond, Robert et al. (2010) stated that high temperature may amplify the degradation of the properties which may lead to conservative prediction of long-term properties. This inherent conservativeness justifies further research by separating the high temperature from a specific degradation mechanism.

Unavailability of data for natural ageing of FRP-concrete bond can be observed in the existing literatures, which suggests the importance of the investigation on FRP-concrete behaviour under natural environment.

Considering the premature failure of FRP-concrete bond system and the identified gaps in the previous research, studies on the effects of environmental conditions on FRP-concrete bond behaviour can be of great importance as the bond behaviour under aggressive environments may be critical. Moreover, determination of reduction factors for FRP-concrete bond system exposed to different environmental conditions and application of such factors in design of FRP strengthened and/or repaired structures may be required.

1.2.2 Repairing of severely damaged reinforced concrete members with FRP

Strengthening of reinforced concrete beams with FRP is well-established and design standards are also available. Guidelines recommended by ACI 440.2R (2008) can be noteworthy. However, the existing equations for strengthening of reinforced concrete beams with FRP are based on the consideration that the beams are loaded up to certain percentage of ultimate load carrying capacity (within serviceable limit) before the strengthening is applied. But local failure of structural members due to extreme loading such as earthquake or blast loading may require retrofitting of the severely damaged members to maintain partial functionality of the structure. A typical example may be where a bridge girder may have undergone some localised failure because of an extreme load event but partial traffic flow needs to be allowed temporarily. But the equations for prediction of load carrying capacity of severely damaged repaired beams, especially,

considering the strain hardening after yielding are not recommended in the studies available in literatures.

Hence, suitability of existing guidelines on the repair of severely damaged reinforced concrete beams should be assessed and if possible, modifications of existing equations for the application in the repair of such members should be carried out.

1.3 Research objectives

Based on the identified gaps in the field of strengthening and repairing of existing reinforced concrete structures with FRP, the primary objective of this research is to investigate the long-term performance of FRP-concrete bond under environmental conditions. The secondary objective is to investigate the effectiveness of typical FRP-strengthening schemes, used for strengthening of reinforced concrete beams, in the repair of reinforced concrete beams.

The objectives stated above can be elaborated further as follows:

- study the effect of temperature cycles (up to one year), wet-dry cycles (up to 18 months) and outdoor environment (up to 18 months) on the bond strength of carbon fibre reinforced polymer (CFRP) and glass fibre reinforced polymer (GFRP)-concrete bond under direct shear (pull-out) loading
- study the effect of temperature cycles, wet-dry cycles and outdoor environment on the fracture energy of CFRP and GFRP-concrete bond under direct shear loading
- investigate the effect of concrete and FRP material properties on the bond strength of CFRP and GFRP-concrete bond and on the fracture energy of CFRP-concrete bond exposed to three environmental conditions
- experimental and analytical study on the effectiveness of typical FRP strengthening schemes for the repair of three severely damaged conventional (made from concrete with cement, water and aggregate) and non-conventional (made from concrete with additives such as fibres and rubbers) RC beams with CFRP
- study the effect of residual strength of steel reinforcement on the repair of damaged RC beams with CFRP

1.4 Significance of the research

Although research on the FRP-concrete bond available in the literature consider the effects of high temperature, cyclic temperature, wet-dry cycles at different temperatures, freeze-thaw cycles, immersion in salt water, immersion in alkaline water and UV radiation, the effect of natural ageing of bond is missing in the database. Hence, the results obtained in this study will be of great importance in the design of CFRP and GFRP strengthening schemes for the rehabilitation of structures which are exposed directly to outdoor environment.

The application of very high temperature, even more than the glass transition temperature of epoxy, to accelerate the ageing rate (using Arrhenius Principle) of any specific ageing mechanism can be found to be a common practice in the previous research. But the controversy of using high temperature as an accelerating agent was reported by Robert et al. (2010). The use of high temperature not only increases the degradation rate but also induces deterioration due to high temperature itself and may cause over degradation. However, in reality, structures may not be exposed to such high temperatures. Hence, the effect of temperature cycles and the wet-dry cycles on the CFRP and GFRP concrete bond were studied separately in this study. The maximum temperature for temperature cycles was selected as 40^{o} C which was below the glass transition temperature of adhesive (epoxy resin) and temperature cycles were generated in a drying oven to incorporate the sole effect of temperature on the FRP-concrete bond. The wet-dry cycles were selected in such a way that the temperature was close to ambient temperature and the maximum relative humidity for wetting was at least 95%. Therefore, the results of these two conditions will be conducive to understanding the effect of two major environmental conditions, namely, temperature cycles and the wet-dry cycles, separately on the CFRP and GFRP-concrete bond.

The experimental and analytical study on the repairing of three damaged beams with CFRP will be helpful to understand the efficacy of typical strengthening schemes provided in the design guidelines and codes. As the steel reinforcements of the beams before repairing with CFRP reached or exceeded the yield strain, the analytical study considering and ignoring the residual strength of steel reinforcement for the prediction of load carrying capacity of repaired beams and comparison of the analytical results with experimental ones may provide valuable information for the future improvement or

modification of available design guidelines. In addition, the proposed equations for the prediction of load-carrying capacity of repaired beams considering the strain hardening of steel will contribute to the design of repair schemes as no previous studies considered strain hardening of steel for repairing of damaged beams. Moreover, the selection of one beam from conventional concrete and two beams from non-conventional concrete will provide information regarding the effect of concrete types on the CFRP repairing.

1.5 Layout of the thesis

The thesis has been divided into nine chapters. Each chapter is associated with sections and subsections based on different aspects and foci of the chapters. In addition, figures and tables have been included to explain the findings of the study. Additional figures and tables, which are not included in the chapters for explanations, have been provided in appendices. Among the chapters, Chapter 8 has been dedicated only to the repairing of damaged reinforced concrete beams.

Chapter 1 provides a general introduction and background of strengthening and repairing of reinforced concrete structures with FRP. Also, problem identification, objectives and significance of the research have been included in this chapter.

Chapter 2 has focused on a comprehensive summary of research undertaken to-date on the bond between FRP and concrete, long term performance of FRP-concrete bond and prediction models, as well as strengthening of reinforced concrete beams with FRP. Also, background information on the FRP composites and a critical review on the research to-date have been provided.

Chapter 3 discusses the experimental program undertaken to investigate the long term performance of FRP-concrete bond subjected to three environmental conditions. The material properties and the change of material properties for three environmental exposures have also been included in the chapter. In the last part of this chapter, the test results for unexposed FRP-concrete bond are provided.

The findings of the long term performance of FRP-concrete bond subjected to temperature cycles, wet-dry cycles and outdoor environment have been discussed in Chapters 4, 5 and 6, respectively.

Chapter 7 focuses on determination of fracture energy from the shear stress-slip relation of CFRP-concrete bond under three environmental conditions. The changes of peak shear stress and fracture energy with exposure durations have been explained for three environmental conditions in this chapter. In addition, shear stress-slip relationships for exposed conditions have been proposed based on an existing model.

In chapter 8, experimental and analytical study on the short term performance of CFRP-repaired beams have been included. Finally, comparison of analytical results with experimental ones has been provided.

In the final chapter; i.e. Chapter 9, conclusions from the findings of both long term performance of FRP-concrete bond and short term performance of CFRP-repaired reinforced concrete beams have been drawn. At the end of this chapter, suggestions for future studies have been provided.

CHAPTER 2

LITERATURE REVIEW

2 Literature review

2.1 Introduction

This chapter focuses on providing a summary of previous research, available in literatures, on long term performance of FRP-concrete bond system and short term performance of RC beams strengthened/repaired with FRP. Literature review on short and long term performance of reinforced concrete structures retrofitted with Fibre-Reinforced-Polymer (FRP) composites can be divided into several categories in the context of basic information on FRP composites, bond strength and bond strength models of FRP strengthened concrete structures, durability of FRP and FRP concrete structures, long-term prediction models, durability of FRP-concrete bond and repairing/strengthening (short term performance) of reinforced concrete (RC) beams with FRP. Section 2.2 of this chapter mainly introduces the FRP composites and describes briefly the formation of FRP composites, its mechanical behaviour and usage in reinforced concrete structures. Whereas sections 2.3 to 2.6 provide information on the bond strength of FRP-concrete structures and bond strength models, durability of FRP and FRP-concrete structures, long term prediction models on the durability of FRP and FRP-concrete structures, and previous experimental studies conducted on the durability of FRP-concrete structures. Section 2.7 provides a brief description on the repairing of reinforced concrete beams with FRP and includes a summary of previous research on the retrofitting of concrete beams with FRP and design guidelines recommended by different researchers. Finally, a critical review on the previous research in the field of FRP-concrete bond, durability of FRP-concrete structures and strengthening of RC beams with FRP is presented in section 2.8.

2.2 Fibre Reinforced Polymer (FRP) composites

FRP composites consist of two parts: continuous fibres and resin matrix. The continuous fibres which can be carbon, glass or aramid, are embedded in a resin matrix. Fibres are the main load carrying components, while, resin matrix is used to bind the

fibres together. The common types of resins used are epoxy resins, polyester resins and vinyl ester resins. Polymeric resins can be used both to provide matrix for the FRP and to provide adhesive bond between FRP and concrete. Epoxy resins are usually used when bonding function is of high importance, such as, in the flexural and shear strengthening of beams. Figure 2.1 shows the schematic cross section of a FRP sheet formed in wet lay-up method.

FRP composites can be classified into three types based on the types of fibres used in the composites: Carbon-Fibre-Reinforced-Polymer (CFRP) composites, Glass-Fibre-Reinforced- Polymer (GFRP) composites and Aramid-Fibre-Reinforced-Polymer (AFRP) composites.

2.2.1 Methods of forming FRP composites

There are two common methods of forming FRP composites for strengthening of RC structures, namely, wet lay-up method and pre-fabrication of FRP composites (Teng 2002). The wet lay-up method is the most common method which is the in-situ application of resin either to woven fabric or a unidirectional tow sheet. Tow sheet is a fibre product that consists of continuous flat fibres held together by a very lightweight scrim cloth (Bank 2006). The second method includes pultrusion of plates for flexural strengthening and filament winding of shells for column strengthening.

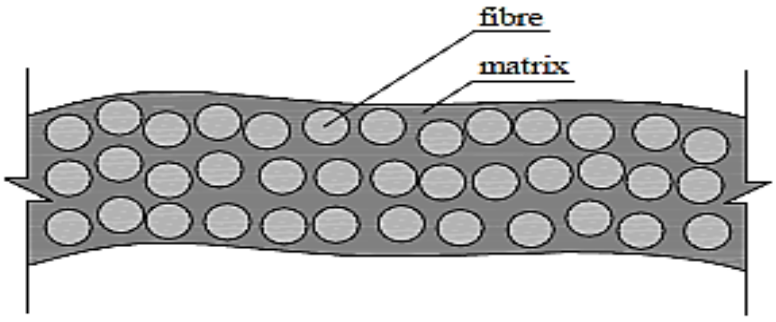

Figure 2.1 Cross section of a FRP sheet formed by wet lay-up process (taken from Shrestha (2009))

The wet lay-up method facilitates versatile site applications as it is applicable for bonding to curved surfaces and wrapping around corners, whereas, prefabrication assures better quality control. A third method, namely resin infusion method, which is similar to wet lay-up method but is not commonly used for structural engineering applications. In this process, dry fibre forms, usually fabrics, are arranged on moulds and then the entire fibre form is infused with resin and cured (Bank 2006).

2.2.2 Mechanical properties of FRP composites

All three types of FRP, namely, CFRP, GFRP and AFRP are linear elastic up to final brittle rupture in tension. Table 2.1 provides the mechanical properties of three types of FRP composites, taken from Head (1996), for FRP composites with unidirectional fibres. The ranges shown in this table are indicative only and a product may have the properties beyond these ranges depending on the fibre content and thickness of the FRP composite.

Figure 2.2 depicts typical tensile stress-strain curves for CFRP, GFRP and mild steel Teng (2002). These curves show the strength differences between these materials as well as a clear contrast between the ductile behaviour of steel and the brittle nature of FRP composites. The brittle nature of FRP has two major structural consequences. First, their brittleness may limit the ductile behaviour of RC members strengthened with FRP as they do not possess the ductility that steel has. Second, redistribution of stresses is restricted due to the lack of ductility. Therefore, the design of FRP strengthened structures cannot follow the existing design methods for RC structures with FRPs simply treated as equivalent steel reinforcement. Consequently, existing design methods for RC structures need to be modified considering the brittleness of FRPs based on research.

The tensile properties of FRP composites are usually determined by preparing flat coupons according to a suitable test standard (e.g. ASTM D3039/D3039M (2008)).

Table 2.1 Typical mechanical properties of CFRP, GFRP and AFRP composites (Head 1996)

Unidirectional advanced composite materials	Fibre content (% by weight)	Density (kg/m^3)	Longitudinal tensile modulus (GPa)	Tensile strength (MPa)
Carbon/epoxy CFRP laminate	65-75	1600-1900	120-250	1200-2250
Glass fibre/polyester GFRP laminate	50-80	1600-2000	20-55	400-1800
Aramid/epoxy AFRP laminate	60-70	1050-1250	40-125	1000-1800

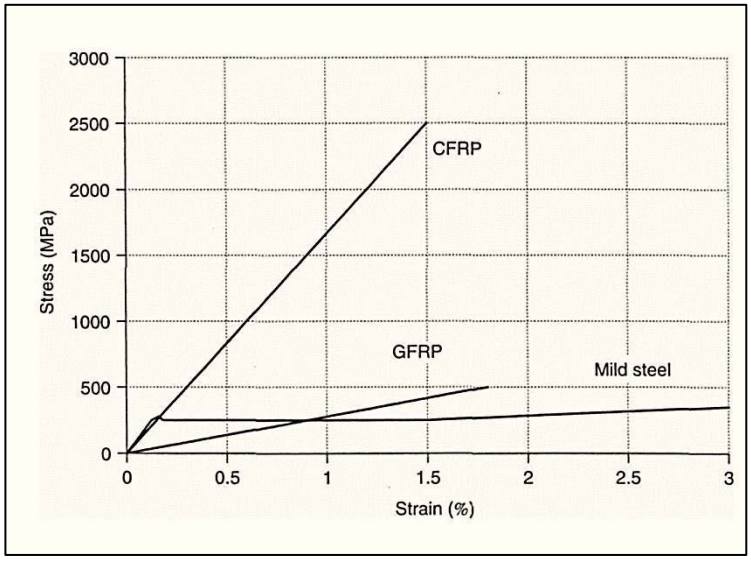

Figure 2.2 Typical FRP and mild steel tensile stress-strain curves (Teng 2002)

2.3 Bond strength and bond strength models

The strengthening of reinforced concrete structures with FRP are usually accomplished by external bonding of FRP to concrete using epoxy resins. The effectiveness of the strengthening mainly depends on the effective stress transfer between FRP and concrete. In reinforced concrete (RC) beams with flexural strengthening, two distinct stress transfer mechanisms are liable to cause interfacial or local concrete failure. The first one is interfacial stress transfer from the highly stressed FRP plate to concrete under a major flexural crack and the failure occurs by the crack propagation in the concrete parallel to the bonded FRP plate and adjacent to the adhesive-concrete interface. This failure mode can be referred to as intermediate flexural crack induced debonding (Teng 2002, p. 11). Although the interfacial stress developed at intermediate flexural crack has both shear and normal stress components, the shear stress is the dominant one in this stress transfer mechanism and is usually simulated by single or double shear tests of FRP strip bonded concrete prisms and referred to as Mode II fracture in fracture mechanics. The other type of interfacial stress which develops at the ends of FRP plate is known as interfacial peeling stress (stress normal to the plate surface) and the debonding due to peeling stress is referred to as Mode I fracture in the context of fracture mechanics.

According to Chen & Teng (2001) there are six possible types of failures for single or double shear tests of FRP-to-concrete bonded joints. The failure modes are as follows:

- Concrete failure
- FRP tensile failure
- Adhesive failure
- FRP delamintation for FRP-concrete joints
- Concrete-to-adhesive interfacial failure
- FRP plate-to-adhesive interfacial failure

Among these failure modes, FRP delamination from concrete substrate is the most common mode of failure in a FRP-to-concrete bonded joints and the location of failure is generally a few millimetres from concrete-to-adhesive interface.

One of the most recognised definitions of 'interface' was provided by Yuan et al. (2004) as the adhesive layer which represents not only the deformation of the actual adhesive layer but also that of the materials adjacent to the adhesive layer.

Studies over the past two decades have tried to develop constitutive laws in order to model the interface between FRP and concrete and predict the delamination of FRP from concrete. These proposed models can be divided into three categories: i) empirical models, ii) fracture mechanics based models and iii) damage mechanics based models. A brief explanation of some of the proposed models is presented in this section.

Empirical models were developed directly by the regression of test data from a variety of test set-ups with different specimen, geometries and material properties (Hiroyuki & Wu 1997; Maeda et al. 1997; Tanaka 1996). But these models are only applicable for similar test set-ups.

Tanaka (1996) provided a simple empirical relationship between the average bond shear stress at failure τ_{max} and bond length L (mm) based on shear tests:

$$\tau_{\max} = 6.13 - \ln L, \text{ MPa} \tag{2.1}$$

Hiroyuki & Wu (1997) also proposed a similar relationship based on a set of double shear tests on carbon fibre sheet (CFS) strengthened reinforced concrete members as follows:

$$\tau_{\max} = 5.88L^{-0.669}, \text{ MPa} \tag{2.2}$$

where the bond length (L) is measured in cm.

The above two models used ultimate bond strength of the bond as P_{max} given by multiplying τ_{max} by the width b_f and bond length L of the bonded area.

Maeda et al. (1997) developed a model in which effective bond length was considered. In this model, the following relationship was proposed between τ_{max}, modulus of elasticity E_f (MPa) and thickness t_f (mm) of the bonded plate.

$$\tau_{\max} = 110.2 \times 10^{-6} E_f t_f, \text{ MPa} \tag{2.3}$$

The ultimate bond strength P_{max} can be determined by multiplying τ_{max} by the effective bonded area $L_e b_f$ where L_e is given by the following equation:

$$L_e = e^{6.13 - 0.580 \ln E_f t_f}, \text{ mm} \tag{2.4}$$

where $E_f t_f$ is in GPa-mm.

Although the model proposed by Maeda et al. (1997) considered the effective bond length, the relationship is invalid when bond length $L < L_e$ (Teng 2002, p. 15).

Linear elastic fracture mechanics (LEFM) were used by some of the researchers (Bazant, Daniel & Li 1996; Täljsten 1996) in order to determine the mode II (pure shear) fracture energy of CFRP-concrete and steel- concrete interfaces.

Täljsten (1996) studied the FRP or steel-concrete beams by LEFM and proposed the directly proportional relationship between the maximum transferable load and the square root of the interfacial fracture energy in an adhesive-bonded joint. Both symmetric and non-symmetric joints were considered in his study. In a further study by Täljsten (1997), the concept of the effective bond length (the length of the bonded steel or FRP plate beyond which no further load can be carried by the plate) was introduced. Some other studies also included the effective bond length in their studies and Yuan et al. (2004) provided a definition of effective bond length as the length of the bond required for reaching the 97% of the applied load, whereas Lu et al. (2005) defined that

the effective bond length is the length of the bonded plate at which 99% of the bond strength is achieved. Ali-Ahmad, Subramaniam & Ghosn (2007) in their numerical analysis showed that increasing the bond length beyond the effective length results in snap-back i.e.; both the load and displacement decrease simultaneously.

Bazant, Daniel & Li (1996) showed the effect of specimen sizes on the strength of quasi-brittle materials and this size effect results in difficulties to compare the test results of different studies carried out with different materials and specimen geometries.

A series of double shear tests were carried out by Neubauer & Rostasy (1997) on CFRP-concrete bonded joints and concluded that the shear stress-slip relationship of FRP-concrete joints can be represented by a triangular model (Figure 2.3) with an ascending trend followed by a descending trend.

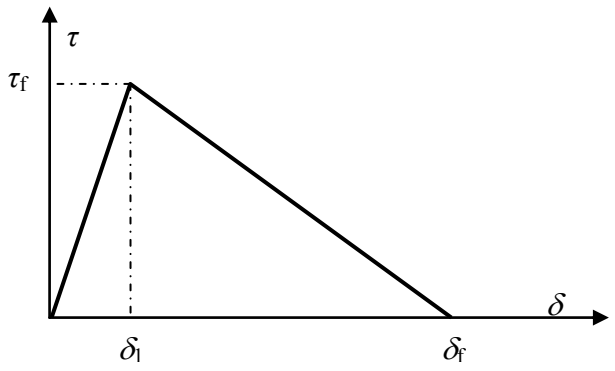

Figure 2.3 Triangular shear-slip model

Also, Neubauer & Rostasy (1997) provided a relationship between the fracture energy, G_f and concrete surface tensile strength f_{ctm} (MPa) as:

$$G_f = c_f f_{ctm}, \text{ N-mm/mm}^2 \quad (2.5)$$

where the average value of c_f (a constant obtained from the regression analysis) was 0.204 mm with a standard deviation of 0.053 for 51 specimens. They proposed a model for bond strength P_{max} applicable both for CFRP and steel plates:

$$P_{\max} = 0.64 k_f b_f \sqrt{E_f t_f f_{ctm}} \text{ if } L \geq L_e \tag{2.6}$$

$$\text{or } P_{\max} = 0.64 k_f b_f \sqrt{E_f t_f f_{ctm}} \frac{L}{L_e}\left(2 - \frac{L}{L_e}\right) \text{ if } L < L_e$$

$$\text{where } L_e = \sqrt{\frac{E_f t_f}{2 f_{ctm}}} \tag{2.7}$$

and k_f = is a geometrical factor related to the width of bonded plate b_f and width of the concrete member b_c and was expressed as follows:

$$k_f = \sqrt{1.125 \frac{2 - b_f / b_c}{1 + b_f / 400}} \tag{2.8}$$

Barenblatt (1962) introduced the Cohesize Zone Model (CZM) to overcome some limitations involved in LEFM. This model was developed to simulate mode I fracture and was extended for mode II fracture by Högberg (2006) considering the tangential traction and separation instead of normal ones.

The non-linear fracture mechanics approach (NLFM) was used by many of the researchers in the study of FRP-concrete interface (Ali-Ahmad 2006; Dai, Ueda & Sato 2005; Mazzotti, Ferracuti & Savoia 2004; Yuan et al. 2004; Yuan, Wu & Yoshizawa 2001). The non-linear fracture mechanics approach was supported by the results of experimental research conducted by Chajes et al. (1996), Bizindavyi & Neale (1999) and Yao, Teng & Chen (2005).

Qiao & Chen (2008) used damage mechanics approach to simulate mode I fracture of FRP-bonded concrete beams. Also, same approach was adopted before by Camanho & Davila (2002) to develop a bilinear interface law for composite laminates but the model was not for FRP-concrete interface.

Several constitutive laws were suggested by researchers to model the FRP-concrete interface subjected to pure shear loads considering different parameters (Ali-Ahmad 2006; Bizindavyi & Neale 1999; Chajes et al. 1996; Chen & Teng 2001; De Lorenzis, Miller & Nanni 2001; Maeda et al. 1997; Mazzotti, Ferracuti & Savoia 2004; Nakaba et al. 2001; Wu, Yuan & Niu 2002; Yuan et al. 2004; Yuan, Wu & Yoshizawa 2001) but none of them are generally accepted.

The bond and load transfer mechanism in FRP plates bonded to concrete were studied by Chajes et al. (1996) using a single shear test set-up. It was observed that interfacial strength is affected by the concrete surface preparation. They also found that the ultimate interfacial shear strength is proportional to the square root of compressive strength of concrete $\sqrt{f_c'}$.

Bizindavyi & Neale (1999) investigated the shear mode between the FRP sheets and concrete beams through single shear tests. It was found that the effective bond length depends on the properties and geometry of the specimens and on the surface preparation. It was further shown that the bond strength of externally bonded FRP laminates mainly depends on the quality of the surface preparation, and the quality of the concrete itself.

De Lorenzis, Miller & Nanni (2001) investigated the parameters affecting the behaviour of bond between FRP and concrete and observed that the bond strength is not affected by the FRP width. Subramaniam, Carloni & Nobile (2007) studied the effect of the width of the FRP laminate on the interface properties in more details. They concluded that the fracture properties of the central portion of the interface away from the edges are independent of the width of the FRP which is similar to the conclusion of De Lorenzis, Miller & Nanni (2001) but the maximum load was found to be higher for wider laminates.

Dai, Ueda & Sato (2005) investigated the behaviour of FRP-concrete interface under shear loads. Different FRP materials (carbon, glass and aramid fibres), FRP stiffness and adhesives were used in their study. An analytical method to define non-linear bond stress-slip models of FRP sheet-concrete interface through pull-out tests was proposed in this study. This method does not require attaching many strain gauges on the FRP sheets to obtain strain distributions and local bond stress-slip relation, instead, the relationship between pull-out forces and loaded end slips can be applied to derive local bond stress-slip relations. Dai, Ueda & Sato (2005) used two LVDTs, at free end and loaded end of the bonded area, to determine the relative slip between the FRP and concrete. The assumption behind their model was that a unique relationship exists between the FRP strain and interfacial slip as follows:

$$\varepsilon = f(s) \tag{2.9}$$

where ε is the strain in FRP sheets at any location and s is the corresponding relative slip between FRP and concrete at that location.

An exponential expression was fitted to the experimental results of shear tests for finding the relationship between the strains in FRP sheets and slips at loaded ends as follows:

$$\varepsilon = f(s) = A(1 - \exp(-Bs)) \tag{2.10}$$

where A and B are experimental parameters.

A first order derivative of ε with respect to x gives the following equation:

$$\frac{d\varepsilon}{dx} = \frac{df(s)}{ds}\frac{ds}{dx} = \frac{df(s)}{ds}\varepsilon = \frac{df(s)}{ds}f(s) \tag{2.11}$$

Therefore, the interfacial bond stress for FRP-concrete interfaces can be expressed as:

$$\tau = E_f t_f \frac{d\varepsilon}{dx} = E_f t_f \frac{df(s)}{ds} f(s) \tag{2.12}$$

Finally, the interfacial shear stress is obtained as a function of relative slip by substituting Equations 2.10 into Equation 2.12:

$$\tau = A^2 B E_f t_f \exp(-Bs)(1-\exp(-Bs)) \quad (2.13)$$

where $E_f t_f$ is the stiffness of FRP sheets (multiplication of modulus of elasticity and thickness).

Also, the interfacial fracture energy can be obtained by the area under the stress-slip curve and leads to the following expression:

$$G_f = \frac{1}{2} A^2 E_f t_f \quad (2.14)$$

The above equation provides the relationship between parameter A, interfacial fracture energy and FRP stiffness.

The theoretical maximum pull-out force can be obtained from the following equation:

$$P_{\max} = b_f \sqrt{2 E_f t_f G_f} \quad (2.15)$$

Based on the experimental maximum pull-out force and the Equation 2.15, the interfacial fracture energy can be calculated.

Equation 2.15 was modified by adding an additional width $2\Delta b_f$ considering the effect of concrete on both sides of the attached FRP sheets:

$$P_{\max} = (b_f + 2\Delta b_f)\sqrt{2 E_f t_f G_f} \quad (2.16)$$

The empirical constants in this model were obtained by regression analysis of experimental results. It was observed that the interfacial fracture energy G_f is affected by the properties of concrete, adhesives and FRP stiffness. The shear stiffness of adhesive affects the interfacial fracture energy most, whereas the effect of concrete strength is much less than that of the adhesive but slightly greater than that of the FRP stiffness. The parameter B increases infinitely with the increase in FRP stiffness and significantly with the shear stiffness of adhesive.

Mazzotti, Savoia & Ferracuti (2008) used Popovics' non-linear equation to analyse the data from push-pull single-shear tests. Popovics' (1973) non-linear equation, mainly

introduced to relate the concrete strength and the strain distribution, was modified to apply for FRP-concrete interface as follows:

$$\frac{\tau}{\tau_{\max}} = \frac{s}{s_{\max}} \frac{n}{(n-1)+\left(s/s_{\max}\right)^{n}} \tag{2.17}$$

where τ_{max} is the peak shear stress, s_{max} is the corresponding slip and $n>2$ is a parameter governing the softening branch of the τ-s curve.

The fracture energy $G_{f,}$ which is the area under τ-s curve, is written as:

$$G_f = g_f(n)\tau_{\max} s_{\max} \tag{2.18}$$

where g_f is an analytical function of exponent n:

$$g_f = \pi\left(\frac{1}{n-1}\right)^{1-\frac{2}{n}} \frac{1}{\sin\left(\frac{2\pi}{n}\right)} \tag{2.19}$$

The three unknown parameters i.e. $\tau_{max,}$ s_{max} and n were obtained through least square minimisation and the fracture energy, obtained from the asymptotic value of maximum transmissible force by an infinite bond length, was used as a constraint in the minimisation procedure.

The effect of FRP plate width was also studied by Mazotti, Savoia & Ferracuti (2008) and it was found that the effect of plate width on the interface fracture energy and delamination force was not significant but the maximum shear stress τ_{max} increased with the decrease in plate width. Also, the effect of primary notch was shown by using two test set-ups (with and without primary notch at loaded end of FRP-concrete bond) and for 50 mm bond length about 60% less delamination load was reported for the set-up without primary notch.

Nakaba et al. (2001) also used Popovics' (1973) equation for developing their model. They used double shear test set up for their research. Unlike Mazzotti, Savoia &, who Ferracuti (2008) applied least square minimization to obtain the maximum shear stress,

τ_{max}, Nakaba et al. (2001) proposed an exponential function of concrete compressive strength as follows:

$$\tau_{\max} = 3.5(f_c^{'})^{0.19} \tag{2.20}$$

Using types of fibre and concrete substrate as test variables, they observed that maximum interfacial shear stress τ_{max} was not affected by the type of FRP but increased with the increase in concrete compressive strength.

Popovics' (1973) equation was also adopted by Pham & Al-Mahaidi (2007) to simulate the CFRP-concrete interface behaviour under single shear tests. But the value of *"n"* was chosen equal to 3, in order to simplify the problem, and find the two unknowns, τ_{max} and s_{max}.

Woo & Lee (2010) proposed a bond-slip law with linear hardening and exponential softening branch. The studied the effects of bonded length, width, and concrete strength on the interfacial behaviour and a proposed the bond-slip model from the experimental results.

Yuan et al. (2012) studied the bond behaviour based on two bond-slip laws. Firstly, The used the bond-slip law proposed by Woo & Lee (2010) and a simplified analytical law with linear softening branch for their study. They also obtained the analytical solutions for the simplified analytical law. Finally, they discussed the influences of the FRP bond length and stiffness on load–displacement curve and the ultimate load based on the analytical solutions of two laws. They also studied the effect of stiffness on the effective bond length.

Zhou, Wu & Yun (2010) proposed an analytical bond-slip model which is applicable to both short and long joints. They developed the bond-slip relationship for short FRP-concrete bond (the bond length is less than the effective bond length) for the first time.

Coronado & Lopez (2006) used ranges of tensile strength of concrete between $0.5f_t$ and $2f_t$ (where f_t is the tensile strength of concrete) and reported that debonding is insensitive to concrete strength. Similarly, Qiao & Chen (2008) also stated that the concrete tensile strength does not have any effect on the failure of the FRP-concrete interface. The interface failure is basically the cohesive failure of concrete along the interface due to the fact that the interface cohesive strength is higher than the concrete tensile strength. Hence, the interface fracture behavior is not affected by concrete tensile strength and variation of the concrete tensile strength does not alter the interfacial load-displacement curve.

Lu et al. (2005) carried out an assessment of twelve existing bond-strength models and bond-slip models using the test results of 253 pull-out specimens collected from existing literature and found that the model proposed by Chen & Teng (2001) is the most accurate and recommended it for design due to its simplicity.

Chen & Teng (2001) adopted a linearly decreasing shear slip model (see Figure 2.4) as typical slip values of FRP-concrete bonded joints are δ_1 = 0.02 mm (the slip corresponding to maximum shear stress) and δ_f = 0.2 mm (maximum slip); i.e., δ_1 is small compared to δ_f. Based on their model, the debonding stress in the FRP plate bonded to concrete is given as:

$$\sigma_f = \alpha\beta_p\beta_L\sqrt{\frac{E_f\sqrt{f_c'}}{t_f}} \tag{2.21}$$

The parameters α, β_p, β_L, E_f, f_c' and t_f in the above equation represent an empirical factor (best fit model = 0.427), FRP width factor, FRP length factor, modulus of elasticity of FRP, compressive strength of concrete and thickness of FRP, respectively, and

$$\beta_p = \sqrt{\frac{2-\frac{b_f}{b_c}}{1+\frac{b_f}{b_c}}} \tag{2.22}$$

$$\beta_L = \begin{cases} 1 & if \quad L \geq L_e \\ \sin\dfrac{\pi L}{2L_e} & if \quad L < L_e \end{cases} \tag{2.23}$$

$$L_e = \sqrt{\frac{E_f t_f}{\sqrt{f_c'}}} \tag{2.24}$$

where b_f and b_c are FRP width and concrete width, respectively, and L_e represents the effective bond length.

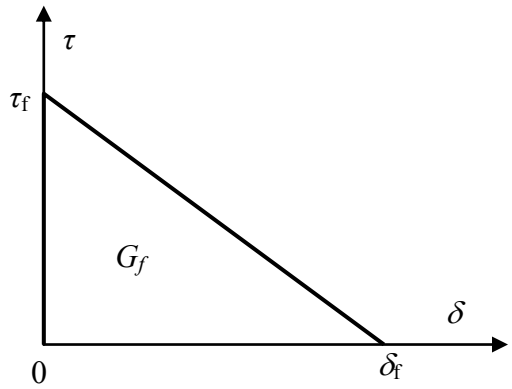

Figure 2.4 Shear slip model (adopted from Chen & Teng (2001))

Biscaia, Chastre & Silva (2013) analysed different existing analytical and numerical solutions for the debonding process of FRP-concrete bond. They used numerical integration process to find the solution of governing differential equation of FRP-concrete bond. In the numerical process, they used five existing bond-slip models including three linear bond-slip relations. The numerical integration process was found to be in a good agreement with the analytical expressions determined for the linear bond-slip models and it was verified that maximum load transmittable to the FRP plate is influenced by the square root of the FRP stiffness and fracture energy even when nonlinear bond-slip relations are assumed.

2.4 Durability of FRP and FRP-concrete structures

According to Cousins, Lesko & Carlin (1998), the durability of structures is the ability of it to maintain its initial performance-properties over time (Imani 2010, p. 36). Karbhari et al. (2003) also defined 'Durability' of a material or structure as "its ability to resist cracking, oxidation, chemical degradation, delamination, wear, and/or the effects of foreign object damage for a specified period of time, under appropriate load conditions, under specified environmental conditions". There are various factors involved in the study of durability of a structural system such as repeated loadings, changes in environmental conditions, chemical exposure and traffic loads. Alternating environmental conditions are considered to be one of the most important environmental effects (Imani 2010, p. 36) on the behaviour of a structural system. Environmental conditions can be referred to as temperature change, wet-dry and freeze thaw cycles, salinity, UV radiation, alkaline environment, acid rain and many other environmental compononents.

Fibre Reinforced Polymer (FRP) composites are being used increasingly in retrofitting of civil engineering structures due to their convenient application methods and resistance to corrosion unlike steel. But the information regarding the long term durability of FRP is sparse. Karbhari (2003) stated that there are a number of myths regarding FRP composites and few of those are:

- Composites can solve all the issues related to degradation of civil infrastructure;
- Composites do not degrade and are not susceptible to environmental influences;
- Glass fibre reinforced composites should only be used for architectural applications due to stress-rupture considerations.
- Carbon fibre reinforced composites are not degradable and have infinite life.

However, the reality is different from the myths stated above. FRP composites can degrade at the level of fibre, polymer, and/or interface under certain circumstances. The resin matrix allows moisture adsorption and may results in the degradation of polymer and fibre. Also, temperature changes, especially when temperature approaches or exceeds the glass transition temperature (T_g), can degrade the performance of FRP composites. Glass transition temperature is the temperature at which resin matrix transforms from hard glass-like material to more rubber-like material. There are other factors which may also degrade the performance of FRP composites used in concrete

structures such as alkalinity, salinity and freezing and thawing. As a result, the effect of various environmental conditions on the FRP composites and the FRP-strengthened structures need to be obtained through extensive research to know the level of performance of the structure and the material itself after long term.

2.5 Long term performance prediction for FRP and FRP-concrete structures

Most of the existing long term prediction models for FRP stiffness and strength for concrete applications are based on the short term accelerated ageing tests. Accelerated ageing tests are carried out by exposing FRP composites and FRP reinforced concrete beams to elevated temperatures or freeze-thaw cycling under water, salt, alkaline, or acidic solution immersion (GangaRao, Taly & Vijay 2006) and accelerated ageing results are correlated to natural ageing. All these accelerated ageing are based on the Arrhenius principle (section 2.5.1).

2.5.1 Arrhenius principle

Arrhenius principle states that the chemical degradation rate depends on temperature. This principle is applied to determine the temperature dependence of polymers exposed to environmental conditions consisting of several temperature levels. The Arrhenius equation is as follows:

$$k = Ae^{\left(-E_a/RT\right)} \tag{2.25}$$

where k = reaction rate constant with respect to a temperature T

A = a constant of the test condition

E_a = the activation energy of the chemical reaction

R = the universal gas constant (8.3145 $JK^{-1}mol^{-1}$)

T = the absolute temperature (K)

In order to apply the Arrhenius equation it is assumed that the degradation is controlled by a single dominant mechanism.

Using Arrhenius principle, short term tests are conducted by using higher temperature to accelerate the degradation in a certain environmental condition. Several temperature levels are chosen to determine load, stress or other parameters at those temperatures and charts are prepared by time-temperature-stress superposition principle based on test results. Finally, accelerated ageing test data are correlated to natural ageing data.

2.5.2 Time-temperature-stress superposition principle

A certain property of polymer composite material such as time-dependent stress at one temperature can be used to find that property at another temperature (under certain limitations) and this principle is referred to as the time-temperature-stress superposition principle. This principle is used to correlate the accelerating aged test data to naturally aged test data and service life prediction can be performed for polymer composite subjected to certain environmental condition (GangaRao, Taly & Vijay 2006).

2.5.3 Existing long term durability prediction models

Long-term prediction models based on Arrhenius equations proposed by different researchers are popular in the study of long term performance of FRP and FRP-concrete structures. Litherland, Oakley & Proctor (1981) , Dejke & Tepfers (2001) and Phani & Bose (1987) proposed models based on Arrhenius principle. But these models are only applicable to certain type of FRP and certain environmental condition. Also, the validity of the assumption that the elevated temperature only increases the rate of deterioration but the deterioration mechanism remains the same is still open for debate. Robert et al. (2010) stated, regarding the use of high temperature as an accelerating factor, that high temperature may amplify the reduction of the properties which may lead to conservative prediction of long-term properties. They also commented that too high a temperature not only accelerate the degradation rate but may also alter the thermo-mechanical induced degradation mechanism which may not be experienced by the structure in real time ageing.

A model to predict the direct tensile strength of glass fibre strands in cement environment and the flexural strength of Glass Fibre Reinforced Cement (GRC) composites exposed to hot water at various temperatures was proposed by Litherland, Oakley & Proctor (1981). They used Arrhenius principle to predict the expected strength of GRC after hundred years of exposure.

Phani & Bose (1987) developed a model to predict the flexural strength of random mat glass fibre reinforced polyester resin specimens exposed to hydrothermal ageing based on Arrhenius equation. Acousto-ultrasonic technique was used to predict the flexural strength in this study. Their research shows that the flexural strength, $\sigma(t)$, after an exposure time, t, follows the following relation:

$$\sigma(t) = (\sigma_0 - \sigma_\infty)\exp\left[\frac{-t}{\tau}\right] + \sigma_\infty \tag{2.26}$$

where σ_0 and σ_∞ are the composite strength at times 0 and ∞, respectively, and τ is a characteristic time, which is dependent on temperature.

Dejke & Tepfers (2001) investigated the long term environmental influence of concrete on GFRP reinforcement bars. GFRP reinforcement bars were exposed to three different environmental conditions, namely, alkaline solution, concrete and tap water. They used elevated temperatures in the range of 7^o C (average outdoor temperature in the south-coast of Sweden) to 80^o C to accelerate the ageing. Some of the specimens were embedded in concrete and exposed to outdoor environment at 100% relative humidity to simulate the real concrete structure in highly humid condition, whereas elevated temperatures were used to accelerate the degradation process and to determine the acceleration factor. The mechanical properties, namely, tensile strength and inter-laminar shear strength were measured in this study. They also commented that time shift factor (TSF) for the ageing of glass fibre reinforced concrete at elevated temperatures suggested by Litherland, Oakley & Proctor (1981) is not applicable to GFRP immersed in alkaline solutions or embedded in concrete. So, they suggested a new approach to

quantify the time shift factor based on the tests of GFRP only. The time shift factor was calculated by the following equation:

$$TSF = \exp\left(\frac{B}{T_1 + 273.15} - \frac{B}{T_2 + 273.15}\right) \quad (2.27)$$

where *TSF* is the time shift factor, *B* is a constant determined using the time shift of two known curves and T_1 and T_2 are two temperatures between which *TSF* is calculated (T_1 is the smaller temperature value)

After obtaining the value of *B* from the tested results at two temperatures, results at a given temperature, *T*, can be obtained by substituting the temperature *T* value in the above equation.

Chen, Davalos & Ray (2006) proposed a procedure based on the Arrhenius relation to predict the long-term behaviour of glass fibre-reinforced polymer (GFRP) bars in concrete structures by obtaining the short term data from accelerated ageing tests. Two types of E-glass-vinyl ester-FRP reinforcing bars were exposed to simulated concrete pore solutions at 20, 40 and 60^{o} C. Determination of tensile strengths of the bars were conducted before and after the exposure for periods of 60, 90, 120 and 240 days. Based on the test results, it was observed that there is a dominant degradation mechanism for GFRP bars in alkaline solutions which does not change with temperature or time. Finally, a modified Arrhenius analysis was included to evaluate the validity of accelerated ageing tests.

According to the approach proposed in this study, first the relationship between tensile strength retention (the percentage of the residual strength over original tensile strength) of GFRP bars and exposure time for the accelerated test was defined as:

$$Y = 100\exp\left(-\frac{t}{\tau}\right) \quad (2.28)$$

where Y = tensile strength retention value (%); t= exposure time: and $\tau = 1/k$.

This equation is a modified form from the study of Phani & Bose (1987) by assuming that GFRP bars degrade completely at infinite exposure time.

In the second step, $\tau = 1/k$ is substituted to another form of Arrhenius equation:

$$\frac{1}{k} = \frac{1}{A}\exp\left(\frac{E_a}{RT}\right) \tag{2.29}$$

Finally, from the Arrhenius plots at different temperature values, long-term prediction was carried out for 20^o C temperature.

Karbhari & Abanilla (2007) studied the durability of unidirectional wet lay-up carbon-epoxy laminates by varying the number of laminate layers. 2, 6 and 12 plies were used in their study and they observed that deterioration rate increased significantly with the increase of number of resin dominated layers. The specimens were immersed in water for 3 years at 23^o C and based on the results obtained from tensile test, flexural test, short beam shear test and in-plane shear test, prediction equations were developed using two popular approaches, namely, Arrhenius method and Phani & Bose (1987) approach. It was observed that both methods were unable to account for the initial post-cure effect in ambient cured/carbon epoxy system. But the Arrhenius approach had better correlation with the experimental results than Phani and Bose approach after the post-cure mechanism ceased. So, Karbhari & Abanilla (2007) provided a general form of equation for the prediction of strength and modulus considering the post-cure effect as follows:

$$P(t) = \frac{P_0}{100}\left[A\ln(t) + B\right]; \quad t > 0 \tag{2.30}$$

where $P(t)$ and P_0 are strength or modulus at time t (in days) and time 0 (unexposed), respectively, and A is constant denoting degradation rate and B is a material constant reflecting the early effects of post-cure progression. The value of B greater than 100 represents the initial post-cure dominance over the moisture induced degradation. And B = 100 indicates fully cured material or null effect of post-cure progression.

2.6 Experimental study on durability of FRP-concrete structures

Although extensive research have been conducted on strengthening of RC structures with FRP, research on long term durability of FRP-concrete bond are very limited. Some research have dealt with durability of concrete beams strengthened with FRP and showed the decrease in ultimate beam strength after various environmental exposures, whereas other research showed the degradation of bond strength between FRP and concrete under aggressive environment. In addition, these research involved variety of test set-ups and environmental factors. A summary of the previous research, carried out experimentally, on the durability of FRP-concrete structures have been included in this section.

Chajes, Thomson & Farschman (1995)

Chajes, Thomson & Farschman (1995) performed two sets of tests to determine the effects of a calcium chloride solution on concrete beams externally reinforced with FRP under freeze/thaw and wet/dry conditions. Three types of FRP, aramid, E-glass and graphite, were used. Each freeze-thaw cycle consisted of 16 hours in a freezer at -17^{o}C followed by 8 hours of thawing at room temperature and a total of 50 and 100 cycles were applied to the beams, whereas, wet-dry cycle consisted of 16 hours of wetting followed by 8 hours of drying at room temperature. The number of wet-dry cycles was 50 and 100. Calcium chloride solution (4 g anhydrous calcium chloride per 100 ml of water) was used for both freeze-thaw and wet-dry cycles. Figure 2.5 shows the schematic diagram of the beam specimen and the test set-up.

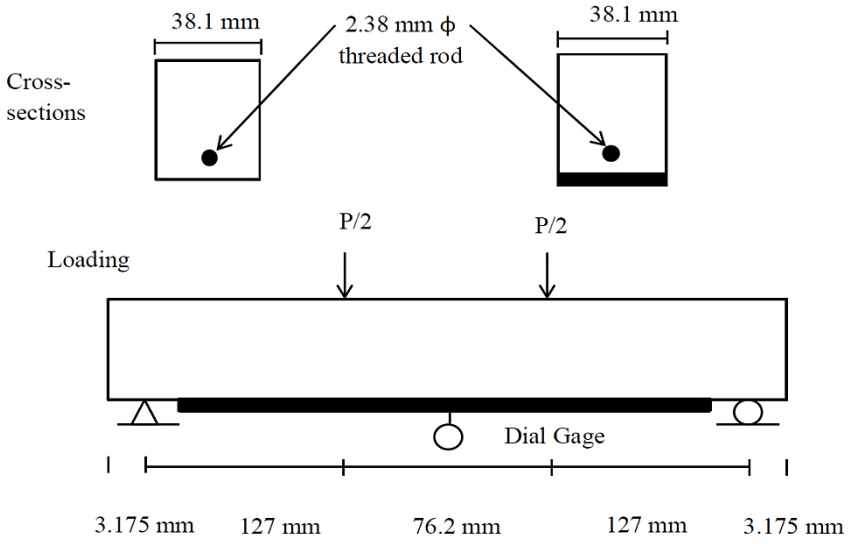

Figure 2.5 Test Set-up (Chajes, Thomson & Farschman 1995)

From the test results it was observed that graphite reinforced beams showed more durable performance than aramid and E-glass reinforced beams. Among the two tested conditions, wet/dry cycles caused slightly more degradation. Also, it was found that degradation can lead to changes in failure mode of the beams in addition to the reduction in ultimate strength. While control beams showed ductile flexural failure, all exposed aramid-reinforced beams failed because of debonding of the fabric. Failure of the E-glass and graphite-reinforced beams indicated deterioration of the concrete-epoxy-fabric bond, evidenced by the lack of adherence of concrete to the fabric.

Toutanji and Gómez (1997)

Toutanji and Gómez (1997) studied the effect of wet/dry cycling using salt water on the performance of FRP-concrete beams and on the interfacial bond between the fibre and the concrete. Four types of FRP (two carbon and two glass) and three different types of two-part epoxy were used. The duration of the wet cycle was 4 hours, and that of dry cycle was 2 hours. Thus, the specimens were exposed for 75 days (300 cycles) and tested in flexure.

From the test results of the specimens exposed to room temperature, it was found that the ultimate flexural load increased significantly by externally bonding FRP sheets to the tension face of concrete beams. The ratio of the ultimate flexural load of strengthened beams to unstrengthened beams, under room temperature conditions, was between 2.2 and 5.1, depending on the type of FRP sheet and the type of epoxy resin system. Even after wet/dry cycles, the beams showed a significant increase in load carrying capacity when FRP sheets were externally bonded to the tension face. Depending on the type of FRP sheets and the type of epoxy resin, the ratio of the ultimate flexural load of strengthened beams to unstrengthened beams was 2.1 to 4.4 under wet/dry cycles. But the increase in the ultimate load was reduced due to wet/dry condition.

Green et al. (2000)

An experimental investigation was carried out by Green et al. (2000) on the effect of freeze thaw cycles on the bond between unidirectional CFRP plates and concrete using both single- lap- joint shear and bond beam specimens. The exposure conditions applied were 0, 50, 150 and 300 freeze-thaw cycles consisting of 16 hours of freezing in cold air at -18^{o} C and 8 hours of thawing in a warm water bath at +15^{o} C. Freeze-thaw cycles up to 300 did not reveal any significant damage of FRP-concrete bond properties.

Myers et al. (2001)

Myers et al. (2001) conducted an experimental program to investigate the durability of bond between concrete and three types of FRP sheets (Carbon, Glass and Aramid) using pre-cracked concrete beams strengthened with FRP. The FRP strengthened beams were subjected to combined environmental cycles under various degrees of sustained loading in an environmental chamber. The exposure cycle consisted of a combination of freeze-thaw cycles, extreme temperature cycles, relative humidity cycles and indirect ultra-violet radiation exposure. After the exposure cycles, the beams were tested under four point bending.

The failure modes of all beams were due to peeling of FRP sheet from the concrete. The post-failure observation of the sheets indicated good bond between FRP and concrete even after the environmental exposure condition, although there was a relative deterioration in the bond. Exposed specimens showed much more rapid increase in strain with the increase in load as compared to control specimens. Specimens conditioned for 5 combined environmental cycles at sustained load of 40% of the ultimate load showed the largest degradation in terms of bond strength. GFRP strengthened beams exhibited more degradation in flexural stiffness than those of AFRP and CFRP strengthened beams.

Homam et al. (2001)

Homam et al. (2001) studied the durability of FRP-concrete bond using FRP bonded concrete prisms. Each specimen was fabricated using two separate concrete prisms with FRP laminates on two sides (Figure 2.6). Two types of FRP, Carbon and Glass, were used to investigate the bond. Specimens were grouped into batches of exposed and control, and placed in respective conditions. Six different exposure condtions were tested as listed below.

a. Control Environment: 22^{o}C and about 50% relative humidity
b. Freeze-thaw: cycling between -18^{o}C and +4^{o}C submerged in water (50, 100, 200, and 300 cycles)
c. UV radiation: exposure to UV-A lamp radiation at 156 watt/m^2 and 38^{o} C (1200, 2400 and 4800 hours)
d. Temperature variations: 4 cycles/day between -20^{o}C and +40^{o}C in dry chamber (28, 56, 112, and 336 cycles)
e. Alkali solutions: submersion in pH 10, pH 12 and pH 13.7 (normal pH 14) NaOH solution at 38^{o}C (7, 14, 28, and 84 days)
f. Water: submersion in water at 22^{o}C room temperature (7, 14, 28, and 84 days)

After the completion of exposure conditions, the specimens were tested by applying tensile load at the ends of the embedded steel rods. The FRP-concrete interface was subjected to shear due to bolts pulling apart. The bond failure took place at the epoxy-concrete interface. In some specimens, small chips of concrete broke off from the

surface of the concrete. The average lap shear strengths of the unexposed CFRP and GFRP bonded specimens were about 3.10 MPa and 2.30 MPa, respectively. The average lap shear strength of GFRP specimens dropped only slightly because of the freeze-thaw exposure compared to that of control specimens. The average lap shear strength of CFRP specimens dropped about 5% due to freeze-thaw exposure. The degradation was slightly more severe than that of GFRP specimens.

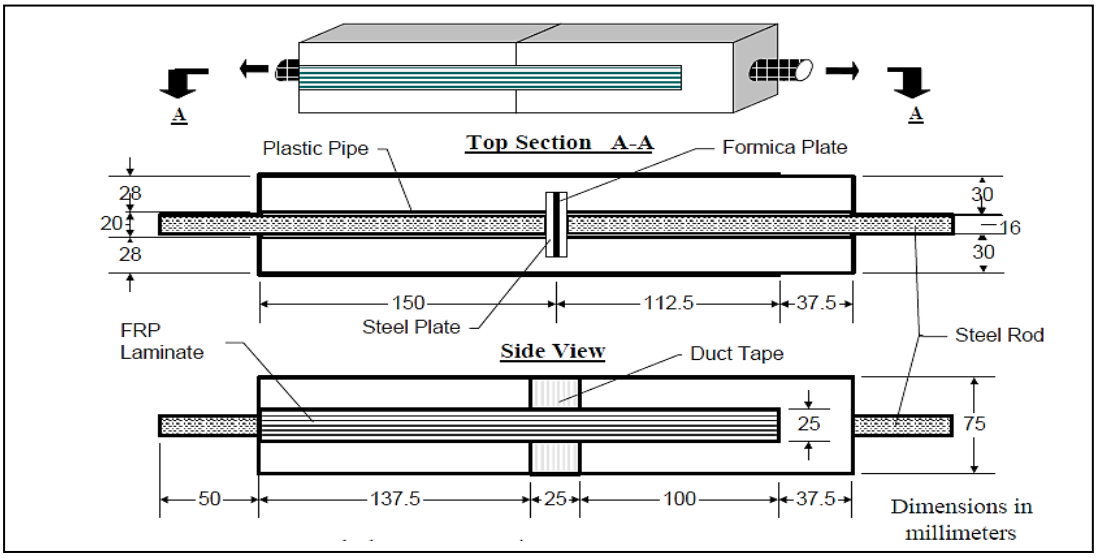

Figure 2.6 FRP bonded concrete prism (Homam, Sheikh & Mukherjee 2001)

Regarding the effect of temperature cycles and pH 10, pH 12 and pH 13.7 NaOH solutions, there were drops of about 10% to 14% in the bond strength of all the exposed GFRP bonded specimens in the early stages of exposure. With the progress of exposure duration, the difference in the strength of specimens exposed to pH 10 and pH 12 solutions and the control specimens disappeared. But the strength dropped about 15% for the temperature exposed specimens and about 5% for the pH 13.7 NaOH solution exposed specimens.

At the early stages of exposure to temperature and pH 10, pH 12 and pH 13.7 NaOH solutions, CFRP-concrete bond strength increased for all exposures, possibly due to the higher temperatures of exposure. However, with the progress of exposure duration, the

strength of control specimens increased and the strength of exposed specimens did not change much. Also, there was a large scatter of the data for this series of tests.

Li et al. (2002)

Li et al. (2002) studied the long-term structural degradation of concrete beams retrofitted with FRP sheets through short-term accelerated conditioning tests. A total of eighteen 1700×152×762 mm steel RC beams were fabricated from 3 batches of concrete. Some of the beams were pre-cracked while some were uncracked and unconditioned. After pre-cracking and surface preparation of the beams, either CFRP or GFRP was bonded to the tensile face of the damaged beams. Seven day exposure to boiling water was used to study the structural degradation of CFRP and GFRP strengthened concrete beams. Also, UV radiation was used for 30 minutes during the exposure to boiling water and for an hour after draining the water out on the seventh day. After conditioning in accelerated or ambient environment, all specimens were tested under four-point bending.

Comparison of the test results of FRP strengthened, pre-cracked and conditioned beams to the corresponding pre-cracked and conditioned control (without FRP strengthening) beams revealed that the average residual load carrying capacity of the FRP retrofitted beams was higher by 5-17%. This observation proved the strengthening ability of FRP even after harsh environmental exposure. However, comparing the FRP strengthened and conditioned beams with its corresponding FRP strengthened and unconditioned beams, it was found that about 57 -76% of strengthening efficiency was lost due to conditioning which implies significant structural degradation. The interesting behaviour was that the conditioning minimised the difference of two types of FRP in the residual increases in ultimate load carrying capacity of FRP strengthened specimens. For unconditioned specimens, increases in load carrying capacity were 44% and 33% for CFRP and GFRP, respectively, whereas for conditioned specimens increases in laod carrying capacity were 17% and 14% for CFRP and GFRP, respectively. The explanation for this behaviour was that the deterioration of the FRP was due to the degradation of FRP matrix and fibres only played a secondary role.

Moreover, the failure mode of all FRP strengthened RC beams was concrete crushing at the compression zone, not by fracturing of the FRP layer which might be due to the high amount of FRP relative to the small specimen size. Therefore, the strength of the FRP layer was not reached, even for the degraded FRP layer. Li et al. (2002) suggested that the best way to enhance the long-term performance of FRP strengthened concrete structures is to increase the water and ageing resistance ability of polymer matrix.

Grace (2004)

Grace (2004) studied the effect of environmental conditions on the CFRP strengthened reinforced concrete beams experimentally by testing 78 beams. Two of the beams were unstrengthened, four (two strengthened with CFRP plates and two with CFRP fabrics) were used as reference beams, not exposed to any environmental condition, and the remaining 72 beams were strengthened with CFRP (36 with CFRP plates and 36 with CFRP fabrics) and were subjected to environmental conditions or repeated loads. The environmental exposure conditions were 100% humidity, dry heat, alkaline solution and saltwater solution with exposure durations of 1000, 3000 and 10,000 hours. Also, sets of four beams were subjected to 350 and 700 freeze-thaw cycles and 35 thermal expansion cycles. After set durations of environmental exposures, the beams were tested under four point bending. The environmental conditions are listed in Table 2.2. The beams tested for repeated loads were not exposed to any environmental conditions but to repeated loads with constant amplitudes of 15, 25 and 40% of the ultimate failure loads at a frequency of 3.25 Hz for 2 million cycles.

Based on the experimental results, strength reduction factors were proposed for RC beams strengthened with CFRP and exposed to various independent environmental conditions.

Grace (2004) concluded that among all conditions (environmental and repeated load) 100% humidity caused the most significant reduction of strength of CFRP strengthened beams and the primary mode of failure of CFRP strengthened beams with or without exposure was delamination of CFRP.

Table 2.2 Environmental conditions used by Grace (2004)

Environmental exposures		
Name of exposure	Properties	Durations (hours/cycles)
Humidity	Constant 100% relative humidity at $38^{o} \pm 2^{o}$ C	1000, 3000 and 10,000 hours
Alkaline solution	pH 9.5 and $23^{o} \pm 2^{o}$ C temperature	1000, 3000 and 10,000 hours
Saltwater	Concentration of 1500 ppm, specific gravity of 1.022 and $23^{o} \pm 2^{o}$ C temperature	1000, 3000 and 10,000 hours
Dry heat	Constant 60^{o} C	1000, 3000 and 10,000 hours
Freeze-thaw cycles	Lowering the temperature of the beams from 4^{o} C and then returning to 4^{o} C (Air and water was used to freeze and thaw respectively)	350 and 700 cycles with each cycle of total 4 hours
Thermal expansion cycles	Raising the temperature of the beams to $48.9^{o} \pm 1.5^{o}$ C and then cooling to $26.7^{o} \pm 1.5^{o}$ C (the heating chamber was programmed for a maximum temperature of 75.5^{o} C and a maximum humidity of 100%	35 cycles with each cycle of total 5 hours

Boyajian, Ray & Davalos (2007)

Boyajian, Ray & Davalos (2007) conducted experimental research on the effect of freeze-thaw cycling under calcium chloride solution on the Mode I fracture critical fracture energy release rates (G_{Ic}) of CFRP bonded single contoured cantilever beam (SCCB) after 50,100, 150 and 300 cycles of freeze-thaw cycles. Figure 2.7 depicts the freeze-thaw cycling scheme applied in the study. They also investigated the weight

change of the specimens and strains initially and after every fifth cycle. Fracture testing after 300 cycles revealed that the efficiency of interface integrity degraded by more than one third of the control case.

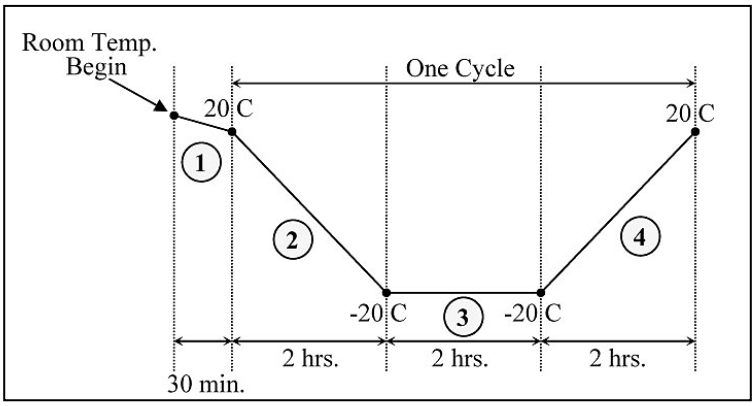

Figure 2.7 Freeze-thaw cycling scheme (Boyajian, Ray & Davalos 2007)

Subramaniam, Ali-Ahmad & Ghosn (2008)

Subramaniam, Ali-Ahmad & Ghosn (2008) demonstrated results from an experimental investigation on the influence of freeze–thaw cycles on the CFRP–concrete interface fracture properties. A direct shear test was used to investigate the FRP–concrete bond behaviour. The cohesive stress transfer between FRP and concrete during the shear test was determined from spatially continuous measurements of surface strains obtained at different stages of applied load by Digital Image Correlation (DIC). The non-linear material law for the interface shear fracture was developed by relating the interface shear stress as a function of relative slip for specimens subjected to freezing and thawing action. A larger percentage decrease in the interface fracture energy due to freeze–thaw cycles, compared to the corresponding decrease in the ultimate nominal stress at debonding, was observed. A decrease in the length of the cohesive stress transfer zone and the maximum interface cohesive stress were also observed with freeze–thaw cycling. But the modulus of elasticity of FRP sheet determined from the maximum strain value at fully debonded zone of FRP-concrete bond, corresponding applied load value and cross sectional area of FRP sheet did not decrease due to freeze thaw exposure.

Ouyang & Wan (2008a)

An investigation on the effect of moisture on externally bonded CFRP-concrete bond deterioration was conducted by Ouyang & Wan (2008a). Modified double cantilever beams bonded with CFRP were used as mode I fracture specimens and deterioration of bond was characterised by interface fracture energy under mode I loading. All concrete specimens were cured under 100% moist environment for 28 days and stored in lab at 35% relative humidity for 10 months. After this period, no further weight change was observed. Control specimens were tested after 7 days of FRP application, whereas other specimens were exposed to full immersion in water for 2, 3, 4, 5, 6, 7 and 8 weeks and tested under mode I loading. A simple method was developed in this study to determine the Interface Region Relative Humidity (IRRH) just after the delamination of FRP from concrete. A relation between interfacial fracture energy and IRRH was obtained in this study. Moreover, a constitutive relation between residual thickness of concrete (RTC) on the detached CFRP plate and IRRH was determined by measuring the RTC. Figure 2.8 shows the relation between normalised RTC (in terms of the residual thickness of concrete of control specimens) and IRRH. Bond fracture energy was also determined numerically as a function of IRRH applying this relation and virtual crack closure technique (VCCT). The observation was that the deterioration of fracture energy was accelerated when the IRRH value was greater than 55% but when the IRRH was greater than 75%, the fracture energy started to become steady and did not show any significant change with the increases in IRRH.

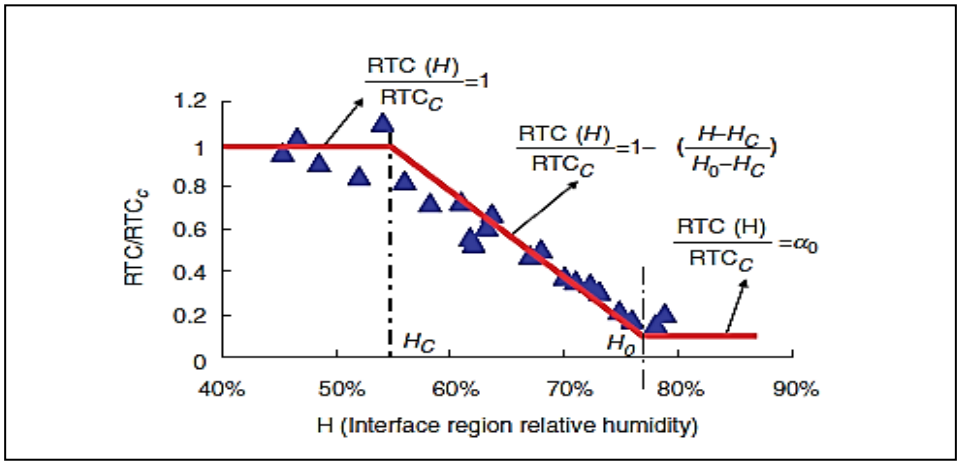

Figure 2.8 Relation between normalised RTC and IRRH (Ouyang & Wan 2008a)

Ouyang & Wan (2008b)

Ouyang & Wan (2008b) derived the moisture diffusion governing equation for the multi layered FRP-adhesive-concrete system by using relative humidity as a global variable in their study in order to model the movement and distribution of moisture in FRP strengthened concrete structure. Diffusion coefficient and the isotherm curve (correlation between environment relative humidity and moisture content at a given constant temperature) at constant 23^{o} C were experimentally determined for each of the constitutive material at different levels of environmental relative humidity. Also, finite element analysis was conducted to study the moisture diffusion in the FRP- adhesive-concrete system. Finally, interface region relative humidity (IRRH) values for different environmental relative humidity, obtained from numerical study, were compared with the values obtained by experimental method developed in a separate study by Ouyang & Wan (2008a). It was observed that error between experimental and numerical IRRH was less than 5% RH which confirmed the good agreement between experimental and numerical results.

Silva and Biscaia (2008)

Silva and Biscaia (2008) studied the effects of cycles of salt fog, temperature and moisture and immersion in salt water on the flexural behaviour of beams externally strengthened with GFRP or CFRP. Their main focus was to study the bond between FRP and concrete subjected to environmental conditions.

In this study, reinforced concrete specimens were fabricated and reinforced with GFRP or CFRP for four point bending test. The specimens consisted of two 100 mm wide prismatic concrete blocks connected through a stainless steel hinge device (Figure 2.9). Two layers of unidirectional GFRP or CFRP strips were bonded to the beam soffit. The effect of ageing was presented in terms of ultimate load-carrying capacity and average bond stress along the length of the bonded GFRP surface. Also, bond slip was modelled in this study and the fracture energy, G_f, was determined based on exponential laws for stress-slip. Moreover, environmental effects on the maximum load carrying capacity of GFRP strip is introduced by a factor, α_E, based on the experimental results. Apart from

the bending test specimens, pull-off tests were conducted on rectangular concrete slabs (600 x 200 x 100 mm).

For accelerated ageing of GFRP specimens, either total immersion in 5% salt water or temperature and salt fog cycles were used. Salt fog cycles were generated with the same salinity (50g/litre water) as used in the immersion tests. Temperature was around 35^{o} C and moisture level was defined by allowing16 hours to dry the specimens followed by 8 hours of fog. The temperature cycles applied in this study consisted of an environment at -10^{o} C for 12 hours followed by +10^{0} C for 12 hours. Specimens were tested after 1000, 5000 and 10,000 hours of exposure.

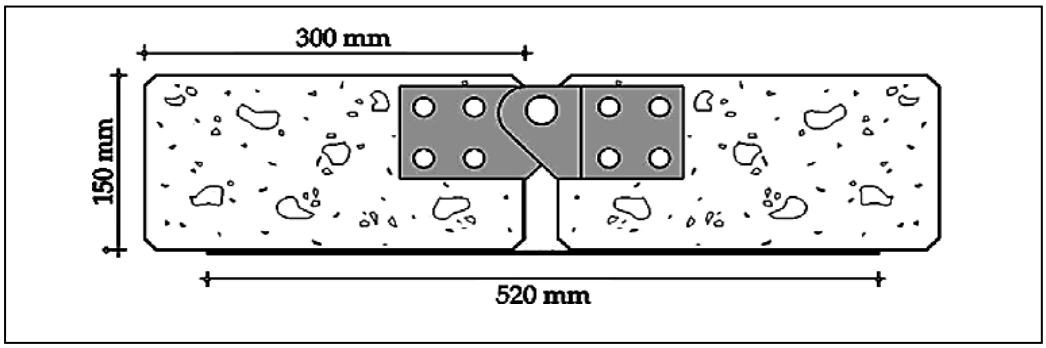

Figure 2.9 Specimen geometry for four point bending test by Silva and Biscaia (2008)

Based on the observations from bending tests and pull-off tests of GFRP specimens, the following conclusions were made:

The freeze-thaw temperature cycles showed the most detrimental effect with a degradation of ultimate load carrying capacity of beams by 31% after 10,000 hours, whereas a gain of 21% at 10,000 hours was observed for immersion tests due to the combined effects of gain in tensile strength of concrete and post-curing of the polymers. The salt fog cycles exhibited an initial increase of strength and after 10,000 hours the load capacity was only 3% below the reference specimens. In terms of failure modes, concrete substrate failure near the adhesive surface occurred for reference specimens and specimens subjected to temperature cycles, whereas failure in the interface between the adhesive and concrete was observed for salt fog cycles and immersion in salt water.

The pull-off tests showed reduction of average pull-out stress for immersion in salt water and salt fog cycles compared to the reference specimens.

Unlike the GFRP bonded specimens, CFRP bonded specimens were only subjected to moisture cycles. Moisture cycles were maintained with relative humidity of 20% for 12 hours followed by 90% for another 12 hours at a temperature of 40^{o} C. For salt fog cycles, same specifications were used as before except the exposure period of 5000 hours replaced by 6000 hours.

Based on the results of bending and pull-off tests of CFRP specimens, Silva and Biscaia (2008) concluded as follows:

Moisture cycles at fixed temperature and salt fog cycles caused approximately the same degradation of load carrying capacity for bending tests. Highest reduction of load carrying capacity was around 20%. The failure occurred in the concrete near surface substrate for both moisture cycles and control specimens, whereas failure was in concrete-adhesive interface for salt fog cycles. Pull-off tests exhibited increase in strength for salt fog cycles due to higher tensile strength of concrete attributed to wet curing by the artificial moisture environment at 35^{0} C.

Lai et al. (2009, 2010)

Lai et al. (2009, 2010) studied the effects of elevated water temperatures on interfacial delaminations of externally bonded CFRP-concrete beams by infrared thermography (IRT) and direct shear tests. The former study mainly focused on the quantification of the changes of delaminations within the adhesive bonding, changes in resistance to direct shear force and changes of failure mode distribution due to three elevated water temperatures: 25, 40 and 60^{o} C for the durations of 5, 15, 30 and 50 weeks. High water temperatures were found to be the single most significant factor for causing degradation of the adhesive layer due to the proximity of the elevated temperatures to the glass transition temperature of adhesive. Lai et al. (2010) used the same environmental conditions as Lai et al. (2009) but their main aim was to quantify the flaws and delaminations by quantitative infrared thermography (QIRT) and by visual image processing after opening-up the CFRP by direct shear.

Leone, Matthys & Aiello (2009)

Leone, Matthys & Aiello (2009) studied the effect of elevated service temperature on bond between externally bonded FRP reinforcement and concrete. They stated that the usual bonding material used for FRP application is a thermosetting polymer, e.g.; epoxy or polyester resin, which are sensitive to temperature increases. For temperatures higher than the glass transition temperature, T_g, the mechanical properties degrade and bonding material changes from a hard and glass-like material to a rubber-like material. In this study, the bond performance between three types of FRP reinforcement, namely, CFRP sheet (wet-layup), CFRP plate (factory made) and GFRP sheet (wet lay-up), and concrete were experimentally investigated by double face shear tests at 50, 65 and 80^o C temperatures. Three temperatures were chosen in this study in such a way that the temperatures represent -10%, +18% and + 45% of the glass transition temperature of the epoxy (55^o C). Test results at elevated temperatures were compared to those at room temperature (20^o C). Conclusions based on the experimental observations were as follows:

-Although the bond stress–slip curves with increasing service temperatures showed a similar qualitative shape as that of control specimens, a significant variation of some relevant parameters such as dropping of initial slope of the ascending branch of the curves, decrease in maximum bond stress with service temperature above glass transition temperature of the adhesive were observed. The reductions of maximum bond stress at 80^o C of 54% for CFRP sheet, 72% for GFRP sheet and 25% for CFRP laminate were observed.

-The type of failure changed with increasing test temperature. Specimens tested at 50^o C showed cohesion failure within the concrete, whereas at 80^o C, an adhesion failure at the interface was observed. At temperatures similar to or higher than the *Tg*, the adhesion strength of the adhesive drops below that of the concrete, causing the bond failure at the FRP reinforcement–adhesive interface.

-The strain values along the reinforcement significantly increased with temperature.

-The initial transfer length increased with the test temperature while the maximum force remained almost constant.

Dai et al. (2010)

Dai et al. (2010) investigated the effects of moisture on the initial and long-term bonding behaviour of fibre reinforced polymer (FRP) sheets to concrete interfaces by means of two types of tests (bending tests and pull-off bond tests). Effects of (1) moisture at the time of FRP installation (construction moisture), consisting of concrete substratum surface moisture and external air moisture; and (2) moisture which normally varies throughout the service life of concrete (service moisture), were studied.

The test variables included pre-conditioned concrete substrate moisture content (dry and wet) at the time of FRP bonding, air relative humidity (RH), 40 and 90%, during the FRP composite curing, adhesive primer type (normal and hydrophobic), bonding adhesive type (normal and ductile), and exposure durations (not exposed, 8 months, 14 months, and 2 years) to wet/dry cycle consisting of a four-day immersion in 60°C sea water and a three-day exposure to dry air exposure in a laboratory. A new type of CFRP sheet, carbon strand sheet (CSS) was used in this research.

Results of the tests showed that surface moisture at concrete substrates during the installation of FRP composites adversely influenced the bond performance of FRP-to-concrete interfaces. However, the effects were much less when a hydrophobic type of primer was used. Different air curing RH values up to 90% had a marginal effect on the bond performance of FRP-to-concrete interfaces. Bond failure always occurred at the primer to concrete interfaces in the specimens exposed to wet/dry cycles, whereas, in the unexposed specimens, bond failure occurred in a very thin mortar layer. The global interfacial shear bond strength (obtained from bending tests) either decreased or increased with the increase in the number of wet/dry cycles depending on the type of adhesive used, whereas, the local bond stiffness (obtained from pull-off tests) degraded monotonically with the increase of exposure duration.

Imani et al. (2010)

Imani et al. (2010) investigated the combined effects of temperature and water immersion using fracture mechanics approach based on Mode II single shear test on CFRP-concrete interface. They adopted this test method because debonding of

externally bonded FRP mainly occurs due to Mode II fracture. The simultaneous environmental conditions used in this study were: 1) immersion in de-ionised water varying from 0 to 15 weeks and 2) exposure to controlled temperature varying from 25^o to 60^o C. Also, a new method was proposed to determine the fracture energy release rate and cohesive law based on J-integral, by only measuring load and slip at the debonding end and it was verified by traditional strain-based method. The effect of environmental conditions was characterised by the fracture energy release rate. Test results showed that considerable degradation of interface integrity occurred due to increased temperature and moisture.

The final output of J-integral was defined as follows:

$$J = \frac{1}{2}\frac{P_f^2}{A_f^2} \times \frac{t_f}{E_f} \tag{2.31}$$

where J is the energy release rate (ERR) at the debonding tip, P_f is the applied load, A_f is the cross sectional area of FRP sheet, t_f is FRP sheet thickness and E_f is elastic modulus of FRP.

When P is the maximum load, J is replaced by fracture energy relase rate G_f and P is replaced by P_{max} in the above equation.

A traction separation law was proposed for samples immersed in 25^o C water for 13 weeks based on best fitting of experimental results as follows:

$$\tau = -1154.96 \times \left(e^{-157.96\delta} - 1\right) \times e^{-157.96\delta} \tag{2.32}$$

where τ is interface shear stress and δ is slip.

Silva & Biscaia (2010)

Silva & Biscaia (2010) described the effect of artificial ageing on the strength and bond between external GFRP reinforcement of RC beams and concrete based on extensive bending and pull-off tests. The artificial ageing was introduced by saline water immersion, salt fogging and cyclic tidal-like action. They also studied the effect of environmental conditions on the mechanical properties of concrete and GFRP

laminates. The tensile tests performed after GFRP tensile specimens were subjected to 10,000 hours of moisture cycles, consisting of 12 hours at 20% relative humidity followed by 12 hours at 90% relative humidity and keeping the temperature at 40^{o} C, showed 11% degradation of tensile strength compared to reference tensile specimens. On the other hand, the salt fog cycles caused more than 12% degradation of tensile strength at 10,000 hours. Dynamic Mechanical Thermal Analysis (DMTA) revealed that salt fog cycles reduced the glass transition temperature, T_g by 4^{o} C from its initial value of 66^{o} C and this supports the tensile strength degradation of GFRP. Moreover, a 2D and 3D finite element modelling was carried out to study the bond-slip and beam response considering the post-aged constitutive properties of components and non-linear material properties. Also, shear tests were designed to develop the Mohr-Coulomb envelope in this study to determine the interface cohesion c and friction angle Φ. These two parameters were required for interface finite element in the computer code library which was based on fracture mechanics and simulated the contact between GFRP and concrete. Figure 2.10 shows the tests set-up proposed in this study for determining the Mohr-Coulomb envelope.

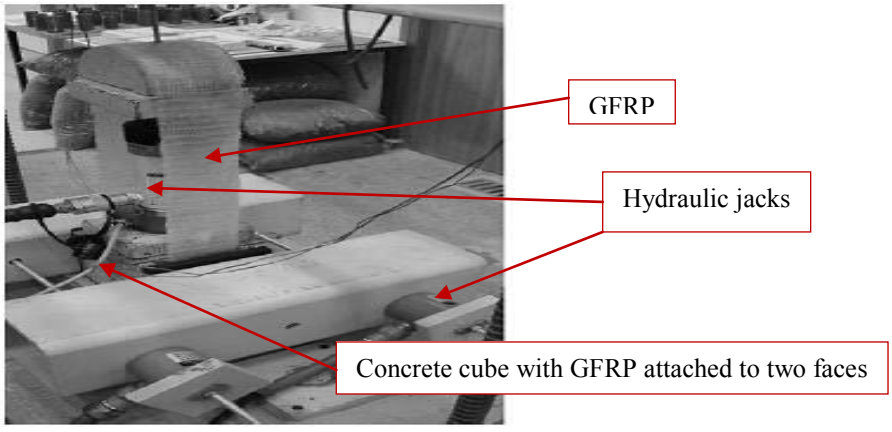

Figure 2.10 Shear tests for characterisation of Mohr-Coulomb Silva & Biscaia (2010)

Cromwell, Harries & Shahrooz (2011)

An extensive experimental investigation was conducted by Cromwell, Harries & Shahrooz (2011) to study the performance of FRP materials and FRP-concrete bond subjected to nine different environmental conditions, namely, water exposure, salt water

exposure, alkaline exposure, dry heat exposure, diesel fuel exposure, weathering exposure (UV radiation), freeze heat exposure and freeze thaw exposure. Three types of FRP, pre-formed CFRP plate, unidirectional CFRP fabric and unidirectional GFRP fabric, were investigated and the specimens were tested under four test methods - tension test, short beam shear test, bond to concrete test and beam flexure test. A summary of the test conditions applied is listed in Table 2.3. The test results of exposed specimens were compared with control specimens and revised environmental knock down factors were proposed.

Table 2.3 Environmental conditions applied by Cromwell, Harries & Shahrooz (2011)

Exposure	Duration	Description
Baseline		Laboratory condition (22^{o} C and 70% RH
Water ASTM D2247	1000, 3000 and 10,000 hours	100% RH at 38^{o} C
Salt water ASTM D1141	1000, 3000 and 10,000 hours	Immersion in salt water at 22^{o} C
Alkaline	1000, 3000 and 10,000 hours	Immersion in pH 9.5 $CaCO_3$ solution at 22^{o} C
Dry heat ASTM D3045	1000 and 3000 hours	60^{o} C
Diesel ASTM C581	4 hours	Immersion in diesel fuel at 22^{o} C
Weathering ASTM G23	1000 cycles (4000 hours)	2 hours of UV at 63^{o} C then 2 hours at 100% RH
Freeze heat	20 cycles (480 hours)	9 hours at -18^{o} C then 15 hours at 100% RH at 38^{o} C
Freeze thaw ASTM C666	360 cycles (1583 hours)	70 min at -18^{o} C then 70 min at 4.5^{o} C and UV

Yun and Wu (2011)

Yun and Wu (2011) studied the durability of FRP-concrete bond interface under freeze-thaw cycling using conventional single shear pull-out test. Variables considered in the study were exposure condition, concrete grade and number of freeze-thaw cycles. Figure 2.11 shows the dimensions of the specimens and test set-up. After the application of FRP, concrete blocks were exposed to an accelerated freeze-thaw cycling in an environmental chamber. After the environmental exposure, the specimens were pulled monotonically under a displacement control loading rate of around 0.005 mm/s up to failure.

The failure modes of all specimens were debonding but the thickness of the concrete peeled off from the specimens varied with the type of solutions, the number of freeze-thaw cycles and the type of concrete. The peak load was also reduced due to freeze-thaw cycles. After 67 freeze-thaw cycles, the specimens from 30 MPa concrete grade retained only 55% of their strength, whereas, specimens from 45 MPa concrete retained only 13% of their strength.

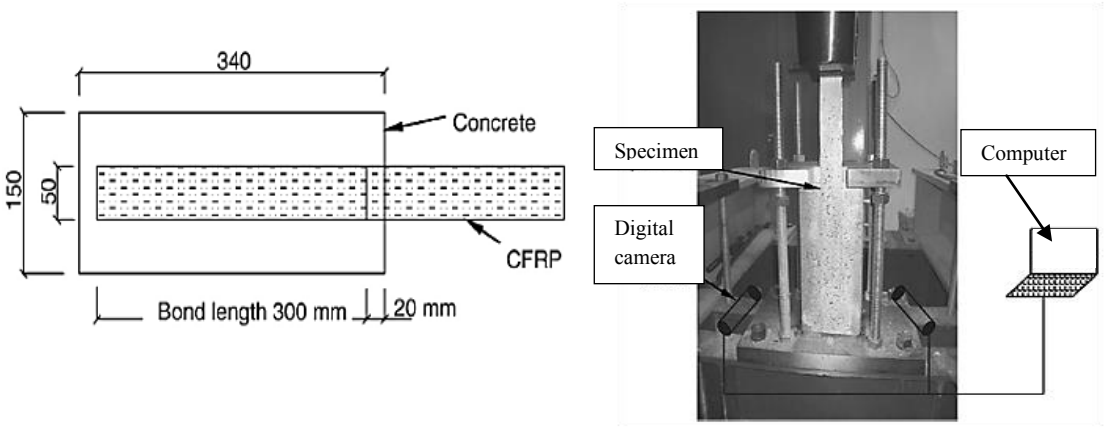

Figure 2.11 (a) Specimen dimensions and **(b)** test set-up Yun and Wu (2011)

In terms of the effects of different types of solutions on the bond strength, the rates of bond strength degradation under two different solutions were almost the same for 30 MPa concrete specimens (W/C ratio above 0.5). However, for the 45 MPa concrete

specimens (W/C ratio below 0.4), bond strength deterioration was much faster in salt water than that in tap water after 33 cycles of freezing and thawing. Similar trend was seen for the effect of two types of solutions on the decreasing rates of maximum slip of 30 MPa concrete specimens. For 45 MPa concrete, the maximum slip under the salt water appeared to be linearly decreasing. However, the decreasing rate of the maximum slip under the tap water was faster under lower cycle numbers, and reduced after 33 cycles. Also, it was noticed that the effective bond length increased with the increase in freeze-thaw cycles; which implies that a long bond length is required for FRP-concrete joint under freeze-thaw cycles.

Benzarti et al. (2011)

Benzarti et al. (2011) used two sets of tests to investigate the long-term performance of FRP-concrete bond exposed to constant hydrothermal ageing condition (40^{o} C temperature and 95% relative humidity).

In the first set, Benzarti et al. (2011) studied hydrothermal ageing (ageing period of 20 months) of concrete slabs strengthened with two types of FRP, carbon fibre sheet (CFS) and pultruded unidirectional carbon fibre plates (CFRP), with the help of pull-off tests. All strengthened slabs were exposed to saturated humidity in a climatic chamber (relative humidity of at least 95%) at 40^{o}C temperature. After exposure to hydrothermal ageing, pull-off tests were conducted. For the composite strengthened specimens with non-carbonated concrete surface, hydrothermal ageing caused progressive and significant decrease in the pull-off strengths of bonded interfaces for both types of FRP. Moreover, the failure mode changed from substrate failure towards a mixed or interfacial failure. The surface preparation had a slight effect on the strength level of the bonded surface.

In the second set, pull-off and single-lap-joint shear tests were used to study the accelerated ageing (for a period of 13 months) behaviour of both the FRP strengthened concrete blocks and the constitutive materials (concrete, epoxy adhesive and composite element) separately. The specimens were exposed to the same accelerated ageing conditions as in the previous set of tests (40^{o} C and RH higher than 95%). Finally, pull-off and single-lap-joint shear tests were performed. From the test results, it was found

that epoxy adhesives used for the bonding exhibited a decrease in mechanical strength during humid ageing, as well as pronounced elasto-plastic behaviour. For the FRP strengthened concrete blocks, shear loading tests revealed an evolution of the failure mode, from a substrate failure towards a cohesive failure within the polymer joint in the case of CFRP strengthened specimens, and even towards interfacial failure in the case of CFS reinforced blocks. In spite of the changes in the failure modes, no change in the maximum shear loads were observed during ageing regardless of the type of specimen. Pull-off characterisations were not always consistent with those of the shear experiments and it was concluded that the latter method has a higher sensitivity and should be used for adhesive bonded joints.

Tuakta & Büyüköztürk (2011a)

According to Tuakta & Büyüköztürk (2011a), long-term performance and durability issues regarding debonding behaviour in Fibre reinforced polymer (FRP) retrofit systems for concrete structures still remain largely uncertain and unanswered. They also stated that the effectiveness of the strengthening system depends significantly on the properties of the interface between the three constituent materials, namely concrete, epoxy, and FRP. In this study, effects of moisture on concrete/epoxy/FRP bond system was characterised by means of the tri-layer fracture toughness obtained experimentally from peel and shear fracture tests. The details of the environmental conditions and specimens will be discussed in the summary of another study by Tuakta and Büyüköztürk (2011b). The results of the experimental study exhibited an irreversible weakening of bond strength in fracture specimens under moisture cyclic condition. Also, interface moisture content was predicted numerically in this study and finally fracture toughness was related to the ratio of transient and threshold interface moisture content. Threshold moisture content (C_{th}) was defined as the moisture content beyond which no additional degradation was observed. Finally, based on the experimental results of fracture specimens under variable moisture conditions, an empirical model was developed to predict service life of FRP-strengthening system.

Tuakta and Büyüköztürk (2011b)

Tuakta and Büyüköztürk (2011b) investigated the degradation of FRP-concrete bond system under moisture with the help of fracture mechanics. In this study, the degradation of bond strength of FRP/concrete interface was quantified by tri-layer (FRP, epoxy and concrete) fracture toughness. In order to investigate the effect of continuous moisture ingress and its reversibility, both quantitatively and qualitatively, peel and shear fracture tests were performed. Peel and shear fracture specimens are shown schematically in Figure 2.12. Specimens were exposed to moist environment at 23^{o} C in a water tank and at 50^{o} C in an environmental chamber for 2, 4, 6 and 12 weeks. Also material characterisations of concrete, epoxy and CFRP under moisture were accomplished. After the required exposure durations, peel and shear fracture specimens were tested as shown in Figure 2.13.

Test results showed that prolonged exposure to moist condition can cause significant degradation of the CFRP-concrete bond strength (fracture toughness). Degradation can be as much as 70% for specimens conditioned for 8 weeks. After a certain period of time, the bond strength approaches equilibrium and no further significant loss of strength may occur thereafter. Moreover, moisture reversal and cyclic moisture conditioning tests revealed that the adhesive bond cannot regain its original bond strength after successive wet-dry cycles. The residual bond strength decreased with the increase in the number of wet/dry cycles and in the intermediate conditioning duration. Also, the failure mode changed in the specimens exposed to moisture with the weakening of the interface between concrete and the epoxy.

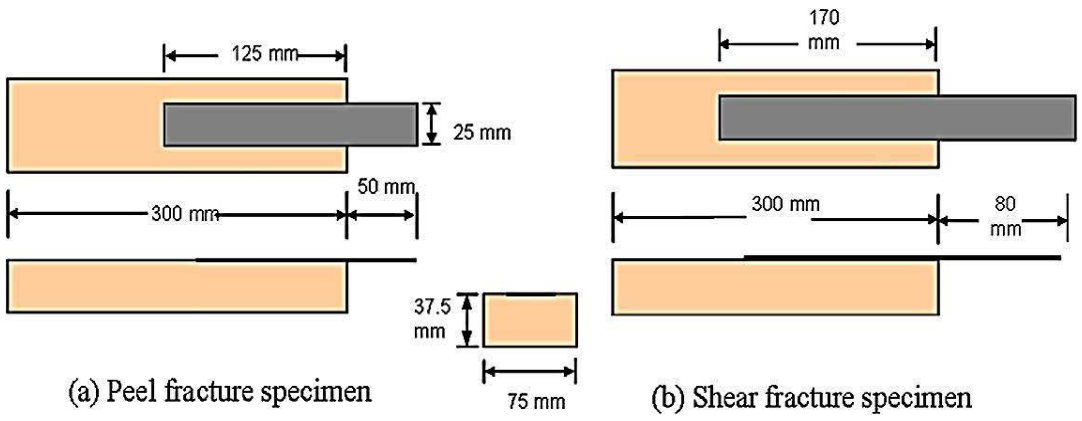

Figure 2.12 (a) Peel and **(b)** shear fracture specimens (Tuakta & Büyüköztürk 2011b)

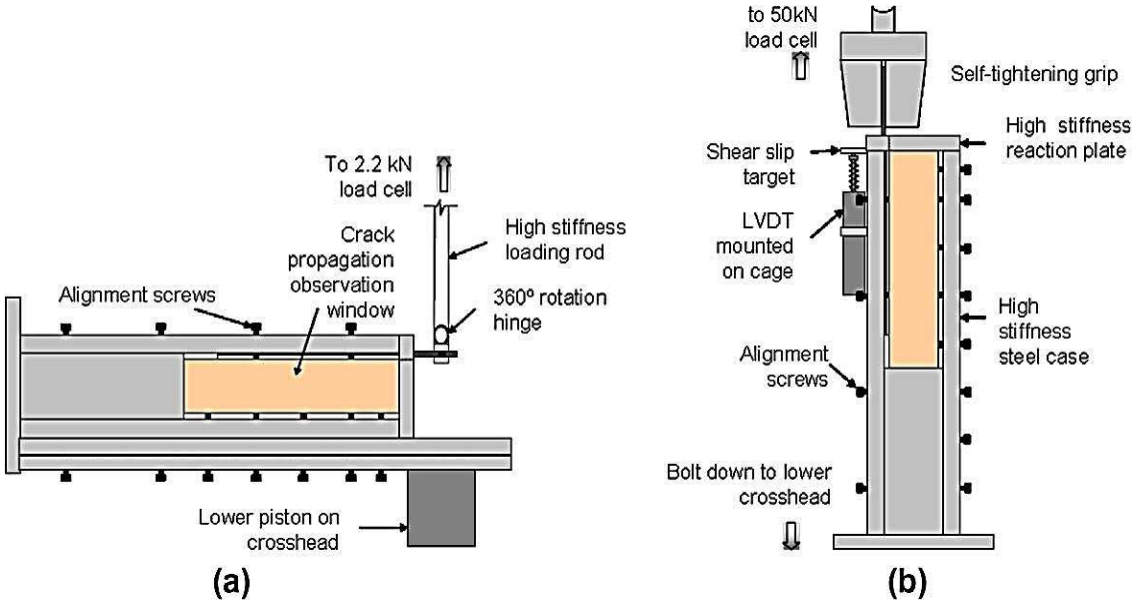

Figure 2.13 (a) Peel and **(b)** shear test set-ups (Tuakta & Büyüköztürk 2011b)

In addition to the above mentioned research found in literatures, few studies were devoted to the environmental effects on the FRP-concrete bond under sustained loads. Ulaga & Meier (2001) and Haber, Mackie & Zhao (2012) experimentally investigated the effects of environmental conditions on concrete beams strengthened with CFRP under sustained loads, whereas Gamage, Al-Mahaidi & Wong (2010) performed both experiments and finite element modelling on the combined effects of cyclic temperature, humidity and mechanical stress on CFRP-concrete interface.

2.7 Repairing of RC beams with FRP

Extensive research have been carried out on flexural and shear strengthening or retrofitting of reinforced concrete (RC) beams with FRP, both experimentally and analytically. Some of the researchers also provided design guidelines for flexural and shear strengthening. A summary of some previous research have been discussed in this section. The previous research on the shear strengthening is out of the scope of this study. So, a summary of some of the previous research on flexural strengthening of reinforced concrete beams has been provided in this section.

Saadatmanesh and Ehsani (1991) experimentally investigated the static strength of reinforced concrete beams strengthened with glass-fibre-reinforced-plastic (GFRP) plates. Five rectangular beams and one T-beam strengthened with GFRP plates bonded to the tension flanges, with three different steel reinforcement ratios, were used to investigate the effect of steel reinforcement on the strengthening. The beams were tested under four-point bending. The test results indicated that significant increases in the flexural strength could be achieved by bonding GFRP plates to the tension face of reinforced concrete beams. Application of FRP also resulted in reduction of crack size in the beam but also caused reduction in ductility of the strengthened beams. Strength gain was more profound in beams with lower steel reinforcement ratios.

An, Saadatmanesh & Ehsani (1991) provided an analytical model based on the compatibility of deformations and equilibrium of forces to predict the stresses and deformations in concrete beams strengthened with FRP plates bonded to the tension face of the beams. Beams with both rectangular and T cross sections were considered in their model. The assumptions behind their analysis were as follows:

- Linear strain distribution through the full depth of the beam
- Small deformations
- No tensile strength in concrete
- No shear deformations
- No slip between composite plate and concrete beam

In regard to the stress-strain relationships of the materials, steel rebar was assumed to be elastic-ideally plastic, glass-fibre was assumed to have linear elastic behaviour and Hognestad's parabola of idealised stress-strain curve for concrete in uni-axial compression (Park & Paulay 1975) was considered (Figure 2.14). An incremental deformation technique was used to calculate strains, stresses and curvature at mid-span in FRP plate, steel re-bar and concrete.

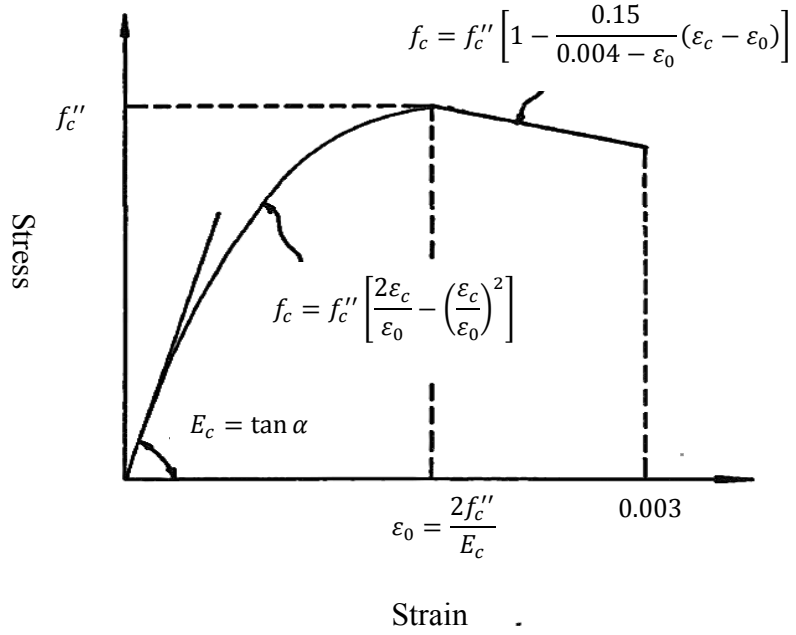

Figure 2.14 Idealised stress-strain curve for concrete in uni-axial compression (An, Saadatmanesh & Ehsani 1991)

Also, a parametric study was conducted to investigate the effects of plate area, plate stiffness and strength, concrete compressive strength and steel reinforcement ratio on the strengthening.

Chajes et al. (1994) applied three different types of FRP (aramid, E-glass and graphite) to the tension face of fourteen under-reinforced rectangular concrete beams for flexural strengthening. The beams were loaded monotonically to failure in four-point bending. The increases in flexural capacities for aramid, E-glass and graphite FRP were 53.2, 45.6 and 45.0 %, respectively. The beams also showed approximately 40% increase in flexural stiffness. Chajes et al. (1994) also presented an analytical model based on the stress-strain relationships of the concrete, steel and composite fabrics.

Picard, Massicotte & Boucher (1995) provided a theoretical model to study the effects of various parameters on the flexural behaviour of strengthened beams with FRP plates. In their model, the stress-strain curve for concrete in uni-axial compression was similar

to An et al. (1991) but an equivalent uniformly stressed compression zone was assumed to compute ultimate moment M_u by relating the depth of equivalent zone to the actual depth of the compression zone by a parameter β_1 (Figure 2.15).

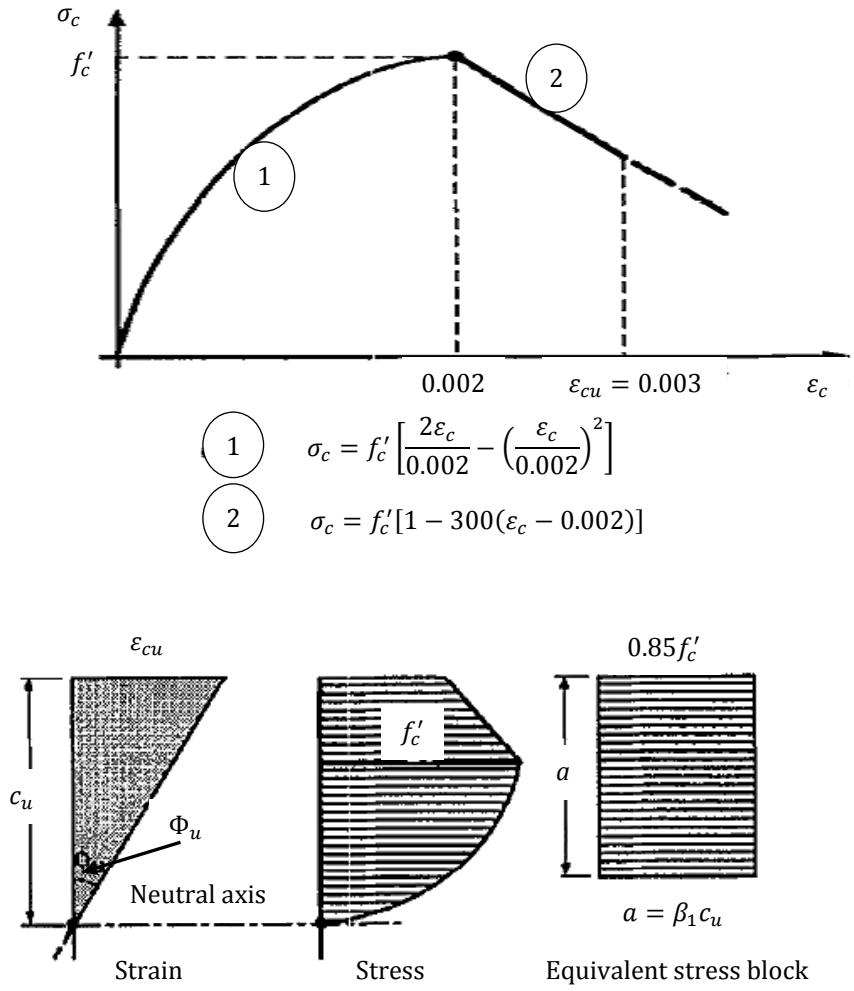

Figure 2.15 Stress-strain diagram for concrete and stress block assumption (Picard, Massicotte & Boucher 1995)

Also, based on a parametric study to investigate the effects of design parameters such as modulus of elasticity of the composite material, the thickness of the strengthening plate

and the compressive strength of concrete; the most significant factor was found to be the compressive strength of concrete.

Arduini and Nanni (1997) investigated the behaviour of pre-cracked RC beams strengthened with carbon FRP (CFRP) sheets. They fabricated 18 RC beams among which 10 were pre-cracked by applying loads of 30% of the nominal capacity of the member.

Two beams were control (without FRP) and the remaining beams were strengthened with unidirectional CFRP sheets bonded at the soffit of the beams except for one beam in which CFRP were applied on the sides (one ply 0^o and 90^o) as well as at the soffit (two plies 0^o). Specimens were tested under four-point bending. From the results it was concluded that the strengthening technique with externally bonded CFRP sheets can result in significant increases in ultimate load capacity and, to a lesser extent, in flexural stiffness. Moreover, the performance of a strengthened pre-cracked beam is not significantly different from that of a strengthened virgin beam. Also, carbon fibre stiffness, fibre direction and number of plies have an important effect on the performance of strengthened beams. Wrapping a sheet at 90^o is very effective for the anchorage of the 0^o plies.

Norris, Saadatmanesh & Ehsani (1997) fabricated nineteen concrete beams. Each beam had a 127 mm × 203 mm cross section. Thirteen of the beams (flexural test specimens) were over-reinforced for shear by closely spacing the stirrups. The remaining six specimens (shear test specimens) were fabricated with stirrups spaced at a distance more than the effective depth *d* so that shear cracks can develop easily. Among these nineteen beams, there were two control (not retrofitted) beams (one for flexure and one for shear). All beams were pre-cracked except for three (two for flexure and one for shear). Beams were retrofitted with three types of fibre/epoxy systems and six types of FRP orientations and tested under four-point bending loads. Test results showed that CFRP sheet increased strength and stiffness and the magnitude of the increase and the mode of failure were related to the direction of fibres. Both for flexural and shear cracks, CFRP fibres placed perpendicular to the cracks showed a large increase in strength and

stiffness but caused brittle failure due to concrete crushing as a result of stress concentration near the ends of the CFRP. On the other hand, when fibre directions were oblique to the crack, smaller increase in strength and stiffness were observed but the nature of failure was more ductile.

Saadatmanesh and Malek (1998) provided design guidelines for flexural strengthening of RC beams with FRP plates considering different failure modes of strengthening. Also, they included multi-step loadings (before and after upgrading) in their design guidelines. The effect of initial stress before strengthening is considered in their design guidelines. The top fibre strain of the concrete beam due to a service moment, M_o (without any load), before upgrading was expressed as:

$$\varepsilon_{c0} = \frac{M_0 c_0}{E_c I_{tro}} \tag{2.33}$$

where c_o = depth of neutral axis; I_{tro} = moment of inertia of the transformed cracked section based on concrete; and E_c = modulus of elasticity of concrete.

The initial tensile strain at the bottom face of the concrete, ε_{fo} can be calculated considering the linear variation of strains along the section of the beam as:

$$\varepsilon_{f0} = \varepsilon_{c0}\left(\frac{h - c_0}{c_0}\right) \tag{2.34}$$

Finally, the strain on the FRP plate is obtained by subtracting the initial tensile strain of concrete from the total strain on the FRP computed from linear variation of the strains in cross section and further used to calculate the stress in FRP plate, f_f, as follows:

$$f_f = E_f\left(\varepsilon_f - \varepsilon_{f0}\right) \tag{2.35}$$

where E_f = modulus of elasticity of FRP plate and ε_f = axial strain at the level of the FRP plate based on linear variation of strains along the section.

Rasheed and Pervaiz (2003) provided closed form equations for the design of FRP flexural strengthening. They used a direct approach for the computation of the depth of compressive stress block. Also, Rasheed and Pervaiz (2003) proposed equations for the

design of doubly strengthened section for the first time. Design guidelines were also provided by other researchers (Chaallal, Nollet & Perraton 1998; El-Mihilmy & Tedesco 2000).

Al-Amery & Al-Mahaidi (2006) studied the effect of coupled flexural-shear strengthening of RC beams by experimental investigation. They reported that the use of FRP straps for shear strengthening also delays the debonding of external FRP used for flexure.

Benjeddou, Ouezdou & Bedday (2007) conducted experimental studies on damaged reinforced concrete beams repaired by external bonding of CFRP composite laminates to the tensile face of the beam. Two sets of beams: a) control (without CFRP) and b) repaired damaged beams; were tested under four-point bending in this study. Parameters investigated included amount of CFRP, damage degrees, CFRP laminate widths and concrete strength classes. The load carrying capacity and the rigidity of the repaired beams of all degree of damages were found to be significantly higher than those of control beams.

Based on the results of extensive research, ACI 440.2R (2008) provided design guidelines for strengthening of concrete beams. According to the guidelines, bonding of FRP reinforcement to the tension face of a concrete flexural member (e.g. soffit of the beam as shown in Figure 2.16 with fibres oriented along the length of the member is capable of increasing the flexural strength ranging from 10 to 160%. However, increases of 5 to 40% are more reasonable considering the ductility and serviceability limits. In order to prevent debonding at the ends of the soffit plates, mechanical anchors in the forms of FRP U-strips or prefabricated steel can be installed (Teng 2002).

Shear strengthening of reinforced concrete beam can be done by wrapping or partially wrapping the member with FRP. Orienting the fibres transverse to the axis of the member or perpendicular to potential shear cracks is effective in providing additional shear strength (ACI 440.2R 2008). There are three types of FRP wrapping schemes used

to increase the shear strength: Completely wrapping the FRP system around the section, wrapping the FRP system around three sides of the member (U-wrap) or bonding to the two sides of the member (Figure 2.17). Among these three schemes, completely wrapping the section is the most efficient, followed by the three-sided U-wrap. Bonding to two sides of a beam is the least efficient scheme.

Mahini & Ronagh (2010) studied the effectiveness of FRP sheets bonded to the web of RC beams for the relocation of plastic hinge away from the RC beam-column joint to toward the beam. This technique was used to repair moderately damaged RC joints and found to be effective in restoring the strength of the joints. In addition, they proposed an analytical model based on equilibrium and compatibility to simplify the design and analysis of such scheme.

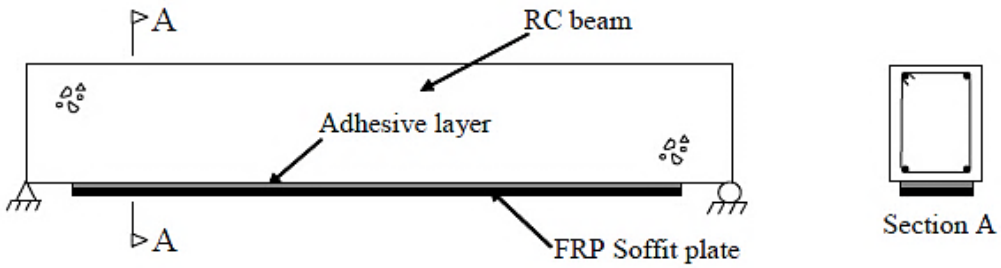

Figure 2.16 Flexural strengthening of RC beams (Teng 2002)

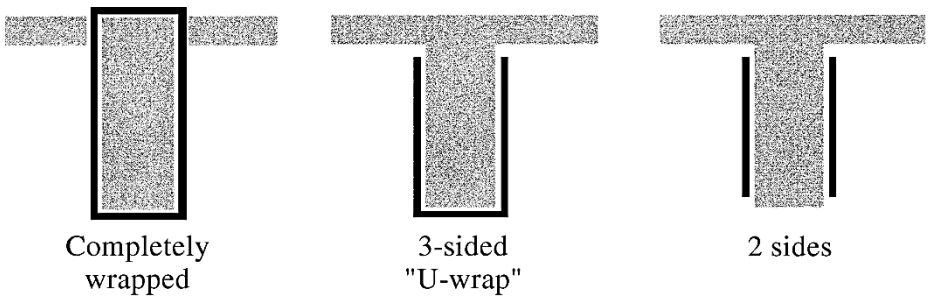

Figure 2.17 Typical wrapping schemes for shear strengthening of beams (ACI 440.2R 2008)

Dong, Wang & Guan (2013) conducted experimental study on the strengthening of RC beams witch CFRP and GFRP. They used external flexural and flexural-shear strengthening scheme and concluded that the latter scheme is much more effective in improving stiffness, strength and hardening behaviour of RC beam.

El-Sayed (2014) studied the effect of flexural shear strengthening scheme on the shear resistance of RC beams by fabricating the RC beams without stirrups (shear reinforcement) and strengthening the beams with CFRP longitudinal reinforcement. As a result of strengthening scheme, shear strength increased up to 35% compared to unstrengthened beams.

2.8 Critical review

Based on the literatures on the bond between FRP and concrete, it has been observed that several research have been conducted to determine the effect of parameters such as specimen geometry, width of FRP, bond length, concrete surface preparation, concrete strength, adhesive and FRP stiffness on the behaviour of bond between FRP and concrete. Also, several constitutive laws have been developed to model the interface between FRP and concrete based on different approaches. Among all of the proposed models to date, the bond failure load predicted by Chen & Teng (2001) best fits the experimental results and has been recommended to be used for design purpose due to its simplicity by Lu et al. (2005).

From the summary of the literatures described in section 2.6, it is clear that durability of FRP-concrete bond, especially the long term durability, is still an area of limited information and it is very difficult to compare the findings of these research studies due to a variety of test conditions applied. Test set-ups used in these studies were four-point bending of FRP bonded beams, single shear (has been referred to as pull-out tests in this dissertation) and double shear tests of FRP bonded concrete prisms, single contoured cantilever and modified double cantilever beam tests under mode I loading, pull-off tests and peel-off tests. According to Benzarti et al. (2011), single-lap-joint shear test is more sensitive to environmental conditions and should be used for adhesive bonded joint. Also, Imani et al. (2010) adopted this test method because debonding of externally

bonded FRP mainly occurs due to Mode II fracture. Therefore, more research should be carried out with similar test set-up to get more information about the long term performance of FRP-concrete bond under various environmental conditions. The environmental conditions applied for the previous research were mainly freeze-thaw cycles, constant immersion in alkaline water, salt fog cycles and immersion in salt water, wet-dry cycles at various temperatures, exposure to high temperatures, cyclic temperature, combined environmental cycles and UV radiation. But the test data related to real outdoor environmental ageing has not been observed in the review of literatures included in this chapter. Also, very few research works were found to be carried out for long term behaviour of FRP-concrete bond. A number of long term prediction models were developed based on short term accelerated ageing mainly for FRP itself and FRP in concrete environment. But the assumption behind those models that using high temperature to accelerate the degradation only increases the rate of degradation but the degradation mechanism remains the same is still a subject for debate.

The research on the strengthening of reinforced beams with external FRP reinforcements were found to be extensive but only a limited number of literatures have been included in section 2.7. Based on the studies included in this chapter, it is evident that strengthening schemes with FRP is already well established and design guidelines have been provided for strengthening of concrete beams by ACI 440.2R (2008). However, the equations for prediction of load carrying capacity of severely damaged repaired beams, especially, considering the strain hardening after yielding are not proposed in the design guidelines available in literatures. Therefore, experimental and analytical research on the performance of FRP in repairing of severely damaged reinforced concrete beams and proposing equations for the repair of damaged beams can be a valuable contribution.

2.9 Conclusions

The aim of this chapter was to cite the previous research available in literatures on the strengthening of reinforced concrete structures with fibre reinforced polymer (FRP) composites. Findings of the various investigations conducted on the behaviour of FRP-concrete bond and its durability were highlighted mainly in this chapter; nonetheless, different aspects of well-established FRP-strengthening schemes and design guidelines

were also discussed briefly. Also, a critical review was made to find out the gaps mainly in the field of durability of FRP-concrete bond and repairing or strengthening of damaged reinforced concrete beams. The gaps identified are summarised as follows:

-The variety of test methods and test conditions applied makes it difficult to compare the findings of various studies. Due to the sensitivity of the mode II debonding to environmental conditions as suggested by Benzarti et al. (2011) and Imani et al. (2010), more experimental studies with various exposure conditions should be carried out with single shear tests.

- The test data on the effect of natural ageing on the FRP-concrete bond is missing in the database which implies the necessity of more investigation for real outdoor exposure.

-Existing long-term prediction models for FRP and FRP in concrete environment bond mainly involves the accelerated ageing by elevated temperatures but using high temperature for acceleration is still a subject for debate.

-In regards to repairing damaged reinforced concrete beams, no design guidelines is proposed considering the effect of residual strength of steel.

CHAPTER 3

EXPERIMENTAL PROGRAM

3 Experimental program

3.1 Introduction

This chapter provides the details of experimental procedures and set-ups used in the study of long term performance of FRP-concrete bond. Also, determination of material properties of CFRP, GFRP and concrete has been described. In sections 3.6 and 3.7, results of the material properties, namely, CFRP tensile properties and concrete compressive properties, for control (unexposed) and exposed conditions are discussed. In addition, the pull-out test results of control CFRP and GFRP-concrete bond are presented in section 3.8. Finally, the findings of the material properties for control and exposed conditions and those of the pull-out tests for control specimens are summarised in section 3.9.

3.2 Overview of experiments

Long term performance of FRP-concrete bond was studied by comprehensive experimental investigations. Single-lap-joint shear test (also referred to as pull-out test) was used to determine the strength of FRP-concrete bond of specimens exposed to three different environmental conditions (temperature cycles, wet-dry cycles and outdoor environment) for duration up to 18 months. In addition to the FRP-concrete bond specimens, FRP coupons and concrete cylinders were also exposed to the same environmental conditions and the material properties of FRP and concrete were identified on the day of each pull-out test. The details of the pull-out tests and material characterisations of FRP and concrete are presented in this chapter.

3.3 Pull-out test of FRP-concrete bond specimens

Long term performance of FRP-concrete bond was studied by single-lap-joint-shear test which is referred to as pull-out test in all chapters of this thesis. As the purpose of this study was to determine the effect of environmental conditions on the bond between FRP

and concrete, pull-out test was chosen for experimental investigation and the maximum load obtained from this test corresponds to the strength of the FRP-concrete bond. The most significant reason for choosing the pull-out test was to simulate the intermediate flexural crack-induced debonding which is an important failure mode (Teng 2002) of RC beams strengthened with FRP for flexure. Although this failure mode is due to both shear and normal stress, direct shear test was chosen because of shear stress being the dominant stress. This test set-up was also recommended by Benzarti et al. (2011) due to the sensitivity of this set-up to environmental conditions. The following subsections will describe geometry and fabrication of pull-out specimens, material properties of the constituent materials, environmental conditions applied in the test, pull-out test set-up and instrumentation and finally, test procedure involved in this study.

3.3.1 Geometry of pull-out specimens

Each of the pull-out specimens consisted of a concrete prism with dimensions of 300 mm × 200 mm × 150 mm and two layers of 40 mm wide FRP strip bonded on the top of concrete prism. The total length of FRP was 400 mm, of which, only 150 mm was bonded to concrete (Figure 3.1). The bond length of 150 mm for all the specimens (control and exposed) was chosen in a way that it satisfies the effective bond length (97.4mm) determined from Chen & Teng (2001) model. A gap of 50 mm was provided between the loaded edge of adhesive bonded joint and concrete edge to prevent the wedge failure in concrete. The FRP strip was extended to 200 mm beyond the concrete prism. This overhanging part was provided to be gripped by the jaws of testing machine in order to exert tensile stress on the bonded FRP.

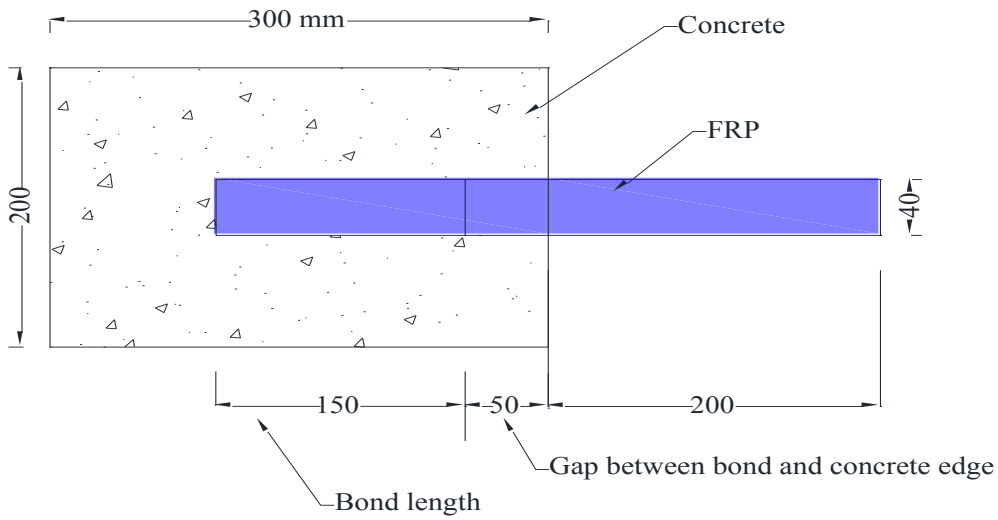

(a)

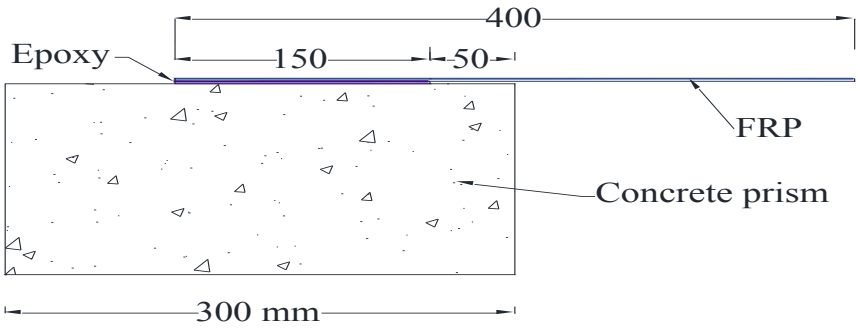

(b)

Figure 3.1 (a) Plan and **(b)** elevation of pull-out specimen

3.3.2 Fabrication of pull-out specimens and material properties

Fabrication of pull-out specimens have been accomplished in several phases. Plywood moulds were used to cast concrete prisms. Two batches of ready mix concrete of target compressive strength: 32 MPa, slump: 80 ± 20 mm and maximum aggregate size: 10 mm were used to fabricate concrete prisms and concrete cylinders. The reason behind using 10 mm coarse aggregate in this study was to accommodate sufficient amount of aggregates in small concrete prisms. Concrete prisms and cylinders were used for fabrication of pull-out specimens and determination of concrete material properties of each set of pull-out test, respectively. All of the concrete specimens (prisms and cylinders) were subjected to moist curing by sprinkling of water and covering the

specimens with plastic sheets for seven days. The demoulding of concrete specimens was carried out on the eighth day and demoulded specimens were subjected to air curing for three weeks. On the 28th days, concrete compressive strength and modulus of elasticity (MOE) were determined by testing a number of cylinders as per AS 1012.9 (1999) and AS 1012.17 (1997), respectively. Table 3.1 provides material properties of two batches of concrete.

Table 3.1 Material properties of two batches of concrete

Concrete Batch	Target compressive strength (MPa)	Measured 28 day cylinder compressive strength (MPa)	Maximum aggregate size (mm)
1	32	36.6	10
2	32	42.0	10

The second phase of fabrication of pull out specimens was surface preparation of the concrete prisms. The surface preparation involved exposing the aggregate layer of the area to be bonded with FRP by the removal of the weakest mortar layer from the top surface. This process was carried out with the help of a needle-gun which works with compressed air pressure (Figure 3.2 (a)). Finally, dust particles were blown off with the help of an air blow-gun (Figure 3.2 (b)).

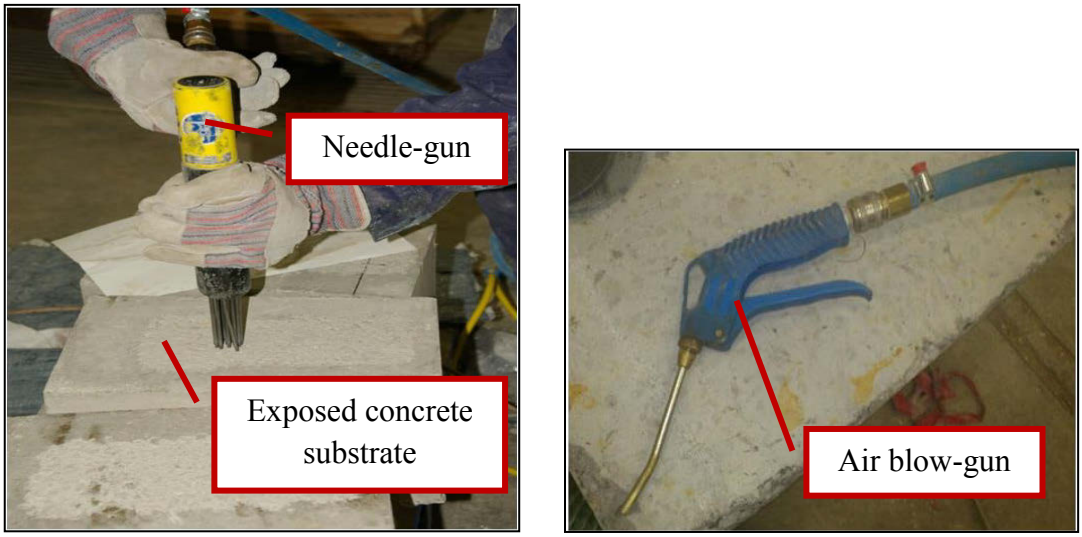

(a) (b)

Figure 3.2 (a) Concrete substrate preparation and **(b)** air blow-gun

The final phase was bonding FRP to exposed concrete substrate by wet lay-up method. Two types of FRP, namely, Carbon (MBRACE CF 120) and Glass (MBRACE EG 90/10A), were chosen for this experimental study. Material properties of the two FRP types are documented in Table 3.2 and Figure 3.3 shows the photos of FRPs used in this study. Sikadur 330, which is a two part epoxy impregnation resin, was used as both matrix for fibres and adhesive for bonding of fibre sheets to concrete. Table 3.3 shows the material properties based on the information in the technical data sheet provided by Sika Australia Pty Ltd (Figure A.26). FRP strips with the dimensions of 400 mm × 40 mm were cut down from the roll of fibre sheets. Two layers of FRP were used for each of the pull-out specimen fabrication. The area of the concrete surface on which FRP was to be bonded was marked and the remaining part was wrapped with masking tape to ensure the bonding of FRP only to the required area. An additional concrete prism wrapped with plastic sheet was used to support the overhanging part of FRP from two specimens placed in a row as shown in Figure 3.4 (a). Epoxy part A and B (4:1 ratio) was mixed in a small bowl for around 2-3 minutes with a stirrer. As "Sikadur 330" acts both as primer and adhesive, no additional primer was applied in this fabrication process. Mixed epoxy was applied on the concrete substrate with a paint brush (Figure 3.4 (a)) and the first layer of FRP strip was bonded to concrete (Figure 3.4 (b)). A plastic roller was used to apply pressure to ensure that epoxy was properly impregnated

into the fibres as shown in Figure 3.4 (c). The same process was repeated for the application of second layer of FRP strip. Fabricated specimens were kept under lab condition (approximately at 23^{o} C) for curing for one week (Figure 3.4 (d)) following which the support blocks were removed carefully without exerting stress on the bonded part.

Table 3.2 Material properties of FRP

FRP Type	Brand Name	Ply Thickness (mm)	*Measured Tensile Strength (MPa)	*Measured Tensile MOE (GPa)
Carbon	MBRACE CF 120	0.117	2886.6	226.2
Glass	MBRACE EG 90/10A	0.154	1657.0	139.3

* Determined by tensile testing of FRP coupons according to ASTM D3039/D3039M (2008)

(a) (b)

Figure 3.3 (a) Carbon fibre and **(b)** glass fibre sheets

Table 3.3 Material properties of epoxy resin

Type of epoxy resin	Tensile strength after 7 days of curing at + 23 ^{o} C (MPa)	Tensile MOE after 7 days of curing at + 23 ^{o} C (GPa)	Coefficient of thermal expansion between - 10^{o} C to + 40 ^{o} C (/^{o}C)	Heat distortion/ glass transition temperature, T_g, after 7 days of curing at + 23 ^{o} C (^{o}C)
Sikadur 330	30	4.5	4.5×10^{-5}	+ 47

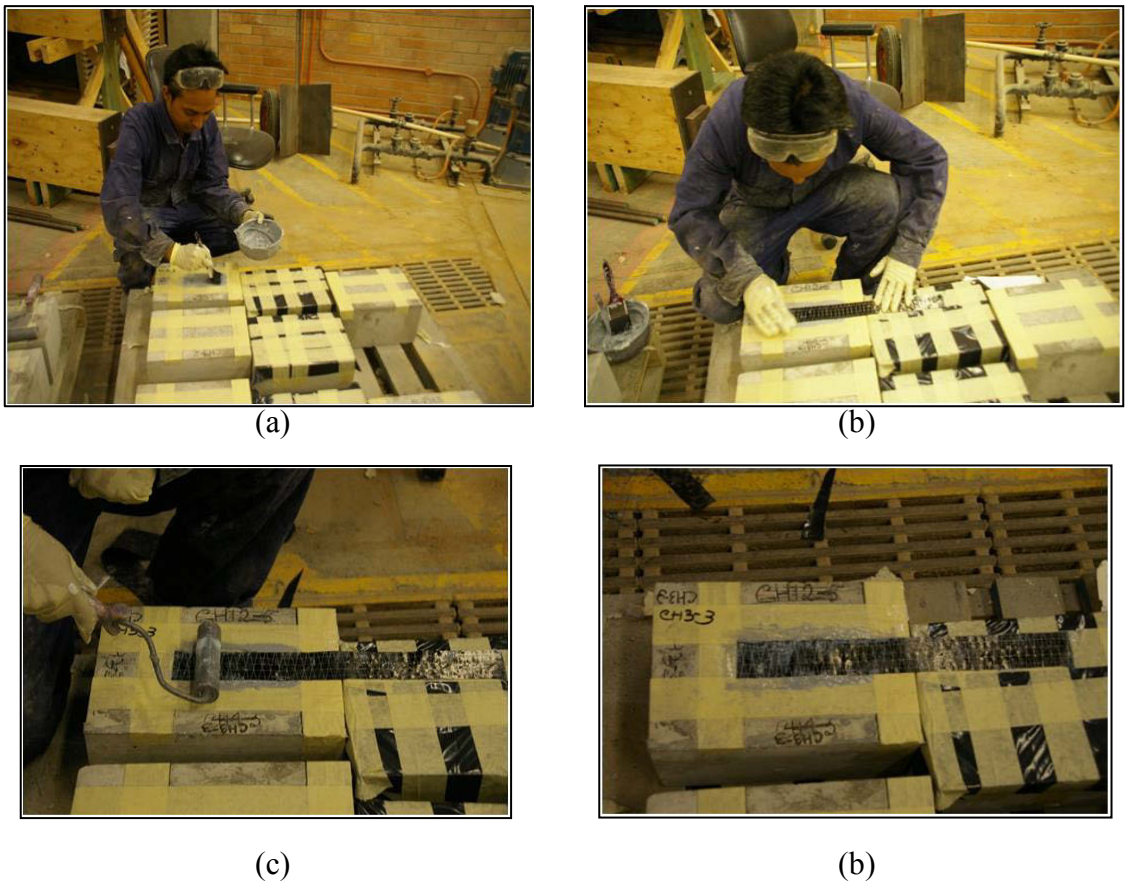

(a) (b)

(c) (b)

Figure 3.4 (a) Application of epoxy, **(b)** bonding FRP to concrete, **(c)** saturation of fibres with a roller and **(d)** fabricated pull-out specimen under curing

3.3.3 Exposure Conditions

3.3.3.1 Control specimens

Ten specimens were used as control specimens (5 for each FRP type) and they were named as CControl-1 to 5 and GControl-1 to 5; where C refers to Carbon and G refers to Glass and numbers from 1 to 5 refer to the specimen number. Control specimens were kept under normal lab conditions before being tested under pull-out load.

3.3.3.2 Exposed specimens

The remaining specimens were subjected to three types of exposure conditions – (i) temperature cycles (ii) wet-dry cycles and (iii) outdoor environment.

- **Temperature cycles:**

The temperature cycles used in this study was targeted to generate the usual highest temperature in Sydney environment, which is about 40^{o} C. In addition, the highest temperature was intentionally kept below the glass transition temperature of epoxy (T_g= 47^{o} C) to avoid any over-degradation of FRP of FRP-concrete bond. Although it was intended to generate the minimum temperature level of 5^{o} C to simulate the lowest temperature in winter, this could not be achieved due to the limitation in the drying oven (Figure 3.5 (a)) used and therefore the minimum temperature of 30^{o} C was used. Typical temperature cycle is shown in Figure 3.5 (b) where each cycle consisted of very sharp rise to 40^{o} C from 30^{o} C within three minutes, constant 40^{o} C for four hours and 57 minutes and a gradual decrease to 30^{o} C over seven hours and two cycles per day were maintained. The reason for using the cyclic temperature instead of constant temperature was to simulate realistic nature of the environment. The sharp increase in temperature was applied mainly to simulate the effect of sudden temperature increase and the gradual decrease in oven temperature for seven hours was chosen to allow the cooling of the specimens. Total of eighteen specimens (nine specimens for each FRP type) were used for this cyclic temperature series and specimens were exposed to 70 cycles (35 days), referred to as CT2 and GT2 series, 180 cycles (90 days), referred to as CT3 and GT3 and 730 cycles (one year), referred to as CT4 and GT4 series.

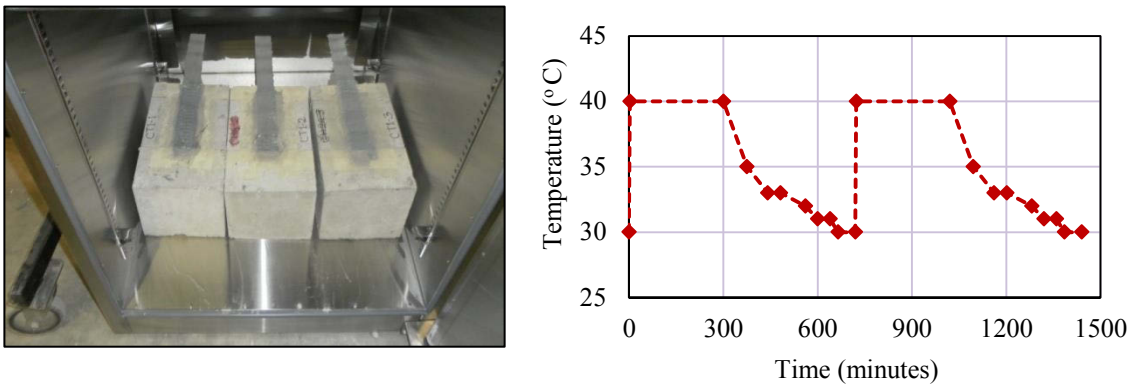

(a) (b)

Figure 3.5 (a) Specimens in drying oven and **(b)** temperature cycles

- **<u>Wet-dry cycles</u>:**

The wet-dry cycles consisted of 1 week wetting followed by 1 week drying and at least 95% RH was maintained for wetting. Although constant immersion in water was observed to be used in a number of previous studies, wet-dry cycles were chosen for this current study to simulate the severe condition of cyclic moisture absorption and desorption of FRP-concrete bond. The one week time for wetting and drying process was selected to allow the specimens to gain and loose sufficient amount of moisture, respectively. Wet environment was created using a humidifier in a small closed chamber. The humidity chamber was fabricated in laboratory with LVLs and plastic sheets. Specimens were stored on the racks in the chamber. Plastic sheets of the two sides of the chamber are removable to help the drying process. During the wetting, care was taken to keep the chamber air-tight so that water vapour generated by the humidifier remained inside the chamber. Figures 3.6 (a) and (b) show the photo of the humidity chamber and the data logger used to measure the temperature and relative humidity of the chamber, respectively. Although the main aim was to maintain constant temperature during wet and dry cycles, steam generated from humidifier raised the temperature to about 30^{o} – 32^{o} C. The humidifier was operated twice in a week for 10 hours each time and the peak of the temperature plot in Figure 3.7 represents the high temperature due to running of humidifier. In drying period, however, the temperature was almost constant in the range of 20 – 23 ^{o} C. The drying environment was created by taking off the plastic cover and letting the specimens dry in lab environment. As the

relative humidity was not controlled during the drying of the specimens, it depended on the lab relative humidity and showed scatters between 30% and 70%. Humidity specimens were subjected to wet-dry cycles for 1 month (CH1 and GH1 series), 6 months (CH2 and GH2 series), 12 months (CH3 and CH4 series) and 18 months (CH4 and GH4 series).

(a) (b)

Figure 3.6 (a) Humidity chamber and **(b)** temperature and humidity data-logger

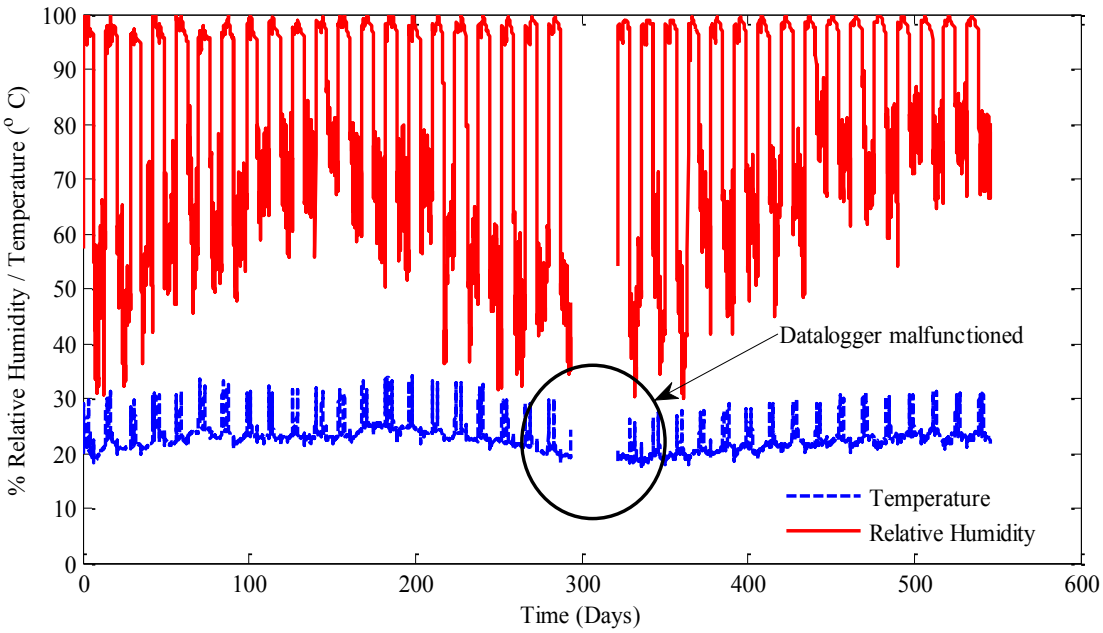

Figure 3.7 Wet-dry cycles with corresponding temperature

- **Outdoor environment:**

A number of specimens were directly exposed to outdoor environment of Sydney, Australia for 2 months (CE1 and GE1 series), 6 months (CE2 and GE2 series), 12 months (CE3 and GE3 series) and 18 months (CE4 and GE4 series). Due to the damage occurred in CE3 series during transferring of the specimens, CE3 specimens and its corresponding control specimens were fabricated again from spare concrete prisms from the second batch of concrete and the control specimens for CE3 series were named as CControl-1 to 5 (B2). Here, B2 refers to specimens from concrete batch 2. Figure 3.8 shows the specimens exposed to outdoor environment whereas the environmental parameters, namely, temperature, relative humidity and solar exposure collected from Australian Government Bureau of Meteorology have been plotted against time (from June, 2011 to December, 2012) in Figure 3.9. The environmental parameters were measured at the data station at Sydney Observatory Hill, which is about 2 km from the location of the exposed specimens. But it can be expected that the collected data would represent the exposed conditions reasonably well.

Figure 3.8 Specimens under outdoor environmental exposure

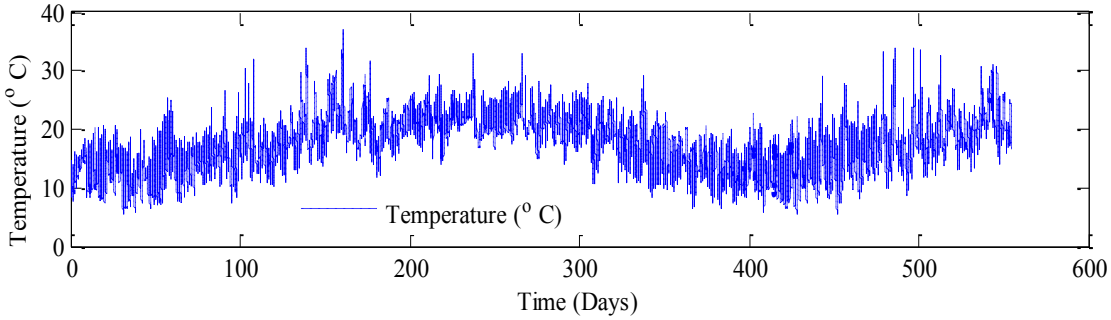

(a) Temperature plot (Sydney Observatory Hill)

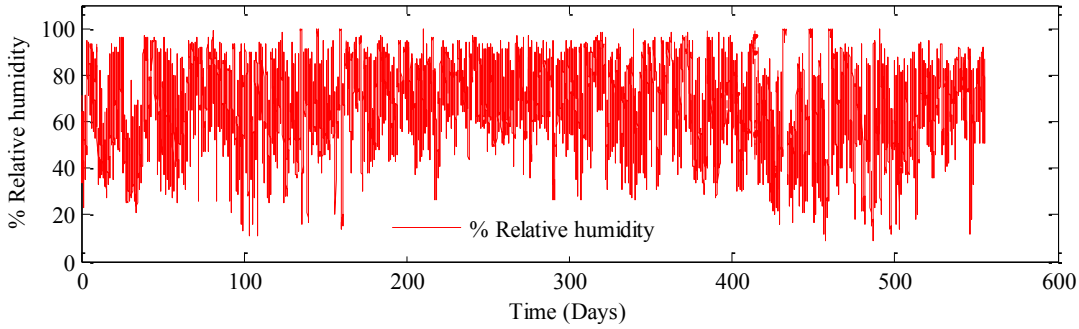

(b) % Relative Humidity plot (Sydney Observatory Hill)

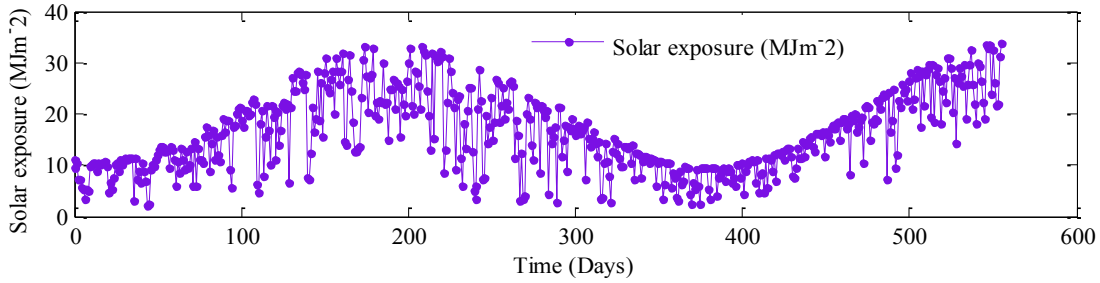

(c) Solar exposure plot (Sydney Observatory Hill)

Figure 3.9 Three environmental parameters for outdoor environmental exposure
Source: Australian Government Bureau of Meteorology

The nomenclature of the tested specimens was chosen such that the first letter represents the type of FRP, i.e., either Carbon or Glass, the second letter represents the exposure condition (T-temperature, H-humid environment/wet-dry cycles and E-outdoor environment, the first number refers to the order of the exposure durations, i.e.; 1st, 2nd, 3rd or 4th and the last number represents the serial number of specimen. The number of specimens exposed to each condition is listed in Table 3.4.

In order to avoid any confusion in the nomenclature, it should be noted that the order of the exposure durations for specimens exposed to temperature cycles started from 2 as a number of specimens from both CFRP and GFRP were fabricated in order to study the effect of constant temperature and named as CT1 and GT1 series. But the specimens were disregarded later from the experimental plan.

Table 3.4 Number of pull-out specimens

Exposure condition	Number of specimens		Name of specimens		Exposure period
	CFRP	GFRP	CFRP	GFRP	
Control	5	5	CControl-1 to 5	GControl-1 to 5	-
	5	-	CControl-1 to 5 (B2)[1]		
Temperature cycle*	3	3	CT2-1 to 3	GT2-1 to 3	5 weeks
Wet-dry cycle**	5	5	CH1-1 to 5	GH1-1 to 5	1 month
Outdoor environment	5	5	CE1-1 to 5	GE1-1 to 5	2 months
Temperature cycle*	3	3	CT3-1 to 3	GT3-1 to 3	3 months
Wet-dry cycle**	5	5	CH2-1 to 5	GH2-1 to 5	6 months
Outdoor environment	5	5	CE2-1 to 5	GE2-1 to 5	6 months
Temperature cycle*	3	3	CT4-1 to 3	GT4-1 to 3	12 months
Wet-dry cycle**	5	5	CH3-1 to 5	GH3-1 to 5	12 months
Outdoor environment	5	5	CE3-1 to 5	GE3-1 to 5	12 months
Wet-dry cycle**	5	5	CH4-1 to 5	GH4-1 to 5	18 months
Outdoor environment	5	5	CE4-1 to 5	GE4-1 to 5	18 months
Total number of specimens	59	54			
	113				

[1] B2 = specimens from concrete batch 2

* 5 hours at constant 40°C followed by 7 hours at gradual decrease to 30°C

** 1 week at around 95% RH followed by 1 week at normal lab condition

3.3.4 Test set-up and instrumentation

"SHIMADZU" universal testing machine with 500 kN loading capacity was used to conduct the pull-out test. The maximum load range of 20 kN was applied as the predicted load capacity for control series was in the range of 12-13 kN. The schematic diagram and photograph of the pull-out test have been provided in Figure 3.10. The specimen was placed vertically with the overhanging FRP heading to the jaws of the upper head of the machine and restrained with two plates connected by two bolts. Monotonic tensile loading was applied to the overhanging part of FRP along the direction of the fibres. The cross head movement from the lower fixed head of the testing machine was measured with a linear variable differential transformer (LVDT) which is capable of measuring displacements in nominal range of ± 50 mm. The LED display of the machine showed the load value during the test. Also, a data taker was used to record load, strain and cross head travel data. Before starting the test, three strain gauges (SG1 to SG3) with 10 mm gauge length and 119.9 ± 0.1 Ohms resistance were attached to the bonded FRP surface to acquire strain profiles along the length of the bond. Instrumentation used in the pull-out test and strain gauge locations is shown in Figures 3.11 and 3.12, respectively.

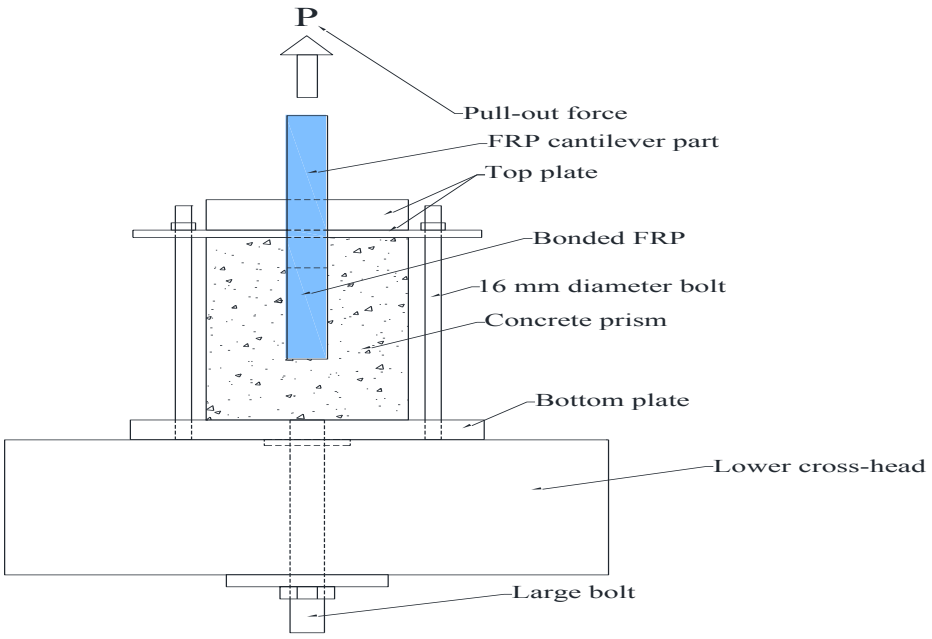

(a)

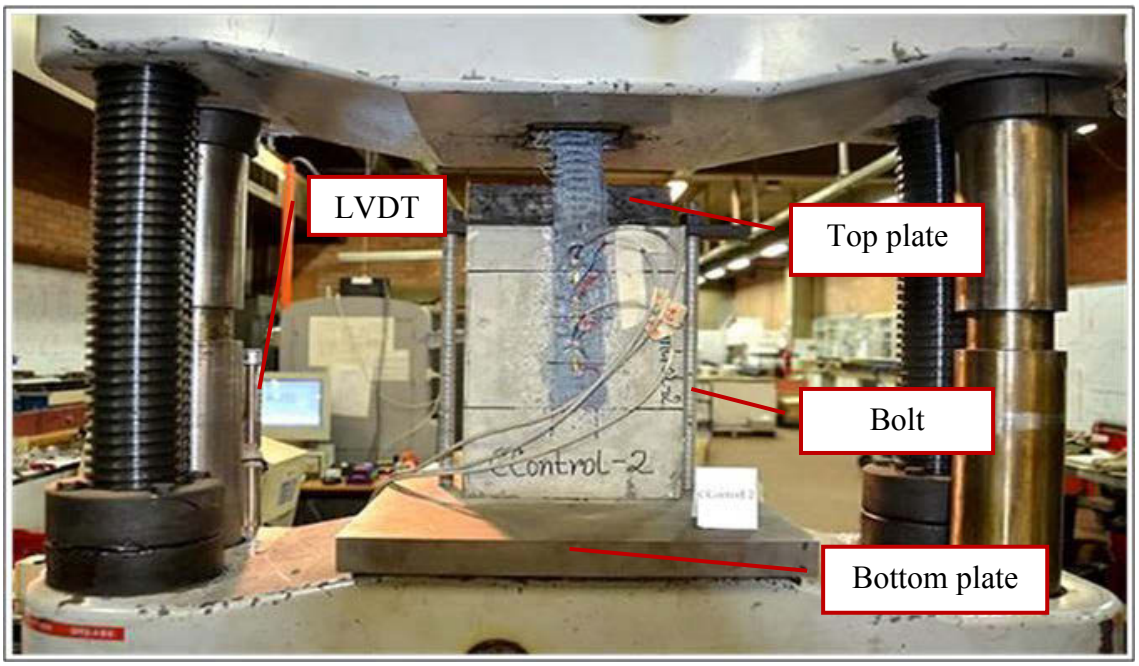

(b)

Figure 3.10 Pull-out test set-up: **(a)** schematic diagram and **(b)** photograph

(a)

(b)

(c)

(d)

Figure 3.11 (a) Data taker, **(b)** BCM Strain gauge, **(c)** jaws used for gripping and **(d)** LVDT

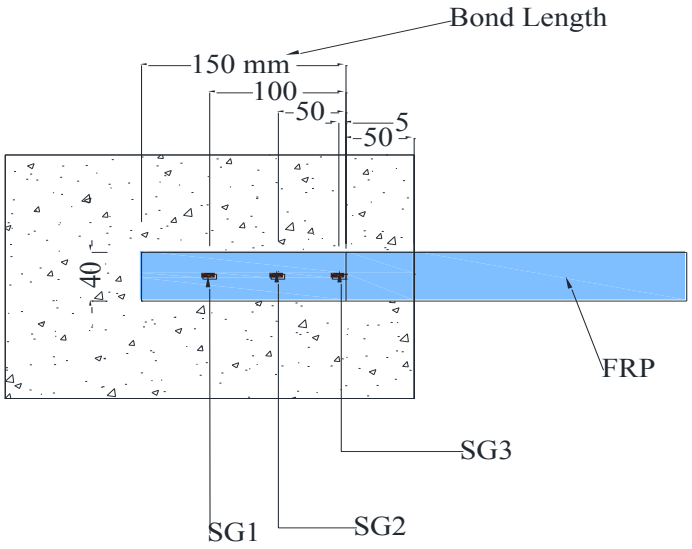

Figure 3.12 Strain gauge locations

3.3.5 Experimental procedure

Pull-out test was performed with a loading rate of approximately 2 mm/min in terms of cross-head travel of the testing machine. The loading rate was selected as per ASTM D3039/D3039M (2008). Although displacement controlled load could not be applied with the machine used in the study, the cross head displacement was constantly monitored and the load rate was adjusted to maintain the constant displacement of cross head. The reason behind adopting the loading rate specified in ASTM D3039/D3039M (2008) was the absence of standard method for pull-out test. After the specimen was placed in the rig and instruments are set up, tensile load was applied monotonically until failure. During the loading, any sound due to crack formation and any visible cracks were noted. Photographs were also taken before and after failure of the specimens to investigate the types of failure modes. Finally, gathered data were analysed in terms of maximum load, strain profiles and failure modes. The maximum load of failure was converted to the maximum axial stress developed in FRP using Equation 3.1:

$$\sigma_{db} = \frac{p_{\max}}{b_f t_f} \tag{3.1}$$

where σ_{db} = maximum axial stress on FRP sheet at debonding, P_{max} = maximum load of debonding, b_f = width of FRP sheet and t_f = thickness of FRP sheet.

In the calculation of maximum axial stress developed in FRP sheet, thickness was taken as the fibre thickness considering the fact that resin matrix has no effect on the load carrying capacity rather it helps in the distribution of stress. The strain values were expressed as micro strains ($\mu\varepsilon$) in all the results presented in this dissertation. After all data were analysed for control and exposed pull-out specimens, the effect of long term exposure to environmental conditions on FRP-concrete bond was studied based on the change in bond strength, strain profiles and failure modes with the time of exposure or cycles of certain environmental conditions. Also, fracture energy release rate of only CFRP bonded specimens were studied for three exposure conditions.

3.4 Tensile test of FRP coupons

In order to determine tensile properties (tensile strength and tensile MOE) of control and exposed FRP, tensile tests were carried out as per ASTM D3039/D3039M (2008). Tensile testing of FRP involved several steps such as fabrication of FRP tensile coupons, curing of specimens and finally, testing of specimens in laboratory. The geometry of FRP tensile coupons, fabrication of FRP coupons and material properties, exposure conditions, test set-up and instrumentation and experimental procedure have been described subsequently in separate subsections.

3.4.1 Geometry of FRP tensile coupons

FRP tensile coupons had total length of 250 mm including end tab length. End tabs at both ends of the coupons had four extra layers (2 layers on the top and 2 layers at the bottom of the main coupon) of same type of FRP with 50 mm length and 15 mm width on both sides of each end. The gauge part of FRP coupons consisted of two layers of 150 mm long and 15 mm wide FRP strip. As two plies were used in this study, the thickness of two plies was considered as the total thickness. Figure 3.13 shows the schematic of coupon geometry.

The selection of coupon width as 15 mm can be endorsed by a recent experimental study by Su (2012), where 15 mm wide FRP coupons performed better in term of ultimate tensile strength than wider FRP strips and in case of wider strips, failure modes were mainly separation of FRP in longitudinal strips. So, the study could conclude that

wider FRP coupons are more susceptible to uneven stress distribution during testing which can cause the unusual failure of FRP coupons at lower level of tensile load. Also, ASTM D3039/D3039M (2008) standard recommends specimen width of 15 mm with overall specimen length of 250 mm, provided that fibre orientation is unidirectional.

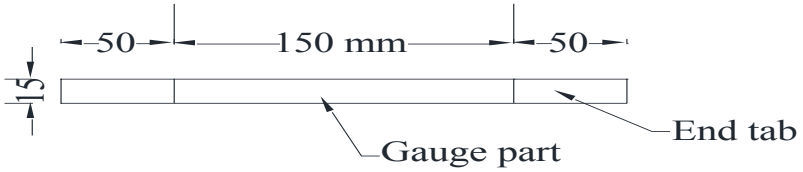

(a)

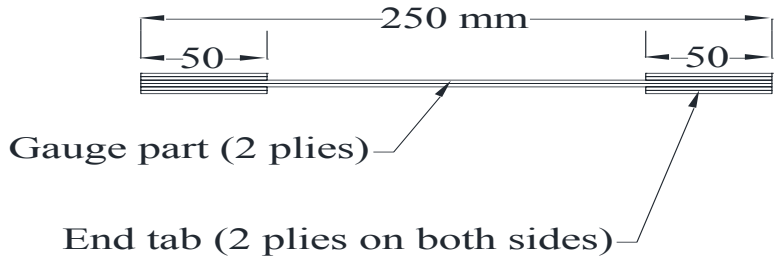

(b)

Figure 3.13 (a) Plan and **(b)** elevation of FRP tensile coupon

3.4.2 Fabrication of FRP tensile coupons and material properties

Fabrication of FRP tensile coupons were similar to the process explained earlier for pull-out specimens except the surface preparation was not involved. Thin aluminium plates were used as moulds for FRP coupons. For this study, FRP tensile coupons were prepared from two types of FRP, namely, carbon and glass. All fabricated specimens were kept in lab condition (at around 23^{o} C) for curing up to seven days. After curing of the specimens, small coupons were machined and the aluminium plate was stripped off from the bottom surface. During the machining of FRP coupons, care was taken to avoid cutting of fibres from the sides. The fabrication of FRP coupons are shown in Figure 3.14.

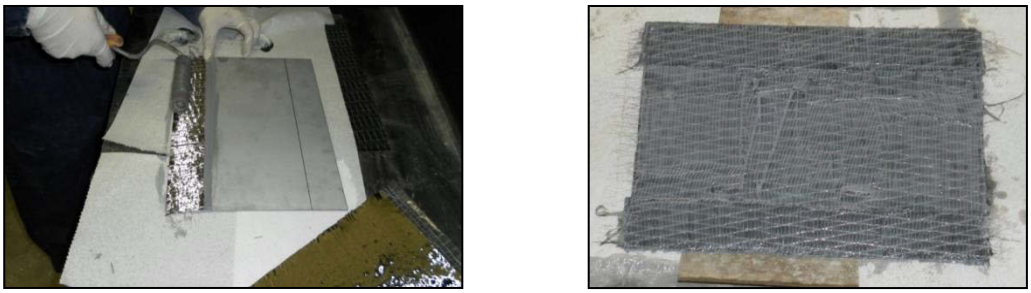

(a) (b)

Figure 3.14 (a) FRP application on mould and **(b)** curing of FRP in lab condition

3.4.3 Exposure conditions

CFRP coupons were fabricated in two batches but the first batch was not used for the study due to fabrication error. Ten coupons (five CFRP and five GFRP) were used as control coupons which were kept in lab condition before testing. In order to perform material characterisation of FRP for exposed conditions, only CFRP coupons were exposed to temperature cycles, wet-dry cycles and outdoor environment and five specimens were used for each of the durations for a certain environmental condition. The GFRP coupons were not exposed to any condition due to unavailability of the same GFRP material which was used for the fabrication of control coupons. In Table 3.5, the number of tensile FRP specimens, exposed to environmental conditions, has been listed.

The nomenclature for control tensile coupons was adopted as follows: CTControl-6 to 10 and GTControl-1 to 5, where the first letter C refers to Carbon and G refers to Glass. The Second letter T stands for Tensile and Control means specimens are exposed to lab condition. In addition, the numbers 6 to 10 after hyphen mean the serial numbers of CFRP specimens and 1 to 5 represent the serial numbers for GFRP coupons. In the nomenclature of exposed specimens, the first and second letters are similar to those of control coupons but the third letter T, H and E stands for temperature cycles, humidity (wet-dry cycles) and outdoor environment. The Number after the third letter refers to the order of exposure periods, i.e.; 1^{st}, 2^{nd}, 3^{rd} and 4^{th} and numbers after the hyphen refer to the serial number of specimens (1 to 5 for GFRP coupons and 6 to 10 for CFRP coupons).

Table 3.5 Number of FRP tensile coupons exposed to environmental conditions

Exposure condition	Number of specimens		Name of specimens		Exposure period
	CFRP	GFRP	CFRP	GFRP	
Control	5	5	CTControl-6 to 10	GTControl-1 to 5	-
Temperature cycle*	5	-	CTT2-6 to 10	-	5 weeks
Humidity cycle**	5	-	CTH1-6 to 10	-	1 month
Outdoor environment	5	-	CTE1-6 to 10	-	2 months
Temperature cycle*	5	-	CTT3-6 to 10	-	3 months
Humidity cycle**	5	-	CTH2-6 to 10	-	6 months
Outdoor environment	5	-	CTE2-6 to 10	-	6 months
Temperature cycle*	5	-	CTT4-6 to 10	-	12 months
Humidity cycle**	5	-	CTH3-6 to 10	-	12 months
Outdoor environment	5	-	CTE3-6 to 10	-	12 months
Humidity cycle**	5	-	CTH4-6 to 10	-	18 months
Outdoor environment	5	-	CTE4-6 to 10	-	18 months
Total number of specimens	60	5			
	65				

* 5 hours at constant 40^{o}C followed by 7 hours at gradual decrease to 30^{o}C

** 1 week at around 95% RH followed by 1 week at normal lab condition

3.4.4 Test set-up and instrumentation

All control and exposed FRP coupons were tested for tensile loads in "SHIMADZU" universal testing machine with a capacity of 500 kN (Only 20 kN was used as the maximum load range of the testing machine) except for few series which are tested in a 50 kN testing machine. The set-up used for tensile testing did not require any special rig but it was necessary to ensure that the gripping and alignment of the test coupons were properly done so that the failure occurs away from the grips and the effect of bending is minimised. Both upper and lower grips used in the experiment had lightly serrated surfaces which is recommended by ASTM D3039/D3039M (2008). A strain gauge of 10 mm gauge length and 119.9 ± 0.1 Ohms resistance was installed at the mid length of the FRP coupons to measure the strain values with the load increment. Also, a LVDT was used to record the cross-head movement during loading. Strain gauge, load cell of the machine and LVDT were connected to a data taker to record all data. Figure 3.15 shows the test set-up for the tensile testing of FRP coupons.

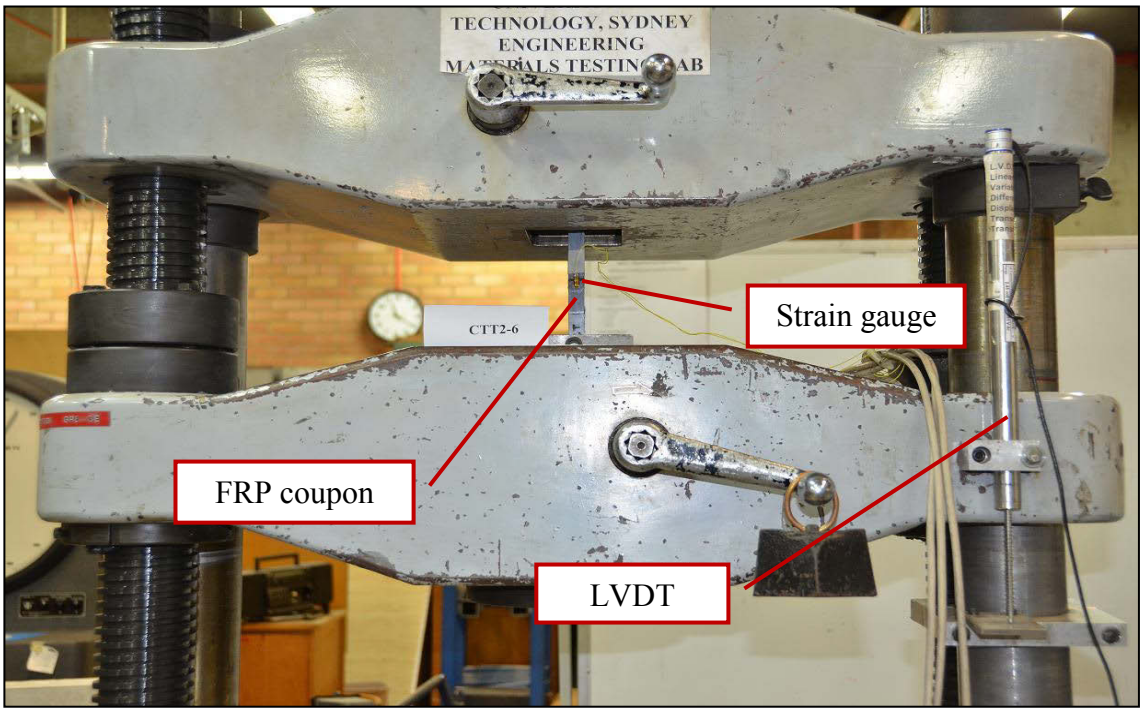

Figure 3.15 Test set-up of tensile testing of FRP coupon

3.4.5 Experimental procedure

Tensile tests of CFRP (control and exposed) and GFRP (control) coupons were conducted as per ASTM D3039/D3039M (2008). The specimens were placed between two grips and alignments of the specimens were checked. Then strain gauge wires were connected to data taker, LVDT was placed in proper position and tensile loading was applied monotonically on the test coupon with loading rate of approximately 2 mm/min of cross head movement specified by ASTM D3039/D3039M (2008). The loading was continued until the specimen failed by the fracture of fibres and notes were taken if any remarkable sound or load drop was observed. Finally, all test data were analysed in terms of ultimate tensile strength, tensile modulus of elasticity and failure modes. Tensile strength is defined as the maximum axial stress developed due to tensile loading, whereas the slope of the stress-strain graph between 1,000 and 3,000 $\mu\varepsilon$ represents the tensile MOE as per ASTM D3039/D3039M (2008).

3.5 Concrete compressive strength and static chord modulus of elasticity test

Material characterisation of concrete was carried out for both control and exposed conditions. Concrete material property tests included the determination of cylinder compressive strength and static chord modulus of elasticity. Concrete cylinders of 100 mm diameter were fabricated as per Australian standard AS 1012.9 (1999) in order to determine compressive strength, whereas cylinders of 150 mm diameter were fabricated as per AS 1012.17 (1997) to determine static chord MOE. Cylinders were cured under identical conditions to the pull-out specimens. Concrete cylinders were tested as per AS 1012.9 (1999) and AS 1012.17 (1997) to determine the compressive strength and static chord MOE, respectively, after 28 days of curing. Three cylinders were used for each test. The rest of the concrete cylinders were exposed to the same environmental conditions applied for pull-out specimens and tested on the day of pull-out test to determine the concrete compressive strength of exposed pull-out specimens.

3.6 Results of Tensile testing of FRP

Tensile strength and elastic modulus of CFRP and GFRP control coupons and those for CFRP exposed coupons have been presented in sections 3.6.1 and 3.6.2, respectively.

3.6.1 Tensile properties of FRP control coupons

3.6.1.1 CFRP tensile properties

A typical stress-strain curve obtained from tensile testing of control CFRP coupons has been shown in Figure 3.16 and the curves for the rest of the specimens have been provided in Appendix A.2. From the stress-strain curve, it is seen that CFRP was linearly elastic up to failure, which implies a brittle failure mode. The tensile strengths and tensile modulus of elasticity of all control coupons have been listed in Table 3.6. Tensile strengths were considered as the maximum axial stress developed in the FRP coupons before failure. In the determination of tensile MOE, the slope of the stress-strain curve was taken between 1000 and 3000 micro strains as specified by ASTM D3039/D3039M (2008) but in presence of any non-linearity in that region, adjustment was made to select the linear portion for calculation. The mean tensile strength was 2,886.6 MPa with a coefficient of variation (CoV) of 6.9 % and the mean tensile MOE was 226.2 GPa with a CoV of 7.5 %.

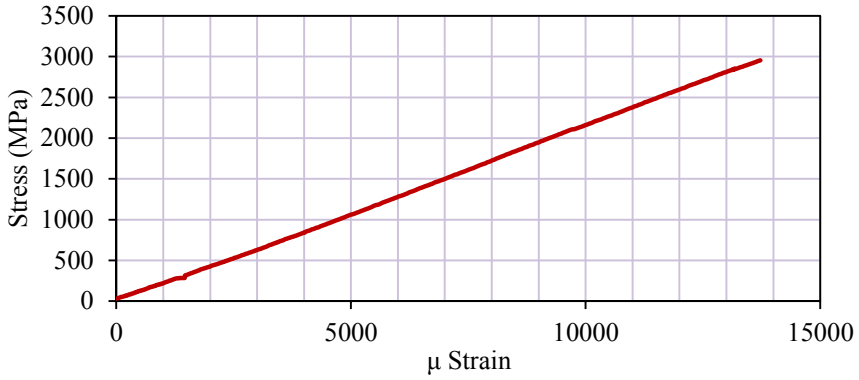

Figure 3.16 Typical tensile stress-strain curve of CFRP control specimens

Table 3.6 Tensile properties of CFRP control coupons

Specimen ID	Tensile strength (MPa)	Mean (MPa)	CoV (%)	Tensile MOE (MPa)	Mean (GPa)	CoV (%)	Comments
CTConrol-6	2954.9	2886.6	6.9	203.9	226.2	7.5	-
CTConrol-7	3135.0			242.7			-
CTConrol-8	2772.9			234.9			-
CTConrol-9	2683.7			223.4			-
CTConrol-10	-			-			Failure extended to end tab

The failed coupons have been shown in Figure 3.17. From the patterns of failure, it can be observed that CTControl-6 and CTControl-7 failed by complete rupture although the locations were very close to both end tabs. CTControl-8 had rupture near the middle of the length along with failure close to one of the end tabs. CTControl-9 showed failure by rupture perpendicular to the loading direction close to one end tab as well as by fracture along the fibre direction. The observation from CTControl-10 was that the rupture occurred close to the mid-length along with longitudinal separation from one end to the other. In addition, the failure in one of the end tabs was observed for this specimen, leading to much lower tensile strength than the other four specimens. Hence, it was ignored from the analysis.

Failure patterns of all control coupons revealed heterogeneity and the reason can be attributed to the difficulty of maintaining proper fibre alignments and epoxy thickness during fabrication, which is a limitation of wet lay-up process.

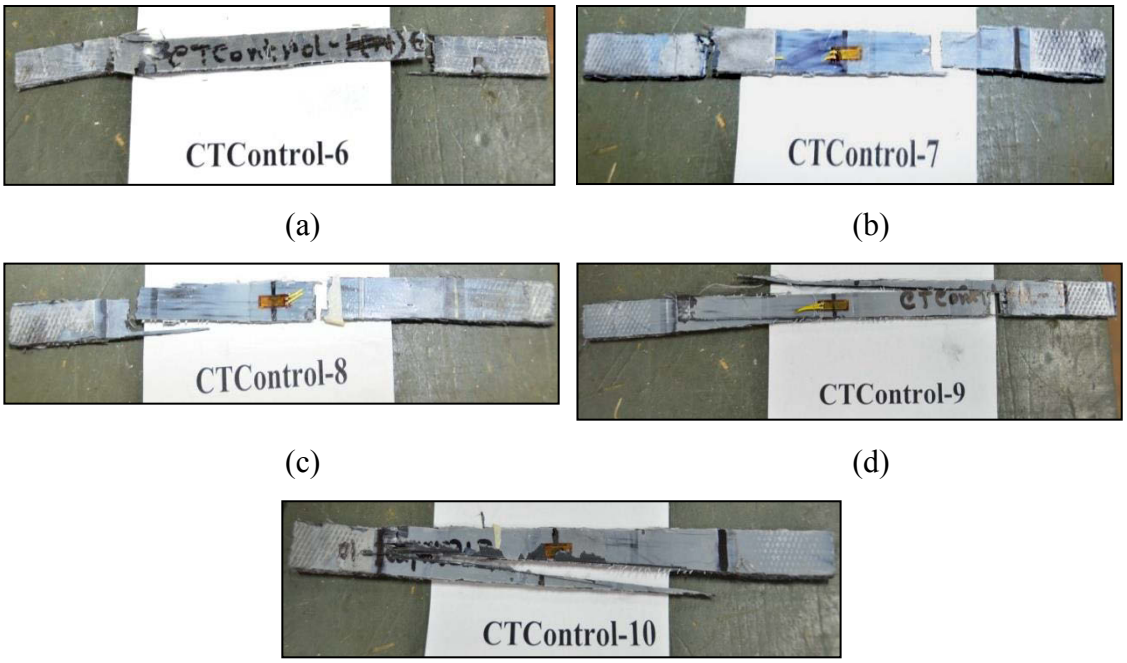

Figure 3.17 Failed CFRP tensile control coupons

3.6.1.2 GFRP tensile properties

The tensile properties, namely, tensile strength and tensile MOE of control GFRP were obtained from tensile tests of five coupons (Table 3.7) as per ASTM D3039/D3039M (2008). The mean tensile strength was 1,657.0 MPa with CoV of 2.0 % whereas the mean tensile MOE was 139.3 GPa with CoV of 5.2 %. A typical stress-strain curve for GFRP control coupon is shown in Figure 3.18 and the curves for rest of the specimens have been provided in Appendix A.2. From the stress-strain curve, it can be observed that GFRP coupon was linearly elastic until failure which represents the typical brittle failure mode of GFRP which is similar to CFRP. However, the slope of the curve suggests a smaller stiffness of GFRP material compared to CFRP material.

Table 3.7 Tensile properties of GFRP control coupons

Specimen ID	Tensile strength (MPa)	Mean (MPa)	CoV (%)	Tensile MOE (MPa)	Mean (GPa)	CoV (%)	Comments
GTConrol-1	1692.9	1657.0	2.0	148.7	139.3	5.2	-
GTControl-2	1671.0			133.3			-
GTConrol-3	1647.4			133.9			-
GTConrol-4	1616.7			141.4			-
GTConrol-5	-			-			Omitted from analysis

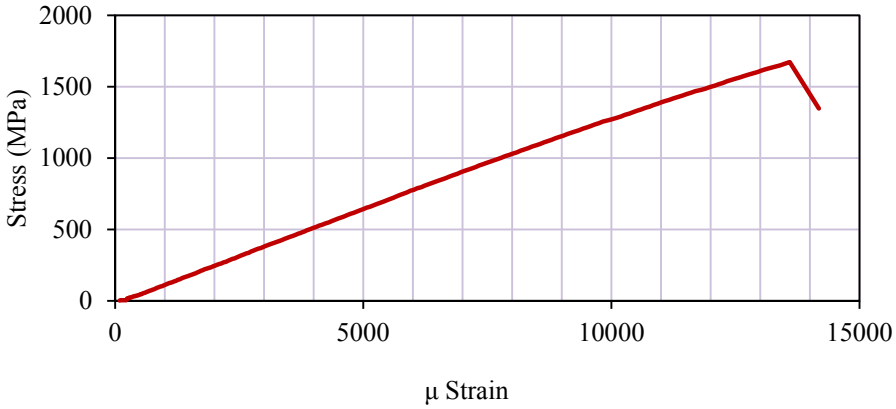

Figure 3.18 Stress-strain curve of GTControl-2

The failure modes of GFRP control coupons can be observed in Figure 3.19 where almost all specimens failed by rupture of GFRP. But rupture in the gauge part of specimen GTControl-5 (Figure 3.19 (e)) extended to the end tab (gripping location) and failure occurred with lower ultimate load value than the other four specimens. Therefore, this specimen was ignored for data analysis.

(a) GTControl-1

(b) GTControl-2

(c) GTControl-3

(d) GTControl-4

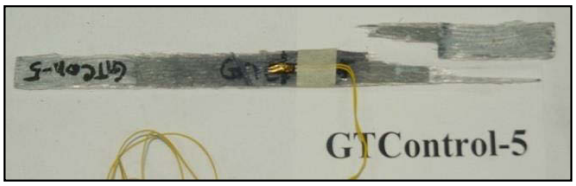

(e) GTControl-5

Figure 3.19 Failed GFRP control coupons

3.6.2 Tensile properties of CFRP exposed coupons

The results of tensile tests on exposed CFRP coupons have been discussed separately for temperature cycles, wet-dry cycles and outdoor environment in this section.

3.6.2.1 Temperature cycles

The tensile strength and tensile elastic modulus of CFRP were determined from CFRP coupons after being exposed to the cyclic temperature for five weeks, three months and one year. The plots for normalised (expressed as the ratio of exposed value to control value) tensile strength and tensile MOE against time of exposure are shown in Figure 3.20. The stress-strain curves, tables containing tensile strength and modulus of elasticity and photos of failed coupons of all the specimens are given in Appendices A.2, A.3 and A.4, respectively.

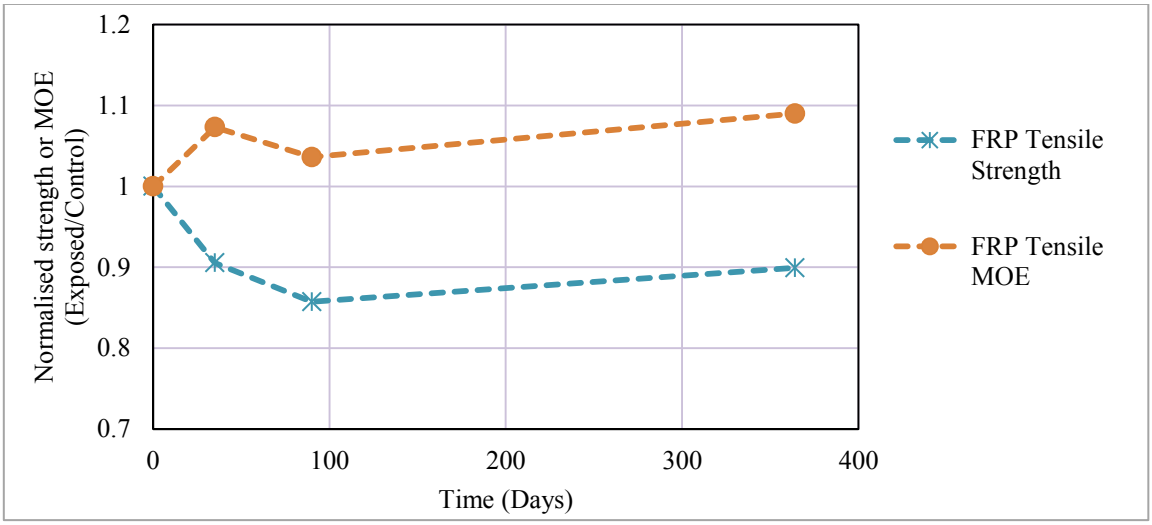

Figure 3.20 Normalised tensile strengths and MOEs of CFRP cyclic temperature series with exposure duration

From Figure 3.20, it can be observed that exposing the FRP coupons to the given temperature cycles resulted in reduction in its tensile strength to about 85.7 % of control value after three months. Only a slight improvement in strength was observed after one year (strength reached up to 89.9 %). Hence, the maximum degradation of tensile strength was 14.3 % due to temperature cycles applied only over three months.

Effect of the temperature cycles on the tensile modulus of elasticity was quite interesting, where unlike the tensile strength, exposure to temperature cycles resulted in an initial increase followed by a decrease in modulus of elasticity and then an increase thereafter. The initial increase in elastic modulus was 7 % after five weeks compared to the control series. After the exposure duration of three months, the modulus of elasticity reached 3.6 % more than the control value and then showed an increasing trend to reach 9 % more than the control elastic modulus. The two different trends of tensile strength and tensile MOE can be explained by the possible increase in the stiffness of fibres itself (Fitzer 1988; Sauder, Lamon & Pailler 2004) and the softening of epoxy matrix due to temperature cycles. As the epoxy matrix hold the fibres together and distributes the stress between fibres, the possible softening of epoxy can lead to the uneven stress distribution and lower strength values of CFRP composites although the MOE increases with the increase in fibre stiffness (Cao, Zhis & Wang 2009).

3.6.2.2 Wet-dry cycles

The results of tensile testing of CFRP coupons exposed to wet-dry cycles for one month, six months, one year and 18 months in terms of change of tensile strength and tensile MOE with exposure durations is presented in this section. The strength values and elastic modulus values for individual specimens for each of the durations are listed in Appendix A.3.

Figure 3.21 shows the changes of tensile strength and elastic modulus with time, where the degradation of tensile strength with exposure duration can be observed due to wetting and drying. The tensile strength continued to decrease from its control value, with almost constant rate, up to exposure period of six months to reach 82.6 % and then showed a decreasing trend with relatively slower rate to reach about 80 % of the control strength (20 % degradation) after one year. Finally, an improvement of strength was observed after 18 months with strength value reaching 91.1 % of the control value.

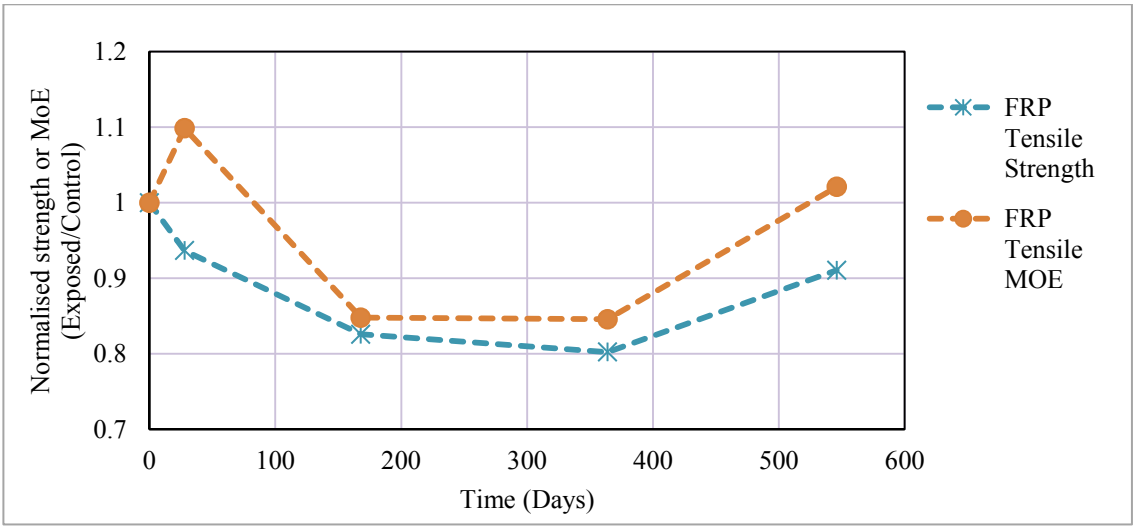

Figure 3.21 Normalised tensile strengths and MOEs of CFRP wet-dry series with exposure duration

The tensile MOE of CFRP coupons (Figure 3.21) also experienced deterioration and almost similar trend to that of tensile strength due to wet-dry cycles with the exception of an initial increase of elastic modulus by 9.9 % from its control value after one month. Then, the modulus of elasticity degraded by 15.2 % compared to its control value after

six months followed by a plateau continuing until one year of exposure duration. But the modulus of elasticity improved significantly and exhibited 2.1 % increase compared to the control value after 18 months.

3.6.2.3 Outdoor environment

The normalised tensile strength and MOE of CFRP coupons exposed to outdoor environment for two months, six months, one year and 18 months are plotted against time in Figure 3.22. The outdoor environment caused the degradation of strength initially by 20.3 % only after two months and then improved the strength gradually. However, the strength value was always lower than the control series. The tensile strength was found to be 94.8 % of control value after 18 months of exposure to outdoor environment.

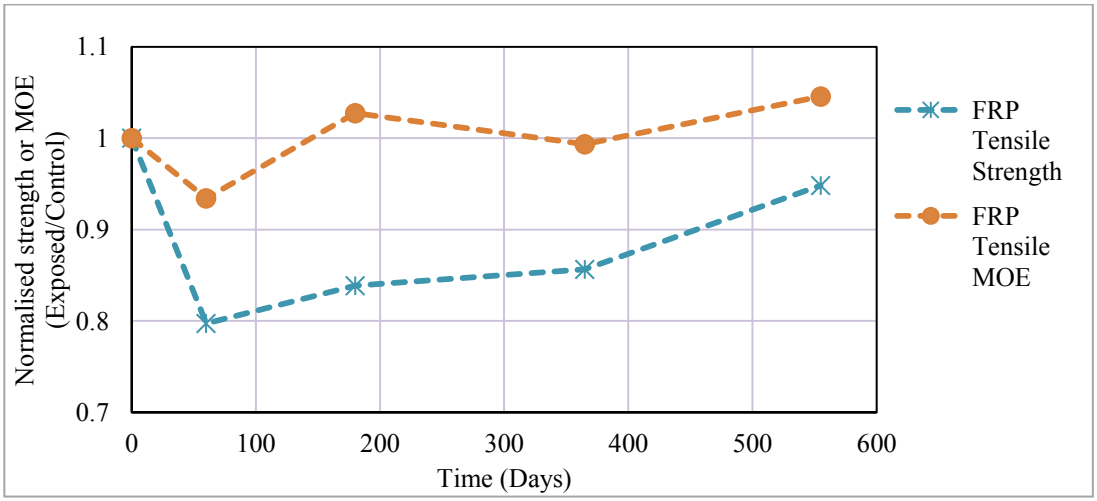

Figure 3.22 Normalised tensile strengths and MOEs of CFRP outdoor environment series with exposure duration

Unlike tensile strength, tensile modulus of elasticity experienced very slight degradation. Although elastic modulus had an initial degradation of 6.6 % after two months, an increase in elastic modulus by 4.6 % from its control value was observed after 18 months of exposure. The decreased tensile strength, in spite of the increase in modulus of elasticity, can be interpreted as the possible softening of epoxy resin.

3.7 Results of compressive testing of concrete

Compressive strength and MOE for control cylinders and only compressive strength for exposed cylinders were determined for the material characterisation of the concrete. The concrete properties were studied mainly to investigate the effects of concrete properties on the changes of FRP-concrete bond strength which has been presented in Chapters 4, 5 and 6. Sections 3.7.1 and 3.7.2 discuss the concrete compressive properties for control and exposed cylinders (from two batches), respectively.

3.7.1 Control cylinders

The average concrete compressive strength and static chord modulus of elasticity with CoVs for control concrete batch 1 (used for CFRP bonded specimens) and 2 (used for GFRP bonded specimens) have been listed in Table 3.8.

Table 3.8 Compressive properties of control concrete cylinders

Concrete batch	Mean compressive strength (MPa)	CoV (%)	Mean elastic modulus (GPa)	CoV (%)
1	31.2	4.8	28.5	10.1
2	35.9	7.0	31.0	5.8

3.7.2 Exposed cylinders

Concrete cylinders were subjected to identical exposure conditions as the pull out test specimens to investigate the effect of exposed conditions on the concrete properties independently. Provided two batches of concrete were used for fabrication of the pull out specimens, two sets of concrete cylinders were used for these tests.

3.7.2.1 Temperature cycles

The changes of normalised compressive strength (expressed as the ratio of exposed to control strength) against the time of exposure for concrete batch 1 and 2 have been plotted in Figure 3.23.

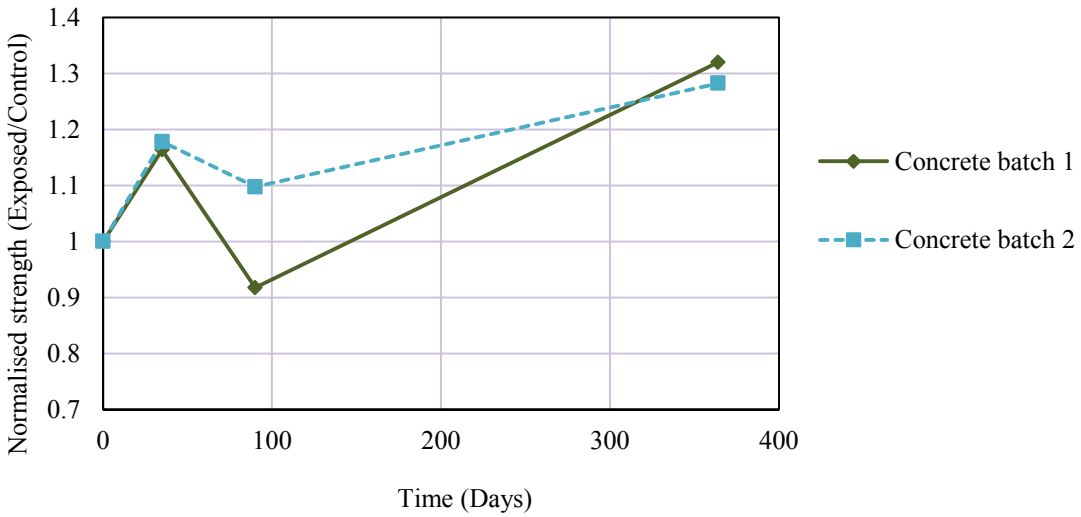

Figure 3.23 Normalised compressive strengths of concrete exposed to cyclic temperature against exposure duration

The average compressive strength values for batch 1 were 36.3 MPa, 28.6 MPa and 41.2 MPa for exposure durations of five weeks, three months and one year, respectively. As plotted in Figure 3.23, the effect of temperature cycles on concrete compressive strength was found to be positive with the exception of about 9 % reduction of strength at three months. The compressive strength value showed about 32 % increase compared to the control specimens after one year.

The average compressive strength values for batch 2 were 42.3, 39.4 and 46.0 MPa for exposure durations of five weeks, three months and one year, respectively. The effect of temperature cycles on the concrete compressive strength of this batch was also positive as strength values were always more than that of control series. The strength increased by 17 % after five weeks and showed a decreasing trend to reach about 10 % more than the control value after three months. The one year exposure series exhibited 28 % gain of compressive strength compared to the control strength.

3.7.2.2 Wet-dry cycles

The wet-dry cycles were found to have positive effect on the concrete compressive strength of concrete batch 1. From Figure 3.24, it is obvious that the compressive strength continued to increase during the exposure period of 18 months due to the suitability of humidity condition for the strength development of concrete, especially, in the early age. The increasing trend became slow after the initial sharp increase by 13 % after the exposure period of one month. The strength increased by 32 % after exposure for 18 months.

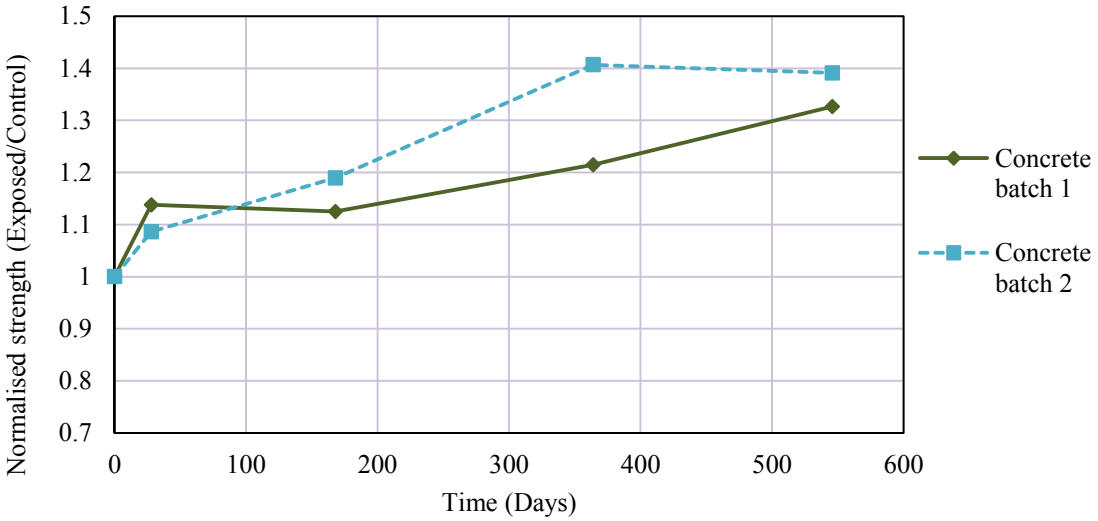

Figure 3.24 Normalised compressive strengths of concrete exposed to wet-dry cycles with exposure duration

Like the first batch of concrete, batch 2 also showed increase of compressive strength up to one year to reach about 40.7 % more than that of control strength. Then it showed slight decrease of strength to reach 39.1 % of the control value after the final exposure duration of 18 months.

3.7.2.3 Outdoor environment

The effect of outdoor environment on the compressive strength of concrete batch 1 was positive as the strength values were always higher than the control strength. This behaviour can be observed from the plot of normalised average concrete strength (ratio

of exposed strength to control strength) against time as illustrated in Figure 3.25. The compressive strength reached the maximum increase of 66.3 % from its control value after one year and then showed a degrading trend to approach the value of 31.6 % more than that of control series.

Similar to batch 1, the positive effect of outdoor environment to compressive strength of concrete was also observed for batch 2 as the strength continuously increased with time. The strength value increased by 23 % from the control value just after two months and then showed a gradual trend of increase. Finally, the normalised compressive strength reached about 59 % more than the control strength after 18 months.

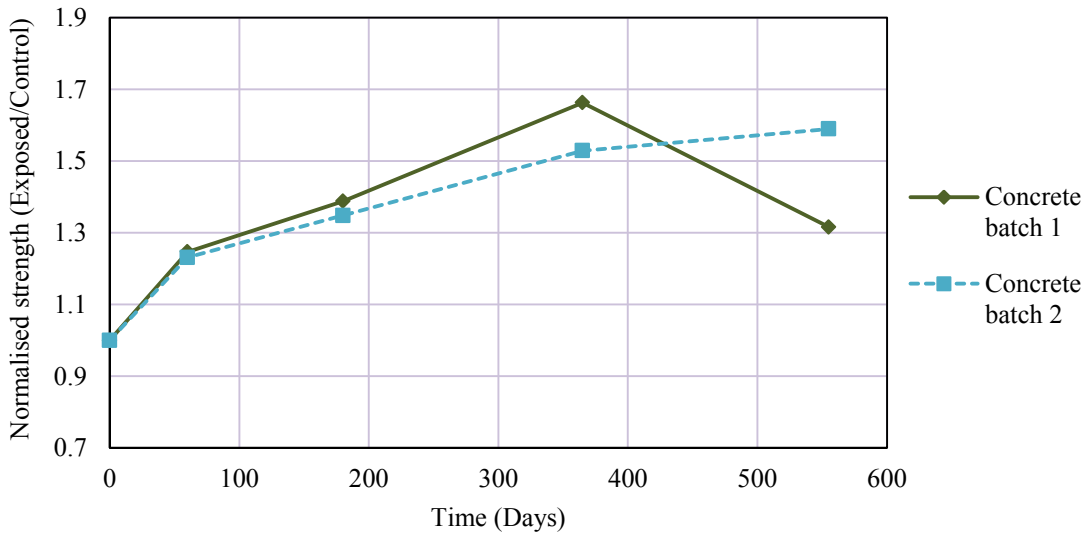

Figure 3.25 Normalised compressive strengths of concrete exposed to outdoor environment with exposure duration

3.8 Test results of control pull-out specimens

The test results of CFRP and GFRP control pull-out specimens are discussed in this section.

3.8.1 CFRP control specimens

3.8.1.1 Pull-out strengths

A total of ten Control CFRP bonded prisms from two concrete batches were tested under direct shear tests and the maximum axial stress developed in CFRP before debonding was considered as pull-out strength of each specimen. Table 3.9 provides the pull-out strength value for each of the specimens from concrete batch 1 together with mean strength and coefficient of variation (CoV).

Table 3.9 Pull-out strengths of control CFRP specimens from concrete batch 1

Specimen ID	Maximum load at debonding P_{max} (kN)	Pull-out strength σ_{db} (MPa)	Mean pull-out strength (MPa)	CoV of σ_{db} (%)
CControl-1	11.1	1183.3	1298.7	12.0
CControl-2	14.6	1563.9		
CControl-3	11.4	1213.4		
CControl-4	12.4	1322.5		
CControl-5	11.3	1210.3		

From Table 3.9, the average pull-out strength for five specimens is found to be 1298.7 MPa with a CoV of 12.0 %. A 12.0 % CoV may be attributed to the fabrication of specimens with wet lay-up process. As FRP fabric consisting of loose fibres is attached to the concrete with epoxy resin manually in wet lay-up method, maintaining the uniform thickness of epoxy and alignment of fibres may not be possible.

The results of five control pull-out specimens from concrete batch 2 have been provided in Table 3.10. The load value of Specimen CControl-5 (B2) reached up to 18.2 kN and was much higher than the remaining four specimens and the reason might be due to the higher thickness of epoxy layer or better surface preparation compared with the other

four specimens. The average pull-out strength considering all the specimens was 1445.2 kN with CoV of 20 %. The higher percentage of the coefficient of variation can be attributed to the strength value of CControl-5 (B2). Hence, the specimen was ignored from the analysis and the average pull-out strength of the remaining four specimens (1320 MPa with CoV of 7 %) was used as the pull-out strength. Control specimens prepared from batch 2 of concrete exhibited relatively higher pull-out strengths and the reason can be attributed to the higher concrete strength of the batch 2.

Table 3.10 Pull-out strengths of control CFRP specimens from concrete batch 2

Specimen ID	Maximum load at debonding P_{max} (kN)	Pull-out strength σ_{db} (MPa)	Mean pull-out strength ignoring CControl-5 (B2) (MPa)	CoV of σ_{db} (%)
CControl-1 (B2)	11.3	1202.2	1320.0	7.0
CControl-2 (B2)	13.3	1422.4		
CControl-3 (B2)	12.7	1357.3		
CControl-4 (B2)	12.2	1298.0		
CControl-5 (B2)	18.2	1945.9		

3.8.1.2 Failure modes

The failure modes of control CFRP pull-out specimens from concrete batch 1 have been shown in Figure 3.26. All specimens failed in the weakest concrete substrate and a concrete layer was found to be attached to all debonded FRP coupons. CControl-1 to 3 exhibited very thick concrete layer attached to the FRP whereas CControl-4 had relatively thinner layer of concrete as well as visible epoxy layer in few locations of the debonded CFRP. The failure mode of CControl-5 was slightly different from other four specimens as epoxy layer was visible in most part of the bond and the thickness of concrete was very small.

The observations suggest that the FRP-concrete bond control specimens failed in concrete few millimetres below the concrete-adhesive interface. Such failure mode is

typical in FRP-epoxy-concrete bond as reported by Chen & Teng (2001) for single or double shear tests.

Control CFRP specimens from batch 2 showed similar modes of failure (Figure 3.27) to those of control specimens from batch 1, i.e. failure in concrete beneath the concrete-adhesive interface. As illustrated in Figure 3.27 (e), CControl-5 (B2) showed partial fracture of CFRP at the edge towards the free end which may be attributed to improper gripping of FRP Imani (2010).

(a) CControl-1

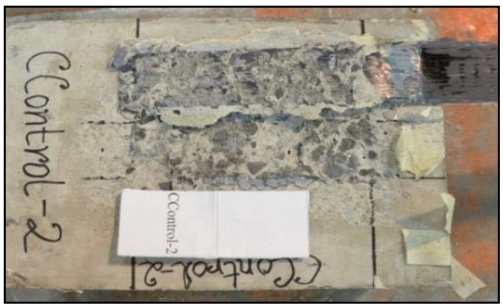

(b) CControl-2

(c) CControl-3

(d) CControl-4

(e) CControl-5

Figure 3.26 Failure modes of control CFRP pull-out specimens

(a) CControl-1 (B2)

(b) CControl-2 (B2)

(c) CControl-3 (B2)

(d) CControl-4 (B2)

(e) CControl-5 (B2)

Figure 3.27 Failure modes of control CFRP pull-out specimens from batch 2

3.8.1.3 Strain profiles

The strain distribution diagrams (*referred to as strain profiles from here onwards*) along the length of the bonded CFRP were plotted based on the readings of three strain gauges (Figure 3.28) at different levels of loads. The distances of three strain gauges were measured from the loaded end as 5 mm, 50 mm and 100 mm. Although strain gauges did not cover the whole length of the bond (150 mm), strain profiles were still capable of providing information on the changes of load/stress-transfer lengths. However, determining the effective bond length by observing the load-transfer length either at 97% of ultimate load (Yuan et al. 2004) or at 99% of ultimate load (Lu et al. 2005) cannot be conducted accurately without mounting strain gauges with close intervals on

the total bond length. Only an assumption on the effective bond length can be made if the load transfer length does not exceed the distance of the far most strain gauge (100 mm from the loaded end) and the comparison of effective bond lengths of exposed specimens with those of control specimens can be conducted to investigate the effect of environmental conditions on the effective bond length. From the strain profiles of CFRP control specimens as shown in Figure 3.29, it can be observed that strain values (in micro strains) at 5 mm from the loaded end continued to increase with the increase in load but strains at 50 mm and 100 mm locations remain almost zero. Therefore, the initial transfer lengths can be considered as 50 mm or less. With the load approaching maximum debonding load, change of load transfer lengths can be observed. Specimens CControl-1 to 4 exhibited the shifting of transfer lengths approximately at 11-12 kN load whereas specimen CControl-5 showed the change of transfer length at lower level of load. The effective bond lengths can be assumed as 100 mm or less for specimens CControl-1, 2 and 4 and more than 100 mm for the remaining two. The observed effective bond lengths were in a very good agreement with the effective bond length (97.4 mm) determined from Equation 3.2 recommended by Chen & Teng (2001).

$$L_e = \sqrt{\frac{E_f t_f}{\sqrt{f_c'}}} \tag{3.2}$$

where L_e = effective bond length, E_f = tensile modulus of elasticity of FRP, t_f = thickness of FRP and f_c' = compressive strength of concrete

The strain value near loaded end for specimen CControl-3 (Figure 3.29 (c)) was lower than the value at 50 mm when the load reached (10.78 kN) close to ultimate. Theoretically, the values should be the same forming a plateau representing the debonded part of FRP sheet. But the fluctuation can be attributed to the local bending of already debonded FRP sheet near loaded end due to thinness of the sheet and roughness of the crack, which was reported by Yuan et al. (2004).

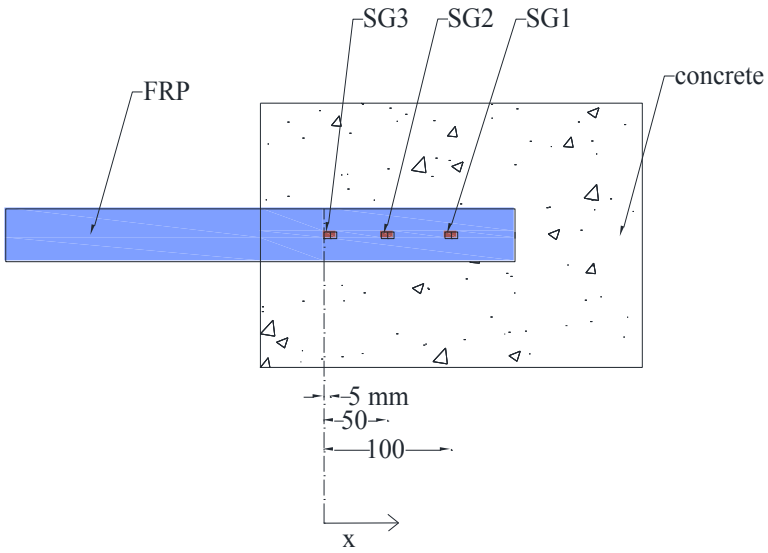

Figure 3.28 Typical strain gauge locations

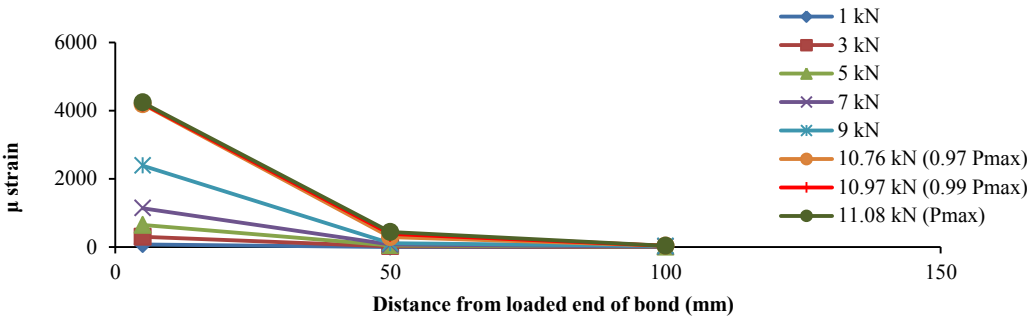

(a) CControl-1

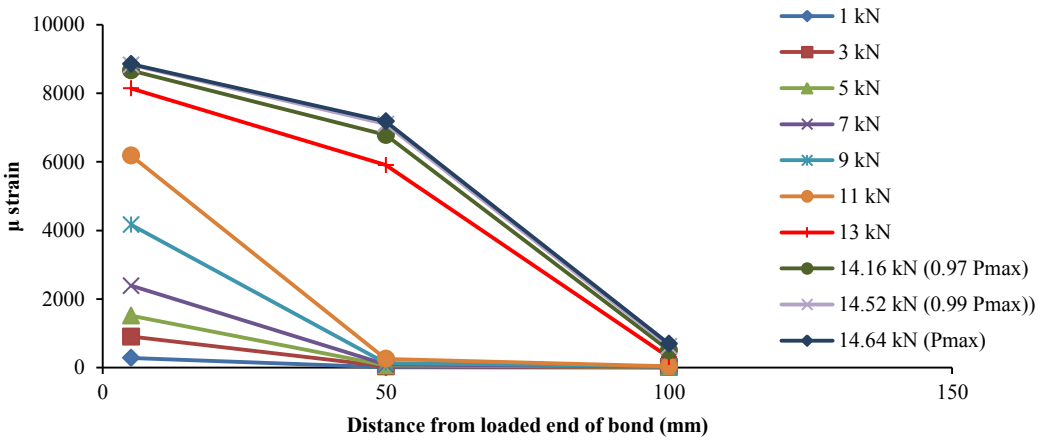

(b) CControl-2

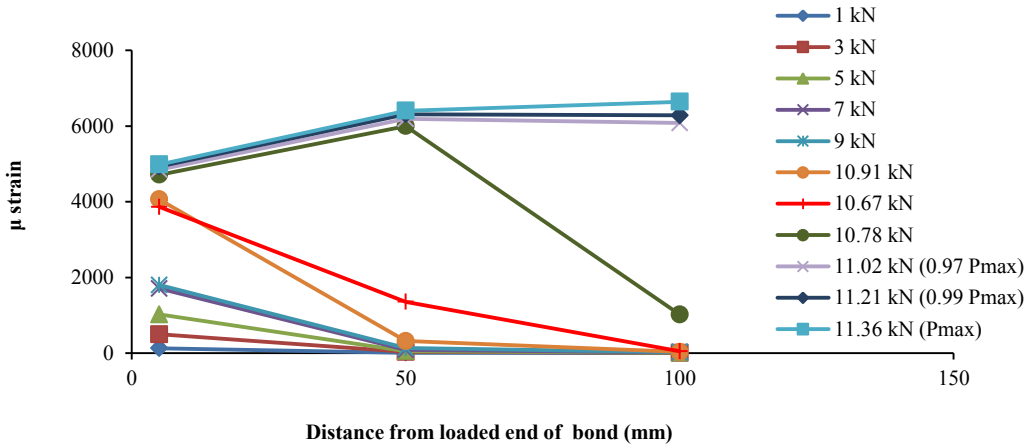

(c) CControl-3

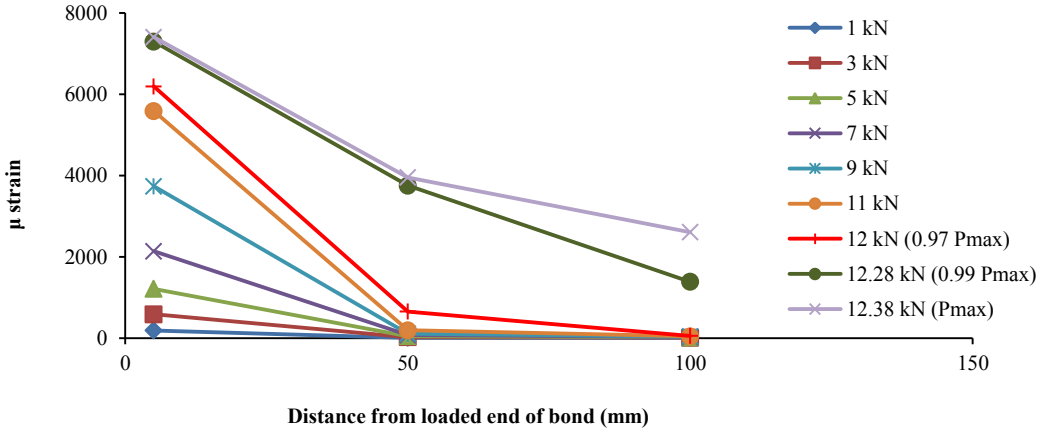

(d) CControl-4

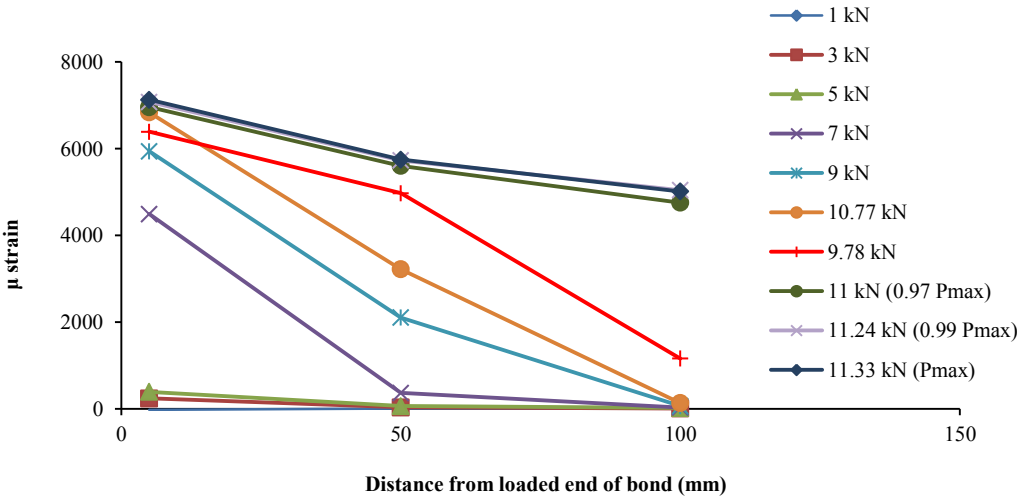

(e) CControl-5

Figure 3.29 Strain profiles of control CFRP pull-out specimens

Similarly, strain profiles for control CFRP pull-out specimens from concrete batch 2 were plotted (Figure 3.30). For specimen CControl-1 (B2), strain values at 5 mm could not be read due to instrumental malfunctioning. However, shifting of the transfer length is still interpretable from the values of the remaining two gauges. Approximately, the load transfer length shifted to 100 mm at 9.40 kN. The change of initial transfer lengths to 100 mm occurred approximately at 11 kN for specimens CControl-2 to 4 (B2). The effective bond lengths of the specimens CControl -1, 2 and 4 were found to be very close to 100 mm. It was only for CControl-3 (B2) where the observed effective bond length was greater than 100 mm. These observed effective bond lengths are close to predicted values using Chen & Teng (2001) model which was 94 mm and close to the experimentally observed ones. The effective bond length values observed from strain profiles of control specimens from both concrete batches will be used later for comparison with the bond lengths of exposed specimens.

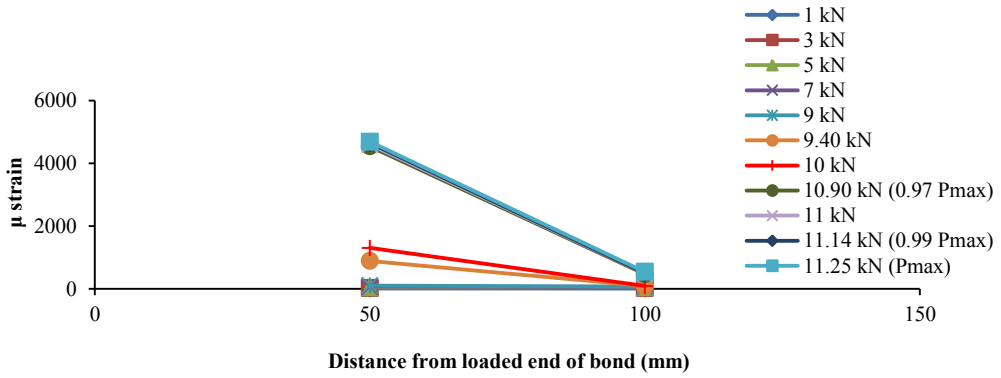

(a) CControl-1 (B2)

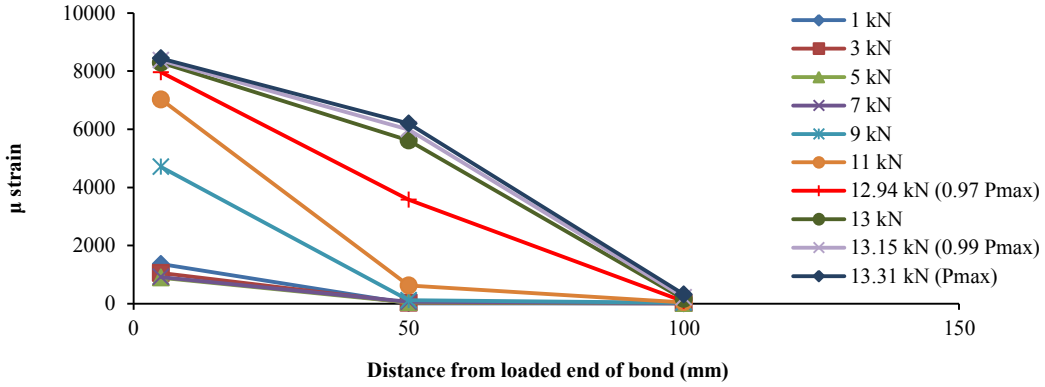

(b) CControl-2 (B2)

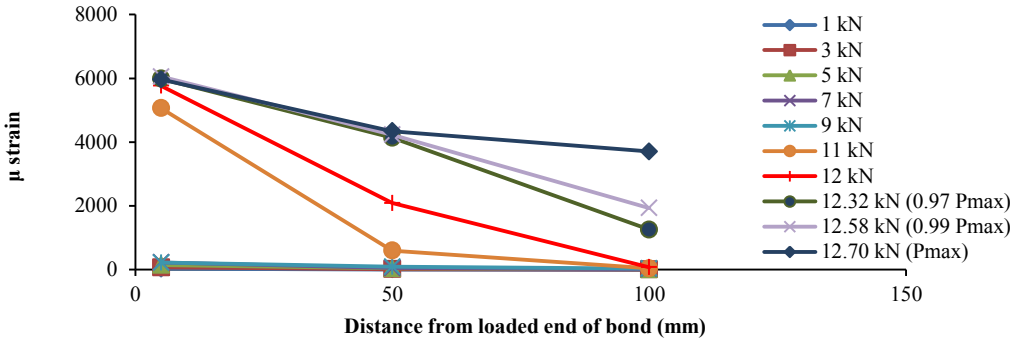

(c) CControl-3 (B2)

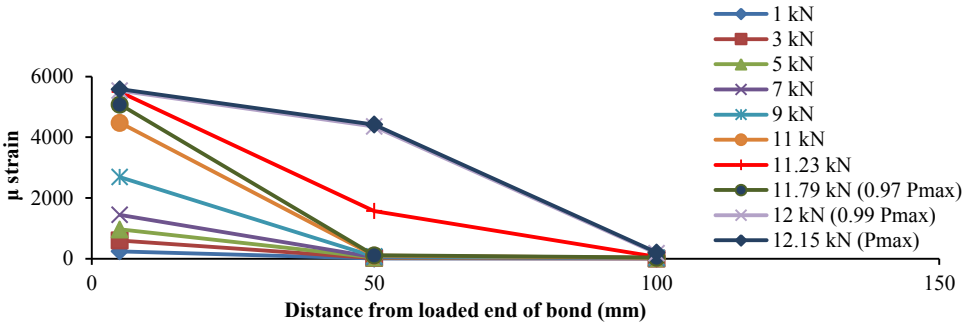

(d) CControl-4 (B2)

Figure 3.30 Strain profiles of CFRP control pull-out specimens from concrete batch 2

3.8.2 GFRP control specimens

3.8.2.1 Pull-out strength

Similar to the CFRP bonded specimens; five specimens were used for GFRP control pull-out tests. The average maximum stress developed in GFRP before debonding was 1027 MPa with a CoV of 6.0 %. The maximum load and stress values for five specimens have been listed in Table 3.11.

3.8.2.2 Failure modes

The failure modes observed after testing were quite similar to those of CFRP pull-out specimens. Most specimens failed in concrete substrate with the exception of GControl-4 which had a very thin layer of concrete as well as visible epoxy layer attached to the debonded GFRP coupon. Figure 3.31 shows the typical failure pattern of this series

along with the failure mode of GControl-4 whereas those for remaining specimens have been provided in Appendix B.2.

Table 3.11 Pull-out strengths of control GFRP specimens

Specimen ID	Maximum load at debonding P_{max} (kN)	Pull-out strength σ_{db} (MPa)	Mean pull-out strength (MPa)	Standard deviation of σ_{db} (MPa)	COV of σ_{db} (%)
GControl-1	12.5	1014.2	1027.0	61.1	6.0
GControl-2	11.7	953.0			
GControl-3	13.0	1054.5			
GControl-4	13.7	1114.9			
GControl-5	12.3	998.4			

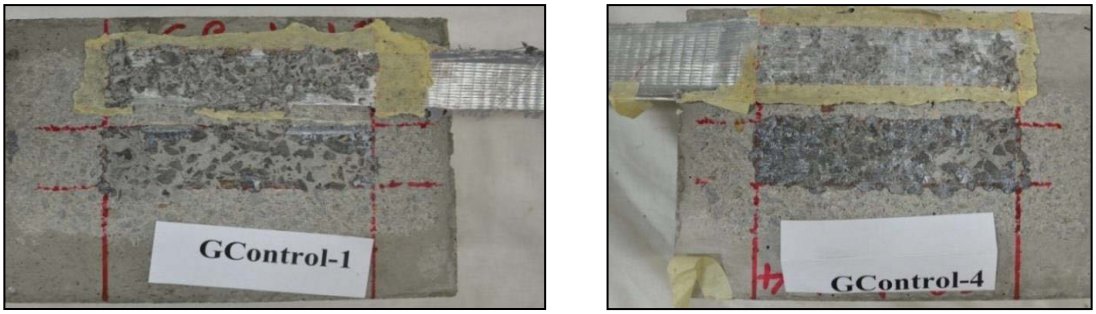

(a) GControl-1 (b) GControl-4

Figure 3.31 Failure modes of Control GFRP pull-out specimens

3.8.2.3 Strain profiles

The strain distribution of the control GFRP specimens was mainly at 0-50 mm location until load value reached very close to the maximum (Figure 3.32). Almost all specimens showed load transfer length (initial transfer length) of approximately 50 mm except when the load reached close to the maximum pull-out forces. This behaviour of GFRP-

concrete bond resembles that of CFRP-concrete bond explained earlier in this chapter. The change of initial transfer lengths of GFRP specimens from 50 mm to 100 mm were observed at about 11 kN load for three specimens, 9 kN load for one specimen and 12.6 kN for the remaining one. Three out of five specimens showed effective bond length of 100 mm or less whereas the remaining two had effective bond length of more than 100 mm according to the definition of effective bond length as the load transfer length either at 97% or at 99% of the maximum load in pull-out test. The effective bond length calculated using Chen & Teng (2001) model was 84.5 mm which is close to the experimental effective bond lengths.

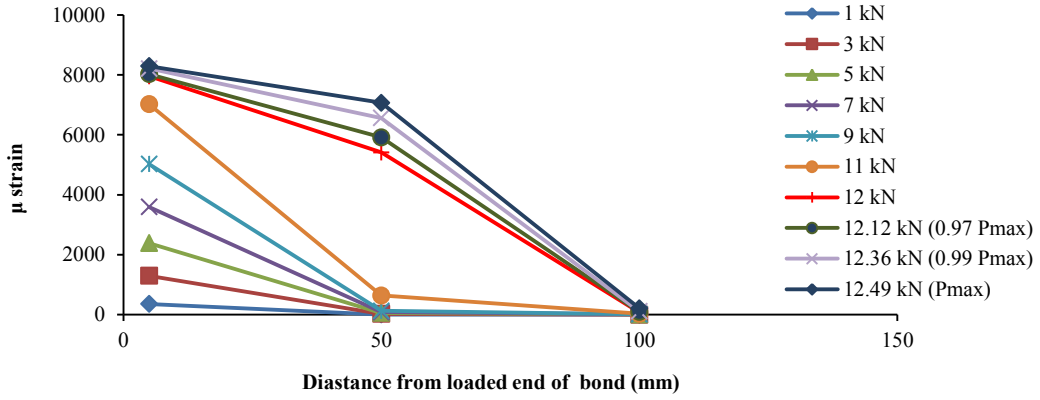

(a) GControl-1

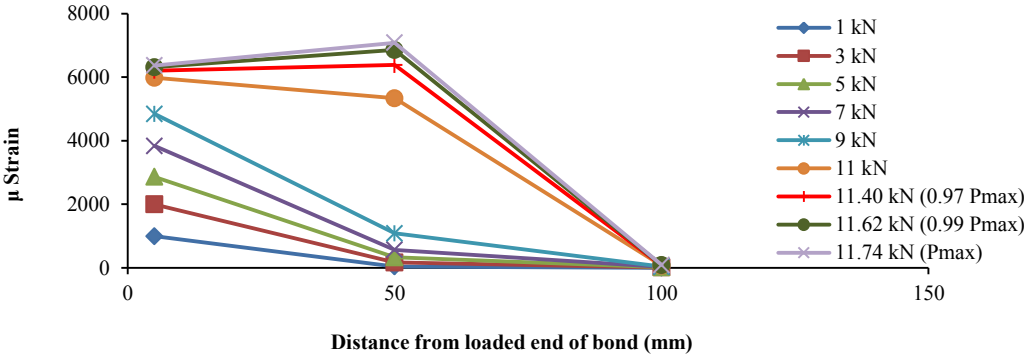

(b) GControl-2

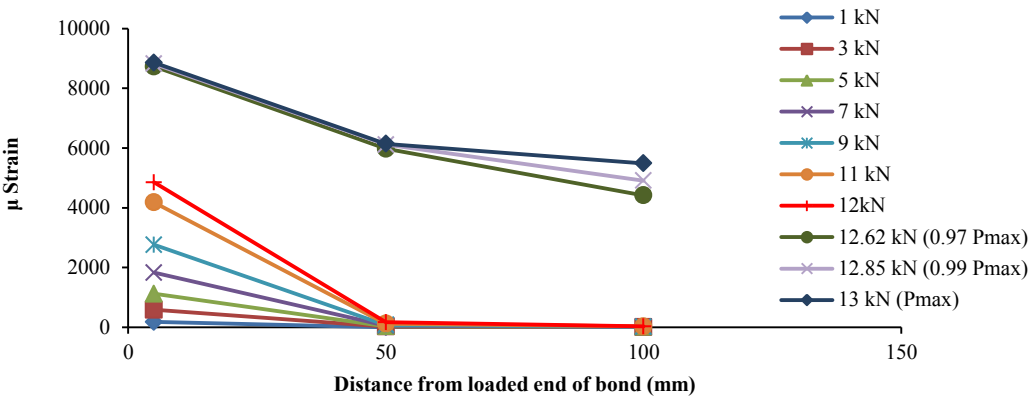

(c) GControl-3

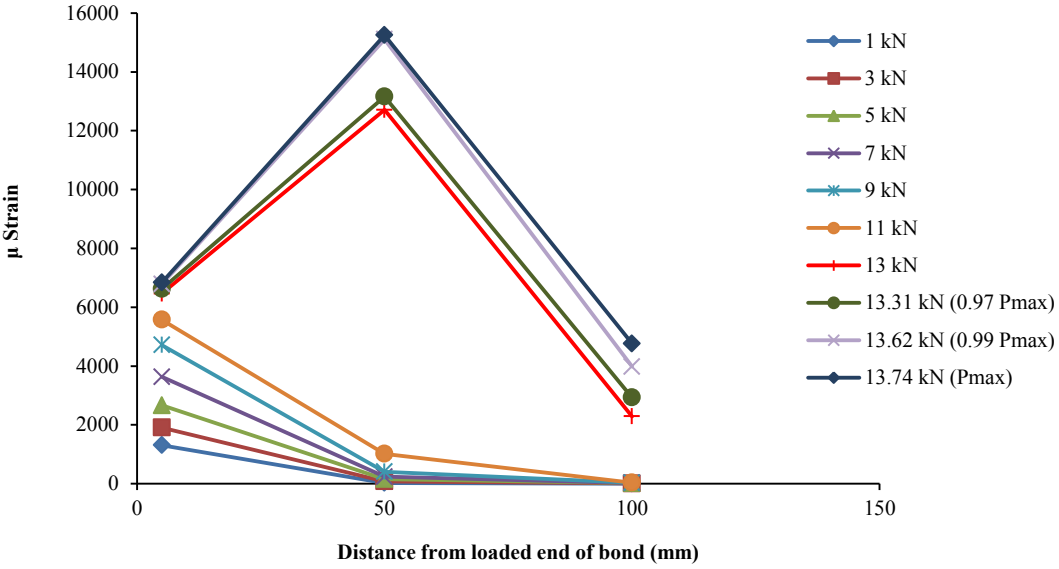

(d) GControl-4

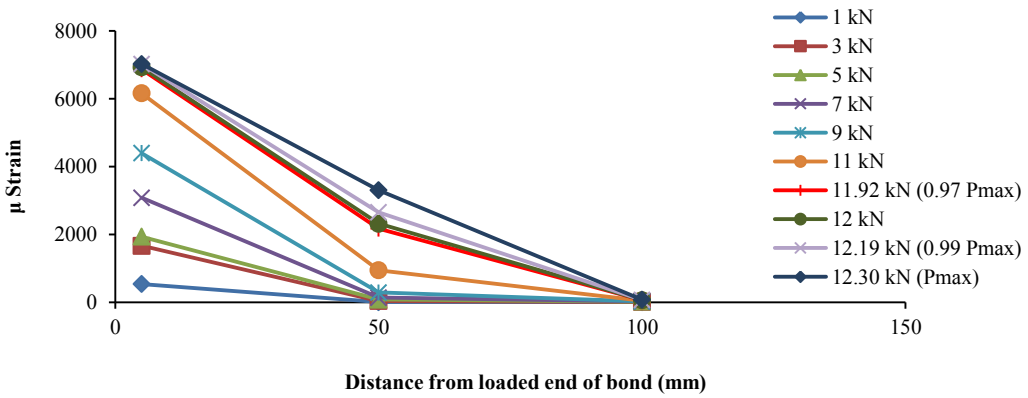

(e) GControl-5

Figure 3.32 Strain profiles of GFRP control pull-out specimens

3.9 Chapter summary

This chapter aimed to explain the methodologies involved in the long term experimental study of CFRP and GFRP-concrete bond as well as the material properties. In addition, behaviour of CFRP tensile properties and two batches of concrete for three environmental exposures, namely, temperature cycles, wet-dry cycles and outdoor environment, was discussed. The test results of control pull-out specimens were also presented in this chapter. The findings of the study can be summarised as follows:

- Temperature cycles did not cause any negative effect on CFRP tensile modulus of elasticity but tensile strength was found to degrade with time. The maximum degradation of tensile strength observed was 14.3 %.

- Wet-dry series caused deterioration of both tensile strength and elastic modulus of CFRP coupons. The maximum degradation of tensile strength was 20 % and that for tensile modulus of elasticity was 15.2 %.

- CFRP tensile strength degraded by 20.3 % due to outdoor environment but the tensile modulus of elasticity showed negligible deterioration of only 6.6 %.

- Concrete compressive strength of only batch 1, subjected to temperature cycles, experienced initial degradation of 9 % compared to control value after three months. However, other exposure conditions applied in this study did not cause any degradation of concrete compressive strength; rather, improved the strength.

- The mean pull-out strength of control CFRP-concrete bond was 1,298.7 and 1,320.0 MPa for the first and second concrete batch, respectively. On the other hand, control GFRP-concrete bond had the pull-out strength value of 1,027.0 MPa

- Failure modes of control pull-out specimens (both CFRP and GFRP) were associated with thick concrete layer attached to debonded FRP.

- Strain profiles of control CFRP and GFRP-concrete bond were mainly distributed over 0-50 mm bond length until the load value reached close to the maximum. The effective bond length can be assumed as 100 mm or less for both types of bond.

CHAPTER 4

EFFECT OF CYCLIC TEMPERATURE ON FRP-CONCRETE BOND

4 Effect of cyclic temperature on FRP-concrete bond

4.1 Introduction

This chapter presents the results of the experimental study on the long-term performance of CFRP and GFRP bonded concrete prisms subjected to temperature cycles. FRP-concrete bond behaviour has been studied based on the pull-out test. Pull-out strengths, failure modes and strain profiles (strain distributions) of CFRP and GFRP bonded specimens are presented. Also, correlation of bond strengths with the material properties has been described in this chapter. Section 4.2 describes the observations from CFRP cyclic temperature specimens, whereas section 4.3 is dedicated to the results of GFRP cyclic temperature specimens. Finally, the chapter summary has been presented in section 4.4.

4.2 Test results of CFRP cyclic temperature series

Experimental results of CFRP-concrete bond exposed to temperature cycles for five weeks (CT2 series), three months (CT3 series) and one year (CT4 series) are discussed in the following sections.

4.2.1 Pull-out strength

The pull-out strengths of CFRP-bonded concrete prisms were determined for CT2, CT3 and CT4 series by testing three specimens per series. The strength values (expressed as maximum stress in CFRP) of all specimens with coefficient of variation (CoV) have been summarised in Table 4.1. The strength value of one out of three specimens for CT4 series has been ignored for the calculation of mean strength due to the failure in the grip region. The change of normalised mean pull-out strength and mean concrete compressive strength (expressed as the ratio of exposed strength to control strength) has been plotted in Figure 4.1 where the vertical lines represent the standard deviations of pull-out strengths. No significant effect of the temperature cycles on the pull-out

strength was observed. An initial increase of strength of 5% was observed after five weeks followed by a descending trend and the strength value reached close enough to the control value after 3 months. After 1 year, bond strength increased by 10% compared to that of control specimens. Such effect of the temperature cycles can be attributed to the maximum temperature limit (40^{o} C) which is fairly below the glass transition temperature (T_g = 47^{o} C) of the epoxy resin. Also, the temperature envelope applied in this research was 30^{o} - 40^{o} C where the difference between the maximum and minimum temperature was only 10^{o} C. Hence, a larger temperature envelope may show degradation of CFRP-cocnrete bond as it may induce more strains (thermal expansion and contraction). The trend of concrete compressive strength was similar to that of pull-out strength and it is understood that pull-out strength is influenced by the change in conrete compressive strength due to exposed condition. The dependence of pull-out strength is further discussed in section 4.2.4 through the failure modes of CFRP-concrete bond.

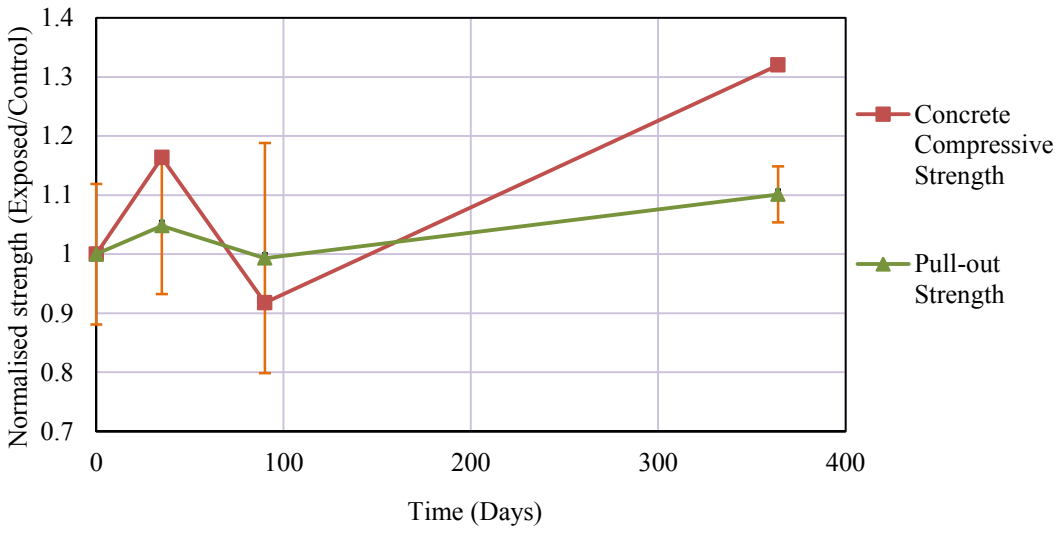

Figure 4.1 Normalised pull-out strength of CFRP cyclic temperature series against exposure duration

Table 4.1 CFRP Pull-out strengths of cyclic temperature specimens

Exposure duration (Days)	Pull-out strength (MPa)	Mean pull-out strength (MPa)	CoV of pull-out strength (%)	Comments
0	1183.3	1298.7	12.0	-
	1563.9			-
	1213.4			-
	1322.5			-
	1210.3			-
35	1440.9	1360.9	11.0	-
	1187.7			-
	1454.2			-
90	1059.8	1290.1	19.6	-
	1248.1			-
	1562.5			-
365	1473.8	1430.0	4.3	
	-			Failure in grip and omitted from analysis
	1386.1			

4.2.2 Failure modes

The change of failure modes due to cyclic temperature, even after the exposure period of one year, was insignificant and there was minimal reduction in the thickness of the concrete on separated CFRP only for three months exposure series. The failure occurring always in concrete layer, leads to the conclusion that concrete was always the weakest of all three constituents, namely, CFRP, epoxy resin and concrete. The failure modes of the each series have been discussed as follows:

- **CT2 series:**

The failure modes of the 5 week temperature (CT2) series were mainly in the concrete layer (Figure 4.2 (a)) and the concrete attached to debonded FRP was thicker than the

control specimens. However, for specimen CT2-3 (Figure 4.2 (b)) epoxy layer was visible in some parts of the FRP.

- **CT3 series:**

CT3 (three month cyclic temperature) series exhibited failure in concrete which was similar to the control series. But a slight reduction of concrete thickness was observed for two specimens (Figures 4.2 (d) and 4.2 (e)) compared to CT2 series and epoxy layer was visible in some locations of the debonded FRP. Only the failure of CT3-1 (Figure 4.2 (c)) was associated with very thick concrete layer attached to the debonded CFRP similar to CT2 series.

- **CT4 series:**

Similar to CT2 and CT3 series, CT4 series also failed with very thick concrete layer attached to debonded FRP (Figure 4.2 (g)). An exceptional mode of failure occurred in CT4-1 as it failed both by debonding and by partial longitudinal fracture of FRP along one edge (Figure 4.2 (f)). The reason for the partial fracture may be attributed to improper gripping of FRP, which was also reported by Imani (2010). Regardless of the unusual failure pattern of this specimen, the debonded FRP was found to have a thick concrete layer attached to it. Specimen CT4-2 was discarded from the analysis as the failure occurred in grip region (Figure B.1 in Appendix B.1).

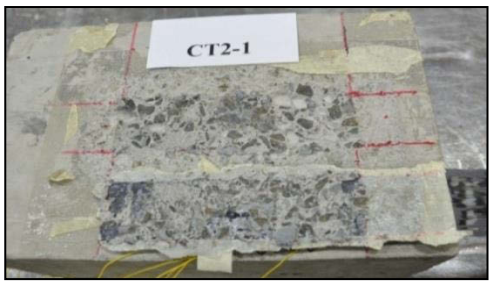

(a) CT2-1

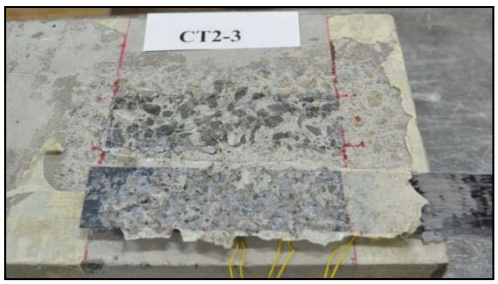

(b) CT2-3

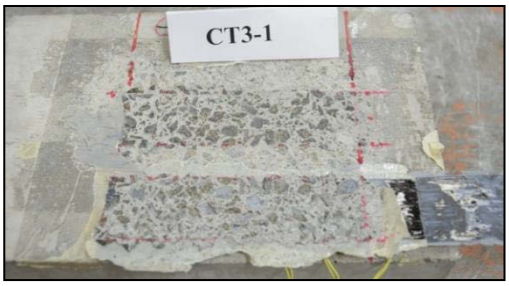

(c) CT3-1

(d) CT3-2

(e) CT3-3

(f) CT4-1

(g) CT4-3

Figure 4.2 Failure modes of CFRP cyclic temperature specimens

4.2.3 Strain profiles

The strain profiles for CT2 and CT3 series were plotted for three strain gauges, located at 5 mm, 50 mm and 100 mm from the loaded end (Figure 4.3 (a)), whereas those for CT4 series were plotted for four strain gauges located at 5 mm, 50 mm, 100 mm and 145 mm (Figure 4.3 (b)).

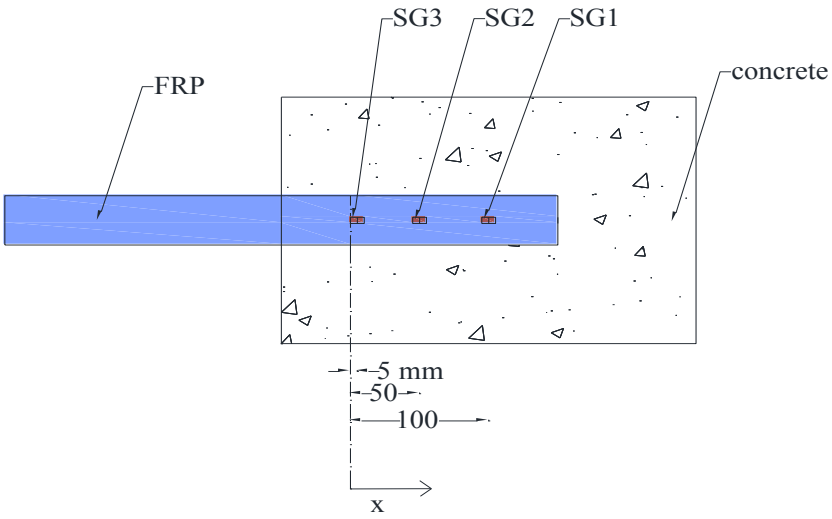

(a)

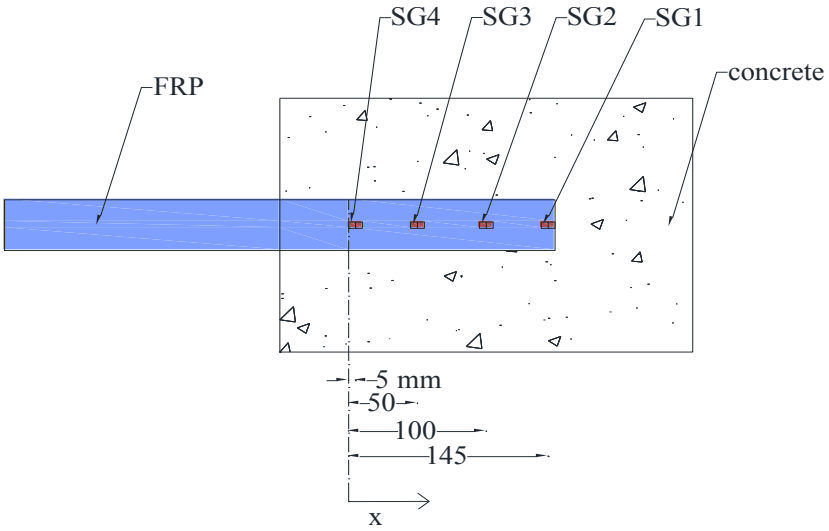

(b)

Figure 4.3 Strain gauge locations

- **CT2 series:**

The strain distributions of five week temperature (CT2) series have been plotted in Figure 4.4. The patterns of strain distribution for all specimens of this series were almost similar to those obtained for CFRP control specimens as provided in section 3.8.1.3. The initial load transfer length was approximately 50 mm up to the load level very close to ultimate load for all specimens. The changes of transfer length occurred at about 11 kN and 13.20 kN in specimens CT2-1 and CT2-3, respectively. But CT2-2

showed the shifting of transfer lengths at lower load value of 9 kN. Based on the definition of Yuan et al. (2004), the effective bond length can be assumed as 100 mm or less for specimen CT2-2 and CT2-3 and slightly more than 100 mm for specimen CT2-1. However, considering the load transfer length at 99% of the maximum load (Lu et al. 2005), the effective bond length of specimens CT2-1 and CT2-3 exceeded 100 mm whereas that of specimen CT2-2 was 100 mm or less.

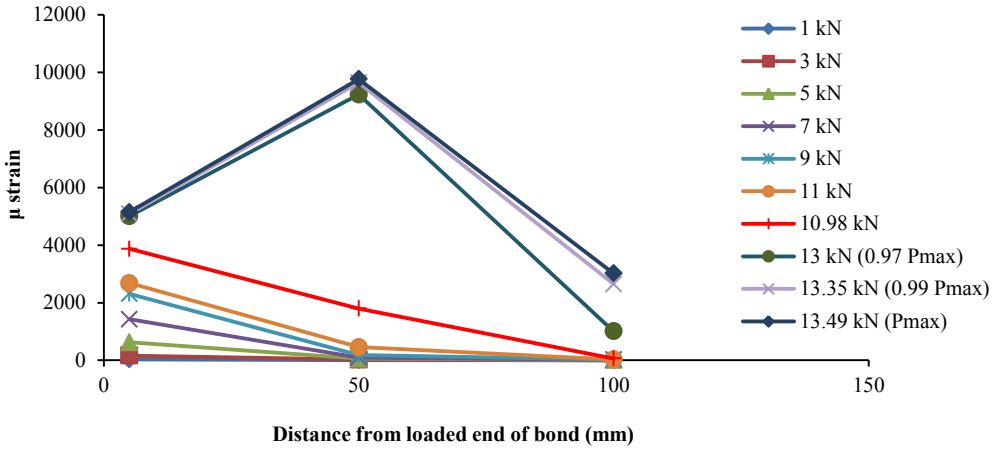

(a) CT2-1

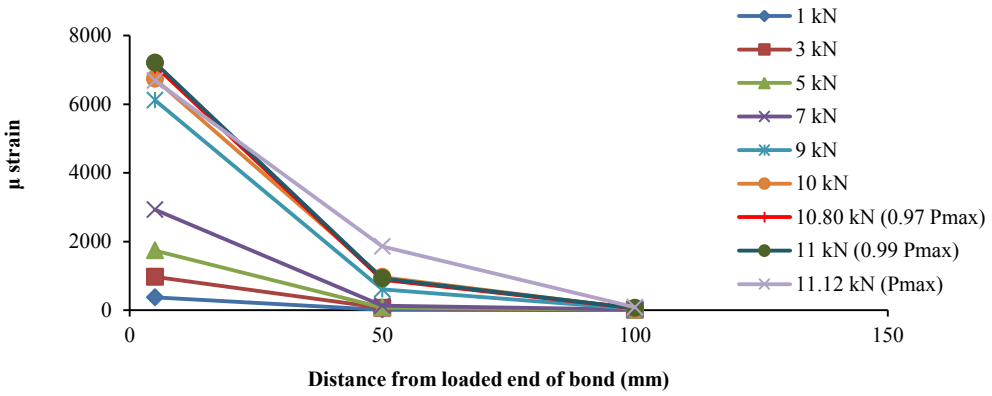

(b) CT2-2

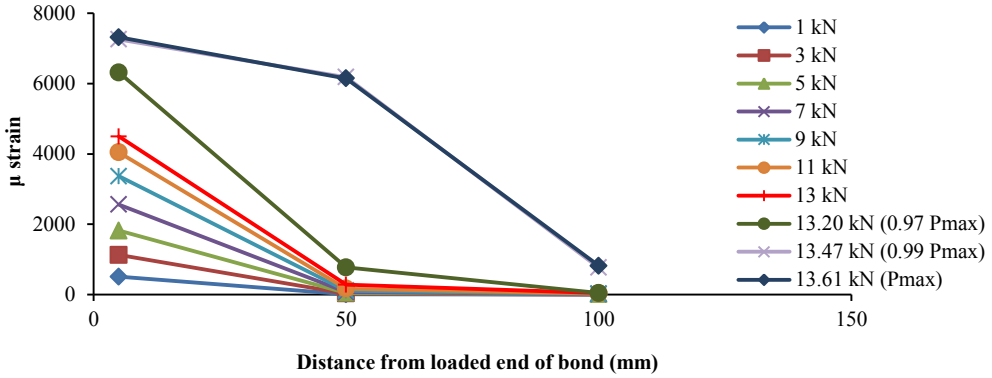

(c) CT2-3

Figure 4.4 Strain profiles of five week CFRP temperature series

- **CT3 series:**

As illustrated in Figure 4.5, the strain profiles of three month cyclic temperature specimens (CT3 series) showed similar behaviour to those of five week temperature (CT2) series except for CT3-1 (Figure 4.5 (a)) which was associated with shifting of initial load transfer length at lower load value of 8 kN. Specimens CT3-2 and CT3-3 experienced the change of initial transfer length at 11 kN and 13.5 kN, respectively (Figures 4.5 (b) and (c)). But the overall trend was retaining the initial transfer length of 50 mm until the load approaches close to the ultimate load, which is exactly as same as observed in the CT2 series. The effective bond length estimated from the strain distributions was 100 mm for CT3-1 and CT3-3 but it was more than 100 mm for CT3-2.

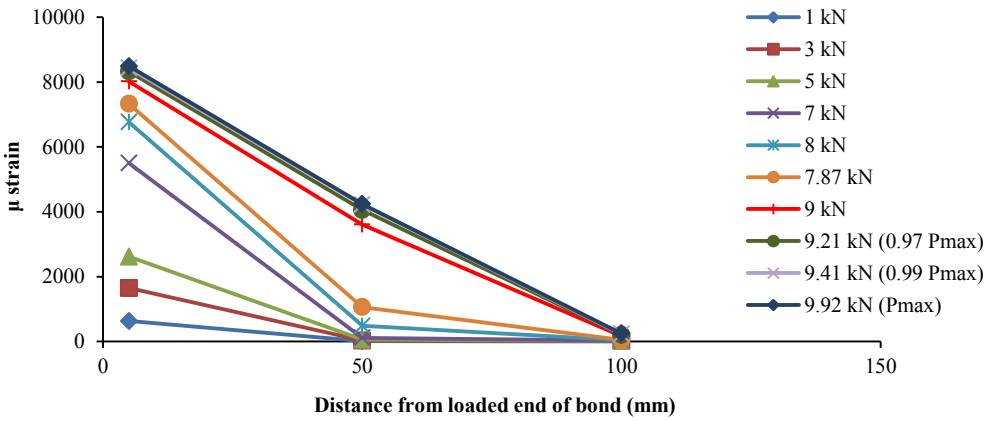

(a) CT3-1

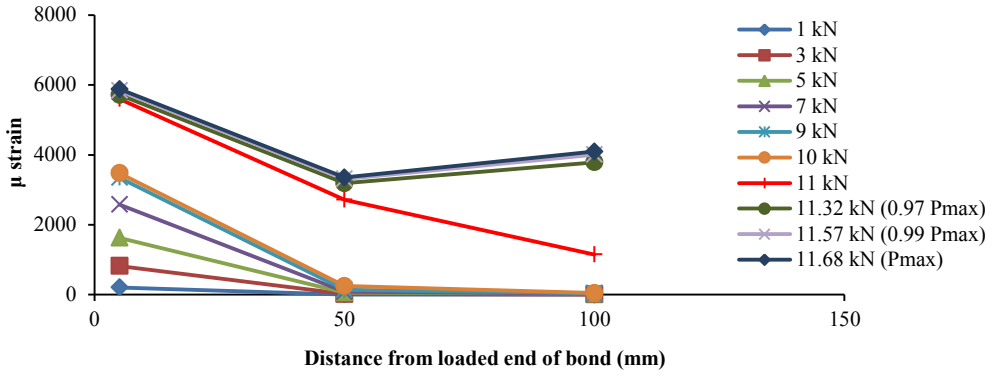

(b) CT3-2

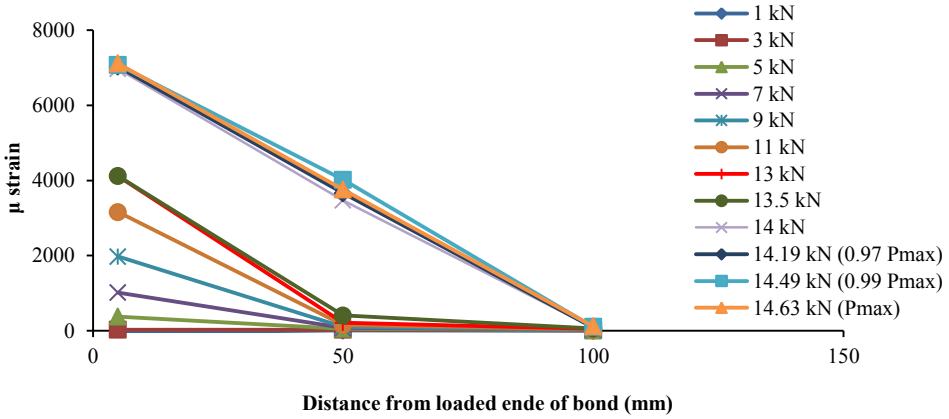

(c) CT3-3

Figure 4.5 Strain profiles of three month CFRP temperature series

- **CT4 series:**

Although three specimens were tested for this series, specimen CT4-2 experienced failure in grip part and was omitted from the analysis of test data.

As observed in Figure 4.6 (a), the strain gauge value at 5 mm from loaded end of specimen CT4-1 was only available up to 7 kN load due to the breaking of strain gauge caused by partial rupture of FRP at that location. However, the change of initial transfer length can be assumed from the available test data. The shifting of initial load transfer length from 50 mm to 100 mm occurred at a very low level of load (approximately at 5 kN) for this specimen which can be attributed to the initiation of CFRP rupture close to that location resulting in the reduction of the capacity to transfer load to concrete. The change of load transfer length approximately from 100 mm to 145 mm (or less)

occurred at 13 kN load. Unlike specimen CT4-1, CT4-3 showed strain profiles distributed only along 50 mm length until the load reached close to ultimate load (Figure 4.6 (b)). The initial transfer length changed from 50 mm to 100 mm at 12.24 kN and no further change of load transfer length was observed. The strain distribution of CT4-3 was very similar to those observed in the previous two series. From the strain profile, the effective bond length of CT4-1 can be assumed as more than 100 mm and less than or equal to 145 mm whereas that for specimen CT4-3 was 100 mm or less (Figure 4.6 (b)).

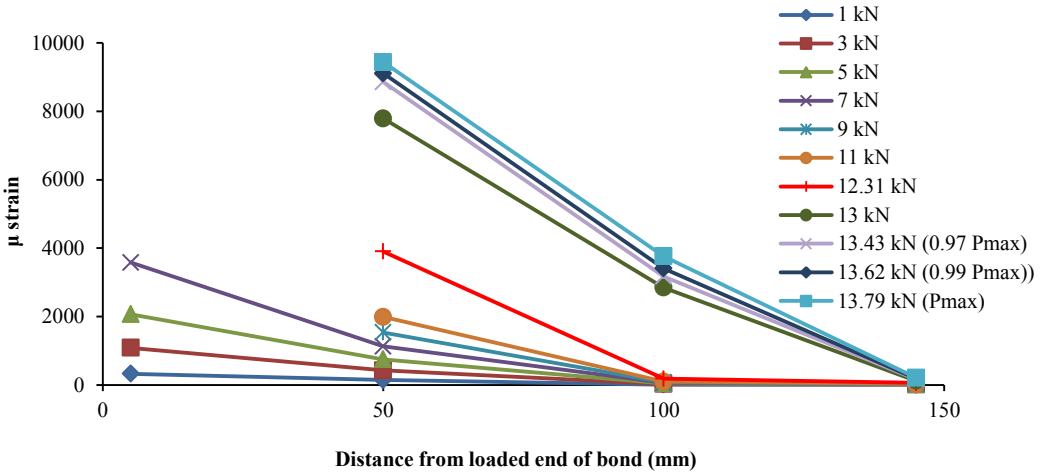

(a) CT4-1

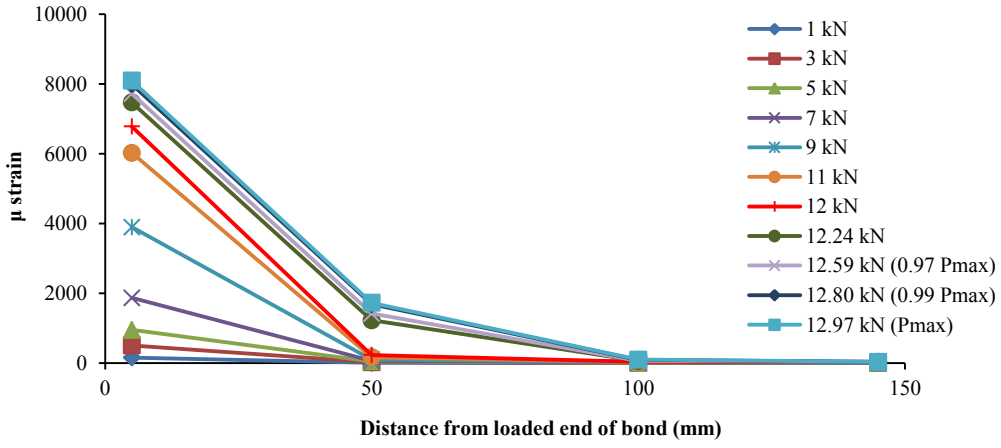

(b) CT4-3

Figure 4.6 Strain profiles of one year CFRP temperature series

4.2.4 Discussion of test results

Based on the test results of CFRP cyclic temperature series, it can be commented that the temperature cycles did not cause any negative effect on the pull-out strength with the exception of only 1% initial deterioration after three months of exposure. As the failure of pull-out specimens always occurred in the concrete adjacent to the epoxy adhesive, the strength of bond were mainly dependent on the concrete compressive properties. This can be confirmed by the trend of concrete compressive strength with exposure durations (described in section 3.7.2.1) observed in this study which was quite similar to that of pull-out strength with time (Figures 4.1). Also, no major change of strain profiles of pull-out specimens was observed. But the increase of effective bond length due to exposure to five weeks of temperature cycles suggests that longer bond length than the effective bond length of unexposed specimens should be used for better performance of CFRP-concrete bond. As the temperature envelope applied in this research was 30^{o} – 40^{o} C with a very small difference between the upper and lower limit, the possibility of bond degradation due to larger envelope cannot be ignored.

4.3 Test results of GFRP temperature series

The test results of GFRP-concrete bond exposed to temperature cycles for five weeks (GT2 series), three months (GT3 series) and one year (GT4 series) have been presented in this section in terms of pull-out strength, failure modes and strain profiles.

4.3.1 Pull-out strength

Pull-out strengths of all GFRP cyclic temperature specimens with corresponding CoVs have been listed in Table 4.2 whereas the change of normalised average pull-out strength (expressed as the ratio of exposed strength to unexposed/control strength) with exposure duration has been illustrated in Figure 4.7. The vertical bars in the graph represent the CoV for the normalised average pull-out strength. Also, the change of normalised concrete compressive strength with exposure duration is shown in the same figure. From Figure 4.7, continuous increase in mean pull-out strength is clearly visible. The increase in bond strength can be divided into two parts where the first part is associated with a rapid increase of strength by about 3% after five weeks compared to

the control strength and the second part shows a gradual linear increase of bond strength until it reaches about 8% more than the control value after the end of the one year exposure. From the observations, it can be stated that the cyclic temperature did not cause any negative effect on pull-out strength of the GFRP specimens even after one year of exposure. Rather, it improved the strength during the whole exposure period. The increase in bond strength can be correlated with the increased compressive strength as shown in the same figure. Although a decreasing trend of concrete compressive strength is visible after three months, the strength value was always more than that of the control series. The gradual increase in pull-out strength after three months may be attributed to the negative trend of the concrete compressive strength.

Table 4.2 GFRP Pull-out strengths of cyclic temperature specimens

Exposure duration (Days)	Pull-out strength (MPa)	Mean pull-out strength (MPa)	CoV of pull-out strength (%)
0	1014.2	1027.0	6.0
	953.0		
	1054.5		
	1114.9		
	998.4		
35	1115.3	1055.8	5.5
	1053.7		
	998.5		
90	1051.9	1064.7	1.9
	1053.5		
	1088.6		
365	1109.3	1112.8	1.7
	1133.5		
	1095.6		

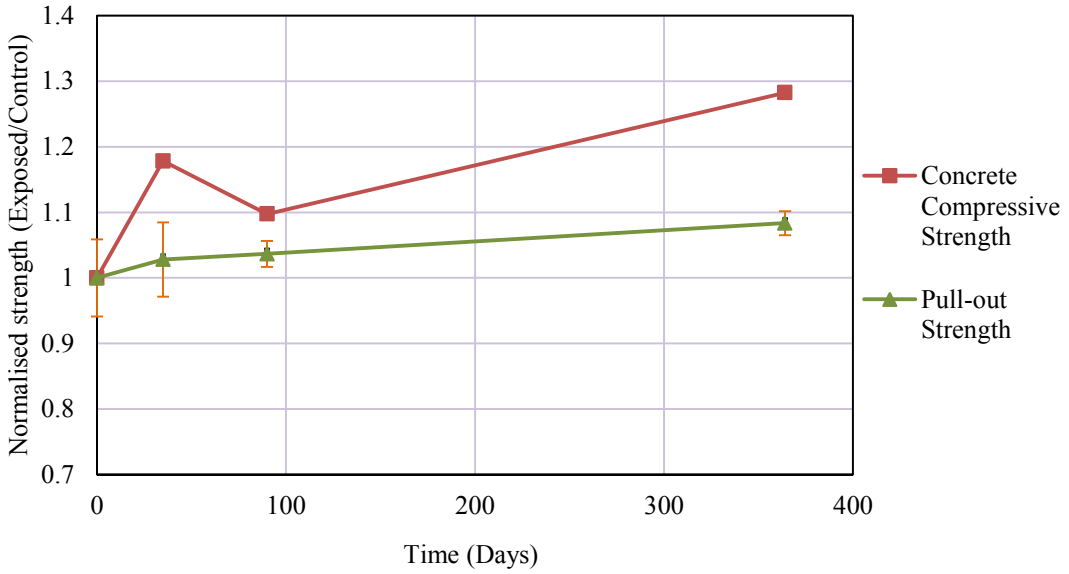

Figure 4.7 Normalised pull-out strength of GFRP cyclic temperature series against exposure duration

4.3.2 Failure modes

Figure 4.8 illustrates the failure modes of two GFRP cyclic temperature specimens per exposure duration and the rest are provided in Appendix B.2. The failure modes of GFRP cyclic temperature specimens were observed to be the same as those of CFRP cyclic temperature specimens.

- **GT2 series:**

Two specimens out of three of the five week temperature (GT2) series failed with very thick concrete layer attached to the debonded GFRP. Only GT2-3 specimen (Figure 4.8 (b)) had relatively thinner concrete layer.

- **GT3 series:**

GT3 (three month temperature) series showed a similar pattern of failure (Figure 4.8 (c)) to GT2 series.

- **GT4 series:**

Only one specimen in one year (GT4) series, namely, GT4-2 was found to have almost no concrete attached to the GFRP coupon (Figure 4.8 (e)). But the remaining two specimens exhibited exactly the same pattern as the other two series.

From the comparison of failure modes of all temperature series (Figure 4.8) with those of control series (section 3.8.2.2), the change of failure patterns with duration of exposure deemed to be insignificant as the failure always occurred mostly in the concrete adjacent to the epoxy layer.

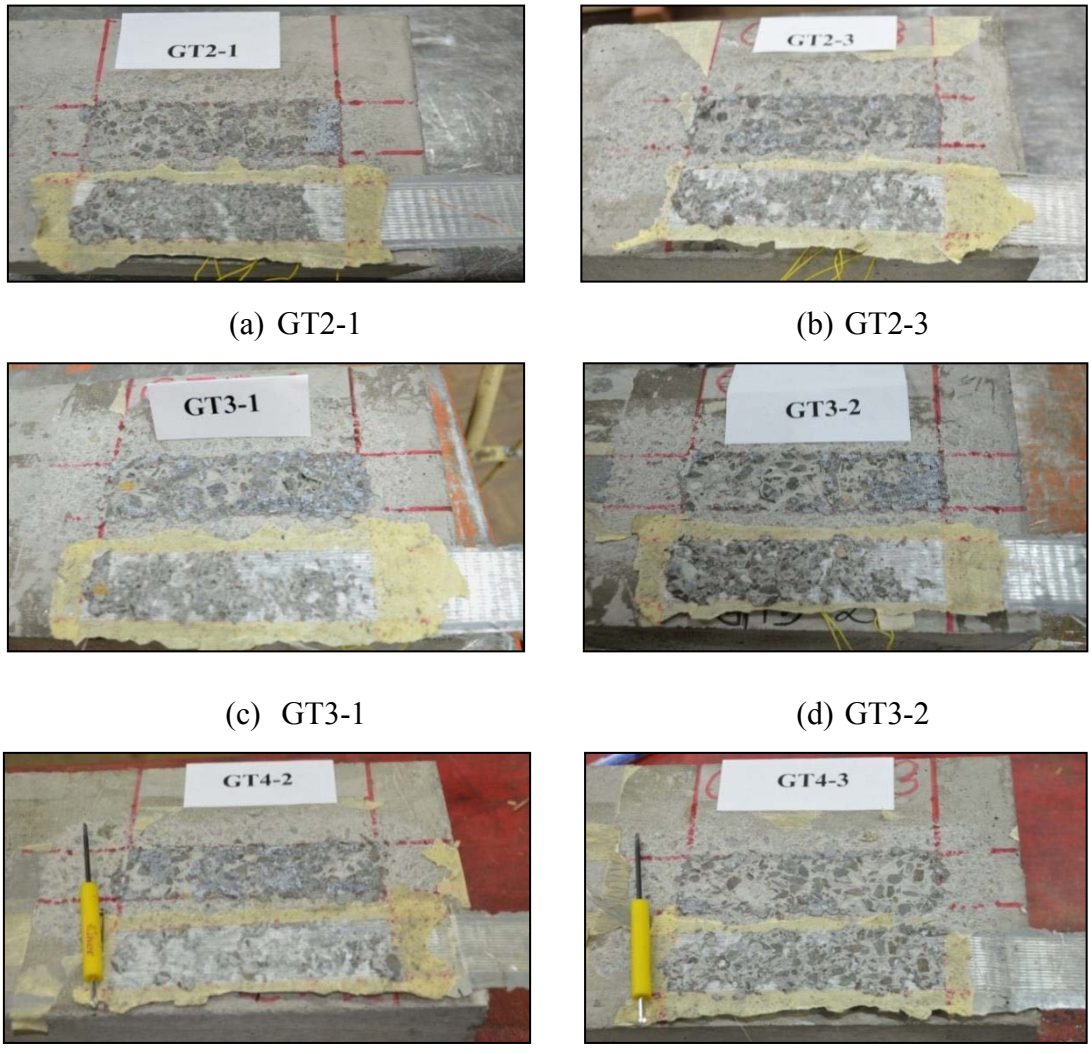

(a) GT2-1 (b) GT2-3

(c) GT3-1 (d) GT3-2

(e) GT4-2 (f) GT4-3

Figure 4.8 Failure modes of GFRP cyclic temperature specimens

4.3.3 Strain profiles

The strain profiles for GT2 and GT3 series were obtained by three strain gauge set-up (Figure 4.3 (a)), and those for CT4 series were obtained by four strain gauge set-up (Figure 4.3 (b)).

- **GT2 series:**

From the plotted strain profiles of five week temperature specimens (Figure 4.9) it can be observed that the initial load transfer length of about 50 mm remained unchanged for all three specimens until the load reached close to the ultimate load. The change of initial transfer length approximately from 50 mm to 100 mm occurred at 12.45 kN, 10.62 kN and 9.52 kN for specimens GT2-1, 2 and 3, respectively. The behaviour of strain profiles of five week GFRP temperature series seems to be almost similar to that found in GFRP control series. The effective bond lengths can be assumed from the definitions by Yuan et al. (2004) and Lu et al. (2005) as more than 100 mm for specimens GT2-1 and GT2-3 and 100 mm or less for specimen GT2-2. Therefore, the change of effective bond length can be seen when compared to the experimental effective bond length of control series where three out of five specimens had effective bond length of 100 mm or less.

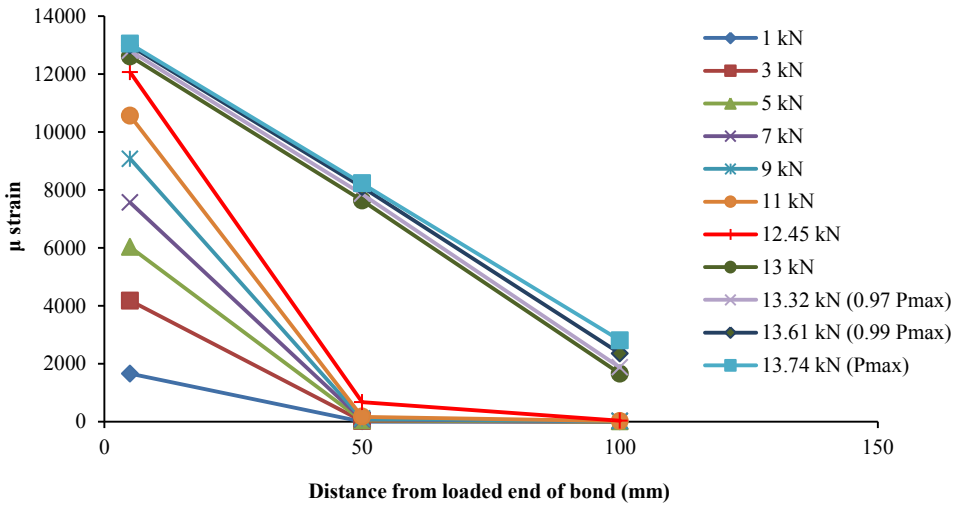

(a) GT2-1

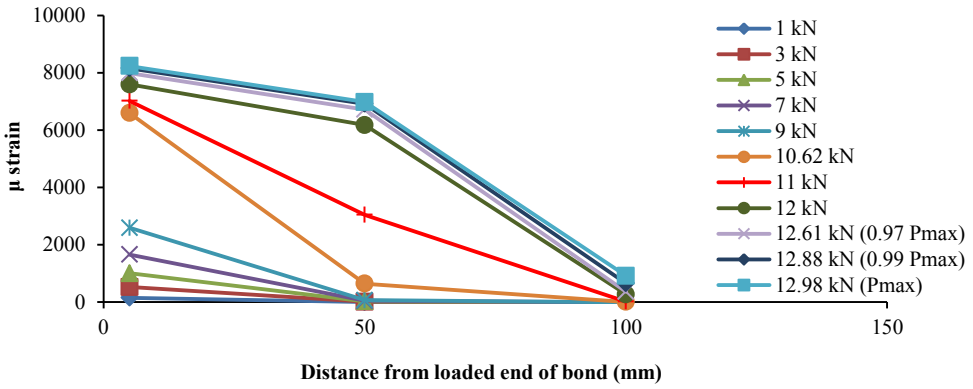

(b) GT2-2

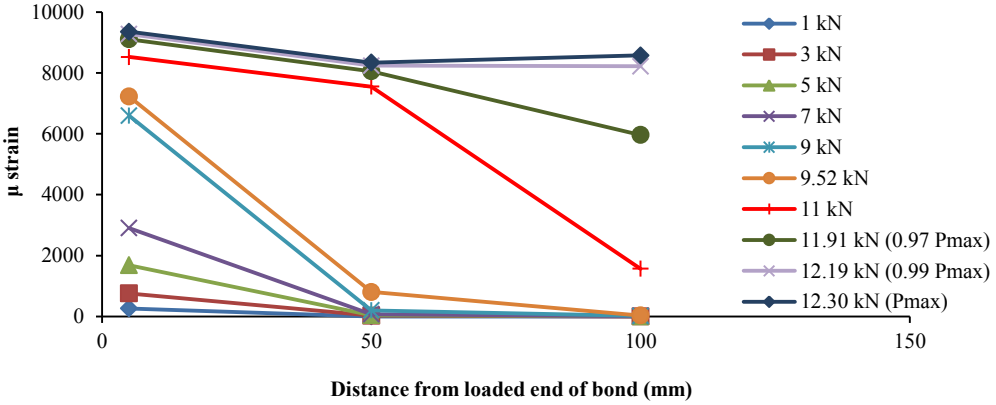

(c) GT2-3

Figure 4.9 Strain profiles of five week GFRP temperature series

- **GT3 series:**

As illustrated in Figure 4.10, strain profiles of three month GFRP cyclic temperature were similar to the control and five week temperature series. The initial load transfer length shifted approximately at 11 kN loads for specimens GT3-1 and GT3-2 and at about 13 kN load for GT3-3. The experimental effective bond lengths can be considered as more than 100 mm for the first two specimens and less than 100 mm for the third one and are exactly as same as those with five week temperature series.

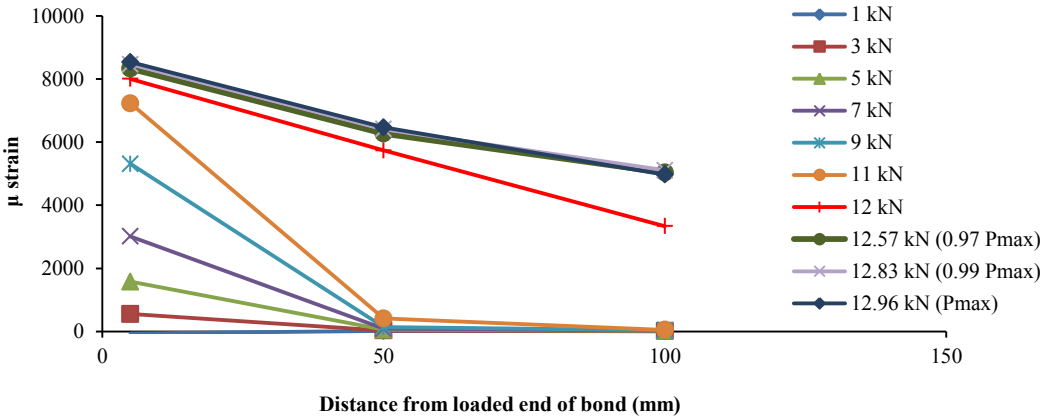

(a) GT3-1

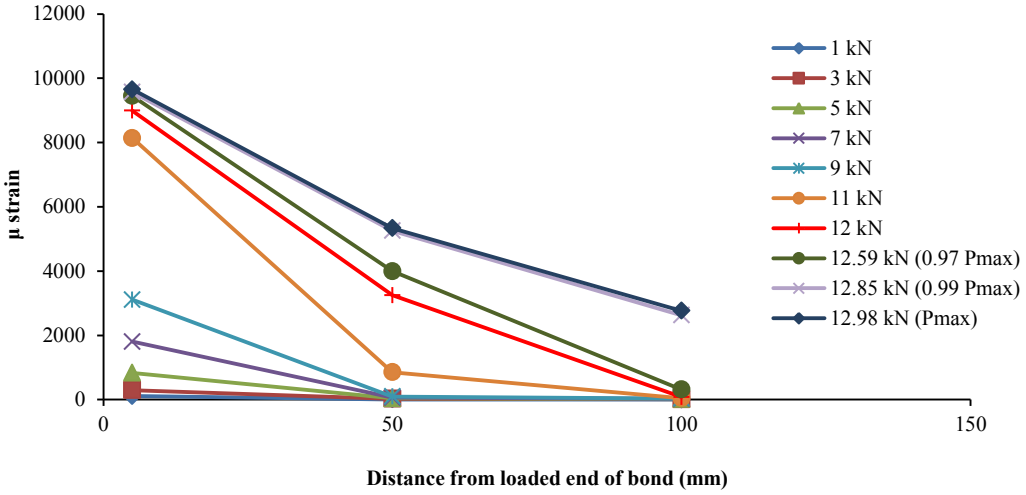

(b) GT3-2

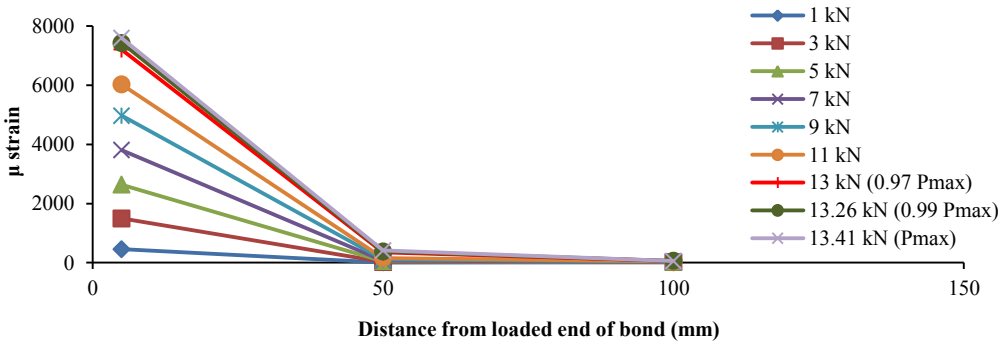

(c) GT3-3

Figure 4.10 Strain profiles of three month GFRP temperature series

- **GT4 series:**

From the plotted strain profiles of one year GFRP cyclic temperature series (Figure 4.11), it can be observed that the load transfer length changed approximately from 50 mm to 100 mm after the load values reached 9.42, 10 and 12.49 kN for specimens GT4-1, 2 and 3, respectively. Then another change of load transfer length is visible from 100 mm to about 145 mm after 13.24 and 13 kN for specimens GT4-1 and GT4-2. Specimen GT4-3 experienced a drop in load after the shifting of transfer length from 50 mm to 100 mm and the second change of transfer length occurred at 12.22 kN. Based on the definitions of effective bond length by Yuan et al. (2004) and Lu et al. (2005), all specimens from one year series had effective bond length of more than 100 mm.

Based on the strain profiles of GFRP temperature series, it can be summarised that although the overall behaviour of strain distributions were quite similar to the control series, the effective bond length exceeded 100 mm which was longer than that in control series.

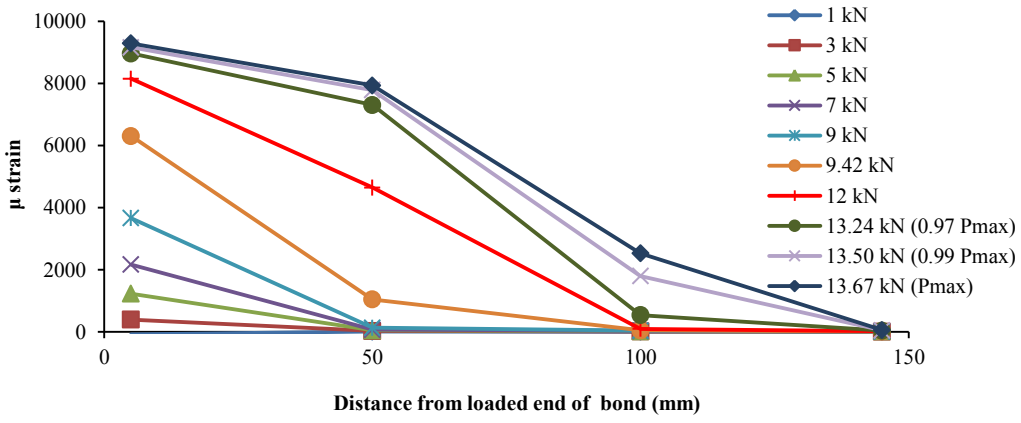

(a) GT4-1

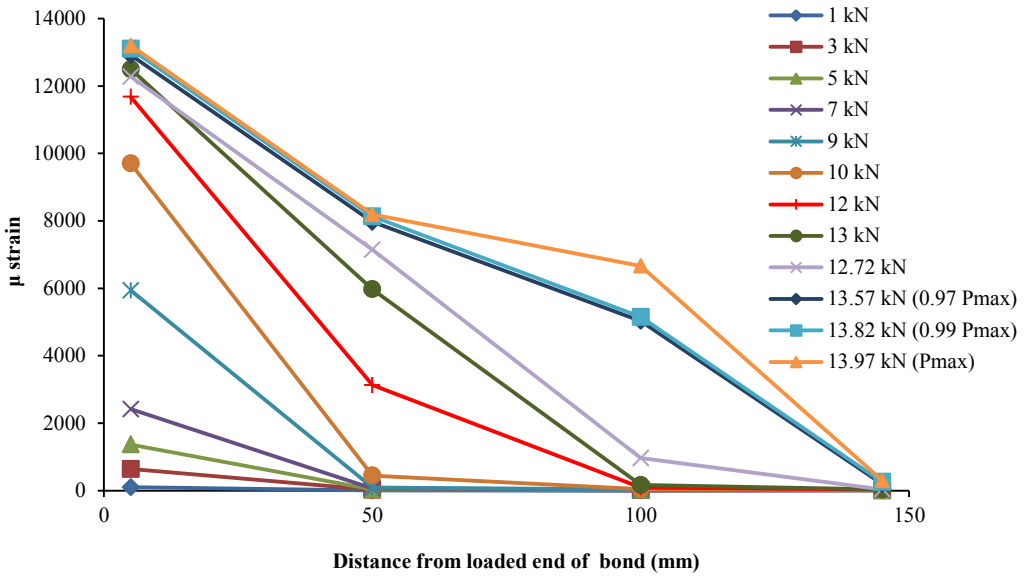

(b) GT4-2

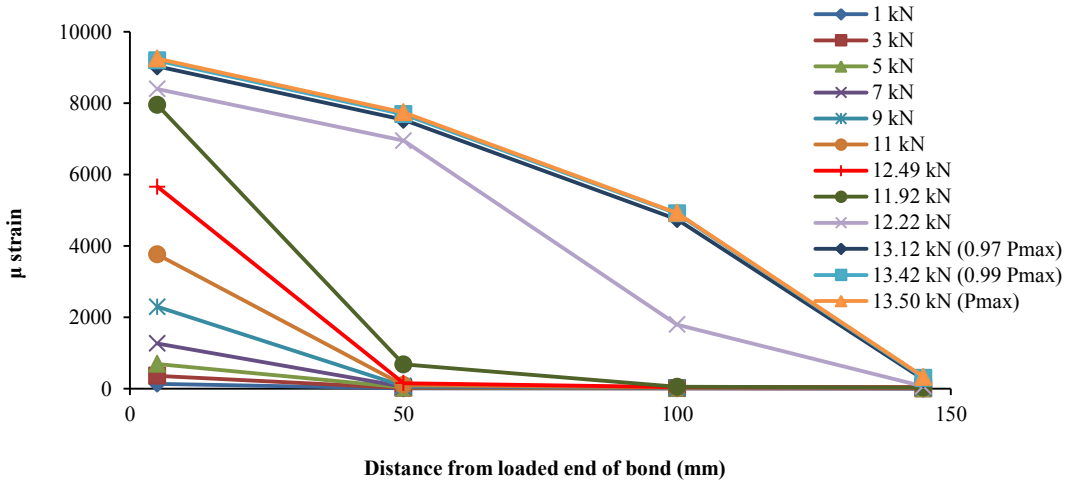

(c) GT4-3

Figure 4.11 Strain profiles of GFRP one year temperature series

4.3.4 Discussion of test results

It is obvious from the test results that the temperature cycles did not cause any reduction of pull-out strength for the GFRP specimens. In fact, the temperature cycles helped to improve the strength provided that the highest temperature (40^{o} C) applied in this study was less than the glass transition temperature of the epoxy resin and the temperature envelope was 30^{o} – 40^{o} C. The gaining of bond pull-out strength can be attributed mainly to the increasing concrete compressive strength (Figure 4.7) with time as the

failure always occurred in the concrete layer adjacent to the epoxy adhesive. However, as GFRP-concrete bond consists of GFRP, epoxy resin and concrete, material characterisation of all three constituents is necessary to understand the effect of material properties on the bond behaviour properly. The effective bond length obtained from the strain distribution plots suggests that the temperature cycles may increase the bond length in the long term and thereby, using longer bond length may improve the performance of GFRP-concrete bond subjected to such environmental condition.

4.4 Chapter summary

Based on the results of the experimental study conducted to understand the effect of cyclic temperature on CFRP and GFRP-concrete bond, the findings were as follows:

- Temperature cycles caused negligible deterioration (by 1% after three months) of CFRP-concrete bond and no degradation of GFRP-concrete bond provided the maximum temperature was always lower than the glass transition temperature (+ 47^{o} C) of the epoxy resin and the difference between the maximum and minimum temperature of the temperature envelope (30^{o}–40^{o} C) was only 10^{o} C.
- No significant change of failure modes was observed in CFRP and GFRP bonded specimens, which suggests the dependence of pull-out strength mainly on the concrete compressive strength.
- Effective bond length increased due to exposed condition for both types of FRP-concrete bond.

From the findings stated above, it can be concluded that although the temperature cycles had insignificant effect on the CFRP and GFRP-concrete bond, the cyclic temperature with a larger envelope may need to be applied for further understanding of the effect of temperature cycles on bond behaviour. Also, for better correlation of pull-out strength with material properties, the study on the adhesive properties subjected to temperature cycles should be conducted. Moreover, as the effective bond length increased due to temperature cycles, higher bond length than theoretical effective bond length for unexposed condition can be conducive to the CFRP and GFRP-concrete bond system to perform better in the long term.

CHAPTER 5

EFFECT OF WET-DRY CYCLES ON FRP-CONCRETE BOND

5 Effect of wet-dry cycles on FRP-concrete bond

5.1 Introduction

The test results of CFRP and GFRP bonded concrete prisms exposed to wet-dry cycles are discussed in this chapter in terms of pull-out strength, failure modes and strain profiles. The effect of material properties on the pull-out strength is also explained from the observed failure patterns of two types of FRP-concrete bond and the change of material properties due to exposed condition. Section 5.2 is dedicated to results of CFRP bonded specimens, whereas section 5.3 reports on the findings of GFRP bonded specimens. In section 5.4, the chapter summary has been presented based on the findings of the study.

5.2 Test results of CFRP wet-dry series

Experimental results of CFRP-concrete bond exposed to wet-dry cycles for one month (CH1 series), six months (CH2 series), 12 months (CH3 series) and 18 months (CH4 series) are discussed in the following sections.

5.2.1 Pull-out strength

The pull-out strength values of all specimens with coefficient of variation (CoV) have been listed in Table 5.1 and the change of mean pull-out strength (expressed as the ratio of exposed strength to unexposed/control strength) against exposure durations has been illustrated in Figure 5.1 along with vertical lines representing the standard deviations. Figure 5.1 also includes the change of normalised concrete compressive strength with time to understand the effect of concrete compressive strength on the changing pull-out strength. The effect of wet-dry cycles on CFRP-concrete bond was of cyclic nature during 18 month exposure. CFRP-concrete bond experienced slight degradation of pull-out strength by about 1% after the exposure duration of one month followed by an increase of 12% compared to the control strength. However, exposure duration of one

year showed the deterioration of pull-out strength by 5% compared to the control strength. Finally, an increasing trend can be observed from the plot with the bond strength reaching close to that of the control specimens after 18 months. Although the concrete compressive strength was observed to increase almost continuously during the exposure for 18 months, only the change of pull-out strength during two periods, namely, one month to six months and 12 months to 18 months, followed the trend of concrete compressive strength. But the pull-out strengths after one month and one year of exposure durations did not follow the trend of concrete compressive strength. The dependence of pull-out strength on the material properties is explained further in section 5.2.4 with the help of observed failure modes.

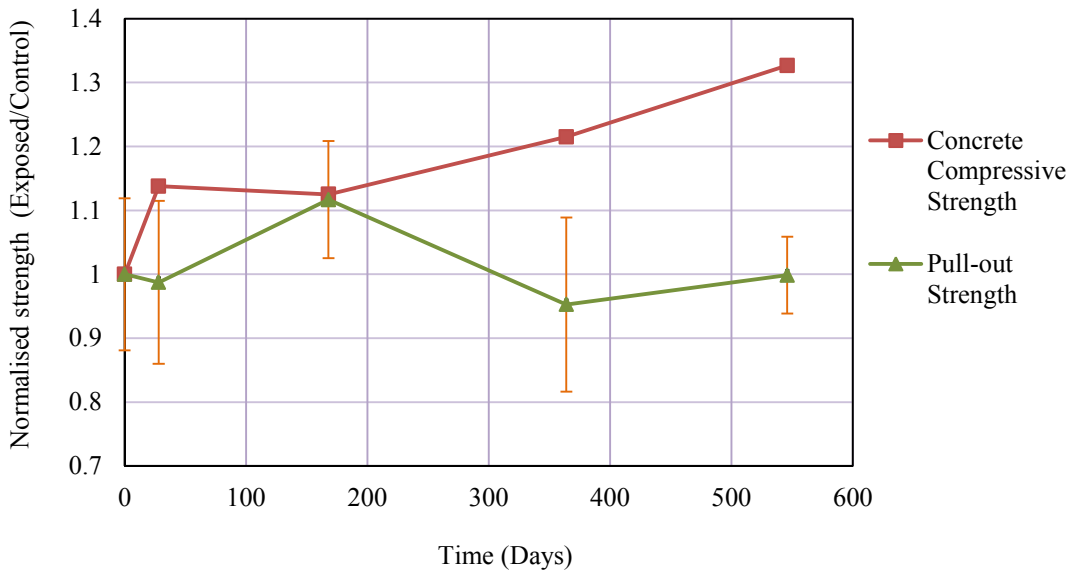

Figure 5.1 Normalised pull-out strength of CFRP wet-dry series against exposure duration

Table 5.1 CFRP Pull-out strengths of wet-dry specimens

Exposure duration (Days)	Pull-out strength (MPa)	Mean pull-out strength (MPa)	CoV of pull-out strength (%)
0	1183.3	1298.7	12.0
	1563.9		
	1213.4		
	1322.5		
	1210.3		
28	1300.7	1282.2	12.9
	1511.3		
	1107.4		
	1354.3		
	1137.3		
168	1433.3	1450.3	8.2
	1280.0		
	1430.0		
	1602.5		
	1505.8		
364	1063.9	1237.3	14.3
	1440.7		
	1238.0		
	1057.5		
	1386.4		
546	1356.3	1296.9	6.0
	1275.4		
	1345.2		
	1338.7		
	1169.0		

5.2.2 Failure modes

The typical failure patterns of CFRP wet-dry series along with any exceptional mode observed from each of the exposure durations have been provided in Figure 5.2 and the rest are shown in Appendix B.1.

- **CH1 series:**

The one month wet-dry specimens showed change of failure modes from the thicker concrete to very thin concrete layer attached to debonded CFRP (Figure 5.2 (b)) compared to control series (section 3.8.1.2). Moreover, epoxy layer was visible on some parts. Three out of five specimens had such failure pattern. As illustrated in Figure 5.2 (a), only CH1-1 had very thick concrete layer attached to the CFRP. Specimen CH1-5 experienced partial longitudinal rupture of CFRP close to one edge of bond apart from the failure with relatively thicker layer of concrete attached to the CFRP coupon (Figure 5.2 (c)).

- **CH2 series:**

Compared to CH1 series, failure modes of CH2 series were associated with relatively thicker layer of concrete attached to debonded CFRP. Therefore, the failure modes of CH2 series seem almost similar to those observed in control specimens. The typical failure mode of this series is represented by Figure 5.2 (f) where thick concrete layer is clearly visible. The exceptional modes were observed in specimens CH2-1 and CH2-2 (Figures 5.2 (d) and (e)) where the former had almost no concrete attached to the debonded CFRP, and the latter showed failure by partial longitudinal rupture of CFRP along one edge as well as by debonding with almost no concrete attached to FRP.

(a) CH1-1

(b) CH1-2

(c) CH1-5

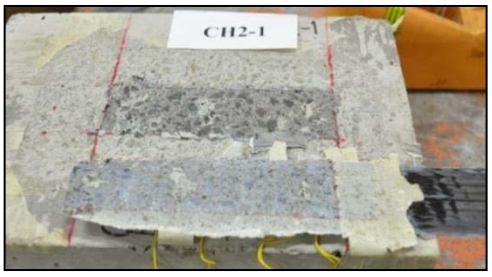

(d) CH2-1

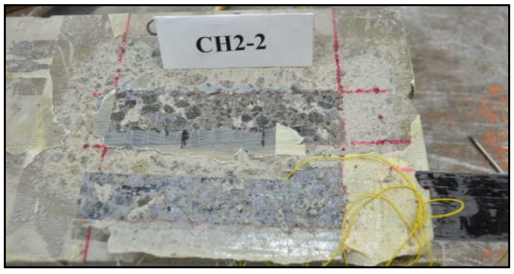

(e) CH2-2

(f) CH2-3

(g) CH3-2

(h) CH3-4

(i) CH3-5

(j) CH4-1

(k) CH4-2

(l) CH4-4

Figure 5.2 Failure modes of CFRP wet-dry specimens

- **CH3 series:**

The observations from the failure patterns of one year wet-dry specimens lead to an interpretation that the thickness of concrete layer on CFRP coupon decreased significantly compared to all previous series. Figure 5.2 (g) represents the typical failure mode observed in this series. Only CH3-4 had thick concrete layer on the debonded CFRP coupon (Figure 5.2 (h)) and CH3-5 experienced partial failure in CFRP by rupture as well as the typical failure of this series (Figure 5.2 (i)).

- **CH4 series:**

Except for CH4-2 as illustrated in Figure 5.2 (k), all specimens of 18 months wet-dry series exhibited very thick concrete layer attached to the debonded CFRP coupon. Epoxy layer was visible in some locations of CFRP coupon of specimen CH4-4, as shown in Figure 5.2 (l), but the thickness of concrete was still thick enough to resemble the typical mode of this series.

From the failure modes of all CFRP wet-dry series explained above, it can be stated that failure modes from thick concrete layer to thinner layer attached to debonded CFRP also revealed the cyclic nature similar to that observed in pull-out strength of this series.

5.2.3 Strain profiles

The strain profiles for CH1 and CH2 series were plotted for three strain gauges , located at 5 mm, 50 mm and 100 mm from the loaded end (Figure 5.3 (a)), whereas those for CH3 and CH4 were plotted for four strain gauges located at 5 mm, 50 mm, 100 mm and 145 mm from the loaded end (Figure 5.3 (b)).

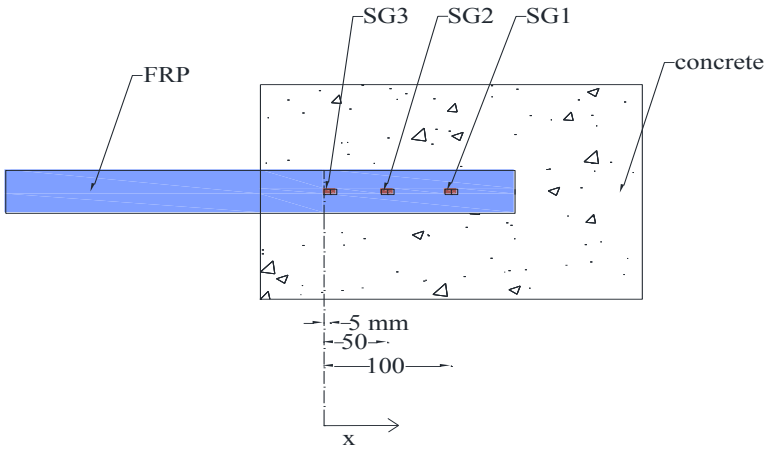

(a) Strain gauge locations for three strain gauge set-up

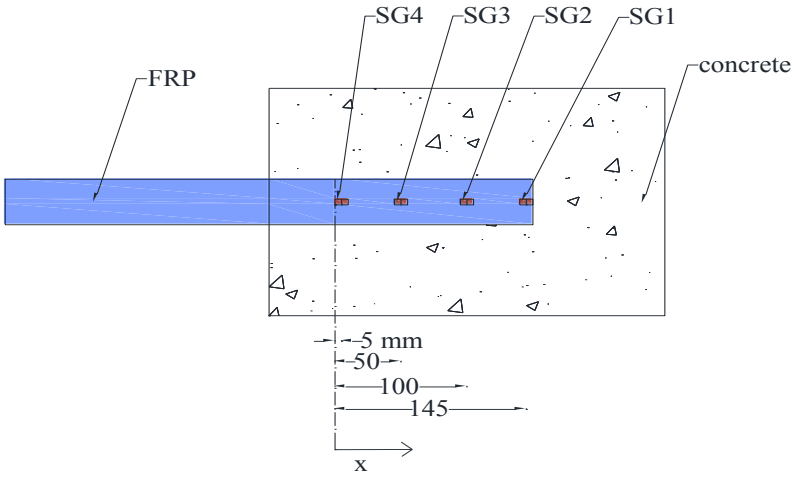

(b) Strain gauge locations for four strain gauge set-up

Figure 5.3 Strain gauge locations

- **<u>CH1 series</u>:**

The strain profiles of CH1 series (Figure 5.4) were found to show some changes from those of control series (section 3.8.1.3) in terms of loads at which the initial transfer length shifted from approximately 50 mm to 100 mm. Most control specimens experienced the change of initial load/stress transfer length at about 10-11 kN load, whereas CH1 series showed this change at a relatively lower level of load; i.e. 8-9 kN load. Only specimen CH1-5 had the change of initial transfer length at a load value more than 10 kN (Figure 5.4 (e)). In addition, higher effective bond length than that of control series was observed in CH1 series. The effective bond length of this series can

be assumed as more than 100 mm according to definitions by Yuan et al. (2004) and Lu et al. (2005).

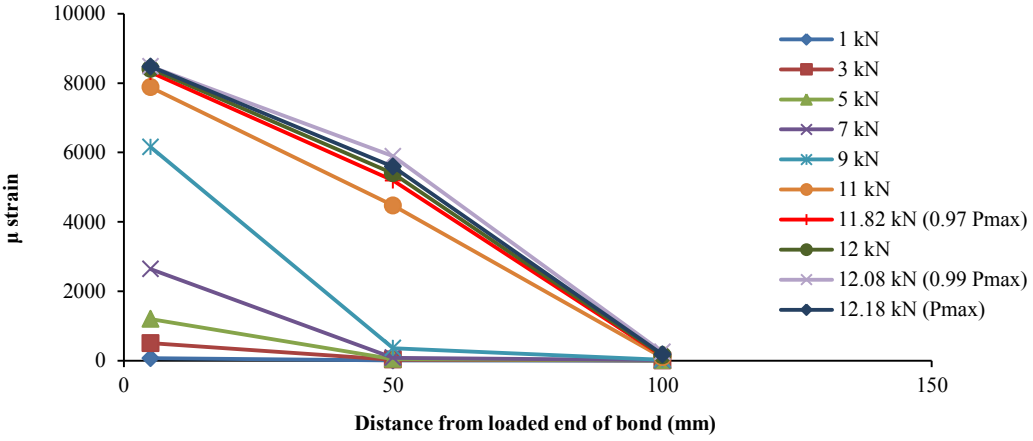

(a) CH1-1

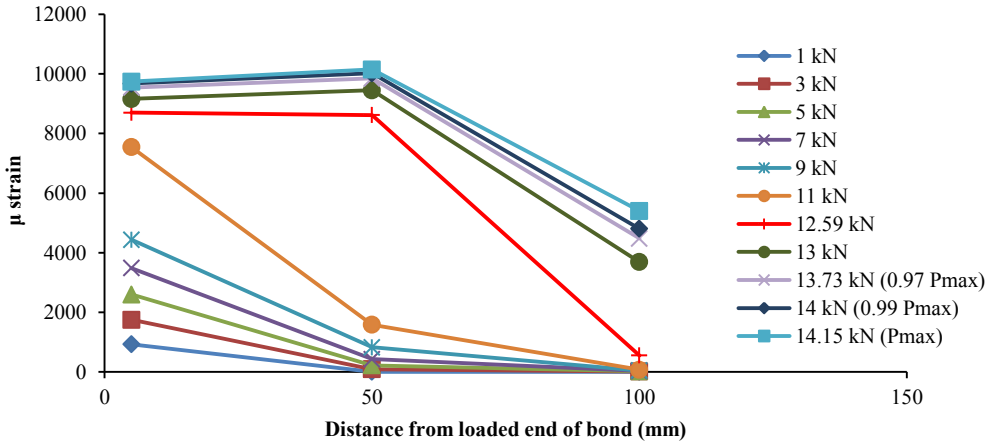

(b) CH1-2

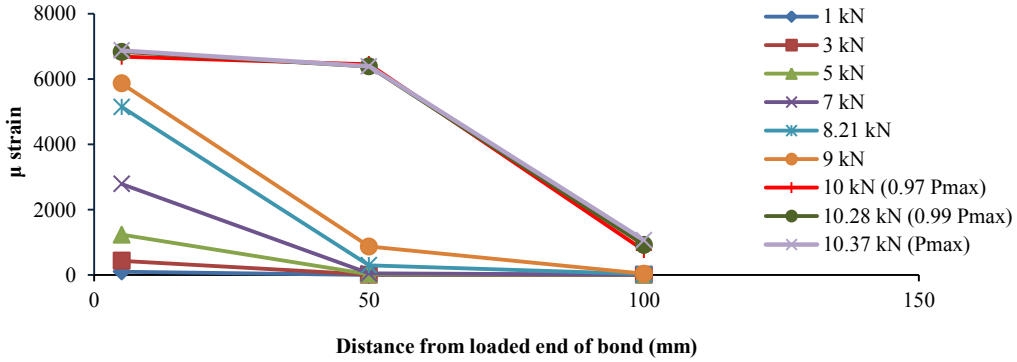

(c) CH1-3

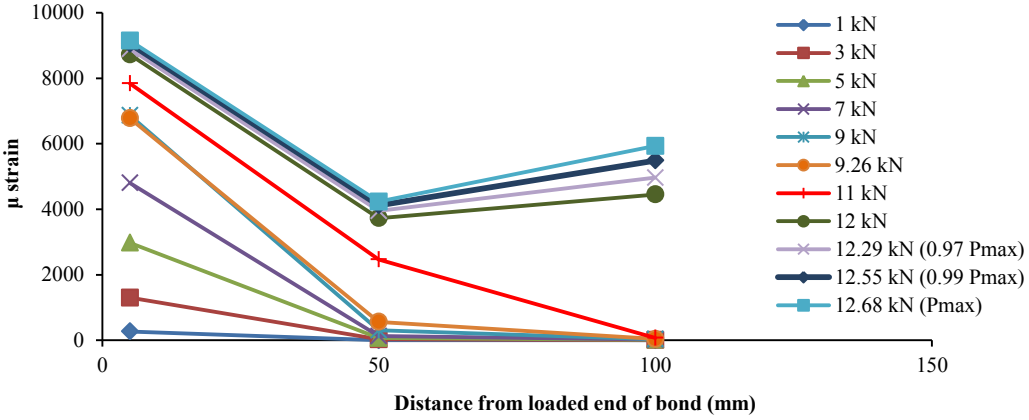

(d) CH1-4

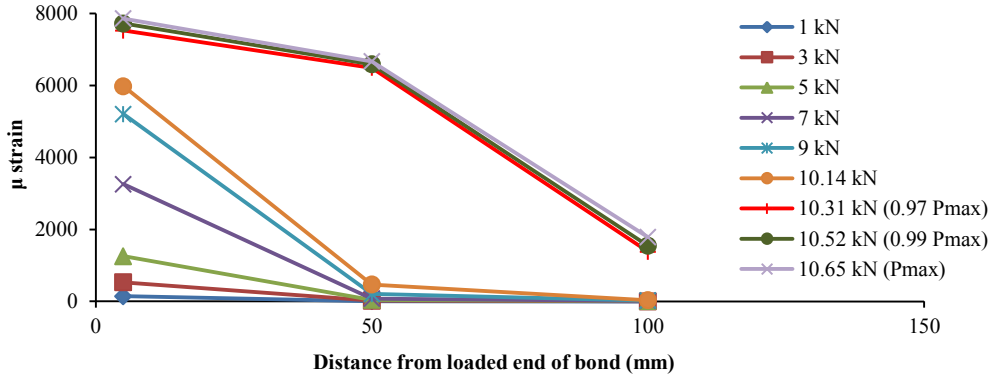

(e) CH1-5

Figure 5.4 Strain profiles of CFRP one month wet-dry series

- **CH2 series:**

Change of initial stress transfer length for six month wet-dry series occurred in the range of 9 -10.5 kN load as shown in Figure 5.5 with the exception of specimen CH2-4 which showed change of transfer length at much lower load value. Compared to the control series, the load level for shifting of initial transfer length was slightly lower. From the trend of strain profiles, the effective bond length of this series can be assumed as more than 100 mm which is quite similar to that observed in CH1 series.

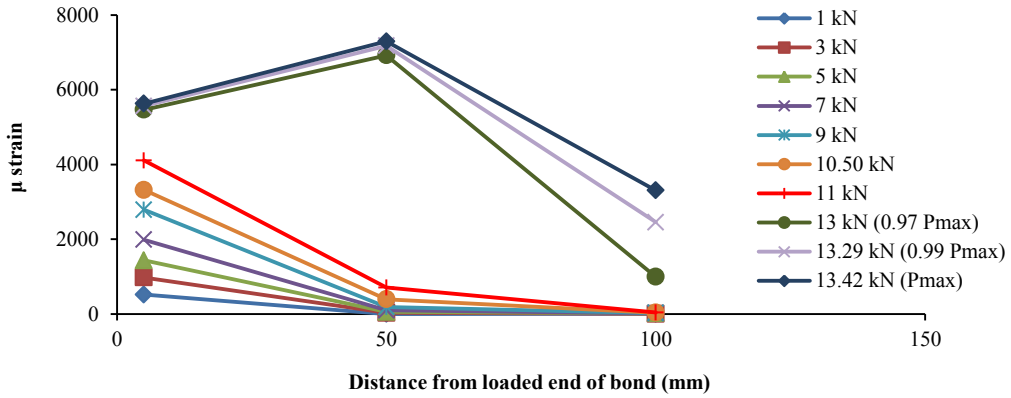

(a) CH2-1

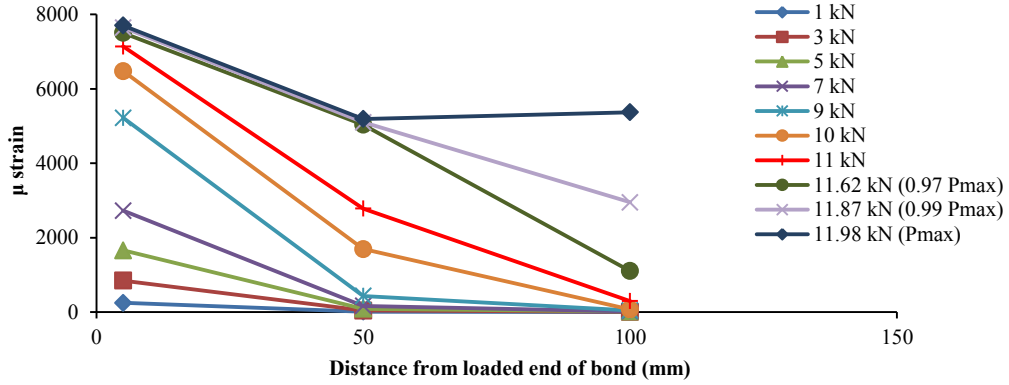

(b) CH2-2

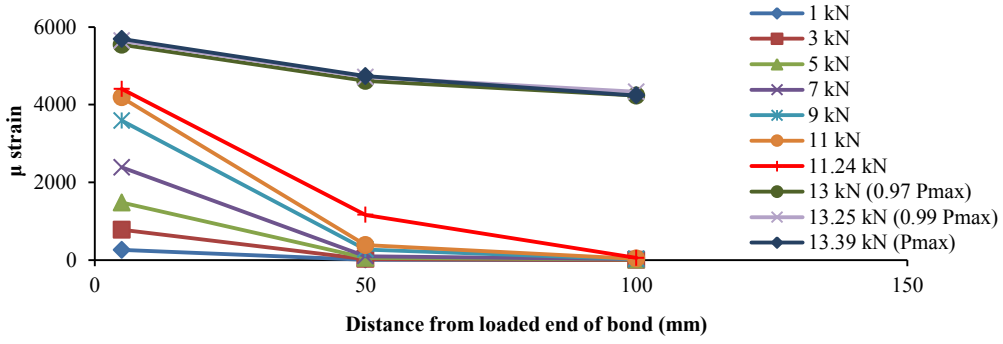

(c) CH2-3

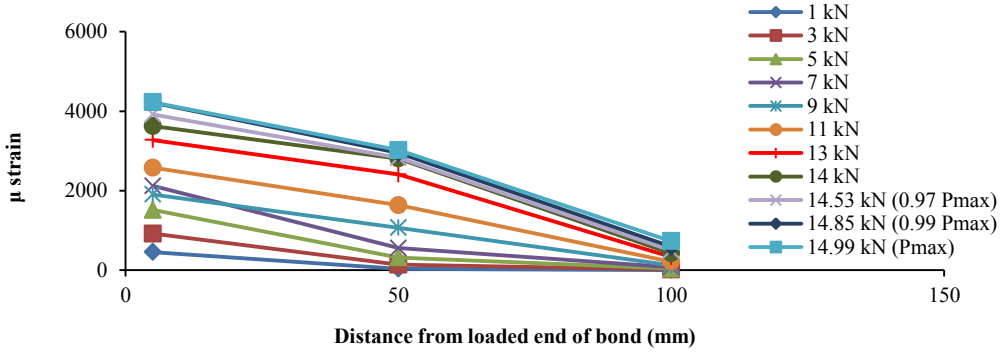

(d) CH2-4

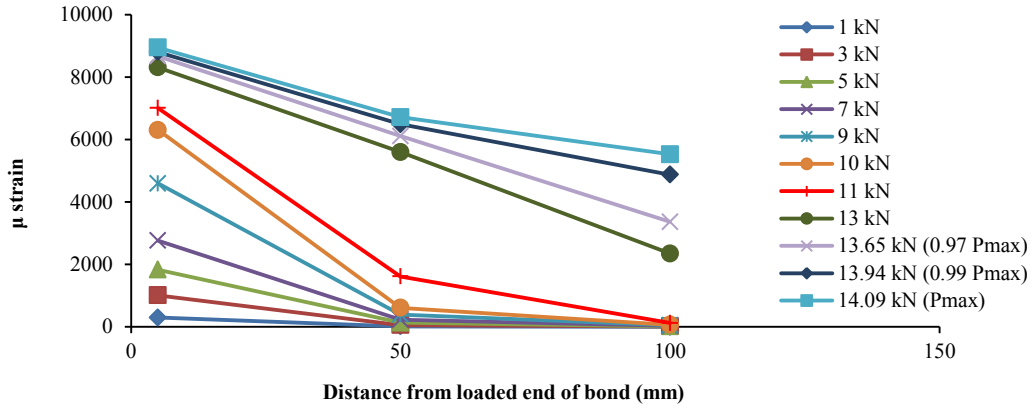

(e) CH2-5

Figure 5.5 Strain profiles of CFRP six month wet-dry series

- **CH3 series:**

The strain distributions of CH3 series were slightly different to those of the control series. The first change of load transfer lengths occurred approximately at 9 kN or less for four of the specimens (Figure 5.6) whereas at 10 kN for specimen CH3-3 (Figure 5.6 (c)) This load, when the first change in load transfer length was observed, is lower than that observed in control specimens (section 3.8.1.3). Similar to CH1 and CH2 series, the effective bond length determined from strain profiles of this series can also be assumed as more than 100 mm.

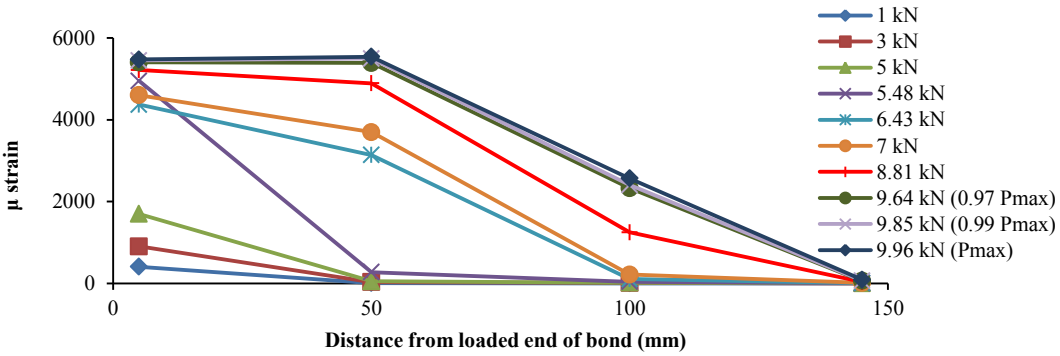

(a) CH3-1

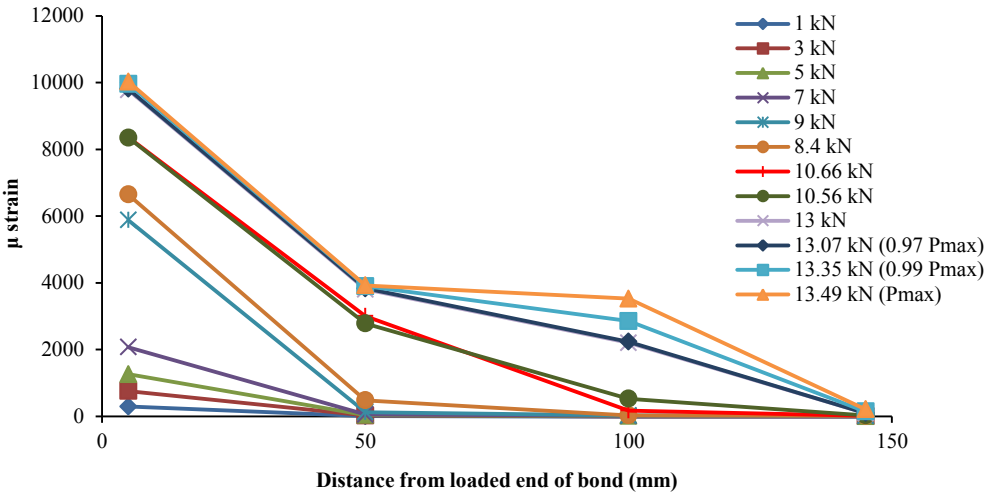

(b) CH3-2

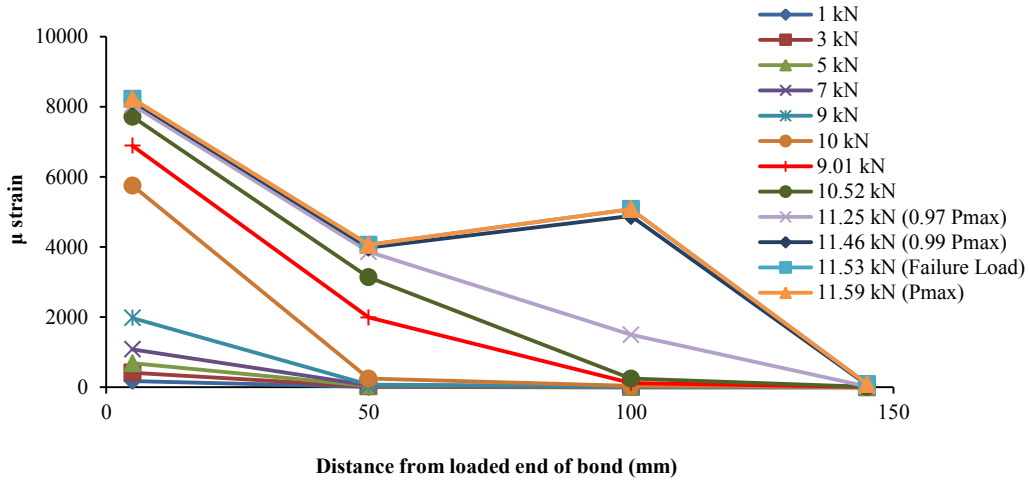

(c) CH3-3

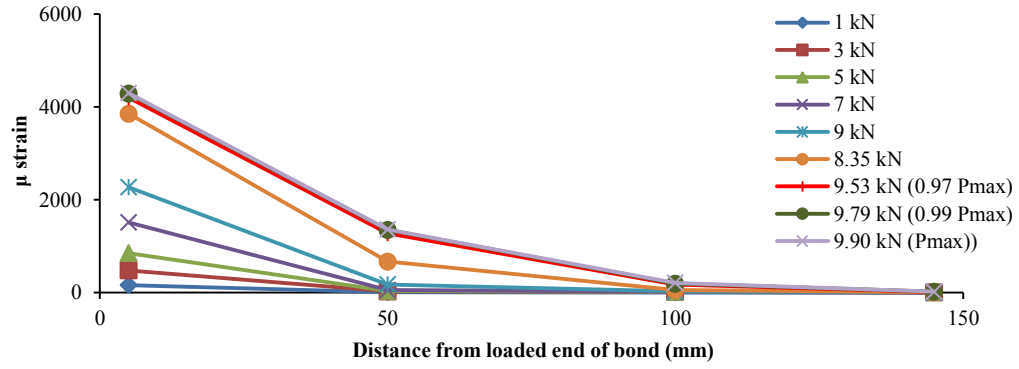

(d) CH3-4

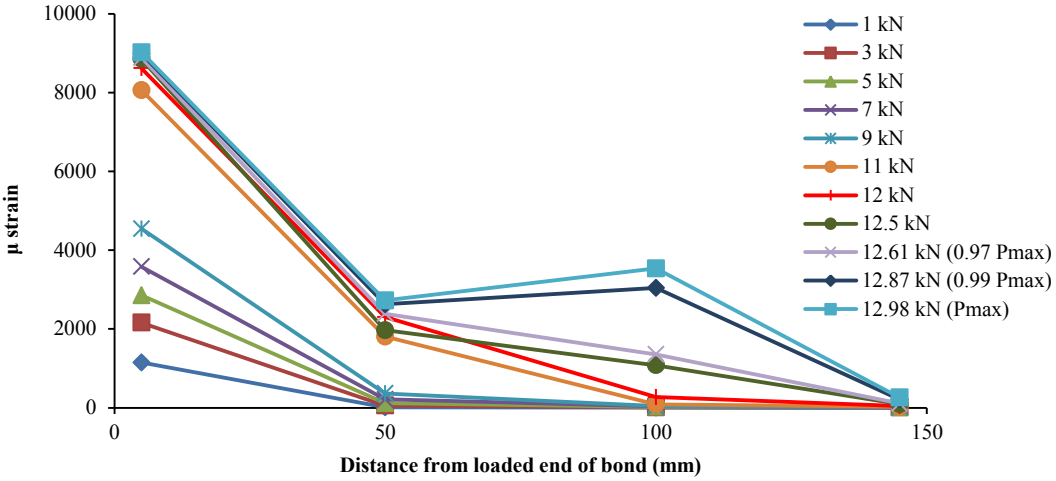

(e) CH3-5

Figure 5.6 Strain profiles of CFRP one year wet-dry series

- **CH4 series:**

Although CH4 series specimens were exposed to humid conditions for extended durations, the strain profiles of the series (Figure 5.7) were found to be almost similar to control series. Three specimens exhibited the shifting of initial transfer length at approximately 11 kN (same as control series) and the remaining two showed this change at about 9 kN. Even the effective bond length of four out of five specimens can be seen to be 100 mm or less from the plotted strain profiles. Only specimen CH4-1 showed effective bond length of more than 100 mm.

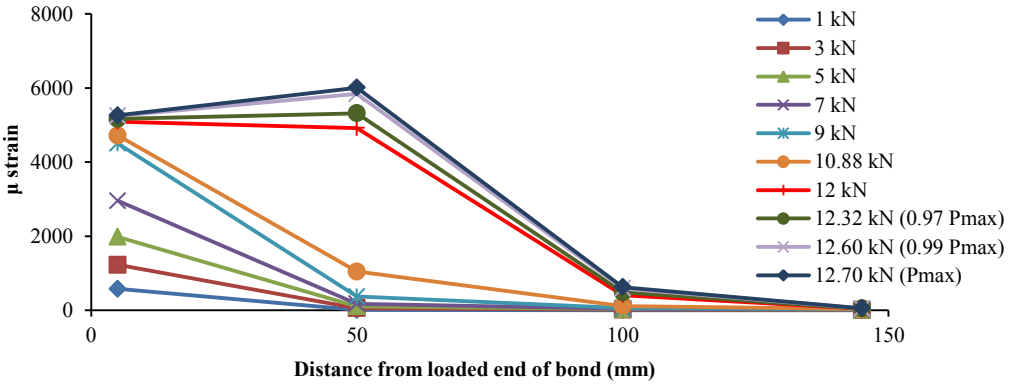

(a) CH4-1

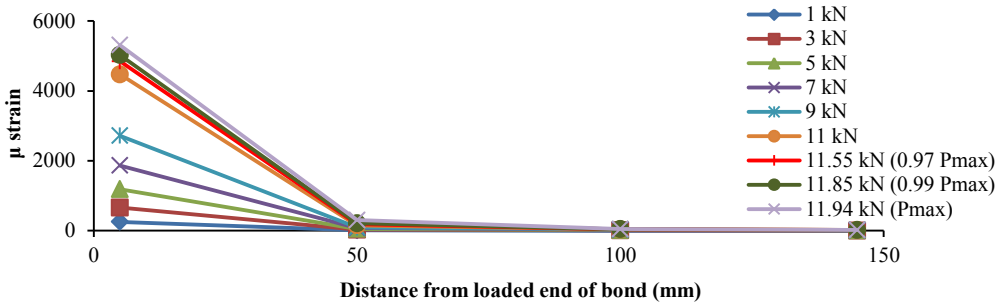

(b) CH4-2

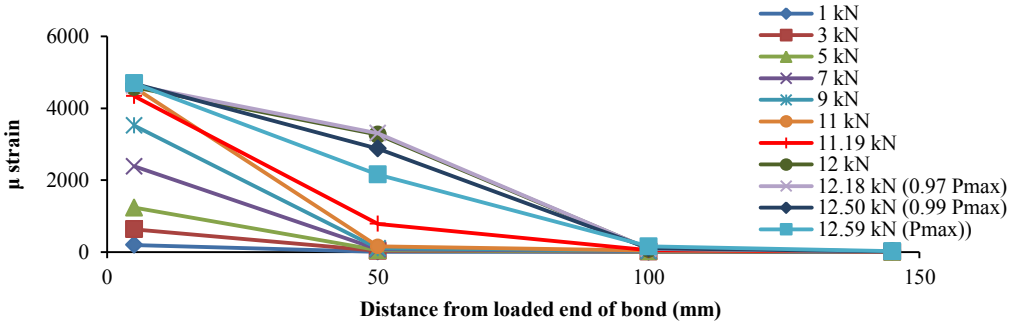

(c) CH4-3

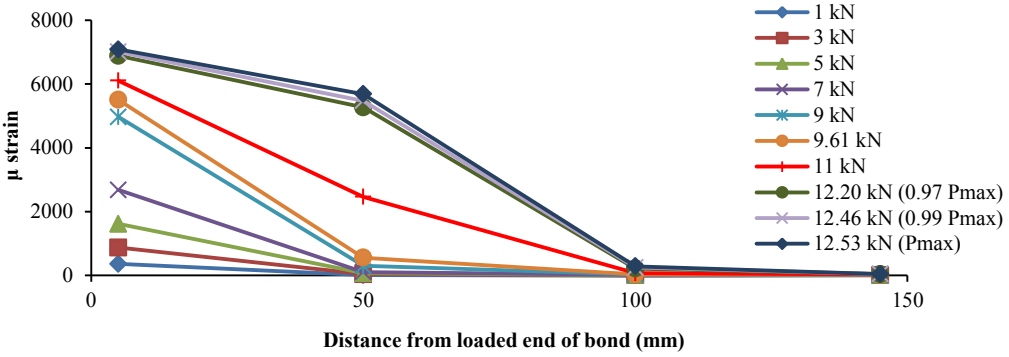

(d) CH4-4

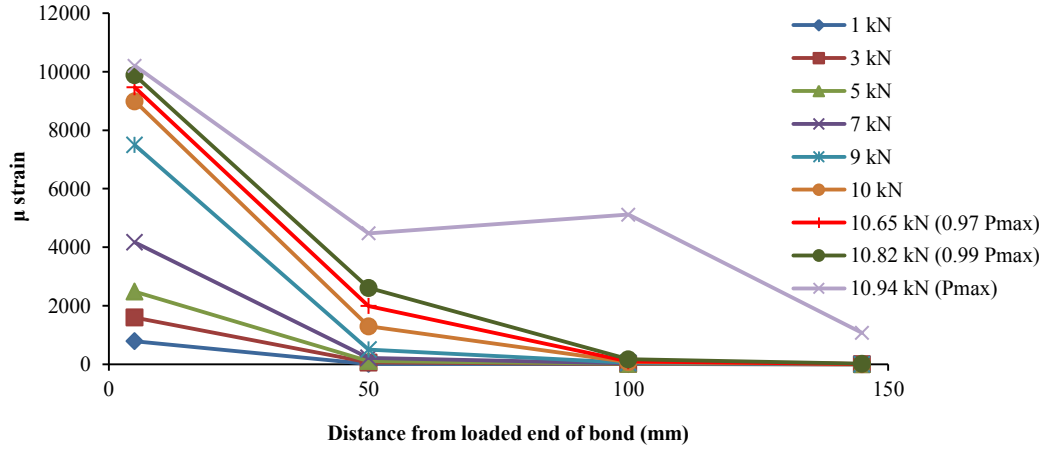

(e) CH4-5

Figure 5.7 Strain profiles of CFRP 18 month wet-dry series

To summarise the strain profiles of all CFRP wet-dry series, it can be stated that the change of initial stress transfer length showed a cyclic nature which was similar to that observed for pull-out strength and failure modes. CH1 series experienced the shifting of initial stress transfer length at lower load level than that of control series whereas CH2 series experienced at a level of load very close to control series. This trend was continued until the CH4 series had this change of initial transfer length at load levels almost the same as the control series. In terms of effective bond lengths, all wet-dry series, except CH4, had longer effective bond length than control series.

5.2.4 Discussion of test results

Cyclic variation in pull-out strength, failure modes and strain profiles were observed from test results for CFRP wet-dry series specimens. There was an initial positive effect of humidity on the pull-out strength and strength increased by 12% compared to control strength after six months. The initial increase can be attributed to the improved concrete compressive strength (Figure 5.1) as the failure occurred in concrete layer after six months of exposure. The maximum degradation of pull-out strength by about 5% after the exposure for one year can also be correlated with the change in failure pattern (from thicker concrete layer to almost no concrete attached to the debonded CFRP). The reason can be the approaching of concrete strength to the epoxy strength and the degradation of epoxy properties due to wet-dry cycles. Although the mechanical properties of epoxy resin due to exposed conditions were not determined in this study, the mode of failure after one year suggests the dependence of bond behaviour more on the epoxy property than that of concrete. Therefore, determination of epoxy properties under the same exposed condition may have to be conducted to better understand the dependence of pull-out strength on the material properties. Moreover, the cyclic nature of bond behaviour suggests the necessity of further study for extended durations until the pull-out strength becomes almost constant. Furthermore, the increased effective bond lengths for exposed specimens were observed from the change of transfer lengths in strain profiles.

5.3 Test results of GFRP wet-dry series

The results of GFRP-concrete bond subjected to wet-dry cycles for one month (GH1 series), six months (GH2 series), one year (GH3 series) and 18 months (GH4 series) have been presented in the following sections.

5.3.1 Pull-out strength

The pull-out strengths of all GFRP wet-dry specimens and CoV have been listed in Table 5.2 and the changes in normalised pull-out strength and concrete compressive strength, expressed as the ratio of the average strength of exposed specimens to that of control specimens, with time have been illustrated in Figure 5.8. From Figure 5.8 , it is seen that wet-dry series degraded the performance of GFRP-concrete bond by about 6.4% compared to the control series after the exposure for six months, although the concrete compressive strength increased. Then, an increasing trend of pull-out strength was observed with the strength value reaching the control strength after 18 months. Therefore, the maximum deterioration of GFRP-concrete bond strength observed in this study was 6.4 %, which was slightly higher than the degradation of CFRP-concrete bond strength. On the other hand, the concrete compressive strength was found to increase continuously up to one year and then, became almost constant. The effect of change in material properties on the pull-out strength is explained later in this chapter (5.3.4) through observed failure patterns of GFRP-concrete bond.

Table 5.2 GFRP pull-out strengths of wet-dry specimens

Exposure duration (Days)	Pull-out strength (MPa)	Mean pull-out strength (MPa)	CoV of pull-out strength (%)
0	1014.2	1027.0	6.0
	953.0		
	1054.5		
	1114.9		
	998.4		
28	1071.8	1021.6	10.8
	1045.6		
	986.3		
	1149.4		
	854.8		
168	1008.8	961.2	12.4
	973.0		
	1114.7		
	791.0		
	918.7		
364	942.9	1011.2	6.9
	936.7		
	1098.1		
	1038.0		
	1040.4		
546	1041.9	1034.4	5.0
	1047.5		
	1087.7		
	1046.3		
	948.8		

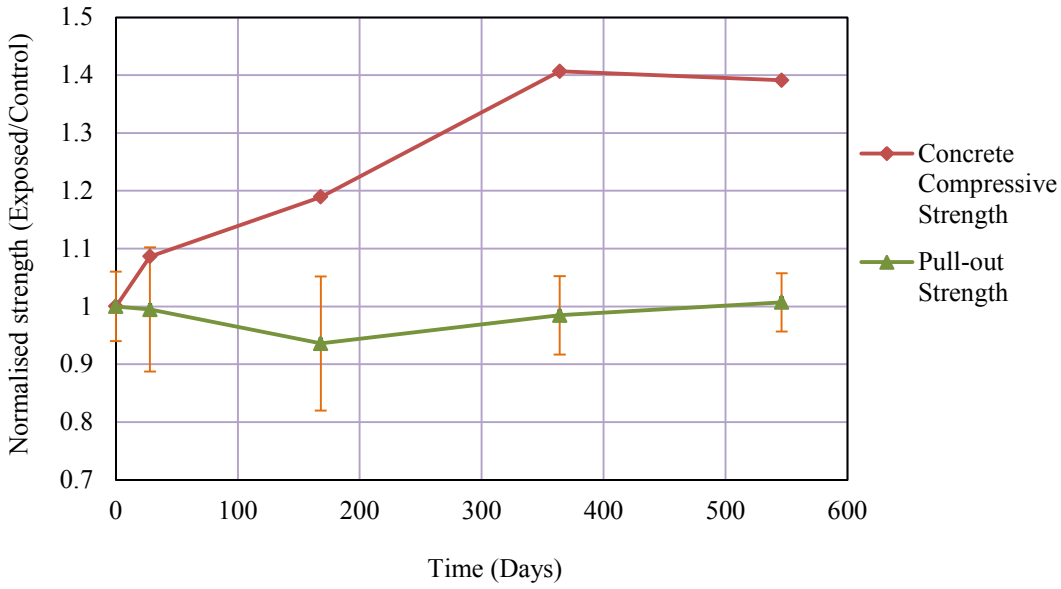

Figure 5.8 Normalised pull-out strength of GFRP wet-dry series with exposure duration

5.3.2 Failure modes

- **GH1 series:**

GH1 series showed failure of specimens with very thin layer of concrete attached to debonded GFRP (Figure 5.9). Only specimen GH1-5 experienced failure in the concrete layer but other four specimens had failure near the interface between concrete and epoxy as illustrated in Figures 5.9 (a) and (b).

- **GH2 series:**

GFRP specimens exposed to wet-dry cycles for six months showed similar pattern of failure to that observed in one month specimens. The thickness of attached concrete on GFRP, although slightly more than one month series, was much less than the control series (section 3.8.2.3). Moreover, epoxy layer was visible in many parts of the debonded GFRP coupons (Figures 5.9 (c) and (d)).

- **GH3 series:**

All specimens, except specimen GH3-3 (Figure 5.9 (e)), from one year wet-dry (GH3) series exhibited thin concrete layer on debonded GFRP (Figure 5.9 (f)).

- **GH4 series:**

18 month GFRP wet-dry series experienced change of failure modes from thin concrete layer to thicker concrete attached to the debonded FRP. Three out of five specimens, namely, GH4-1, 4 and 5 showed this type of failure as illustrated in Figures 5.9 (g) and (i), whereas specimen GH4-2 and GH4-3 (Figure 5.9 (h)) still had the failure pattern associated with very thin concrete mass.

In summary, evolution of failure modes from thick concrete layer attached to debonded GFRP in control series to thinner/very thin layer in exposed series was observed in this study. Only the 18 month wet-dry series (GH4) showed almost similar mode of failure to that of control series.

(a) GH1-2

(b) GH1-5

(c) GH2-3

(d) GH2-5

(e) GH3-3

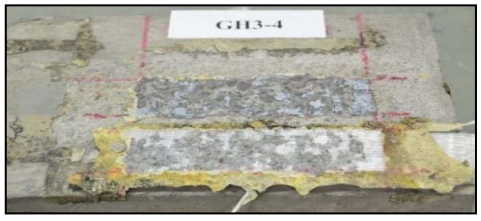

(f) GH3-4

(g) GH4-1

(h) GH4-2

GH4-3

Figure 5.9 Failure modes of GFRP wet-dry specimens

5.3.3 Strain profiles

The strain profiles of GH1 and GH2 series were plotted for three strain gauge set-up (Figure 5.3 (a)), whereas those for GH3 and GH4 series were plotted for four strain gauge set-up (Figure 5.3 (b))

- **GH1 series:**

As plotted in Figure 5.10, strain profiles of GH1 series were similar to those of control series. The change of initial stress transfer length changed from approximately 50 mm to 100 mm at load level of 9 to 12.5 kN for four specimens (Figures 5.10 (a), (b), (c) and (e)) and about 7 kN for specimen GH1-4 (Figure 5.10 (d)). Also, the effective bond lengths of four specimens were 100 mm or less by the definitions of Yuan et al. (2004) and Lu et al. (2005), which is similar to the control series.

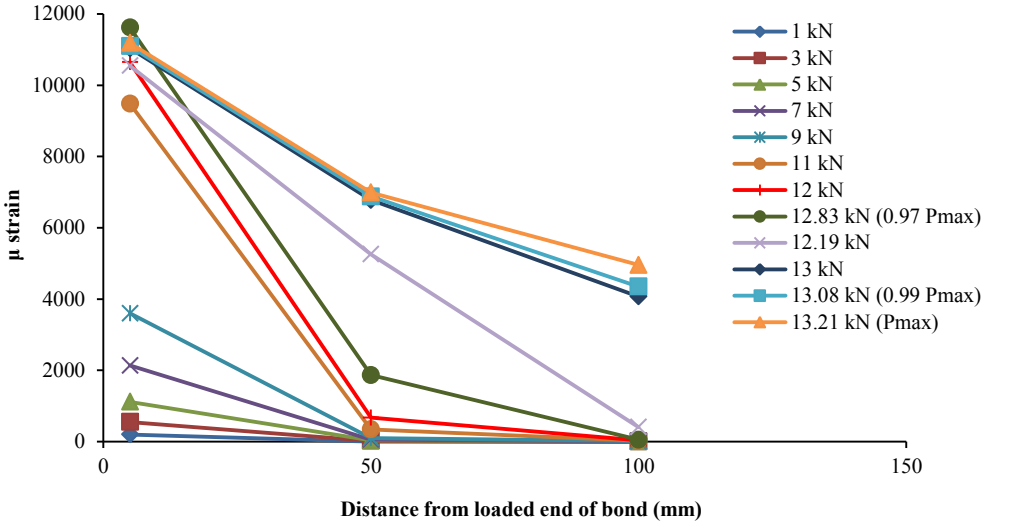

(a) GH1-1

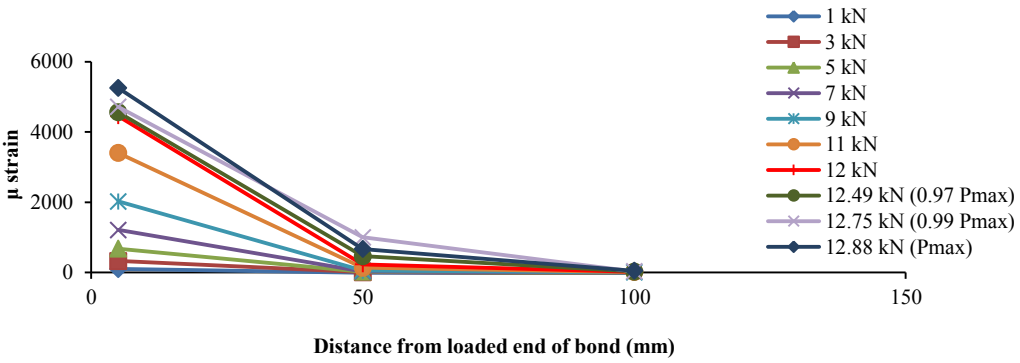

(b) GH1-2

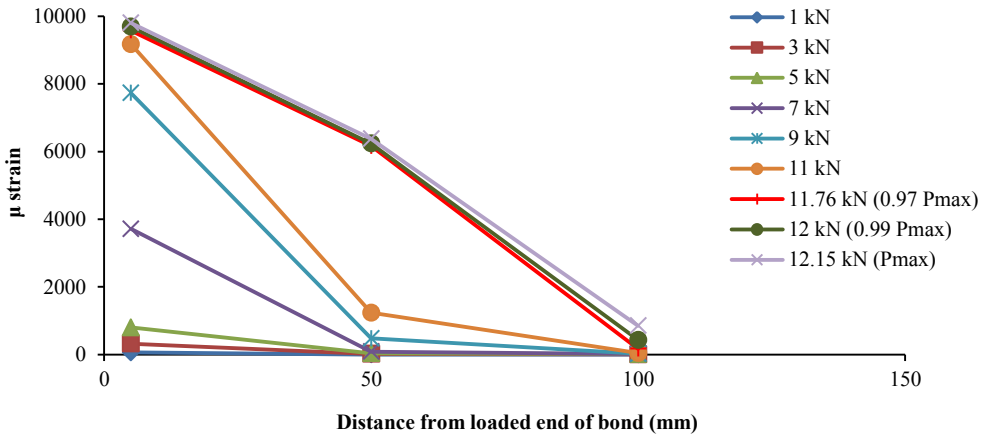

(c) GH1-3

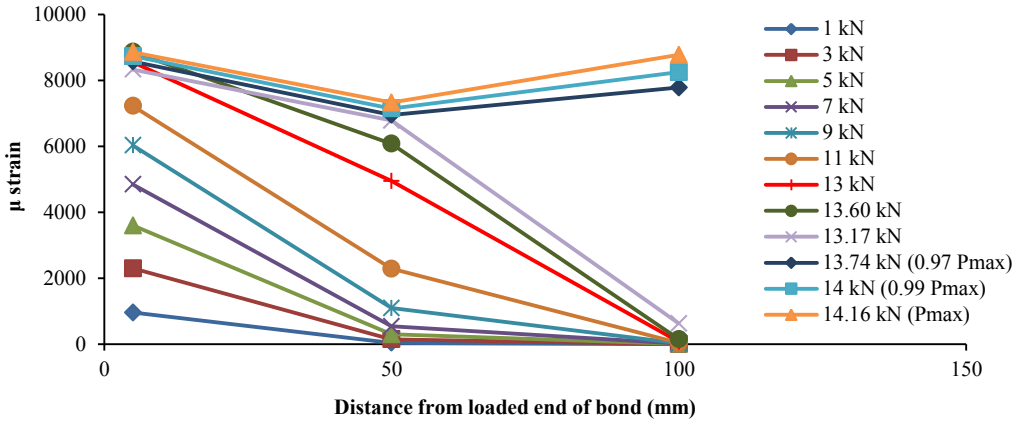

(d) GH1-4

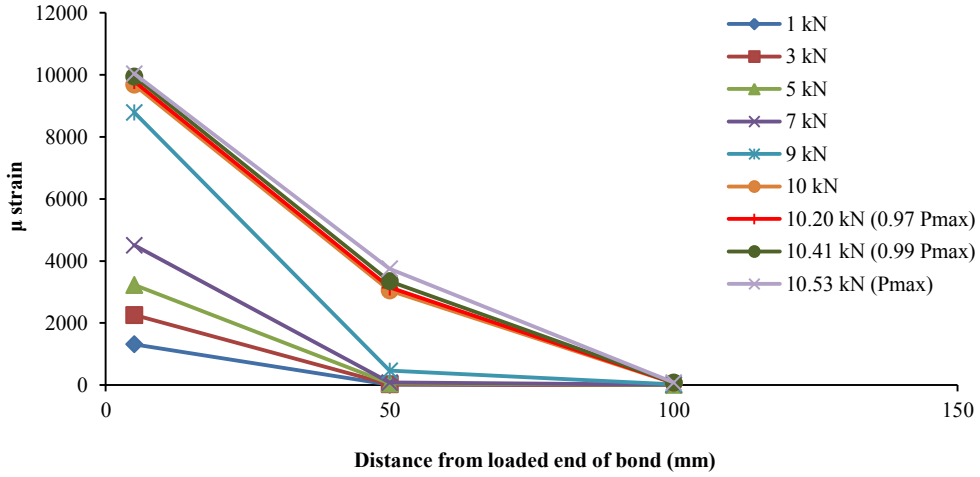

(e) GH1-5

Figure 5.10 Strain profiles of GFRP one month wet-dry series

- **GH2 series:**

Figure 5.11 represents the strain distributions of GH2 series. The initial transfer lengths of GH2 series were found to change at relatively lower load than control series as the load level for two specimens was 8 kN and for one specimen was 10 kN. Only specimen GH1-1 had relatively higher level of load (12 kN) at which shifting of initial transfer length occurred (Figure 5.11 (a)). Specimen GH2-3 showed (Figure 5.11 (c)) an exceptional behaviour with change of initial load transfer length at very low load level and the reason might be weaker bonding of FRP near the loaded end of bond length during fabrication. In terms of effective bond length, four specimens showed similar length to that of control series; i.e. 100 mm or less.

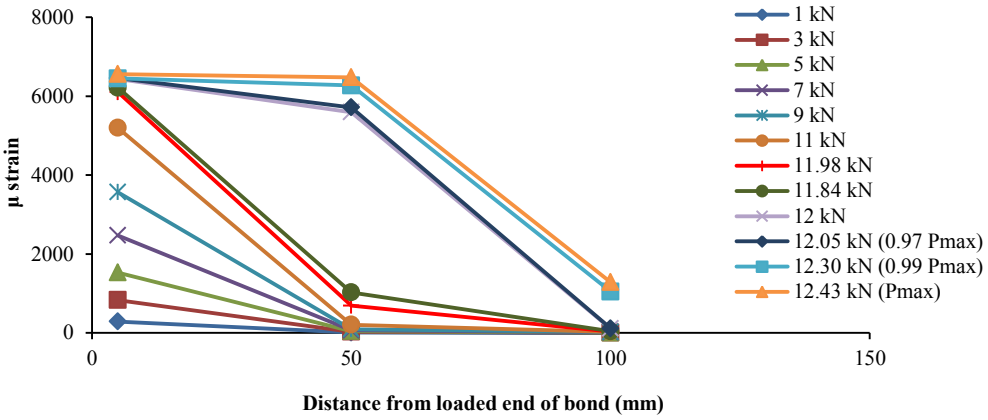

(a) GH2-1

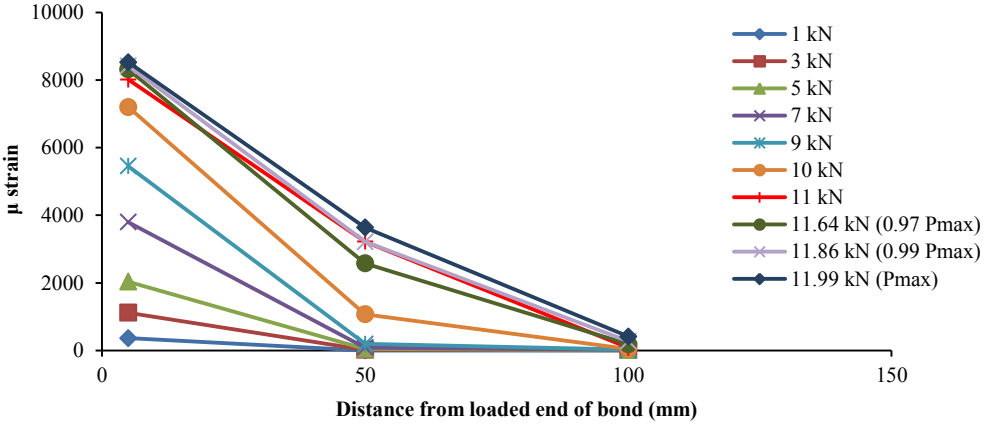

(b) GH2-2

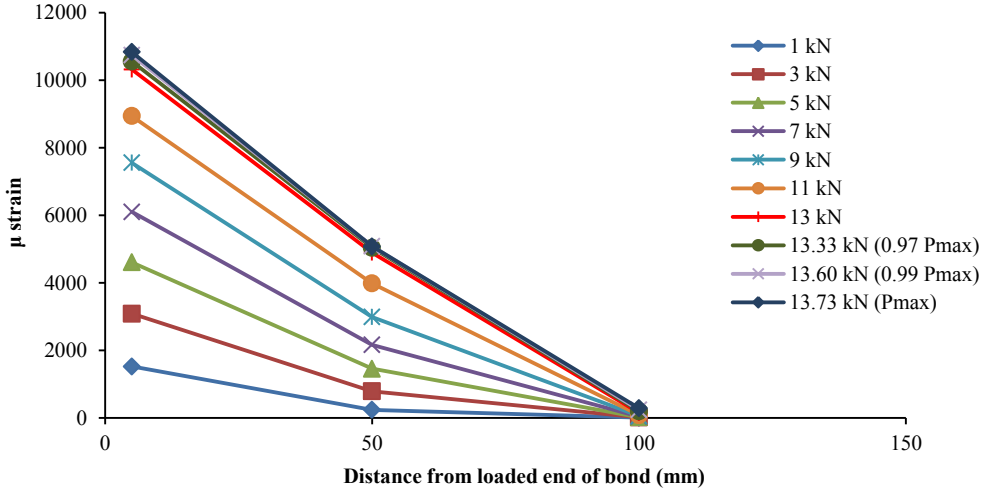

(c) GH2-3

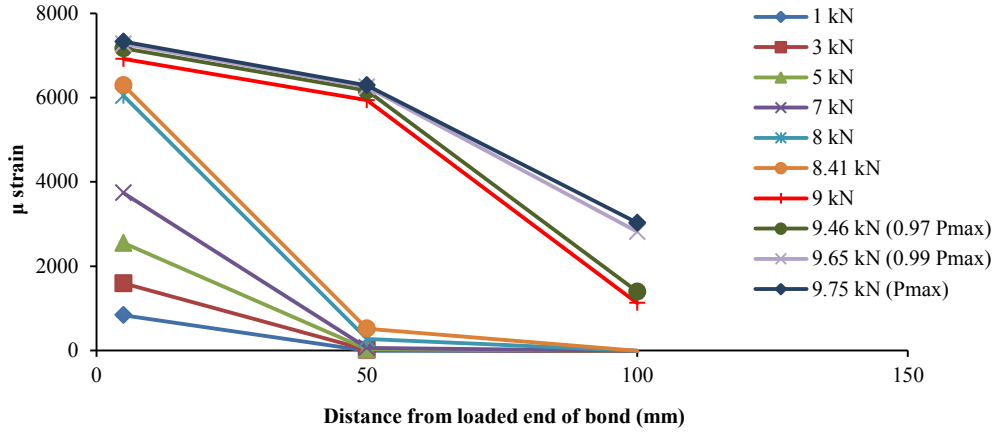

(d) GH2-4

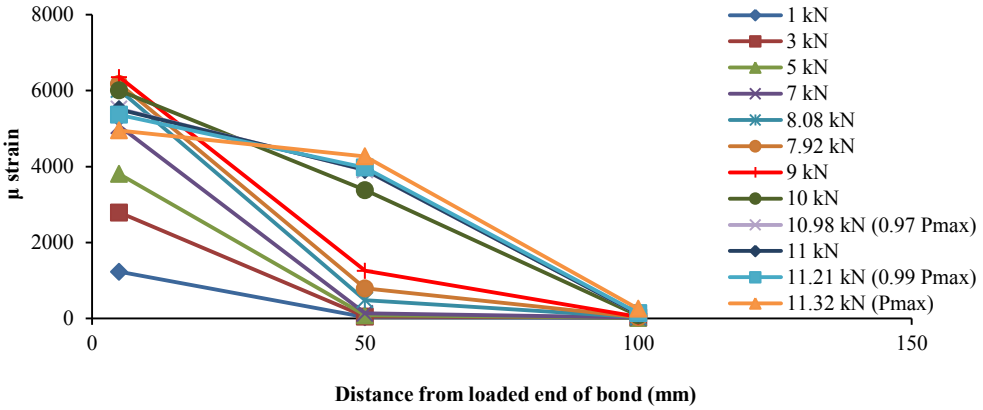

(e) GH2-5

Figure 5.11 Strain profiles of GFRP six month wet-dry series

- **GH3 series:**

From the plotted strain profiles of GH3 series in Figure 5.12, it was found that three out of five specimens showed the change of initial stress transfer length at about 10 kN load. Specimen GH3-5 (Figure 5.12 (e)) even experienced this at higher load (12 kN). But for specimen GH3-2 only, initial transfer length shifted at relatively lower load of 8 kN. Hence, the overall behaviour of the strain distributions, in term of initial stress transfer length, was almost similar to that of control series, although the load level for the shift of initial transfer length was slightly lower than the control series. However, the effective bond lengths were found to be more than 100 mm which was higher than those obtained from control series.

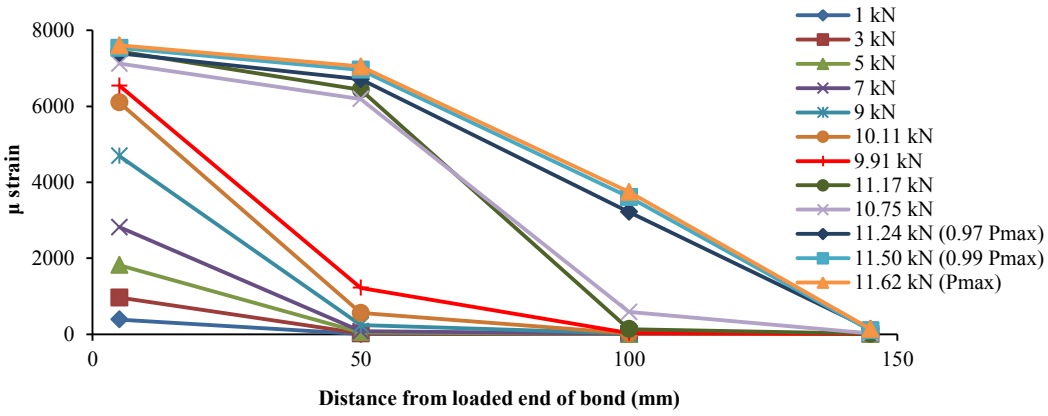

(a) GH3-1

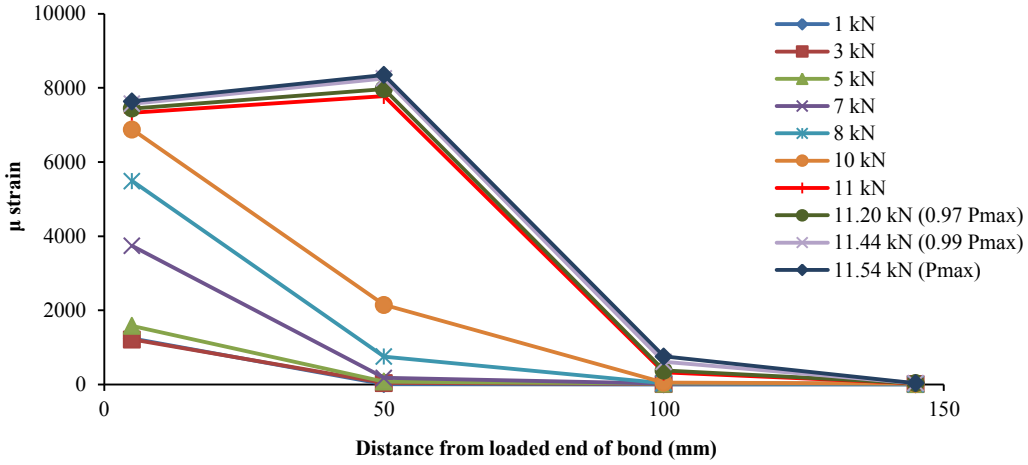

(b) GH3-2

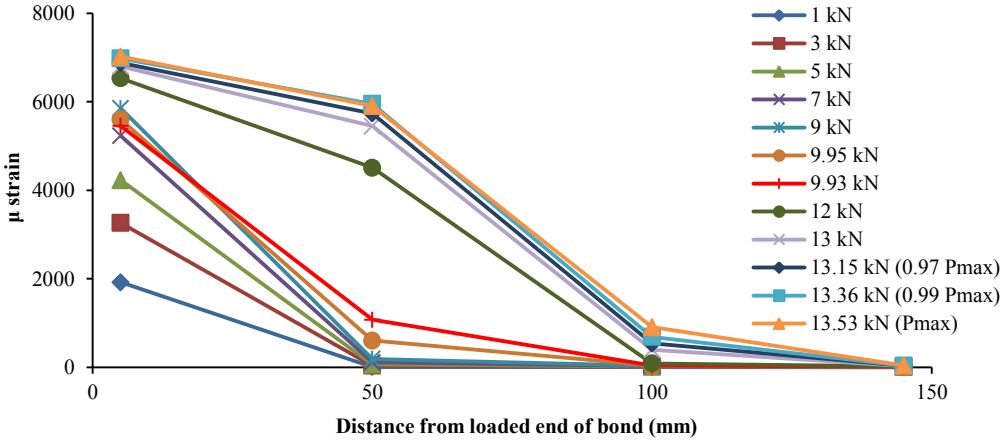

(c) GH3-3

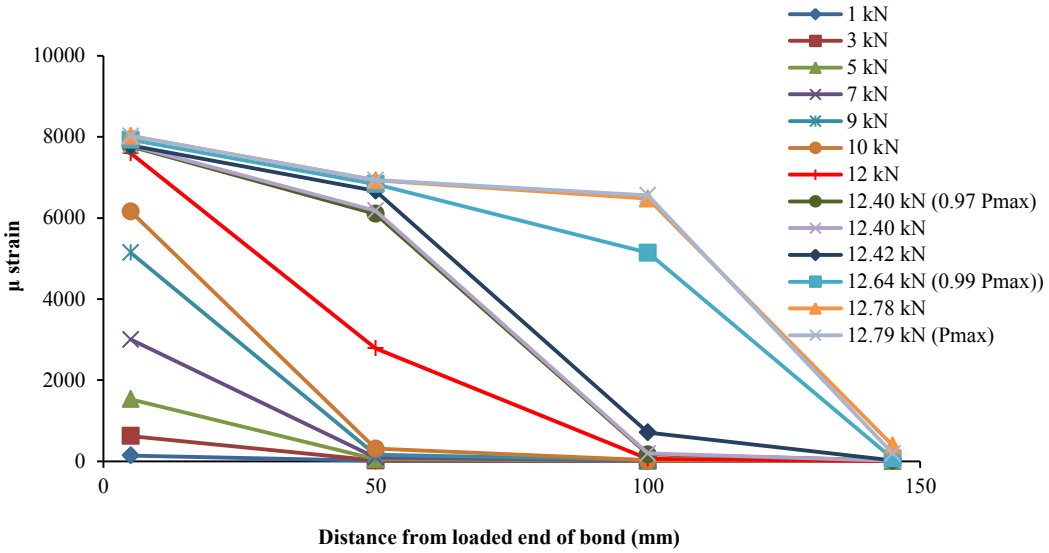

(d) GH3-4

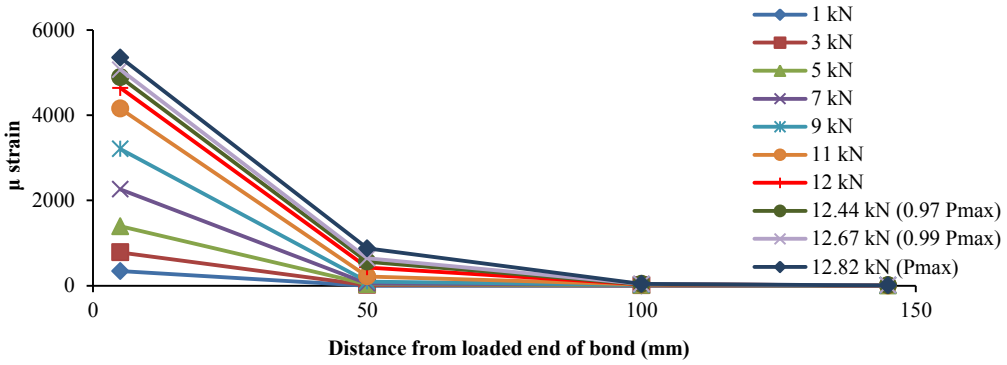

(e) GH3-5

Figure 5.12 Strain profiles of GFRP one year wet-dry series

- **GH4 series:**

GH4 series (Figure 5.13), although showed higher effective bond lengths (more than 100 mm for three out of five specimens) than control series, the load level at which the change of initial stress transfer length occurred revealed quite a similar pattern. Three out of five specimens experienced the shift of initial transfer length at about 11 kN (Figures 5.13 (c), (d) and (e)), one specimen at about 10 kN (Figure 5.13 (b)) and one at 12 kN (Figure 5.13 (a)).

In summary, the strain distributions of GFRP wet-dry series changed with the exposure duration. The change of initial load transfer length for GH1 series occurred almost at the

same level of load as with control series. GH2 series experienced this change at relatively lower load. GH3 specimens showed the change at load level higher than GH2 series but slightly lower than control series. And the GH4 series showed almost a similar pattern to control specimens. In terms of effective bond lengths, no change was observed until the exposure duration was one year. Only GH3 and GH4 series had higher effective bond length (more than 100 mm) than control series.

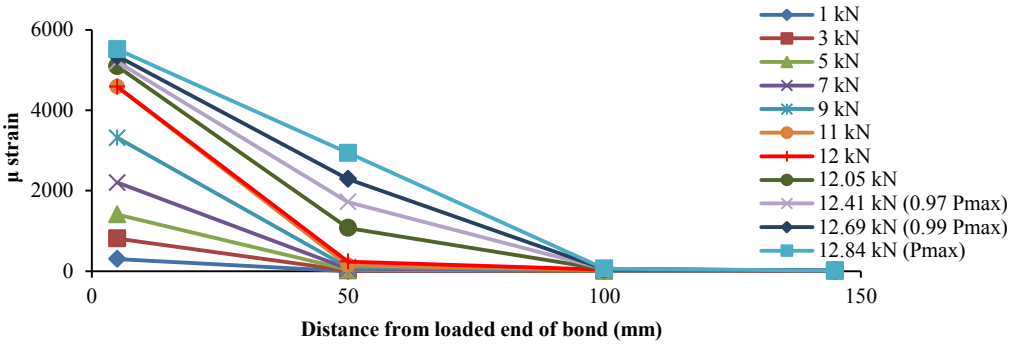

(a) GH4-1

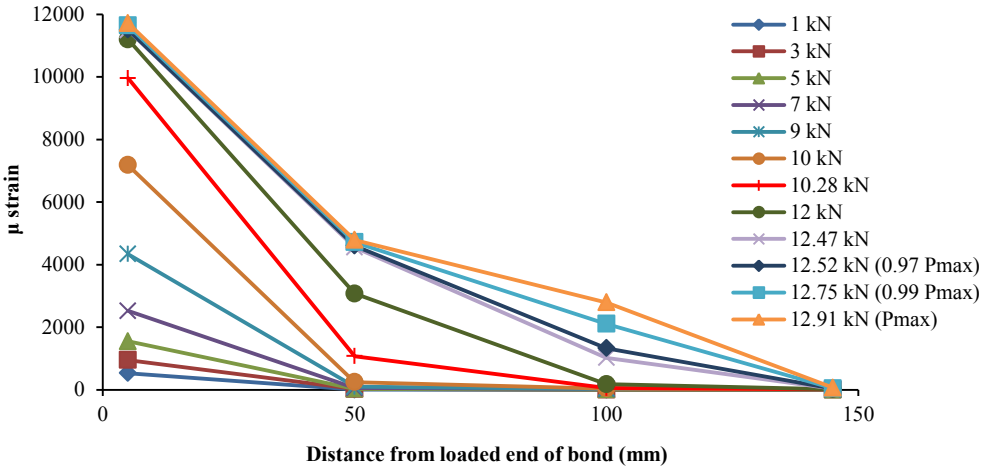

(b) GH4-2

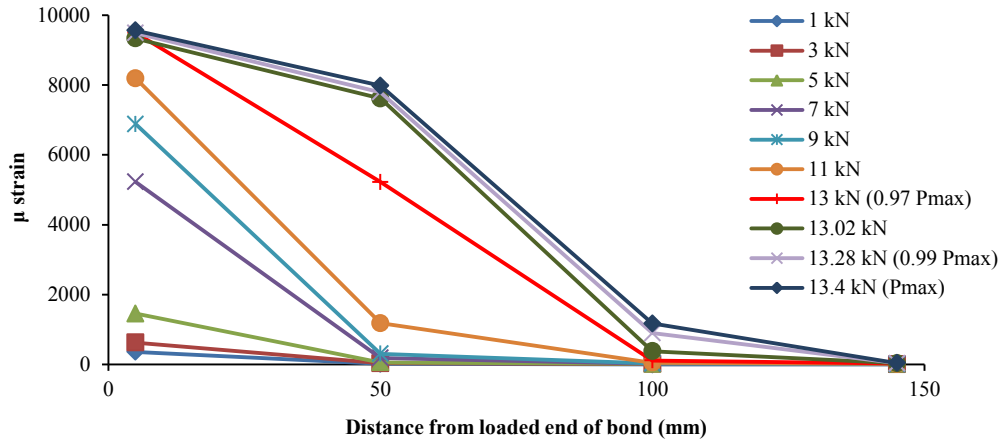

(c) GH4-3

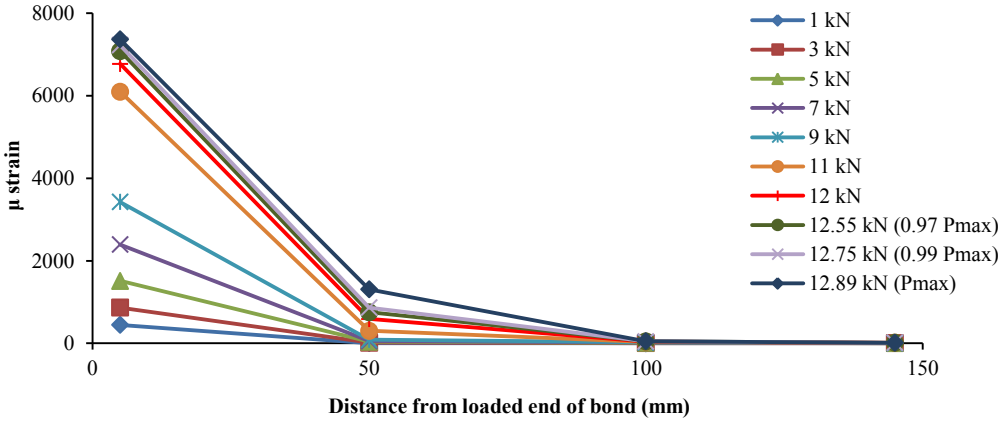

(d) GH4-4

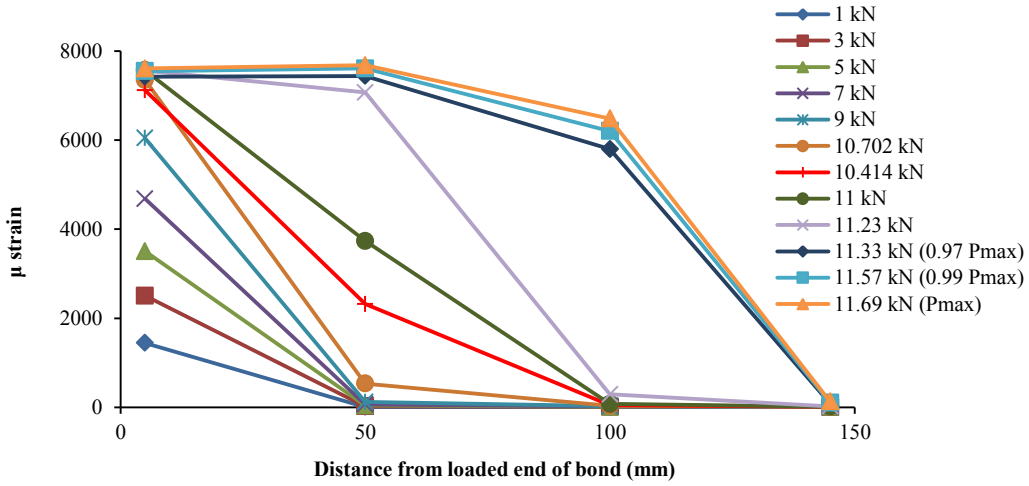

(e) GH4-5

Figure 5.13 Strain profiles of GFRP 18 month wet-dry series

5.3.4 Discussion of test results

From the test results of GFRP wet-dry series, it can be stated that wet-dry condition had an adverse effect on pull-out strength of GFRP-concrete bond. Although the concrete compressive strength increased continuously due to suitable humid condition for the development of concrete strength (Figure 5.8), the bond strength showed degradation up to six months. The degradation can be attributed to the deterioration of epoxy strength as the failure pattern of pull-out specimens changed from thick concrete to thinner concrete layer attached to GFRP compared to the control series. Hence, the bond strength is more likely to depend on the epoxy properties than concrete properties, similar to the observation in CFRP wet-dry series. Since the failure was still in epoxy layer after one year of exposure, the significant improvement of pull-out strength can be because of the improved epoxy properties. The approaching of pull-out strength of exposed specimens to the control strength after 18 months of exposure can also be correlated with the failure mode. As the failure pattern of GH4 series was almost similar to the control series (failure with thick concrete layer attached to GFRP), increased concrete compressive strength helped to improve the bond strength. However, further experimental study on the epoxy properties should be conducted to validate the explanation regarding the dependence of pull-out strength on the epoxy properties. The change of effective bond length from 100 mm or less to more than 100 mm after one year was noticed in this study.

5.4 Chapter summary

The aim of this chapter was to discuss the results of the experimental study on the effect of wet-dry cycles on CFRP and GFRP-concrete bond. The major findings can be summarised as follows:

- The deterioration of pull-out strengths of CFRP and GFRP-concrete bond was minimal due to wet-dry cycles. The maximum reduction of pull-out strength of CFRP-concrete bond was only about 5% after one year. Even an initial increase of pull-out strength by 12% was noticed because of increased concrete compressive strength. The change of pull-out strength of CFRP bonded specimens revealed the cyclic nature. On the other hand, GFRP-concrete bond strength degraded by 6.4%

after six months, which was slightly more than the maximum degradation experienced by CFRP-concrete bond.

- Failure modes of CFRP-concrete bond changed from thick concrete to very thin concrete layer attached to the FRP but this change also followed the cyclic nature similar to that of pull-out strength. In case of GFRP bonded specimens, all exposed series specimens, except for the 18 month exposure, showed change of failure pattern from very thick concrete to very thin concrete layer attached to the debonded FRP.
- Effective bond length for both CFRP and GFRP-concrete bond increased due to exposed condition.

From the findings stated above, it can be concluded that the wet-dry cycles had more prominent effects on GFRP-concrete bond than on CFRP-concrete bond. The change of failure modes from thicker concrete layer to very thin concrete layer for both types of bond due to wet-dry cycles necessitates further experimental study on the epoxy properties to better understand the bond mechanism which is more likely to depend on the behaviour of three constituents, namely, FRP, concrete and epoxy. Moreover, the increased effective bond length of exposed specimens suggests that the longer bond length than the theoretical effective bond length for unexposed condition may improve the long term performance of CFRP and GFRP-concrete bond.

CHAPTER 6

EFFECT OF OUTDOOR ENVIRONMENT ON FRP-CONCRETE BOND

6 Effect of outdoor environment on FRP-concrete bond

6.1 Introduction

This chapter presents the results of experimental study on the long-term performance of CFRP and GFRP-concrete bond subjected to outdoor environment. The test results of CFRP bonded specimens have been discussed in section 6.2 and those of GFRP bonded specimens have been provided in 6.3 in terms of pull-out strengths, failure modes and strain profiles of exposed bonded specimens. In addition, the dependence of pull-out strength of two types of bond on the material properties has been explained based on the change of material strength and/or stiffness and failure modes of bond. Finally, the findings of this research have been summarised in section 6.4.

6.2 Test results of CFRP outdoor environment series

The CFRP Pull-out specimens subjected to outdoor environment were tested after the exposure durations of two months (CE1 series), six months (CE2 series), 12 months (CE3 series) and 18 months (CE4 series). The test results have been presented in the following sections.

6.2.1 Pull-out strength

The strength values for Control (0 days), CE1 (60 days), CE2 (180 days) and CE4 (555 days) specimens with coefficient of variation (CoV) are listed in Table 6.1. As the one year outdoor environment specimens (CE3 series) and their corresponding control specimens were fabricated from concrete batch 2, the strength values of these specimens have been included in Table 6.2 separately.

Table 6.1 CFRP pull-out strengths of outdoor environment specimens from batch 1

Exposure duration (Days)	Pull-out strength (MPa)	Mean pull-out strength (MPa)	CoV of pull-out strength (%)	Comments
0	1183.3	1298.7	12.0	-
	1563.9			-
	1213.4			-
	1322.5			-
	1210.3			-
60	993.7	1178.2	12.0	-
	1159.2			-
	1378.9			-
	1149.5			-
	1209.8			-
180	1034.6	1101.5	11.1	-
	1098.9			-
	998.7			-
	1273.7			-
	-			Damaged specimen
555	1062.1	1186.6	10.6	-
	1125.6			-
	1173.1			-
	1395			-
	1177.2			-

Table 6.2 CFRP pull-out strengths of outdoor environment specimens from batch 2

Exposure duration (Days)	Pull-out strength (MPa)	Mean pull-out strength (MPa)	CoV of pull-out strength (%)	Comments
0	1202.2	1320.0	7.0	-
	1422.4			-
	1357.3			-
	1298.0			-
	-			Ignored from analysis
365	1299.8	1307.3	13.0	-
	1411.3			-
	1326.7			-
	1028.1			-
	1470.5			-

The change of normalised pull-out strength of CFRP-concrete bond and concrete compressive strength (expressed as the ratio of exposed strength to control strength) with exposure durations for outdoor environment can be observed from the plot in Figure 6.1. The plot also represents the standard deviations of normalised pull-out strengths with black vertical lines. In addition, the red vertical dashed line at the time of "0" days represents the standard deviation of pull-out strength of control specimens fabricated from concrete batch 2. It can be seen from the plot that CFRP specimens lost pull-out strength continuously with time due to exposure until it reached the maximum deterioration of bond of 15.2% (84.8% of control) after six months. However, an improvement of strength was observed thereafter and strength value reached very close to control value (99 % of the control value) after one year. Finally, pull-out strength reduced to 91.4% of control value after 18 months. On the other hand, the continuous increase in concrete compressive strength up to one year followed by a drop in strength after 18 month exposure was observed but the concrete compressive strength was still much higher than that of control series. The difference between the trend of the concrete

compressive strength and the pull-out strength has been discussed in detail in section 6.2.4 through failure patterns of CFRP outdoor environment series.

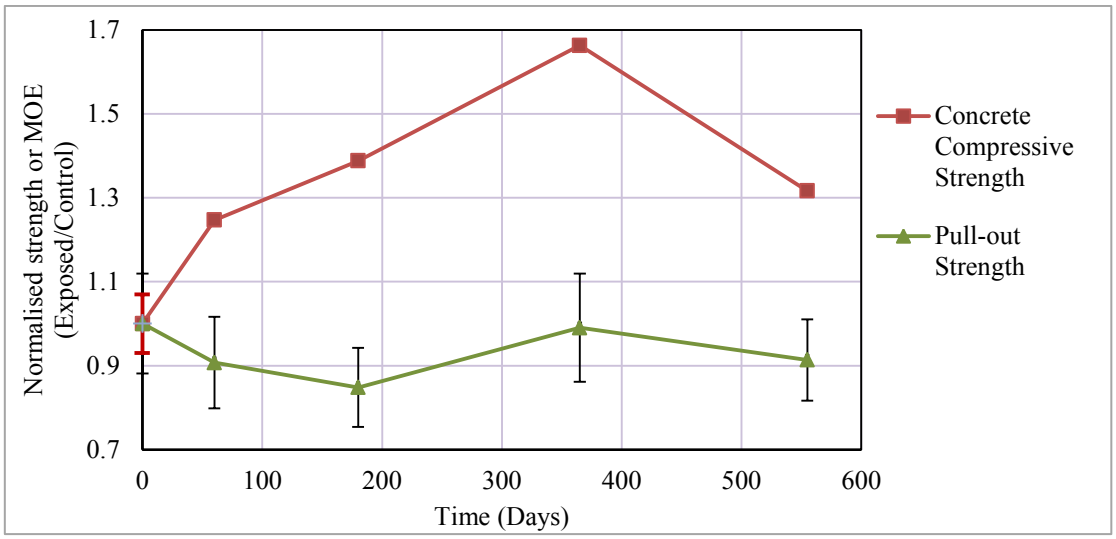

Figure 6.1 Normalised pull-out strengths of CFRP outdoor environment series with exposure duration

6.2.2 Failure modes

- **CE1 series:**

The typical failure modes for CE1 series can be observed in Figure 6.2 (b) where very thin layer of concrete (almost no concrete) was attached to the debonded CFRP. Only specimen CE1-1 had relatively thicker concrete layer (Figure 6.2 (a)) attached.

- **CE2 series:**

Similar to CE1 series, CE2 series also experienced failure with very thin concrete layer attached to CFRP as illustrated in Figure 6.2 (d). Three out of four specimens tested for this series had this mode of failure whereas specimen CE2-1 showed inconsistent failure by partial rupture and partial debonding (Figure 6.2 (c)). This can be due to the improper gripping of the FRP leading to non-uniform stress distribution along the width of the FRP, which was also reported by Imani (2010).

- **CE3 series:**

All specimens of CE3 series, fabricated from concrete batch 2, failed with the same pattern as observed in the previous two series (Figure 6.2 (e)). Qualitatively, the reduction of concrete thickness compared to the control specimens from batch 2 (section 3.8.1.2) was much higher than that observed after two months and six months of exposure and the concrete layer was hardly visible on the debonded FRP.

- **CE4 series:**

The CE4 series failed with similar pattern (Figure 6.2 (g)) to those with previous outdoor environment series, namely, CE1 and CE2 series. However, specimen CE4-1 showed exception with thick concrete layer attached to CFRP (Figure 6.2 (f)). Two specimens, namely, CE1-4 and 5 experienced longitudinal fracture of CFRP along with debonding as shown in Figure 6.2 (h), which can be attributed to the improper gripping of the FRP.

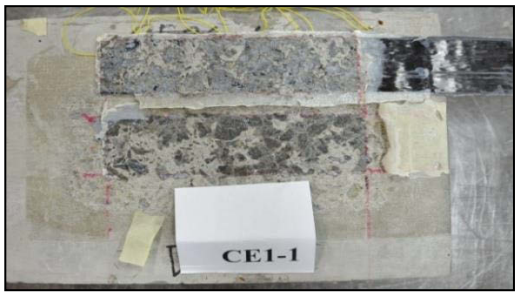

(a) CE1-1

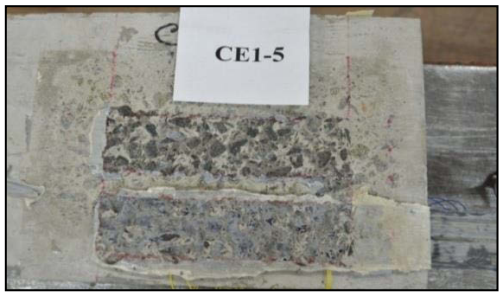

(b) CE1-5

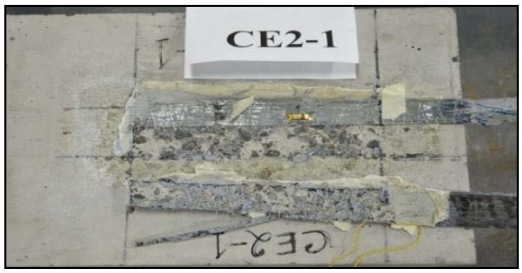

(c) CE2-1

(d) CE2-2

(e) CE3-1

(f) CE4-1

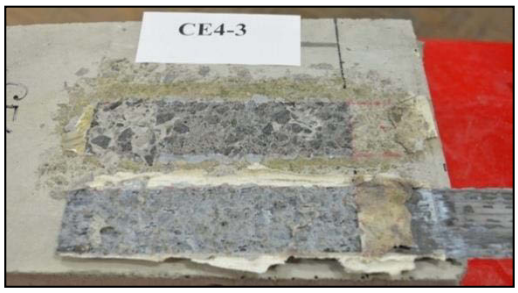

(g) CE4-3

(h) CE4-4

Figure 6.2 Failure modes of CFRP outdoor environment specimens

As a summary of the failure modes, it can be stated that all series experienced failure associated with very thin concrete layer/almost no concrete attached to debonded CFRP and the least thickness of attached concrete was observed in CE3 series specimens.

6.2.3 Strain profiles

Three strain gauges, located at 5 mm, 50 mm and 100 mm (Figure 6.3 (a)) from the loaded end of the FRP-concrete bond, were used to investigate the strain profiles. For CE4 series specimens, an additional strain gauge at 145 mm was also used (Figure 6.3 (b)).

- **CE1 series:**

Figure 6.4 shows the strain profiles of CE1 series. The strain profiles of specimens CE1-3 and CE1-4 have been ignored for analysis as the strains at 5 mm location had erroneous values due to instrument malfunction. It can be observed from the remaining three specimens that the load for the change of initial stress transfer length from approximately 50 mm to 100 mm was about 8.5 – 9 kN which was much lower than that

of control specimens (as discussed in section 3.8.1.3). The effective bond length was found to be 100 mm or less for two specimens and slightly greater than 100 mm for the remaining one according to the definitions by Yuan et al. (2004) and Lu et al. (2005). Hence, the effective bond length can be considered as 100 mm or less for this series.

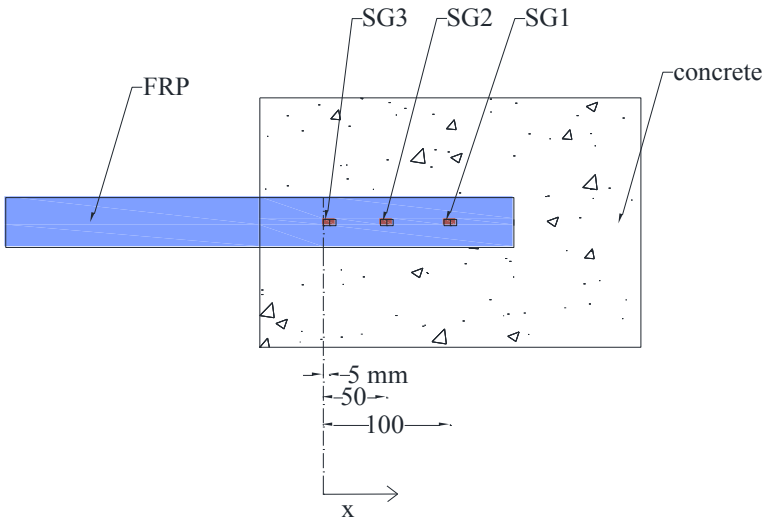

(a) Strain gauge locations for three strain gauge set-up

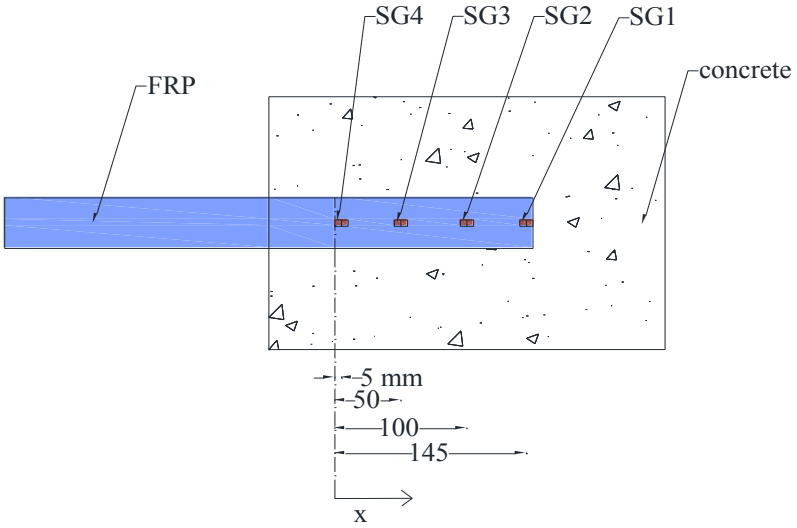

(b) Strain gauge locations for four strain gauge set-up

Figure 6.3 Strain gauge locations

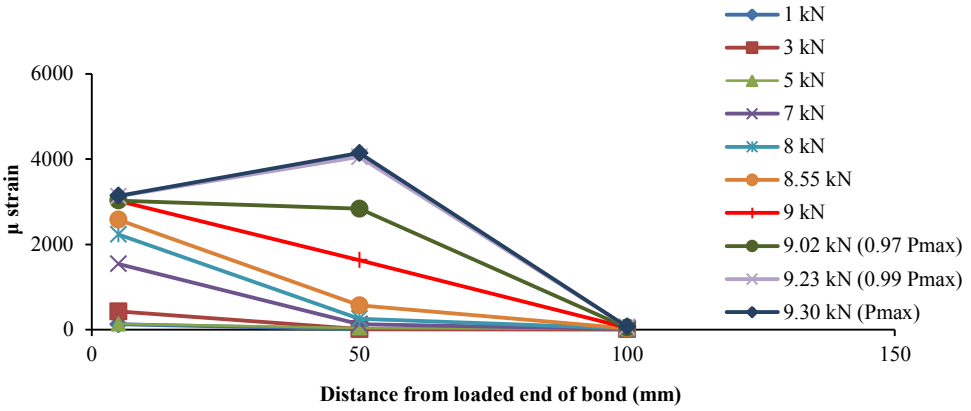

(a) CE1-1

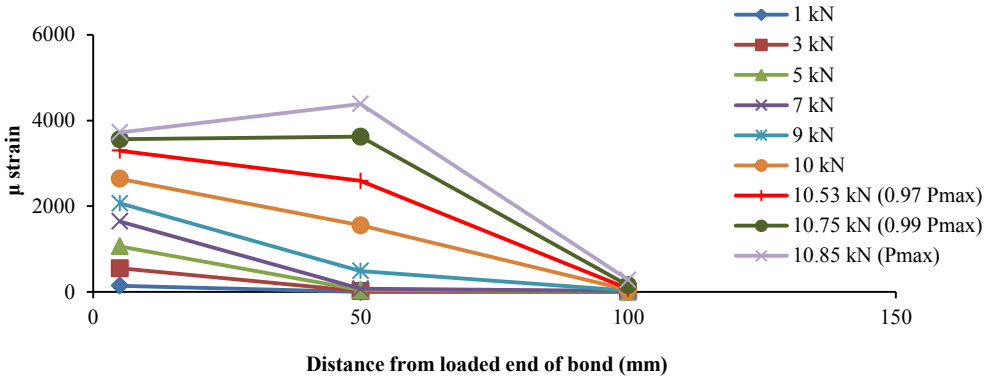

(b) CE1-2

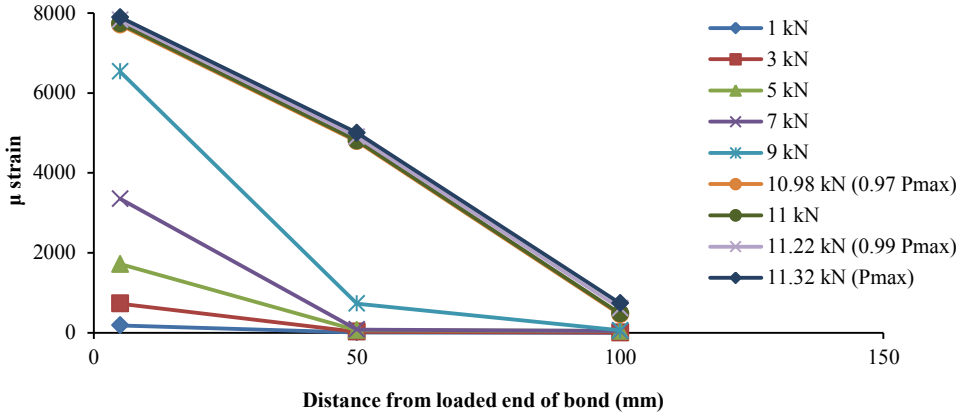

(c) CE1-5

Figure 6.4 Strain profiles of CFRP two month outdoor environment series

- **CE2 series:**

Similar to CE1 series, the load levels at which the initial transfer lengths changed from 50 mm to 100 mm for CE2 series (Figure 6.5), were also lower than the control series. Among four of the specimens tested in this series (specimen CE2-5 was damaged during transferring to laboratory), three specimens experienced the shifting of initial stress transfer length at about 7-8 kN and one at 9 kN. These loads were lower than that for CE1 series specimens. The effective bond lengths of the CE2 series can be assumed as more than 100 mm as three out of four specimens had the stress transfer length of more than 100 mm at 97 and 99 % of the maximum load of debonding.

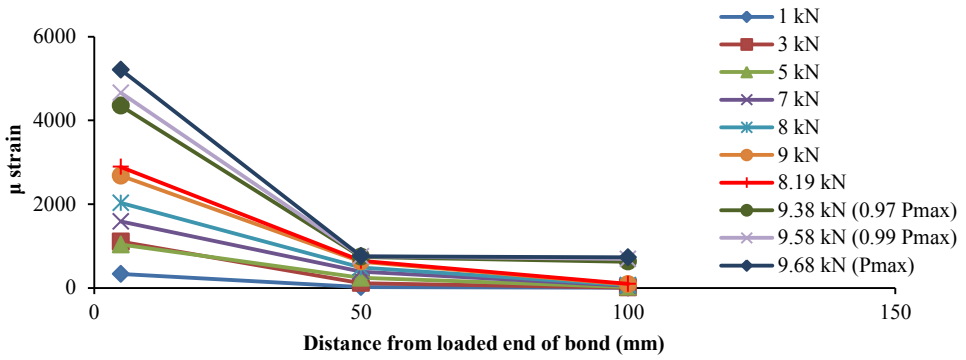

(a) CE2-1

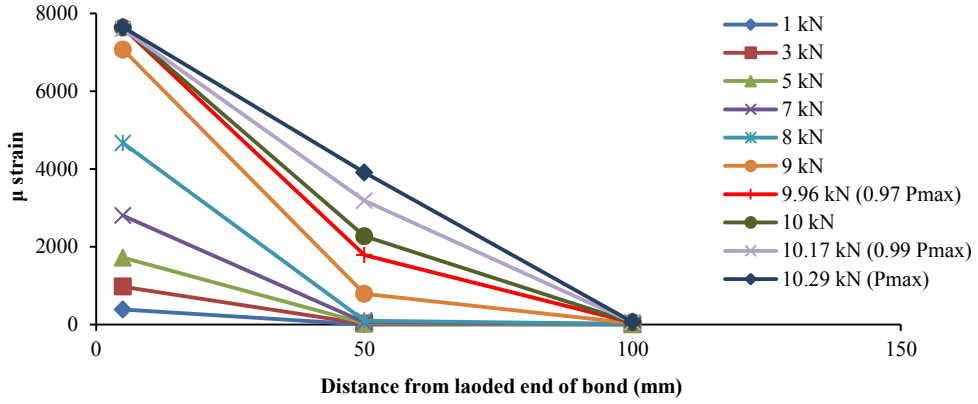

(b) CE2-2

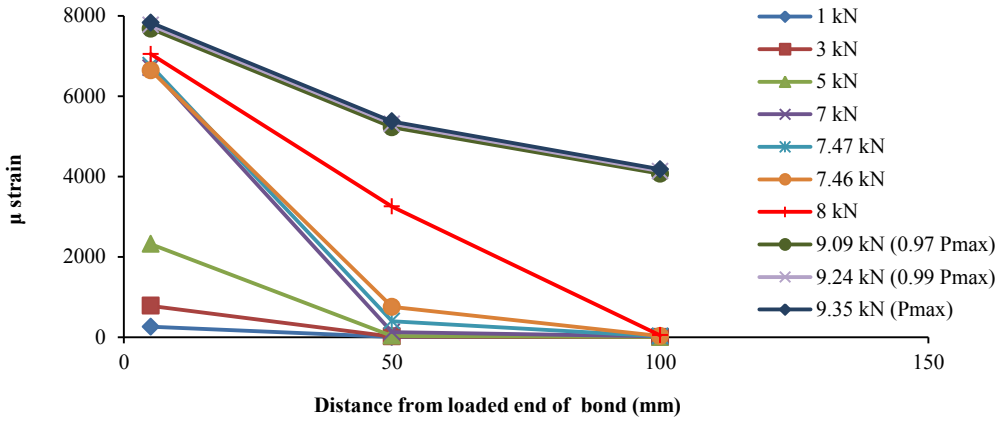

(c) CE2-3

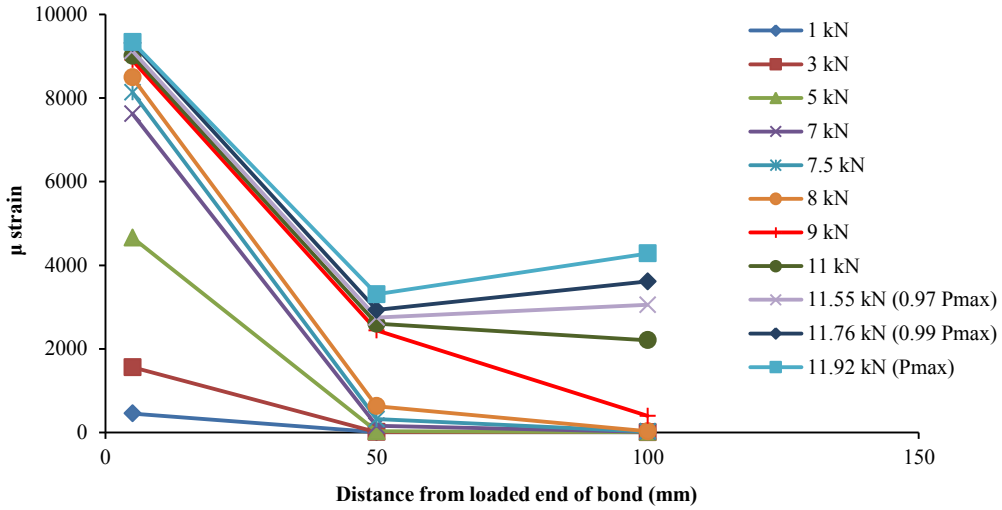

(d) CE2-4

Figure 6.5 Strain profiles of CFRP six month outdoor environment series

- **CE3 series:**

As illustrated in Figure 6.6, the change of initial stress transfer length of CE3 series occurred at 7.5 - 8.4 kN for three specimens and 10-11 kN for the remaining two. Compared to the strain profiles of control specimens, fabricated from concrete batch 2 (section 3.8.1.3), the load levels for CE3 series (also fabricated from concrete batch 2) were much lower. The effective bond lengths determined from the strain profiles of CE3 series for all specimens were observed as more than 100 mm.

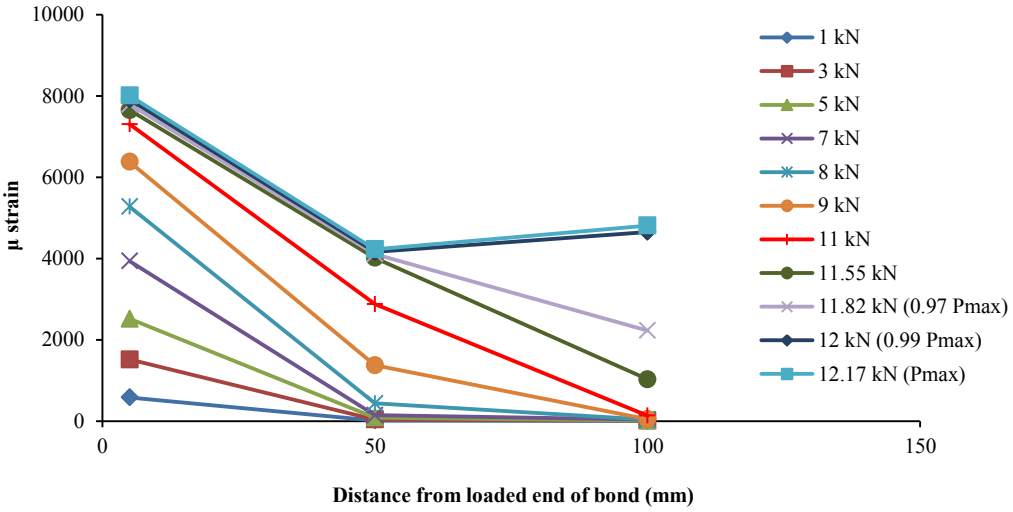

(a) CE3-1

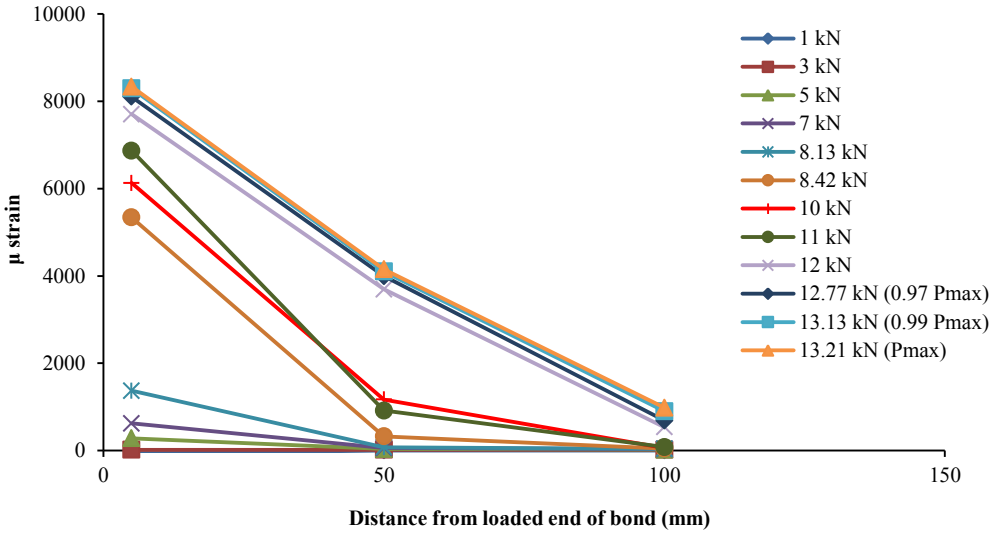

(b) CE3-2

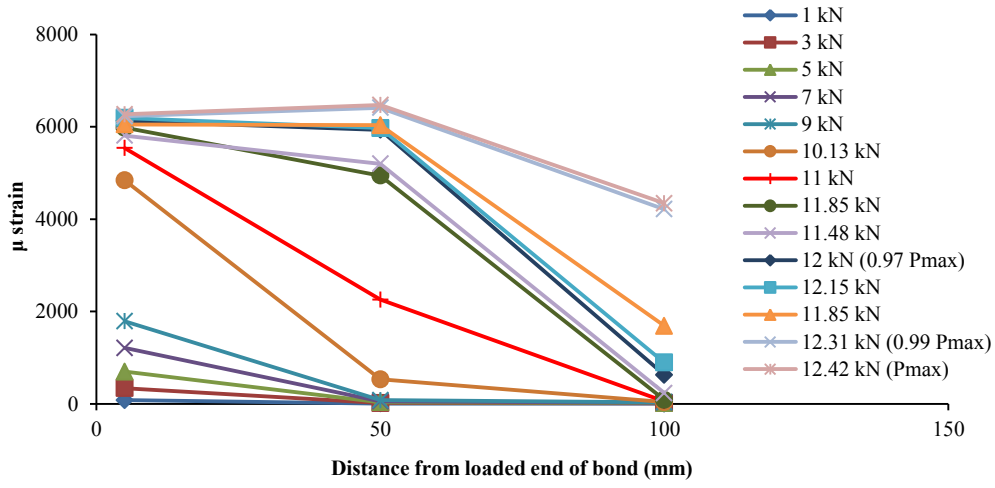

(c) CE3-3

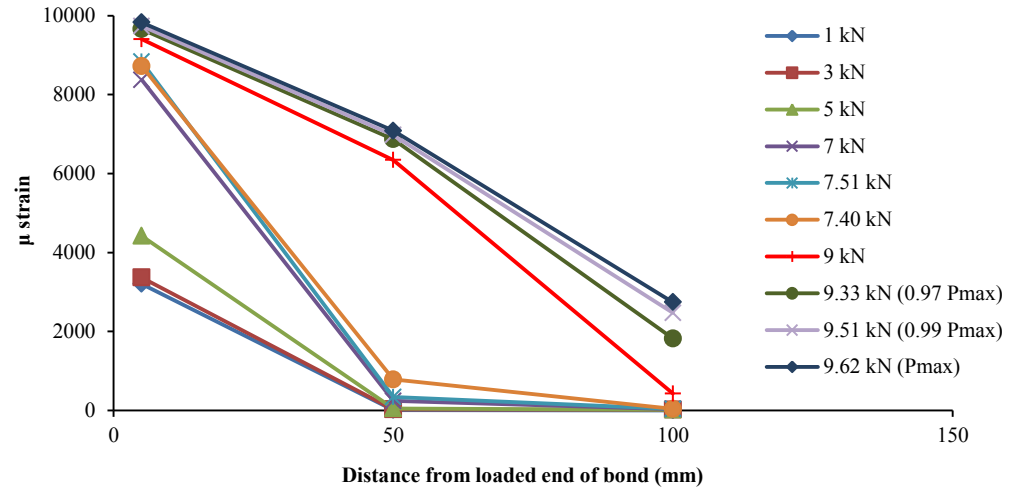

(d) CE3-4

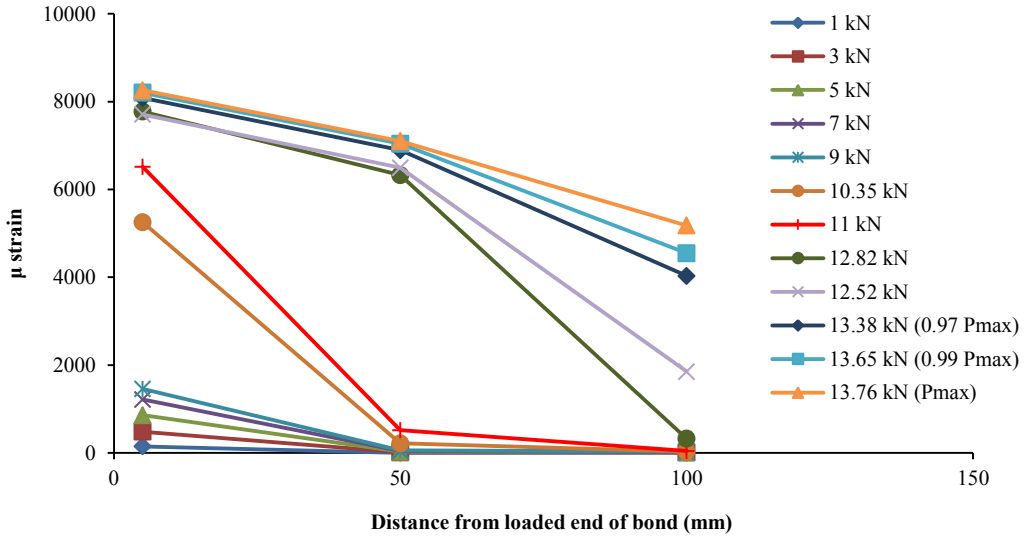

(e) CE3-5

Figure 6.6 Strain profiles of CFRP one year outdoor environment series

- **CE4 series:**

The strain distributions of CE4 series have been presented in Figure 6.7. The load values for the shifting of the initial stress transfer length from 50 mm to 100 mm were 10-11 kN for three specimens and 8 kN for two specimens. These loads at change in transfer length were slightly lower than those observed for the control series. Moreover, three out of five specimens exhibited effective bond lengths of 100 mm or less and the remaining two had those of more than 100 mm. Therefore, the effective bond length of this series can be assumed as 100 mm or less which is similar to control series.

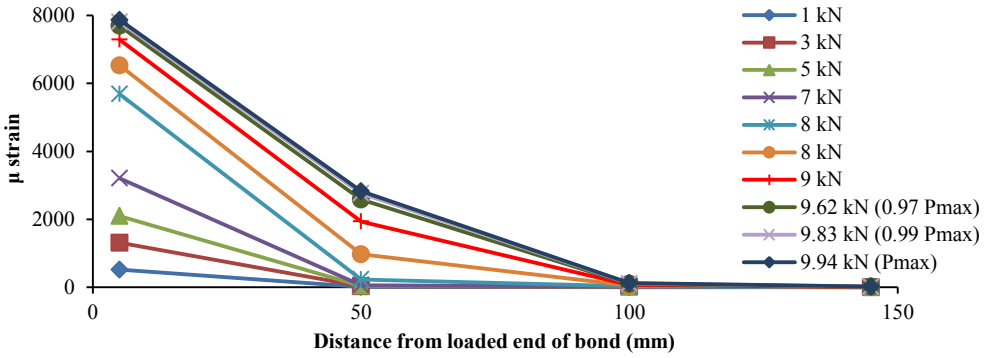

(a) CE4-1

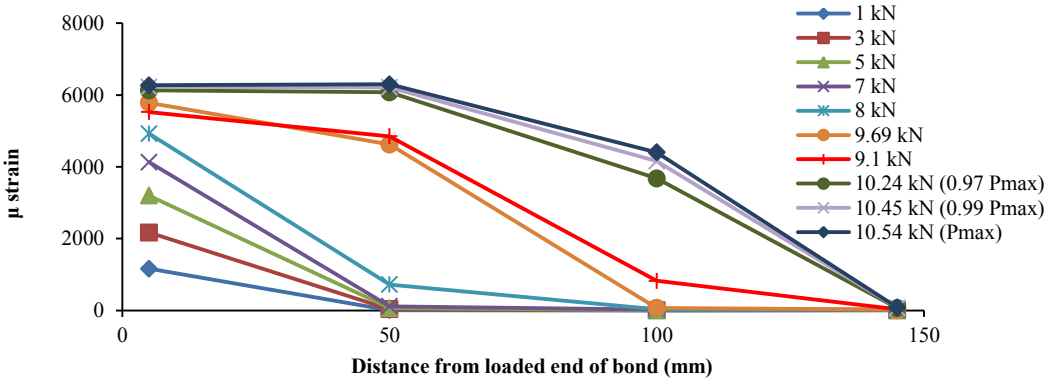

(b) CE4-2

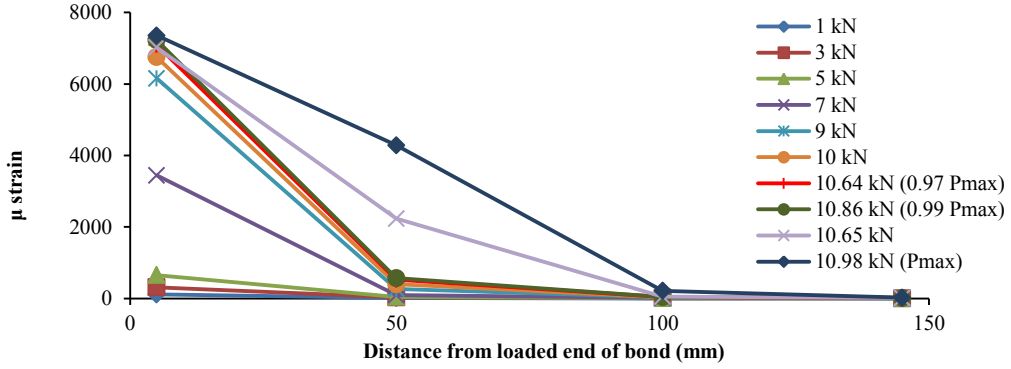

(c) CE4-3

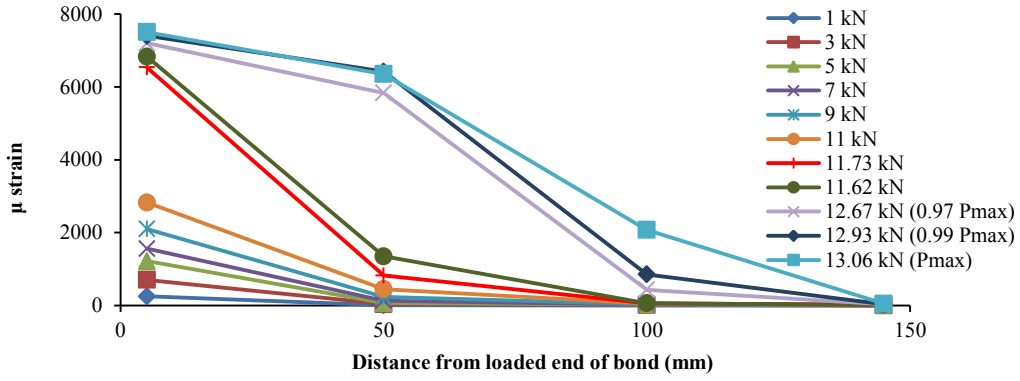

(d) CE4-4

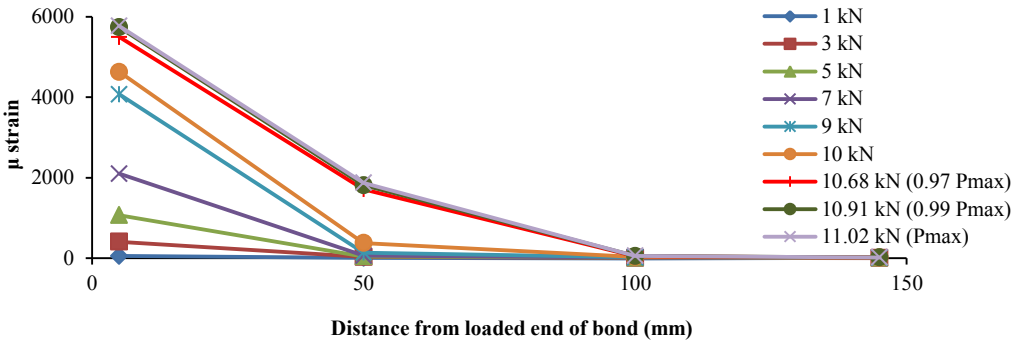

(e) CE4-5

Figure 6.7 Strain profiles of CFRP 18 month outdoor environment series

Based on the plotted strain profiles of all CFRP outdoor environment series, changes in strain profiles with time can be observed. The load level at which the change in initial stress transfer length occurred for all exposed series was lower than that of control specimens, except for CE4 series where this load was similar to the control series. The effective bond lengths for CE1 and CE4 series were similar to the control series and were 100 mm or less. However, effective bond lengths for CE2 and CE3 series were longer than the control series.

6.2.4 Discussion of test results

Exposure to outdoor environment had the most prominent effect on the CFRP-concrete bond and led to deterioration of the bond strength by 15.2 % after six months of exposure compared to the control value although the concrete compressive strength continued to increase (Figure 6.1). The reason can be attributed to the possible degradation of epoxy properties. In addition, the failure modes, shifted from thicker concrete layer to almost no concrete attached to debonded CFRP, suggests the dependence of bond strength more on the epoxy properties than concrete strength. The reason for the improvement of pull-out strength after 12 months can be because of the improvement of epoxy strength as the failure was still at the adhesive-concrete interface. The interesting behaviour of pull-out strength exhibiting deterioration after 18 months can be either of two possible reasons as follows:

1. The decrease in adhesive strength and concrete compressive strength (Figure 6.1) together compared to 12 month series resulted in adhesive-concrete interface failure with relatively thicker concrete attached and reduced pull-out strength. In fact, the thickness of concrete layer was observed to increase slightly after 18 months where some parts of debonded FRP showed concrete debris.
2. The adhesive strength remaining unchanged but the decreasing compressive strength increased the thickness of concrete compared to 12 months series and the pull-out strength decreased as a result of reduced concrete strength.

Hence, the complex behaviour of bond between FRP and concrete under exposed condition necessitates the investigation of epoxy properties under similar condition to understand its contribution to the changing pull-out strength.

The changing nature of strain profiles with exposure durations was also observed. The increased effective bond lengths observed from the strain profiles of exposed series indicate the requirement for longer bond lengths than the effective bond length of unexposed series for better long term performance.

6.3 Test results of GFRP outdoor environment series

The results of GFRP-concrete bond subjected to outdoor environment for two months (GE1 series), six months (GE2 series), one year (GE3 series) and 18 months (GE4 series) are discussed in the following sections.

6.3.1 Pull-out strength

The pull-out strengths of GFRP outdoor environment specimens have been given in Table 6.3. The change of pull-out strength and concrete compressive strength with time due to outdoor environmental exposure is also presented in graphical form in Figure 6.8. The vertical lines in the graph represent the positive and negative value of standard deviation of the normalised mean pull-out strength. From Figure 6.8, it can be observed that there was an initial reduction in the pull-out strength (to 90.7 % after six months) followed by a recovery in the pull-out strength in later stage reaching to 98.2% of the control value after 18 months. On the other hand, concrete compressive strength

increased continuously with time during the whole exposure duration of 18 months. The reason for the degradation of pull-out strength despite the increase in concrete compressive strength is discussed later in section 6.3.4 through observed failure modes.

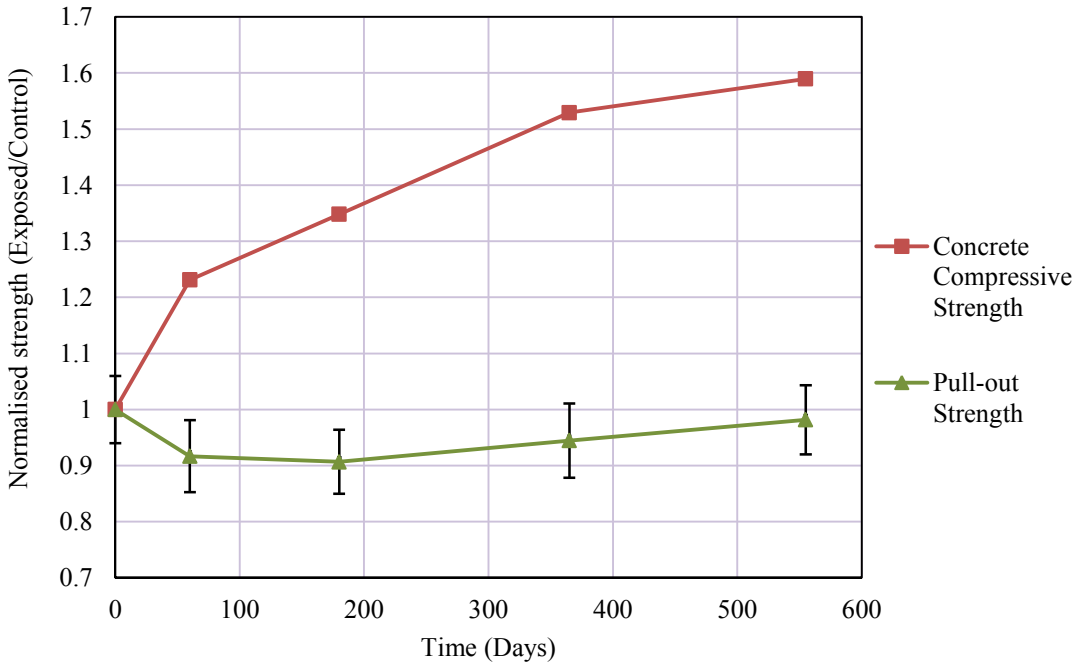

Figure 6.8 Normalised pull-out strengths of GFRP outdoor environment series with exposure duration

Table 6.3 Pull-out strengths of GFRP outdoor environment specimens

Exposure duration (Days)	Pull-out strength (MPa)	Mean pull-out strength (MPa)	CoV of pull-out strength (%)
0	1014.2	1027.0	6.0
	953.0		
	1054.5		
	1114.9		
	998.4		
60	994.2	941.4	7.0
	868.0		
	899.5		
	920.0		
	1025.3		
180	958.0	931.1	6.3
	938.1		
	922.1		
	998.1		
	839.4		
365	872.3	970.0	7.0
	996.1		
	1056.1		
	944.4		
	981.0		
555	953.6	1023.3	6.3
	1125.4		
	992.6		
	1036.9		
	1008.1		

6.3.2 Failure modes

- **GE1 series:**

GE1 series showed shifting of failure modes from thick layer of concrete to very thin layer of concrete attached to debonded GFRP in comparison with the GFRP control specimens (section 3.8.2.2). In fact, visual inspection (Figure 6.9 (a)) confirmed that the failure mainly occurred in hardened cement paste adjacent to the epoxy layer. The epoxy layer was visible on most part of the concrete substrate and debonded GFRP.

- **GE2 series:**

Similar to GE1 series, GE2 series also exhibited failure modes with almost no concrete attached to GFRP (Figure 6.9 (b)).

- **GE3 series:**

GE3 series had hardly any concrete attached to debonded FRP. In addition, mostly, epoxy was visible all over the debonded GFRP strip as illustrated in Figures 6.9 (c) and (d).

- **GE4 series:**

In GE4 series, failure mode similar to GE3 series was observed (Figure 6.9 (e))

(a) GE1-1

(b) GE2-1

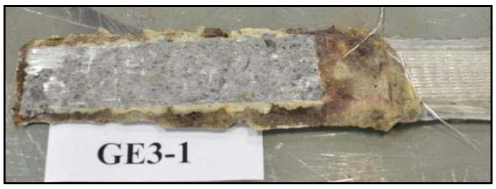

(c) GE3-1

(d) GE3-5

(e) GE4-2

Figure 6.9 Failure modes of GFRP outdoor environment specimens

Based on failure patterns of all GFRP outdoor environment series, it can be summarised that exposed condition changed the mode of failure from very thick concrete layer to very thin concrete layer attached to GFRP coupon compared to control series. Even, GE3 and GE4 series showed hardly any concrete attached to debonded GFRP. Hence, the failure modes for all series can be assumed as concrete-adhesive interfacial failure.

6.3.3 Strain profiles

Strain profiles of all series, except GE4 specimens, were plotted for three strain gauge set-up (Figure 6.3 (a)). Only GE4 series had the set-up with four strain gauges as shown in Figure 6.3 (b). The strain profiles of all series have been discussed separately as follows:

- **GE1 series:**

The strain profiles of GE1 series have been illustrated in Figure 6.10. The initial stress transfer length changed to approximately 100 mm at loads of about 7 kN, 8.7 kN, 10.8 kN, 10.5 kN and 9 kN for specimens GE1-1, 2, 3, 4 and 5, respectively. The load levels were found to be lower than the control series. Also, the strain profiles varied from control series (section 3.8.2.3) in terms of effective bond length as three out of five specimens showed effective bond length of more than 100 mm.

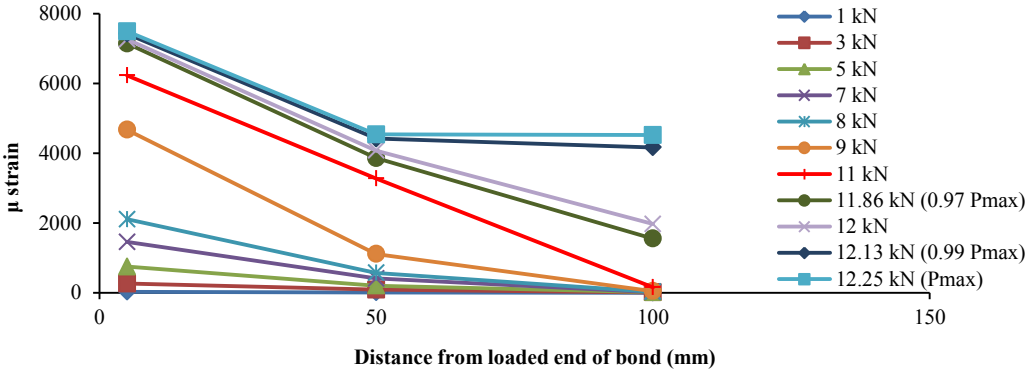

(a) GE1-1

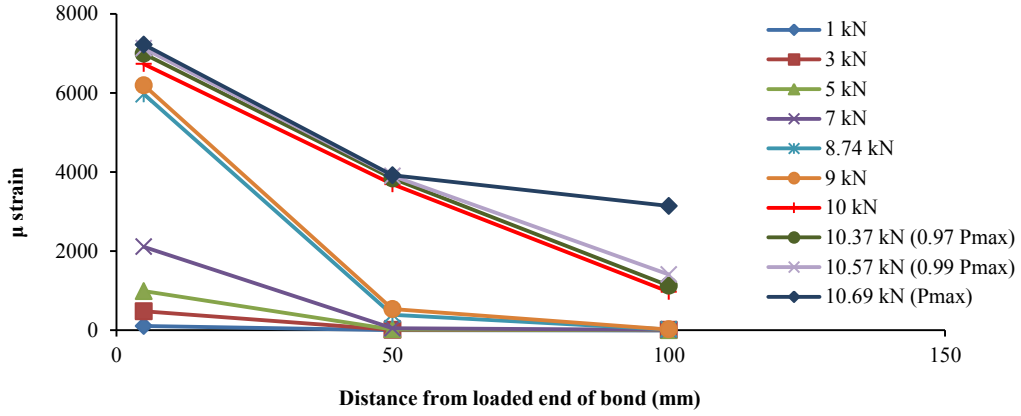

(b) GE1-2

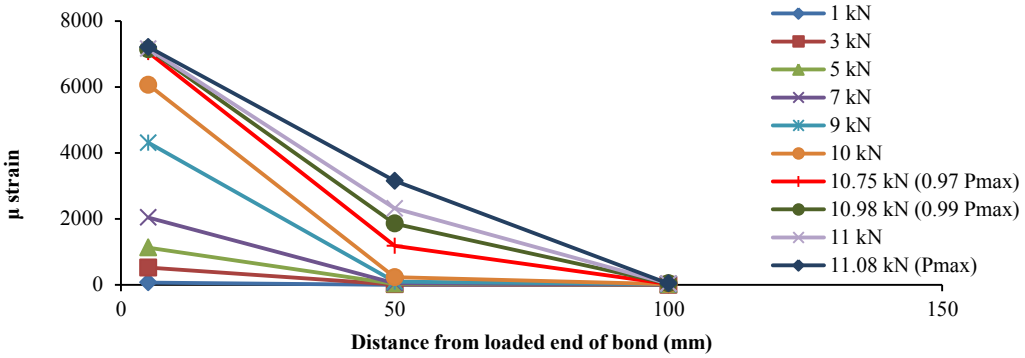

(c) GE1-3

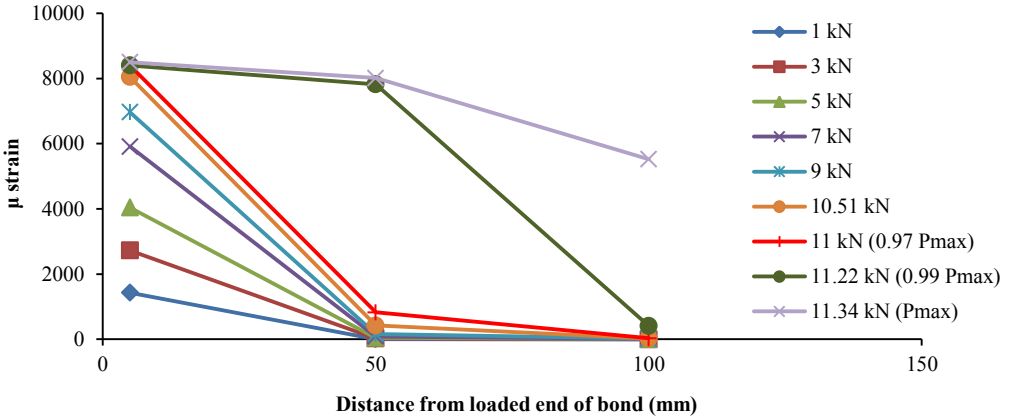

(d) GE1-4

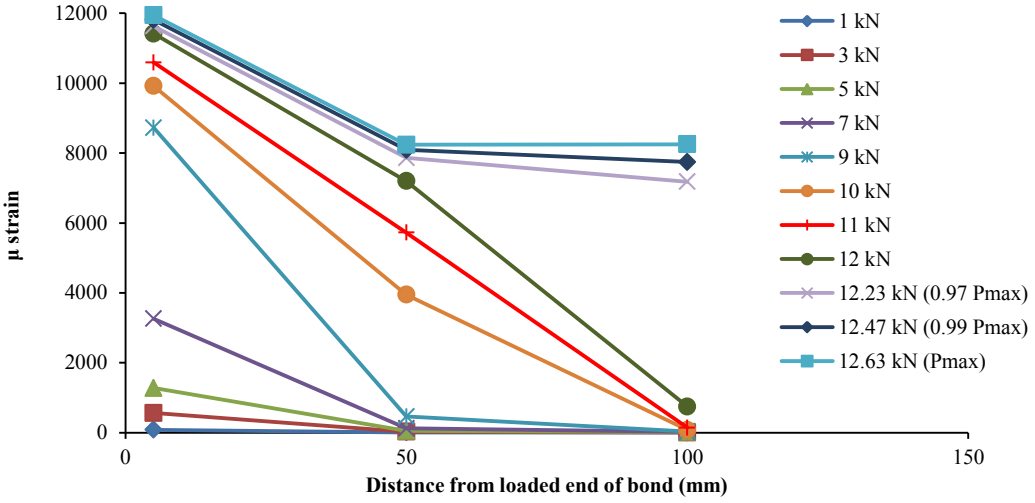

(e) GE1-5

Figure 6.10 Strain profiles of GFRP two month outdoor environment series

- **GE2 series:**

The strain profiles of GE2 series, as illustrated in Figure 6.11, exhibited an interesting behaviour. Only specimen GE2-2 experienced the change of initial load/stress transfer length at about 9 kN load whereas the other four specimens experienced this at much lower loads (approximately 5-7 kN). Also, the strains were distributed to the bonded GFRP gradually with the increase of load and not abruptly like control series. Similar to GE1 series, three out of five specimens of GE2 series had effective bond length of more than 100 mm and thereby, differed from the effective bond length of control series.

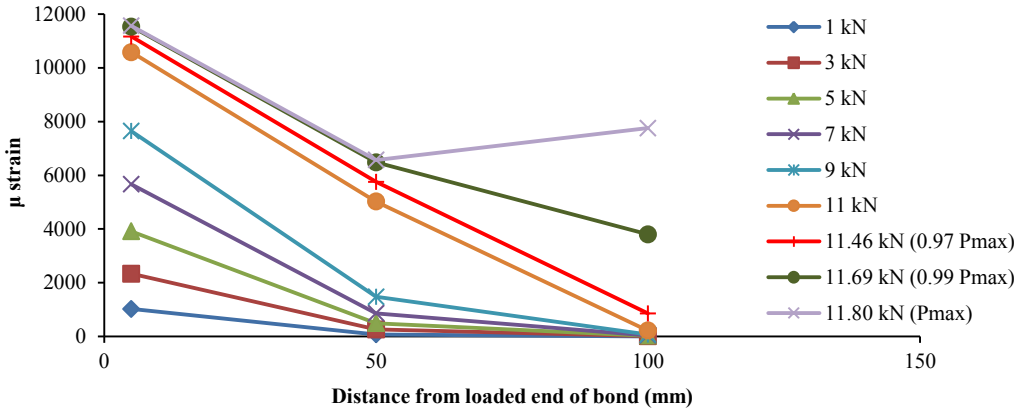

(a) GE2-1

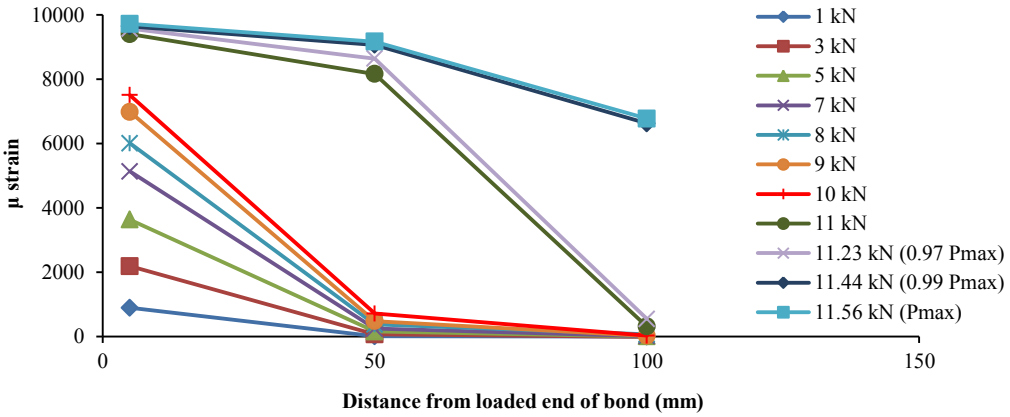

(b) GE2-2

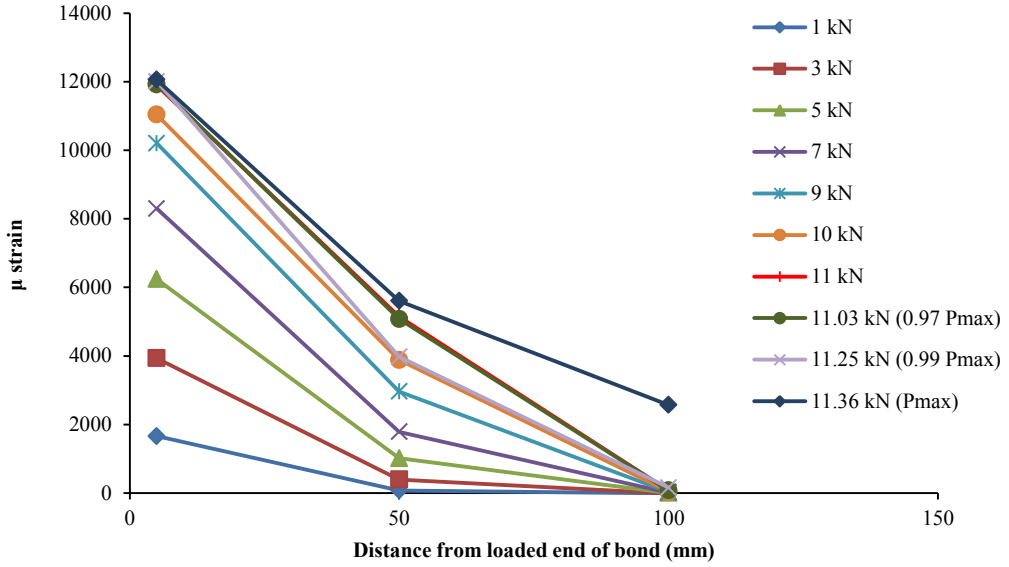

(c) GE2-3

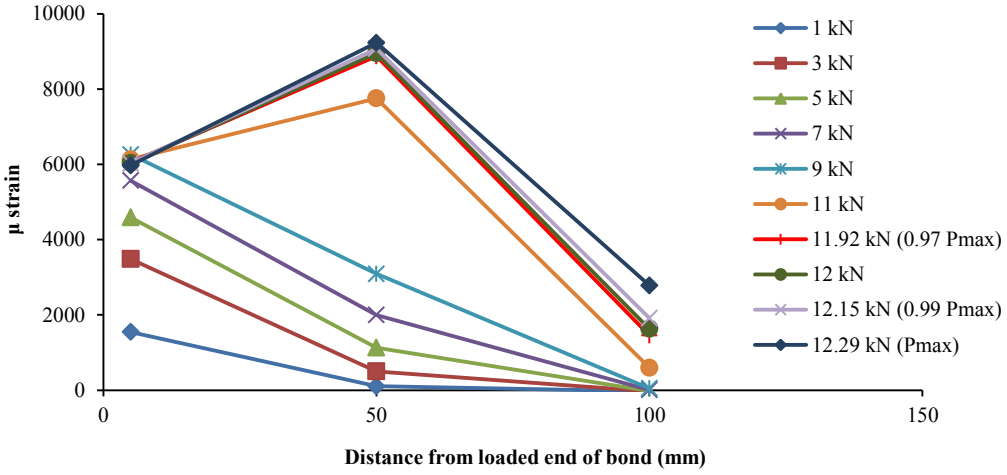

(d) GE2-4

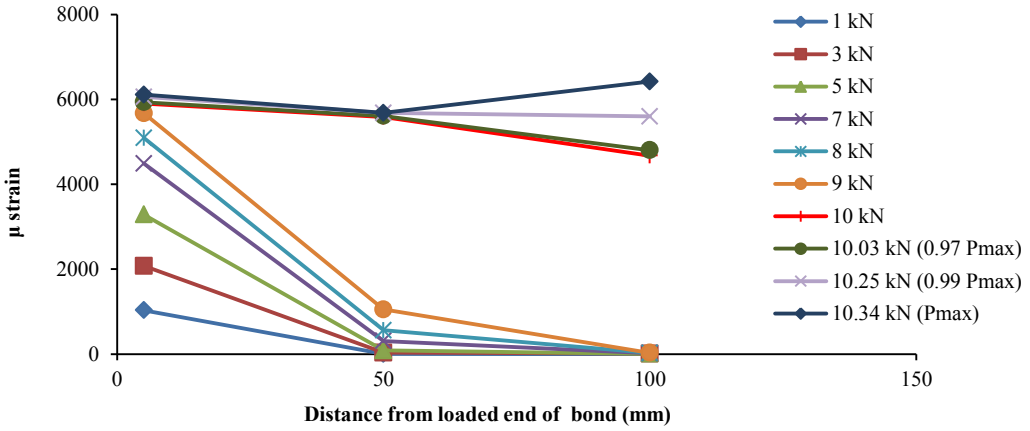

(e) GE2-5

Figure 6.11 Strain profiles of GFRP six month outdoor environment series

- **GE3 series:**

Unlike the GE2 series, initial transfer length from 50 to 100 mm occurred at higher loads for GE3 series. From Figure 6.12, it can be observed that the change of initial stress transfer length occurred at 7.8 kN, 11 kN, 10 kN, 10.5 kN and 10.5 kN for specimens GE3-1 to 5, respectively. These loads are slightly lower than that for the control series but not as much as for GE2 series. However, the effective bond lengths of three of the specimens of this series were more than 100 mm and higher than those observed in control specimens.

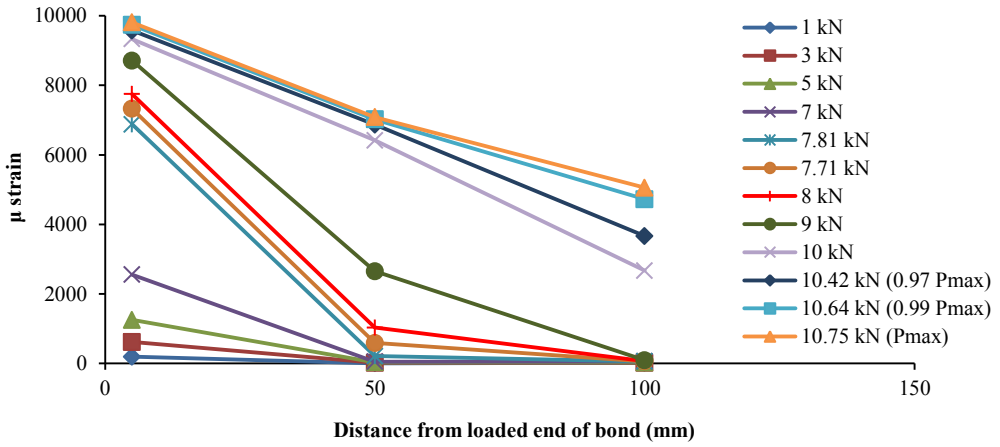

(a) GE3-1

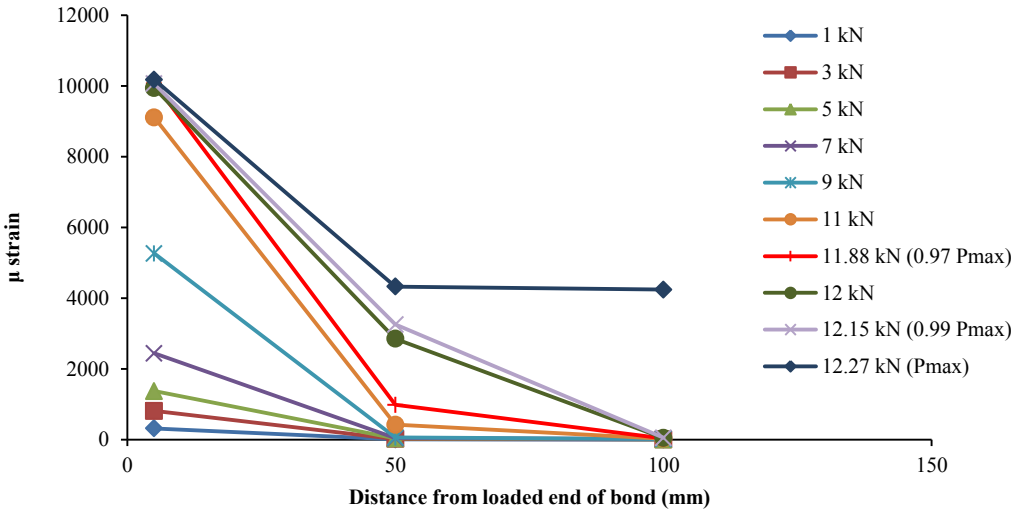

(b) GE3-2

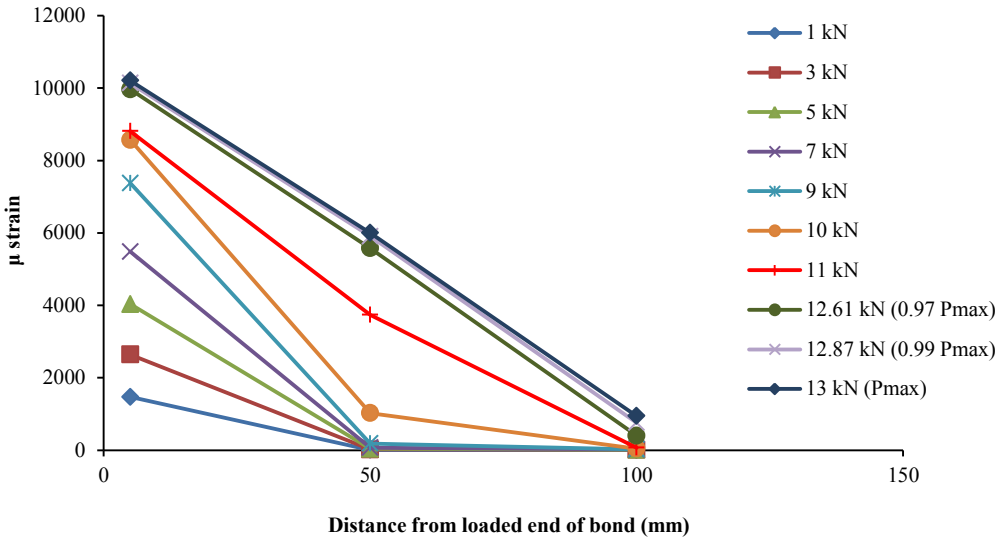

(c) GE3-3

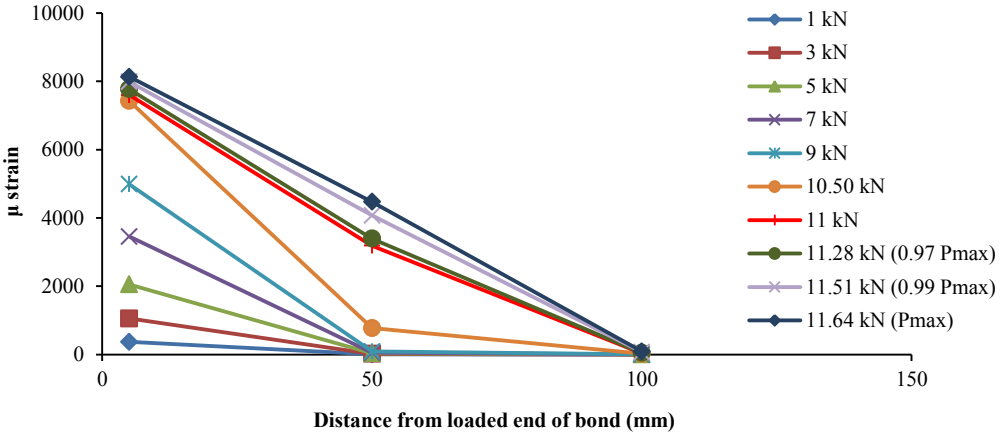

(d) GE3-4

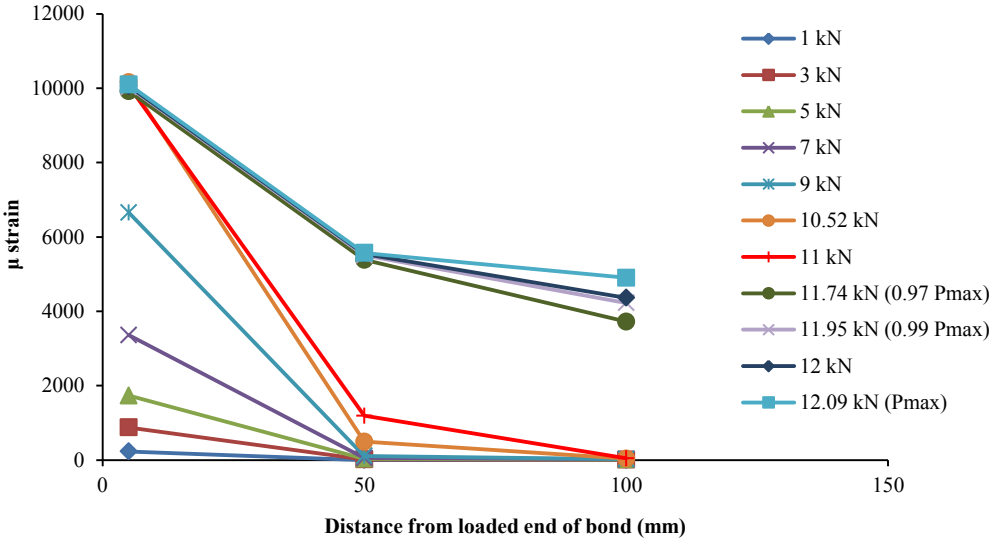

(e) GE3-5

Figure 6.12 Strain profiles of GFRP one year outdoor environment series

- **GE4 series:**

The strain profiles and loads (10.5 to 11 kN for four specimens and 7.8 kN for one specimen) when the shifting of initial transfer length occurred for GE4 series (Figure 6.13) were similar to the control series (section 3.8.2.3). The effective bond lengths of four specimens can be assumed to be 100 mm at least from the consideration of load transfer length at 97% of the maximum load.

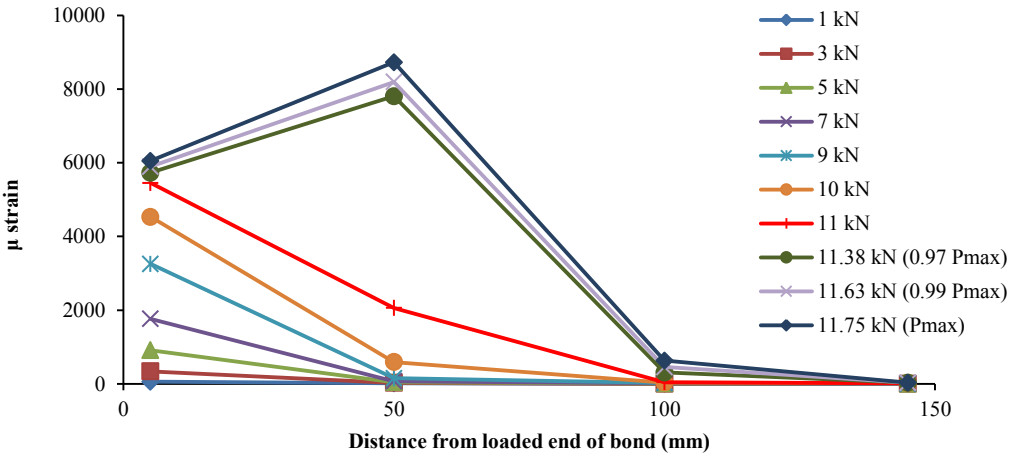

(a) GE4-1

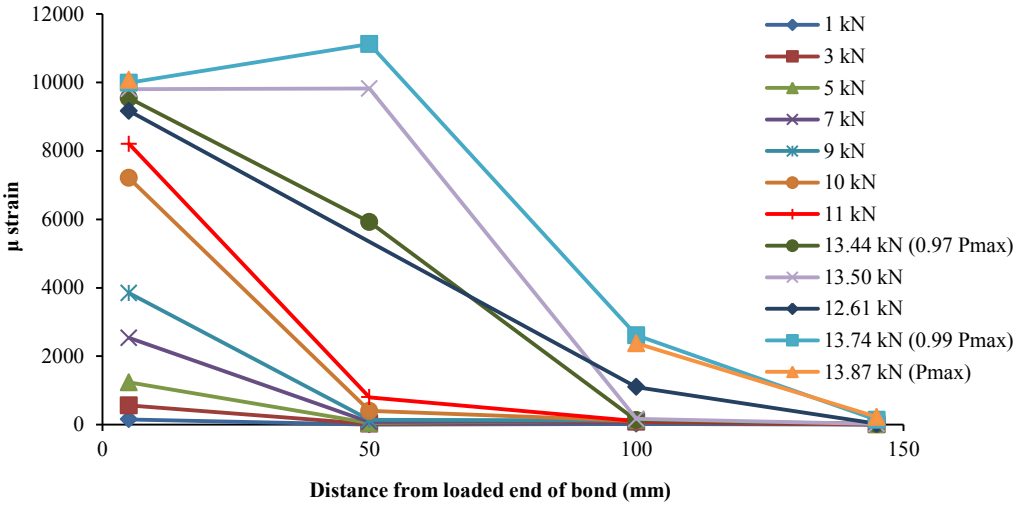

(b) GE4-2

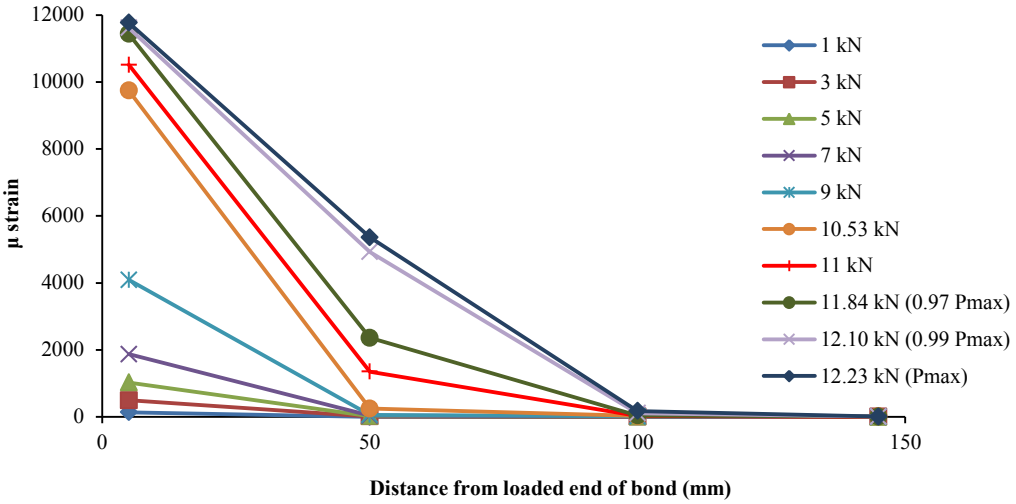

(c) GE4-3

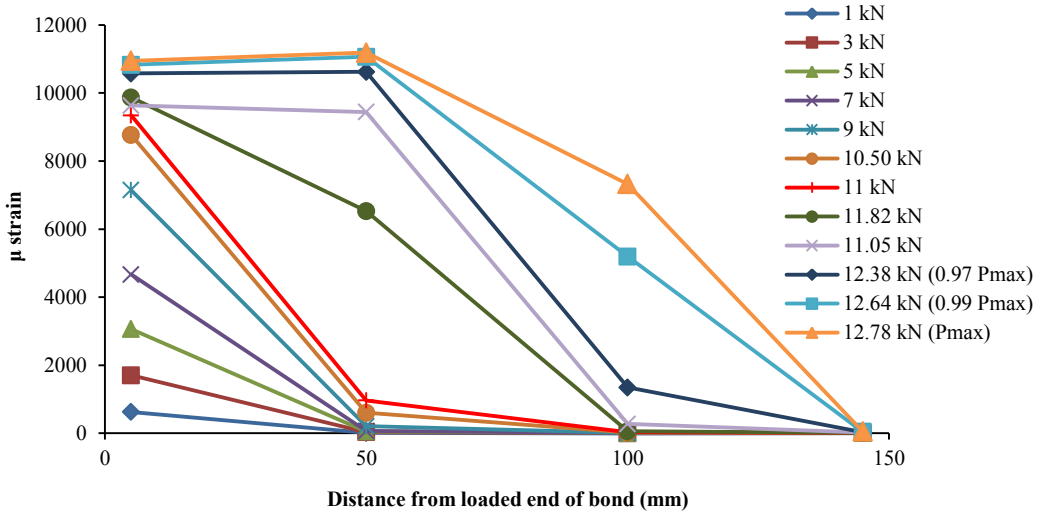

(d) GE4-4

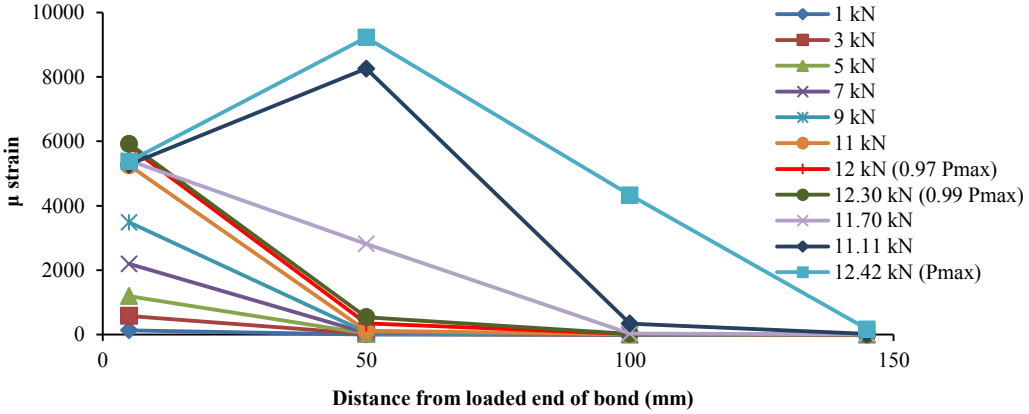

(e) GE4-5

Figure 6.13 Strain profiles of GFRP 18 month outdoor environment series

The strain profiles for GFRP outdoor environment series showed very interesting behaviour in terms of the changes of initial stress transfer lengths. Load at the change in initial transfer length for GE1 and GE2 were much lower than the control but this load increased for GE3 and GE4 series, with the load being almost equal to that for control series. This trend exactly coincides with the change of pull-out strength with time of exposure (Figure 6.8). The effective bond lengths for all series, except for GE4, were more than 100 mm.

6.3.4 Discussion of test results

Although the pull-out strength of GFRP-concrete bond was found to deteriorate with time until the maximum degradation of 9.3% occurred after six months, the degradation of GFRP-concrete bond was much lower than that of CFRP-concrete bond. The deterioration of bond can be due to the possible loss of epoxy properties under exposed environment as the concrete compressive strength increased continuously with time (Figure 6.8) Also, failure modes associated with very thin or almost no concrete attached to debonded GFRP lead to the interpretation that the failure occurred in the concrete-adhesive interface and thereby, epoxy strength had more influence on the bond mechanism than the concrete strength under the exposure of outdoor environment. The gradual improvement of pull-out strength after one year can be attributed to the possible improvement of the epoxy properties as the failure modes were still in the interface. In addition, strain profiles exhibited changing nature with time and the effective bond length increased for exposed specimens compared to control specimens.

6.4 Chapter summary

This chapter aimed to discuss the findings of the investigation on the effect of outdoor environment on CFRP and GFRP-concrete bond. The major findings can be summarised as follows:

-The maximum degradation of pull-out strength for CFRP and GFRP-concrete bond was 15.2% and 9.3% compared to that for the corresponding unexposed specimens, respectively and the main cause of degradation can be degraded epoxy properties.

- Failure modes for both CFRP and GFRP bonded concrete prisms changed from thick layer of concrete to almost no concrete attached to debonded FRP due to outdoor environment.

- Effective bond length increased due to exposed condition for both types of FRP-concrete bond.

From the findings stated above, it can be concluded that the most severe environmental conditions applied in this study was the outdoor environment as it caused significant deterioration of both CFRP and GFRP concrete bond in comparison with the other two environmental conditions. In addition, CFRP-concrete bond was the most affected one between the two types of bond system used in this study. Moreover, changing failure modes from thicker concrete layer to almost no concrete layer for outdoor environmental conditions suggests that further experimental study on epoxy properties under similar conditions is required in order to justify the dependence of bond properties on the epoxy properties. Furthermore, the descending trend of pull-out strength after 18 months of exposure suggests the requirement of further investigation for extended durations.

CHAPTER 7

STUDY ON THE FRACTURE PROPERTIES OF CFRP-CONCRETE BOND EXPOSED TO THREE ENVIRONMENTAL CONDITIONS

7 Study on the fracture properties of CFRP-concrete bond exposed to three environmental conditions

7.1 Introduction

Interfacial fracture energy, G_f, is an important parameter to model adhesive bonded joints (Dai, Ueda & Sato 2005). The debonding of FRP from concrete due to direct shear can be represented as interfacial fracture (Boyajian 2002) and the interfacial fracture energy is a failure criterion of adhesive joints. It can be defined as the energy release rate at a debonding tip at the maximum transmissible force (Imani 2010) where the energy release rate, G, was defined by Irwin in 1956 as the energy needed for the propagation of existing crack by infinitesimal unit area. The interfacial fracture energy of FRP-concrete bond can be determined from the area under the shear stress-slip curve of the bond. The study of interfacial energy of FRP-concrete bond was reported by Bazant, Daniel & Li (1996), Täljsten (1996), Maeda et al. (1997), Neubauer & Rostasy (1997), De Lorenzis, Miller & Nanni (2001), Yuan, Wu & Yoshizawa (2001), Wu, Yuan & Niu (2002), Dai, Ueda & Sato (2005), Mazzotti, Savoia & Ferracuti (2008) and Imani (2010). Therefore, considering the importance of fracture energy release rate in adhesive joints, this chapter aims to discuss the fracture energy release rate due to the debonding of CFRP-concrete bond for both control and exposed specimens. Comparisons of the energy release rates from curve fitting of experimental shear stress-slip data with those from theory and one of the existing stress-slip interface laws have also been included in this chapter. The methodology used in the determination of shear stress, slip and fracture energy from the experimental data of pull-out tests of CFRP bonded concrete prisms has been presented in the first part (section 7.2) of this chapter. In addition, a summary of theoretical fracture energy and an existing shear-slip law has been provided. The second part of the chapter (section 7.3) focuses on the results obtained from the analysis of shear stress-slip relationship of the control and exposed specimens and discusses the effect of the environmental conditions, namely, temperature cycles, wet-dry cycles and outdoor environment on the fracture energy release rate for the debonding of CFRP-concrete bond. In section 7.4, the stress-lip laws

for control and exposed specimens have been proposed based on the determination of unknown parameters by curve fitting of experimental shear stress and slip data. Finally, section 7.5 provides a conclusive summary of the findings of the study on the fracture energy of CFRP-concrete bond under three environmental conditions.

7.2 Determination of shear stress-slip relationship and fracture energy

The shear stress-slip relationships of CFRP-concrete bond for control and exposed specimens have been established from the strain values along the bond length of CFRP bonded concrete prisms and the CFRP stiffness values. As the tensile properties of GFRP exposed coupons were not evaluated in this study, the shear stress-slip relationships for GFRP bonded specimens are not discussed and the discussion is limited to CFRP bonded specimens only.

7.2.1 Shear stress and slip from strains along CFRP bond length

The establishment of shear stress-slip relationship using the strain gauges along the bond length of FRP sheet was first conducted by Täljsten (1997) and further adopted by many researchers (Ferracuti, Savoia & Mazzotti 2006; Nakaba et al. 2001; Pham & Al-Mahaidi 2007). From a typical pull-out test set-up as illustrated in Figure 7.1, the average shear stress, τ, between two successive strain gauges, ε_i and ε_{i-1}, can be determined by Equation 7.1 as follows:

$$\tau = \frac{E_f t_f (\varepsilon_i - \varepsilon_{i-1})}{\Delta x} \tag{7.1}$$

where E_f is the tensile modulus of elasticity of FRP and t_f is the thickness of FRP sheet.

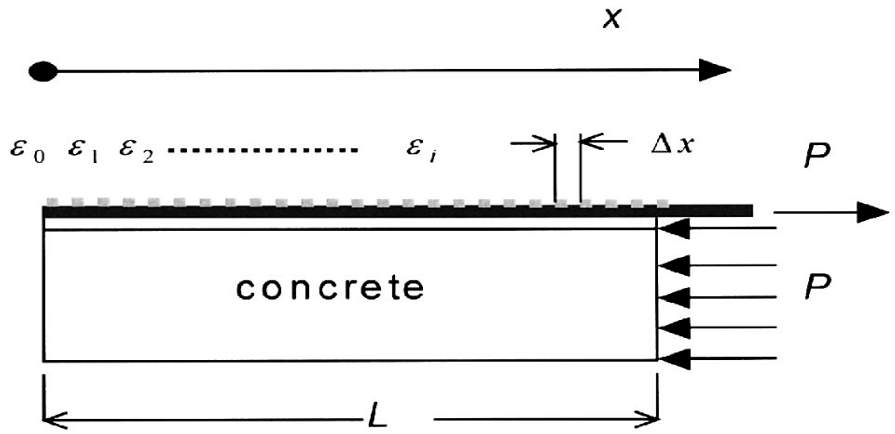

Figure 7.1 Pull-out test set-up (Dai, Ueda & Sato 2005)

The local slip between concrete and FRP due to the strain differences between concrete and FRP can be determined with the assumption that the overall deformation of concrete is negligible compared to FRP deformation provided that the concrete specimen is much larger than the FRP. Hence, the strain in concrete can be ignored. In addition, if a bond length much greater than the effective bond length is used, the slip at the far end (at the location of ε_0 in Figure 7.1) of FRP-concrete bond can be assumed as zero. The slip at any strain gauge location *i* can be obtained by integrating the strain values along the bond length numerically starting from the strain value at the far end; i.e. ε_0. Equation 7.2 represents the slip, s_i, at strain gauge location, *i*.

$$s_i = \frac{\Delta x}{2}(\varepsilon_0 + 2\sum_{1}^{i-1}\varepsilon_j + \varepsilon_i) \tag{7.2}$$

where s_i = local slip at the strain gauge location *i*, ε_0 = strain of FRP at the free end of the bond, ε_j = strain of the *j*th gauge (*j=1* to *i-1*).

Hence, the average slip between the locations *i* and *i-1* can be obtained as follows:

$$s = \frac{s_i + s_{i-1}}{2} \tag{7.3}$$

After obtaining the average shear stress (Equation 7.1) and corresponding average slip (Equation 7.3) at any location for the load values starting from zero to close to failure of the bond, the shear-stress slip plot can be developed for each of the specimens. It should

be noted that a large number of strain gauges with very close intervals (10-20 mm) should be used for better estimation of local bond-slip relation (JCI TC952 1998). If the strain gauge interval is large, the results of average shear stress between two strain gauges obtained from the difference of strain readings as well as the local slip calculated by numerical integration of strain profile are likely to be affected. Although the shape of strain profile is nonlinear, the linear variation of strains between two subsequent strain gauges is assumed in order to integrate the strain profile (Ferracuti, Savoia & Mazzotti 2007) and close intervals of strain gauges are required to increase the accuracy of the results.

Also, the slip at the loaded end of bond can be measured alternatively by attaching Linear Variable Differential Transformer (LVDT). Dai, Ueda & Sato (2005) and Imani (2010) applied this technique in their study to measure the slip only at the loaded end of FRP-concrete bond and thereby, established the shear stress-slip interface laws.

Between two of the methods stated above, the method using strain gauge reading was used in this study as no LVDT was attached to the loaded end of bond. Although, only three strain gauges (SG1 to 3) were attached to most of the specimens (Figure 7.2), the strain at the free end was assumed to be zero to integrate the strains numerically along the bond length. The assumption seems reasonable as the bond length used in this study was much higher than the theoretical effective bond length computed by Chen & Teng (2001) model. As the shear stresses and corresponding slips at the loaded end are sufficient to establish shear-stress-slip relationship, the average shear stress and slip at 5 -50 mm location from the loaded end was only considered. However, the shear stress-slip values at other locations were also assessed and used when the maximum shear stress and slips occurred at those locations.

.

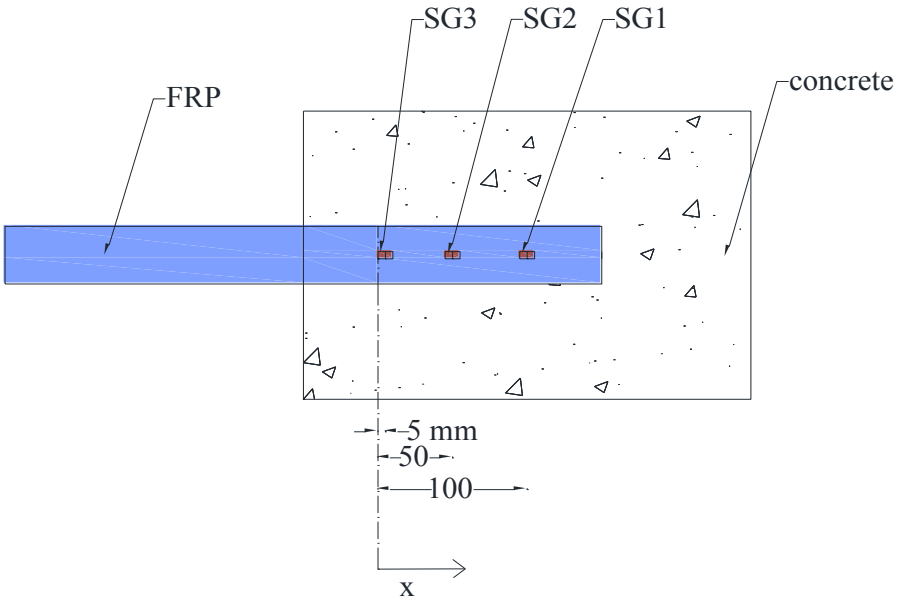

Figure 7.2 Strain gauges used for slip measurements

7.2.2 Determination of Fracture energy release rate

Fracture energy release rate, G_f, for debonding of FRP from concrete can be related to the maximum force, $P_{max,}$ in a pure shear test as follows:

$$P_{\max} = b_f \sqrt{2E_f t_f G_f} \tag{7.4}$$

where b_f = the width of FRP sheet, E_f = the tensile modulus of elasticity of FRP and t_f = thickness of FRP sheet

Equation 7.4 is a well-established formula and was derived by many researchers applying various approaches. Täljsten (1997), Yuan, Wu & Yoshizawa (2001) and Wu, Yuan & Niu (2002) showed the same expression by Linear Elastic Fracture Mechanics (LEFM). Dai, Ueda & Sato (2005) derived it by expressing the shear stress as a function of slip and integrating the shear stress with respect to slip. J-integral approach, adopted by Imani (2010), also revealed the same relation between the maximum pull-out force and fracture energy release rate. Therefore, the fracture energy release rate can easily be calculated from an experimentally obtained pull-out force from the above analytical expression.

The determination of fracture energy can also be conducted by numerical integration of shear stress-slip plots obtained from experimental data. The shear stress and slip can easily be obtained using the strain data and the FRP stiffness value as discussed in section 7.2.1. However, obtaining a smooth curve for shear stress-slip is unlikely unless a suitable curve fitting technique is applied. Hence, in this study, the average shear stresses of the loaded end of bond was fitted against corresponding slip values by curve fitting toolbox of MATLAB software and the fracture energy was calculated from the fitted curve by analysis tool incorporated in the MATLAB Curve Fitting Toolbox. The rational fit of curve fitting toolbox was able to match experimental data very closely for all the control and exposed specimens. The curves fitted to shear stress-slip data had a general form as shown in Equation 7.5.

$$\tau(s) = \frac{p_1 s^2 + p_2 s + p_3}{s^2 + q_1 s + q_2} \tag{7.5}$$

where $\tau(s)$ = regressed value of shear stress (expressed as a function of slip, s) obtained from fitted curve and p_1, p_2, p_3, q_1 and q_2 are unknown parameters of the rational fit.

Although all individual specimens showed very good agreements with Equation 7.5, the values of peak shear stresses or slips showed variations even in the same series of specimens due to scattered nature of experimental data. The scatter of FRP-concrete bond experimental data was also reported by Mazzotti, Savoia & Ferracuti (2009) and Pham & Al-Mahaidi (2007).

The shear stresses against slips were also fitted with a nonlinear model developed by Dai, Ueda & Sato (2005). Equation 7.6 provides the nonlinear relationship of shear stress, τ, with slip, s, as determined by Dai, Ueda & Sato (2005).

$$\tau = A^2 B E_f t_f \exp(-Bs)(1 - \exp(-Bs)) \tag{7.6}$$

where A and B are two unknown parameters of the τ-s fit and can be obtained from the regression analysis. A can be referred to as maximum FRP strain in a pull-out test set-up and the other parameter B can be regarded as ductility index (unit of B is mm^{-1}). The smaller value of B indicates lower initial interfacial stiffness but better ductility as it causes slower softening after the maximum bond stress occurs.

7.3 Results and discussions

The fracture energy release rates determined both from analytical formula and from fitted curves of experimental data have been included in this section for control and exposed specimens separately. Also, the change of fracture energy release rate with time due to exposed conditions has been discussed.

7.3.1 Fracture properties of control specimens

The shear stress-slip curves were fitted for control CFRP specimens fabricated from two batches of concrete. Figure 7.3 (a) shows the rational fit of one of the specimens from control series fabricated from the first batch of concrete whereas Figure 7.3 (b) shows the shear stress-slip curve of the same specimen fitted with Equation 7.6. The curves for rest of the specimens have been provided in Appendix C.1. As illustrated in Figures 7.3 (a) and (b), the peak shear stress for the rationally fitted curve seems slightly higher than the experimental peak, whereas the latter predicted lower value of maximum shear stress. But the overall shape of both fits represents the trend of the shear stress against slip data obtained from pull-out test and both of the fits provided very close integral value; i.e. similar fracture energy. However, maximum shear stress and fracture energy were found to vary from specimen to specimen. Therefore, the data sets for all specimens in a series were fitted with one model curve (Figures 7.4 (a) and (b)) to avoid the scatter of the plots due to the variation generated from material non-uniformity or local defects. Hence, the maximum shear stress, corresponding slip and fracture energy in each series have been presented by single fit (both for rational and Dai, Ueda & Sato (2005) model). Similar approaches have been reported by Dai, Ueda & Sato (2005), Mazzotti, Savoia & Ferracuti (2009), Pham & Al-Mahaidi (2007) and Imani (2010).

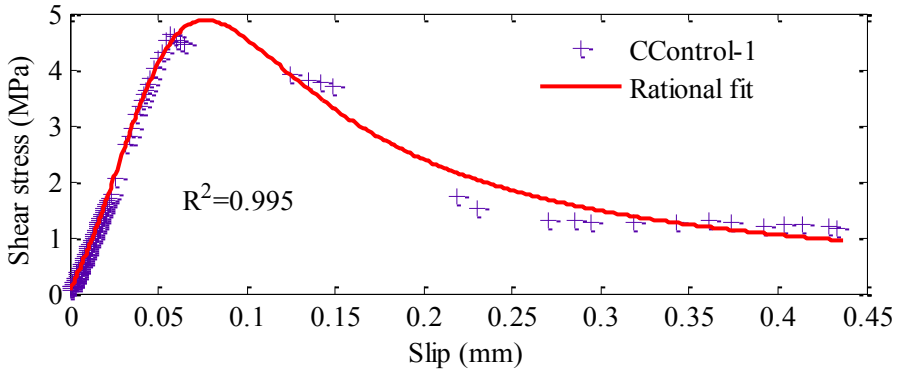

(a) Rational fit

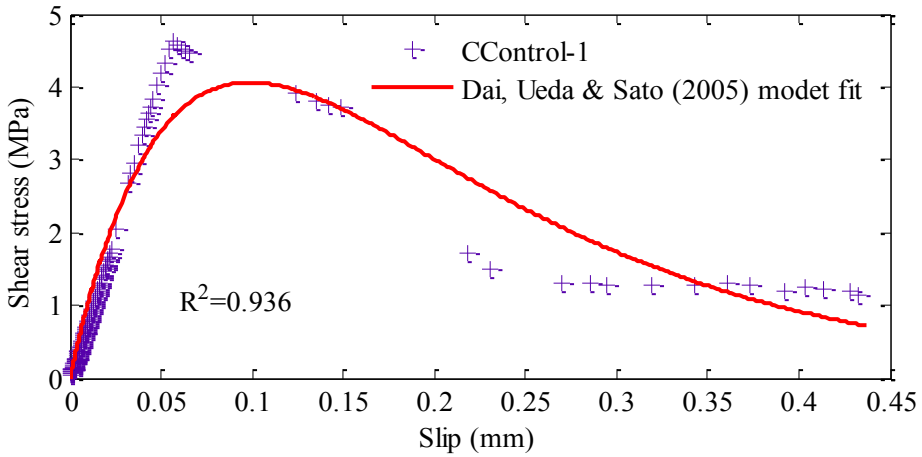

(b) Dai, Ueda & Sato (2005) model fit

Figure 7.3 Fitted curves for CControl-1

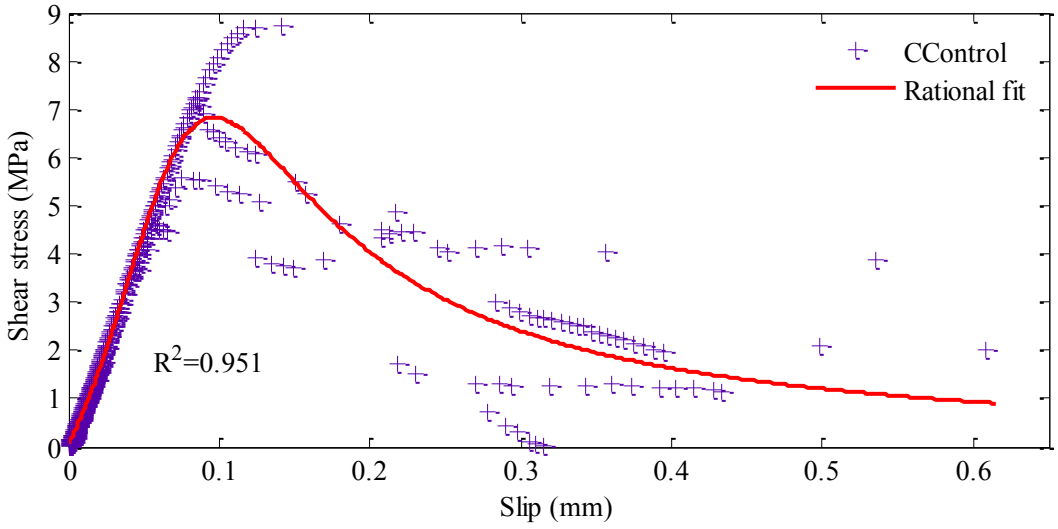

(a) Rational fit

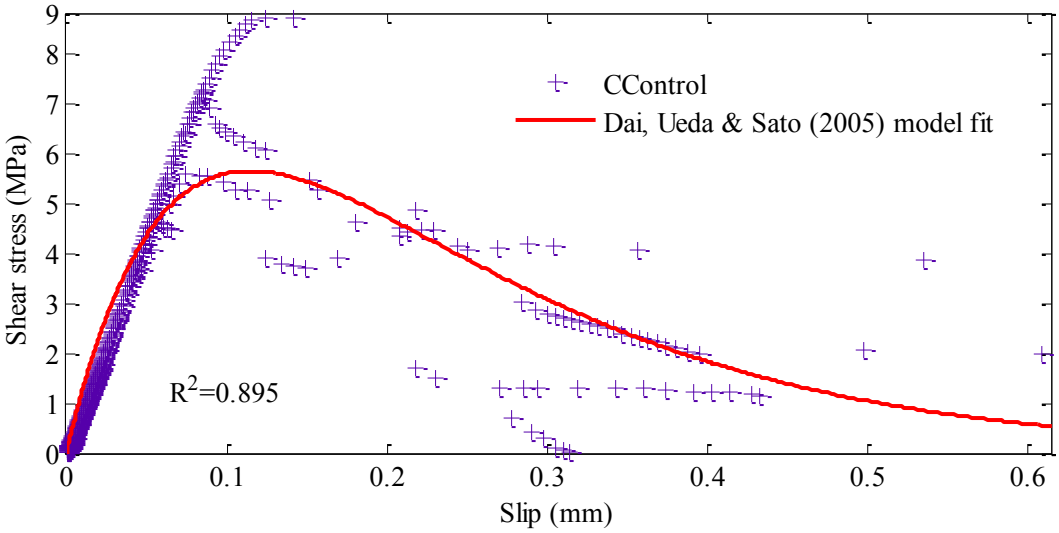

(b) Dai, Ueda & Sato (2005) model fit

Figure 7.4 fitted curves for CControl series

The curve fitting parameters for both fits of control specimens have been provided in Appendix C.2. Only the results in terms of fracture energies (G_f), maximum shear stresses (τ_{max}) and corresponding slips (s_{max}) for the two fits and the analytical fracture energy have been included in Table 7.1. The experimental fracture energies for both fits were determined by integrating the shear stress-slip curve with the limit of slip, s, from '0' to average ultimate slip of the specimens. On the other hand, calculation of analytical fracture energy was conducted considering the average pull-out force of control specimens. It can be observed that the fracture energies obtained from both fits showed much higher values than the corresponding analytical fracture energy. The reason can be attributed to the number of strain gauges used in the measurement of strains along the bond length. As the distance between strain gauges was large, it was difficult to capture shear stresses and slips precisely from the strain profiles. Moreover, higher local strain values due to the roughness of coarse aggregates may lead to higher slip values determined from the integration of strains along the bond length. Although the peak shear stress from Dai, Ueda & Sato (2005) model fit was lower than that observed from rational fit, fracture energies from both fits were similar.

Table 7.1 Shear stress-slips and fracture energies of Control specimens

Specimens	Rational fit			Dai, Ueda & Sato (2005) model fit			Analytical G_f (N/mm)
	τ_{max} (MPa)	s_{max} (mm)	G_f (N/mm)	τ_{max} (MPa)	s_{max} (mm)	G_f (N/mm)	
CControl	6.82	0.095	1.570	5.65	0.115	1.656	0.873

Control specimens fabricated from second batch of concrete were also analysed for shear stress-slip and fracture energy. The rational fit of one specimen has been illustrated in Figure 7.5 (a) and the fit with Dai, Ueda & Sato (2005) model for the same specimen has been provided in Figure 7.5 (b). Similar to control specimens from the first batch of concrete, rational fit showed the peak shear stress very close to the experimental peak whereas the Dai, Ueda & Sato (2005) model predicted a lower value. The maximum shear stress, slip value at maximum shear stress and fracture energy of control series from concrete batch 2, computed from the fitted curve (Figure 7.6) through all data sets, have been included in Table 7.2. Fracture energies from curve fitting were found to be higher than the analytical ones as observed for specimens from concrete batch 1.

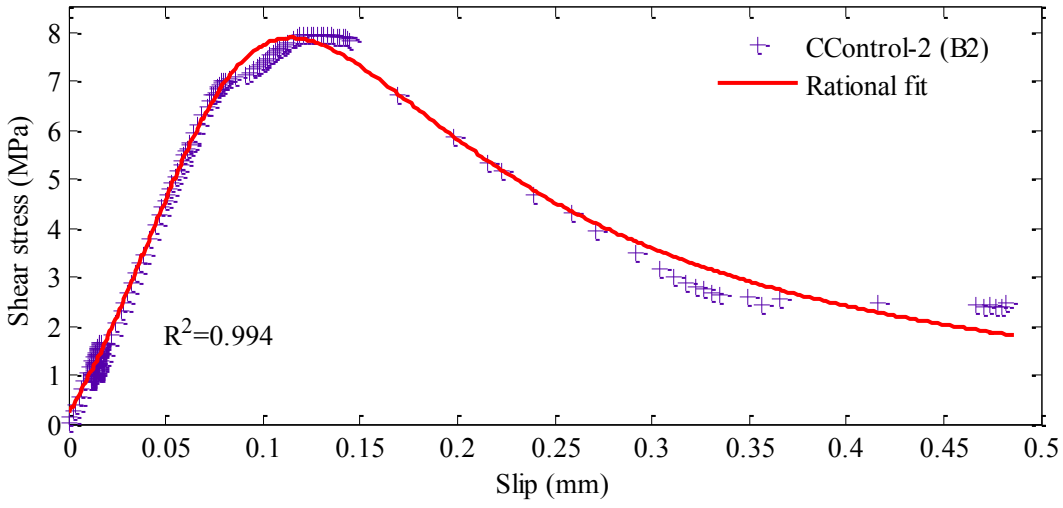

(a) Rational fit

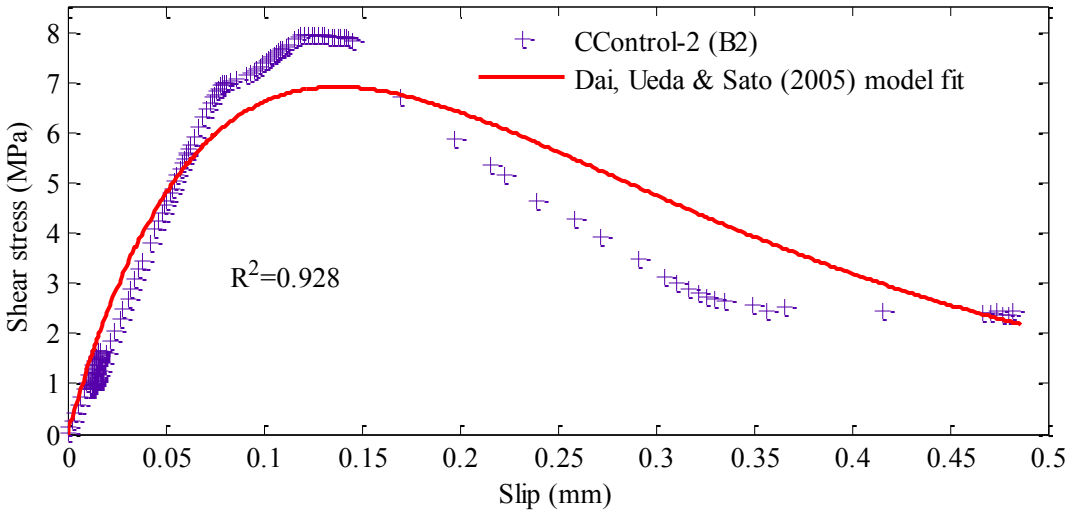

(b) Dai, Ueda & Sato (2005) model fit

Figure 7.5 Fitted curves for CControl-2 (B2)

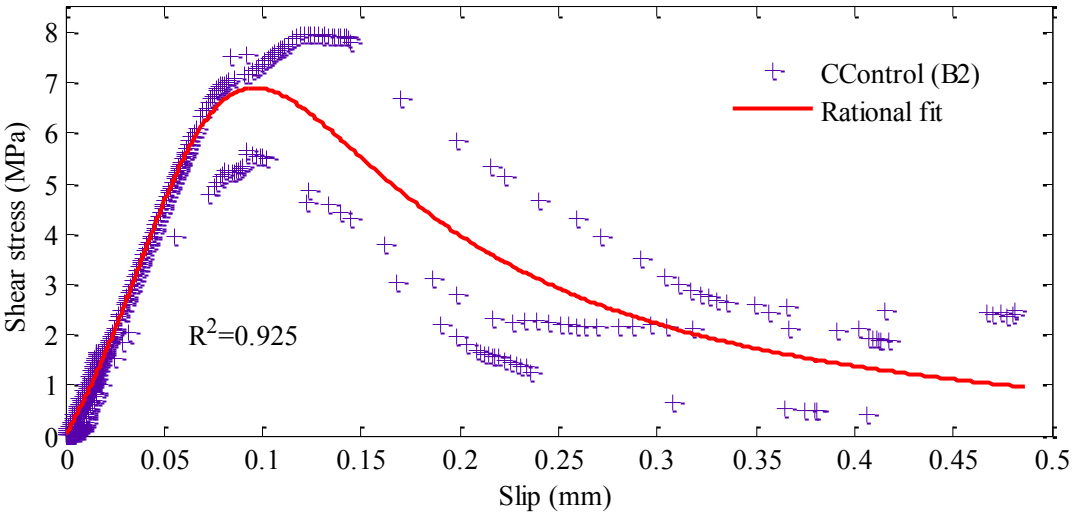

(a) Rational fit

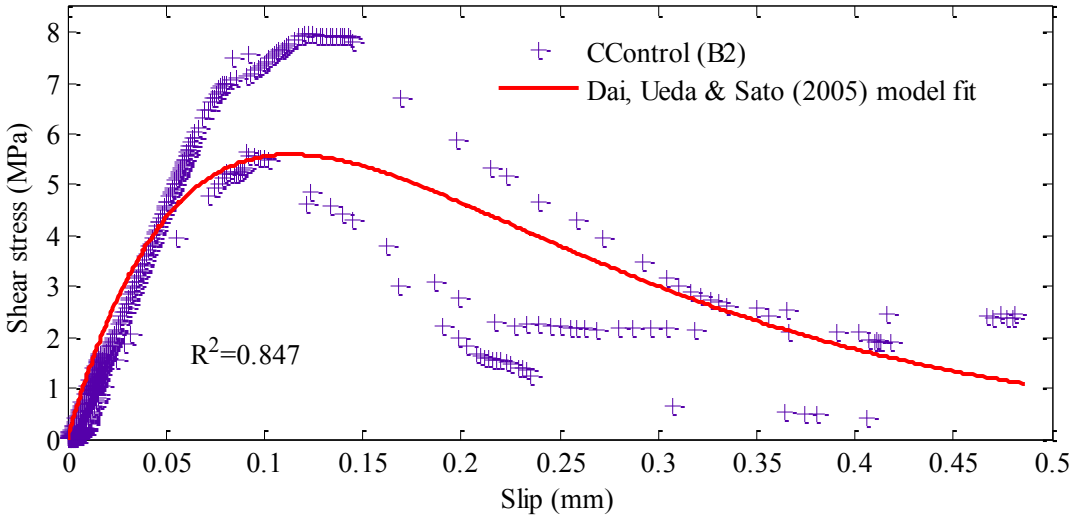

(b) Dai, Ueda & Sato (2005) model fit

Figure 7.6 Fitted curves for CControl (B2) series

Table 7.2 Shear stress-slips and fracture energies of Control specimens from concrete batch 2

Specimens	Rational fit			Dai, Ueda & Sato (2005) model fit			Analytical G_f (N/mm)
	τ_{max} (MPa)	s_{max} (mm)	G_f (N/mm)	τ_{max} (MPa)	s_{max} (mm)	G_f (N/mm)	
CControl (B2)	6.90	0.095	1.489	5.60	0.115	1.584	0.901

7.3.2 Fracture properties of exposed specimens

Fracture properties as well as the change of fracture properties with time for the specimens exposed to temperature cycles, wet-dry cycles and outdoor environment have been included in the following sub-sections. In addition, the change of fracture properties has been explained by correlating it with observed failure modes of CFRP-concrete bond.

7.3.2.1 Cyclic temperature series

The shear stress-slip curves fitted with rational model and Dai, Ueda & Sato (2005) model for five weeks (CT2 series), three months (CT3 series) and one year (CT4 series) cyclic temperature specimens have been illustrated in Figures 7.7, 7.8 and 7.9, respectively, whereas the maximum shear stress, corresponding slip and fracture energy of all three series for both fits have been listed in Table 7.3. As illustrated in shear stress-slip plots, it is evident that the peak shear stress changed with duration of exposure for both fits and the rational fit always predicted higher peak than that by Dai, Ueda & Sato (2005) model fit. However, the fracture energies (Table 7.3) obtained from both fits match quite well with each other. Similar to the control series, the analytical fracture energies of temperature series were much lower than the experimental ones.

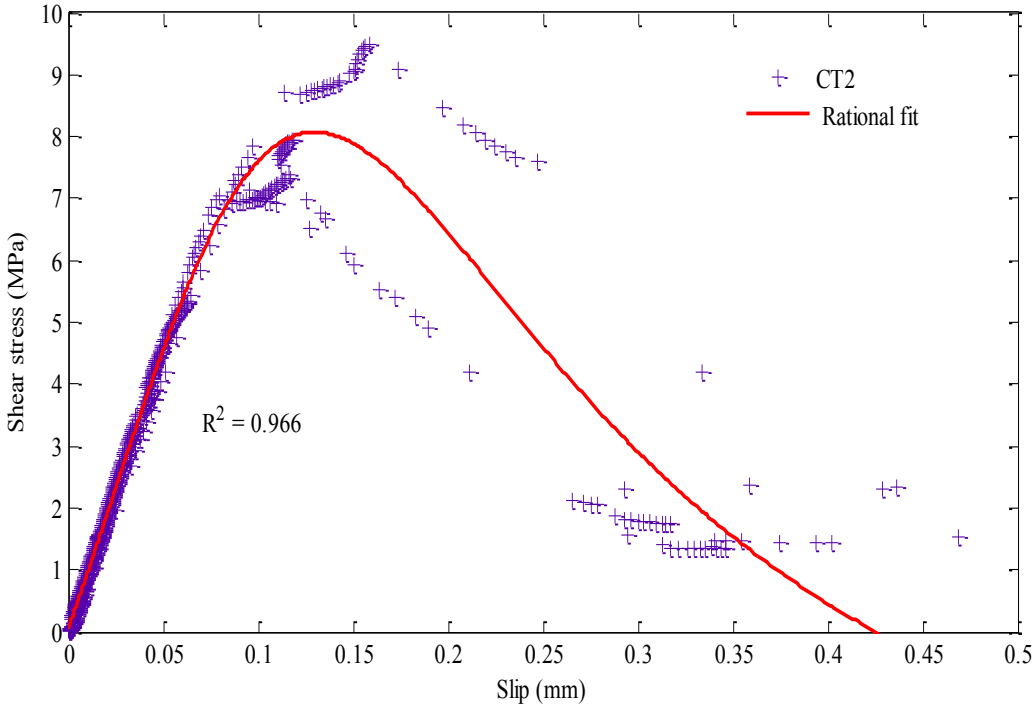

(a) Rational fit

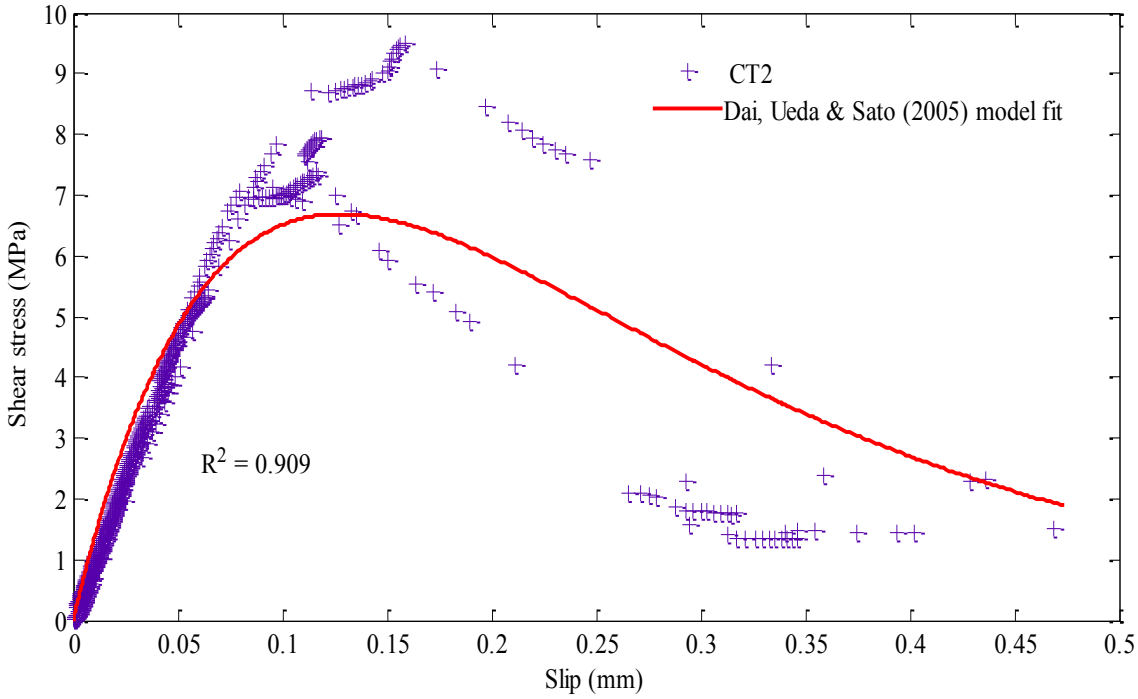

(b) Dai, Ueda & Sato (2005) model fit

Figure 7.7 Fitted curves for CT2 series

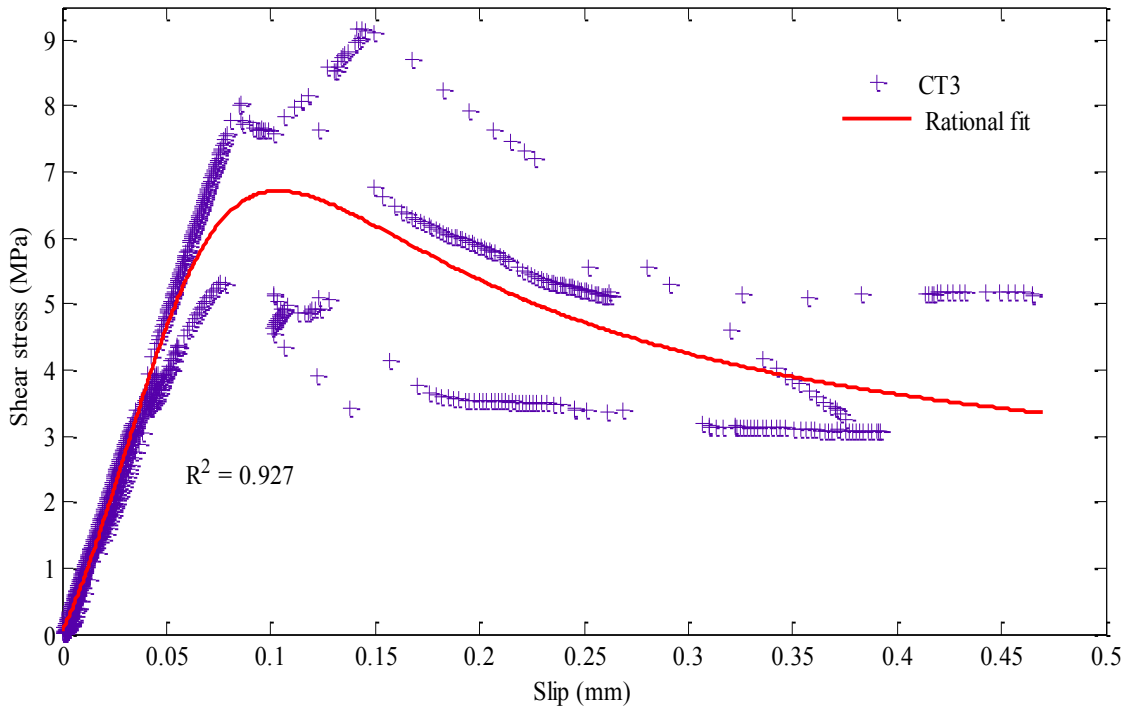

(a) Rational fit

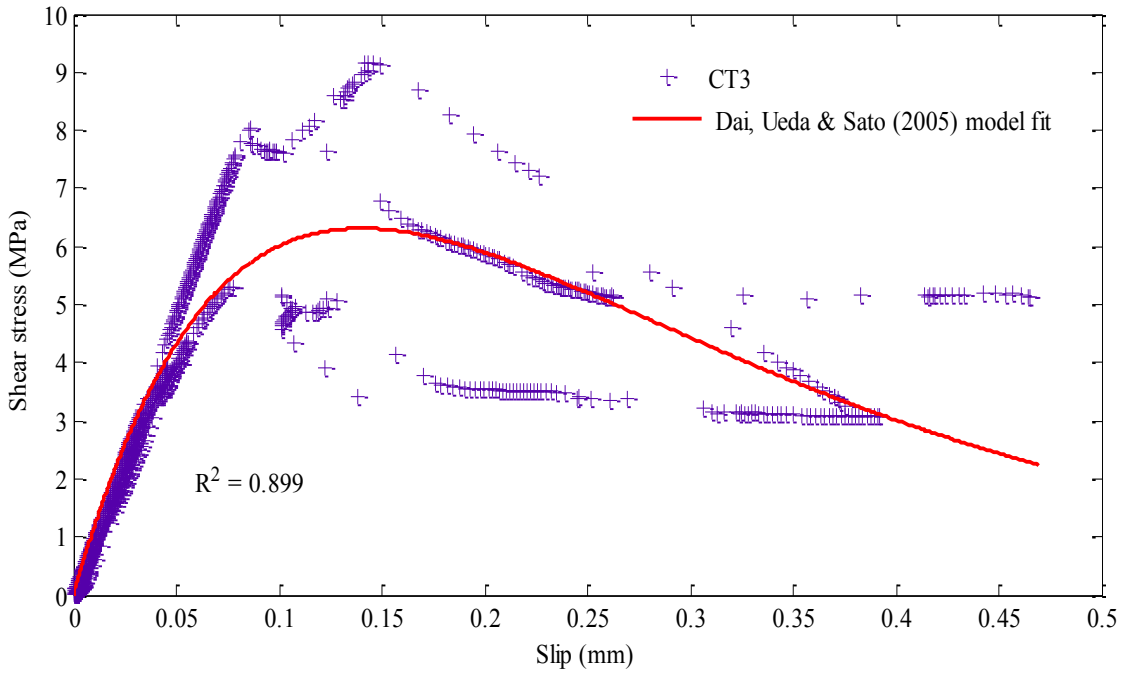

(b) Dai, Ueda & Sato (2005) model fit

Figure 7.8 Fitted curves for CT3 series

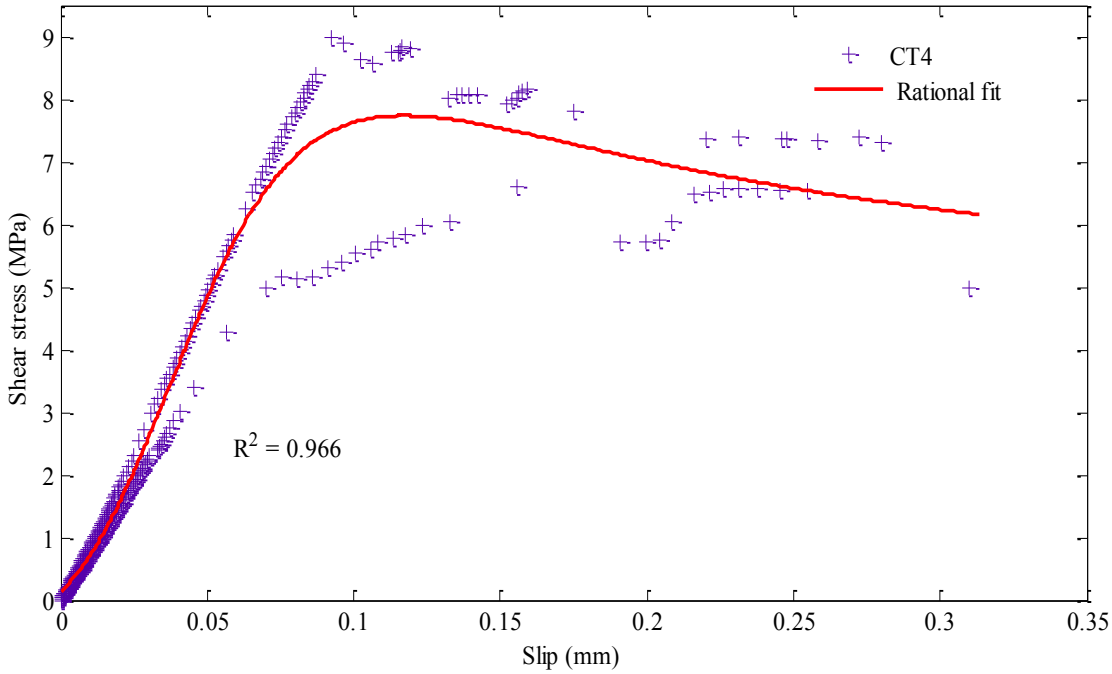

(a) Rational fit

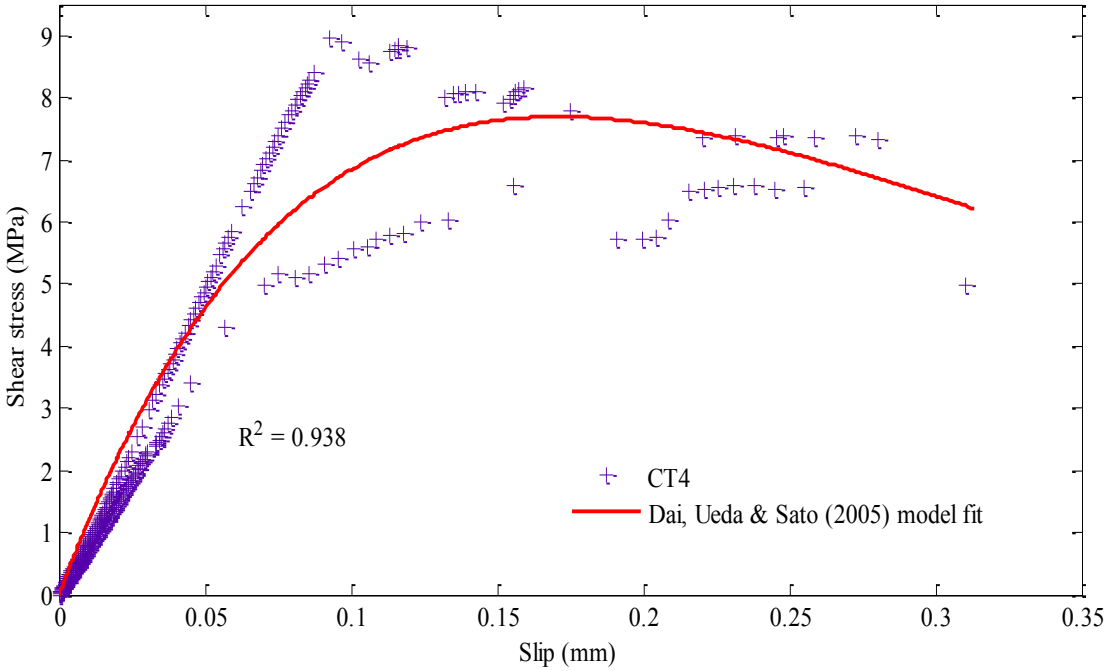

(b) Dai, Ueda & Sato (2005) model fit

Figure 7.9 Fitted curves for CT4 series

Table 7.3 Shear stress-slips and fracture energies of cyclic temperature specimens

Specimens	Rational fit			Dai, Ueda & Sato (2005) model fit			Analytical G_f (N/mm)
	τ_{max} (MPa)	s_{max} (mm)	G_f (N/mm)	τ_{max} (MPa)	s_{max} (mm)	G_f (N/mm)	
CControl	6.82	0.095	1.570	5.65	0.115	1.656	0.873
CT2	8.07	0.130	1.816	6.69	0.130	1.985	1.000
CT3	6.71	0.105	1.932	6.31	0.140	1.925	0.831
CT4	7.74	0.115	1.627	7.69	0.170	1.645	0.970

The change of maximum shear stress values with time due to cyclic temperature can be observed from Figure 7.10 where the maximum shear stresses of exposed specimens have been normalised by dividing them by the maximum shear stress of control specimens. It can be seen that temperature cycles did not cause any negative effect on the maximum shear stress developed in the CFRP-concrete bond. Rational fit and Dai,

Ueda & Sato (2005) model fit both showed similar trends of peak shear stress with time. The trends seem to be quite similar to the trend of pull-out strength (ultimate axial stress) with time as illustrated in section 4.2.1. Initially, an increase in maximum shear stress, 18.3% for rational fit and 18.4% for Dai, Ueda & Sato (2005) model fit, occurred after the exposure for five weeks. Then a decreasing trend was observed where the maximum shear stress values reached 1.6% less and 11.7% more than the control values after 3 months for rational and Dai, Ueda & Sato (2005) model fits, respectively. Finally, the maximum shear stress for the former and the latter fit increased by 13.5% and 36.1%, respectively, after one year compared to their corresponding control values. As the failure modes of all cyclic temperature series were associated with a thick concrete layer attached to debonded CFRP, the peak shear stress is likely to be influenced by the concrete compressive strength and can be supported by the similar trend of concrete compressive strength with the exposure durations explained in section 3.7.2.1.

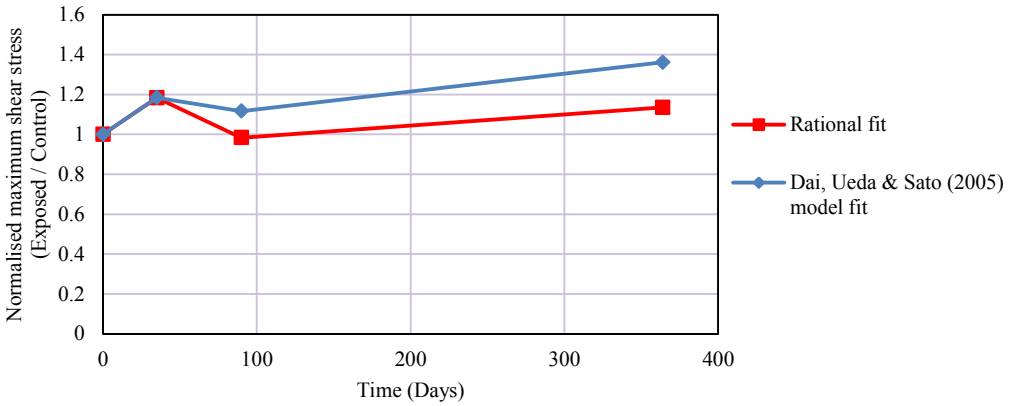

Figure 7.10 Normalised maximum shear stress against days of exposure for cyclic temperature specimens

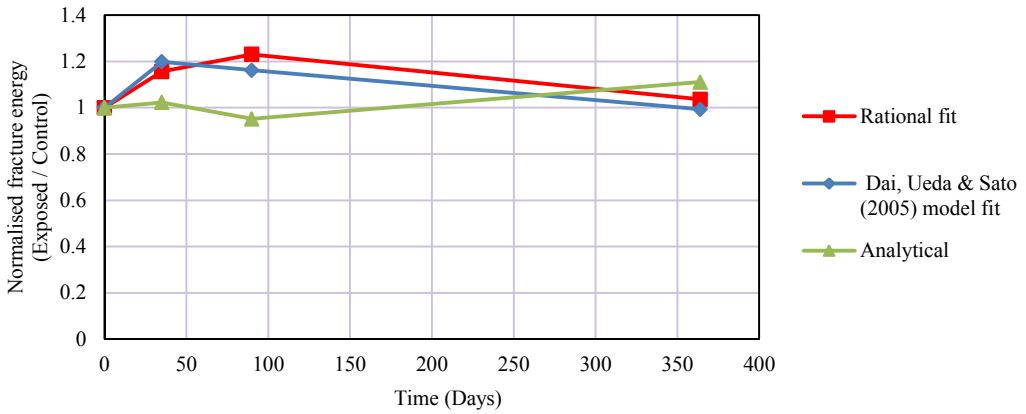

Figure 7.11 Normalised fracture energy against days of exposure for cyclic temperature specimens

Similar to the maximum shear stress, experimental fracture energies determined from both fits revealed the positive effect of cyclic temperature on it and can be observed in Figure 7.11. The maximum increase in fracture energy for rational fit was 23.1% after three months and that for Dai, Ueda & Sato (2005) model fit was 19.9% after five weeks. However, the decreasing trend of the fracture energies was observed after three months and five weeks for the former fit and the latter one, respectively, and finally, fracture energy from both fits reached very close to the control value after one year of exposure. The change of analytical fracture energy with time exhibited quite an opposite trend to those from experimental results. The discrepancy can be attributed to the following:

- The theoretical fracture energy is directly proportional to the square of the maximum pull-out force. Also, the change of stiffness of CFRP contributes to the change of fracture energy with time as the fracture energy is inversely proportional to CFRP stiffness ($E_f \times t_f$). As the CFRP tensile modulus of elasticity (section 3.6.2.1) and pull-out strength (section 4.2.1) of CFRP-concrete bond (directly proportional to maximum pull-out force) behaved similarly with time of exposure, the overall effect of the two similar trends of pull-out strength and CFRP stiffness led to the deterioration of analytical fracture energy.

- On the other hand, the experimental fracture energies, determined from shear stress-slip curve, depended not only on the peak shear stress but also on the area of the softening branch of shear stress-slip curve. The increase in fracture energy in CT2 (five

weeks) series was due to increase in both the peak shear stress and the area of the softening branch compared to those in control series (Figures 7.7 and 7.10). The increase in the area of softening branch can be attributed to the possible softening of epoxy adhesive even though the failure always occurred in concrete layer for all temperature series. The rational fit for three month temperature (CT3) series showed lower maximum shear stress than the CT2 series (Figure 7.10) but much more gradual softening than CT2 after achieving the peak shear stress (Figure 7.8 (a)) and thereby, improvement of fracture energy was observed. But the Dai, Ueda & Sato (2005) model fit for CT3 series exhibited relatively lower peak shear stress than CT2 (Figure 7.10) but with similar shape of softening branch (Figure 7.8 (b)), which can be the cause of descending trend of fracture energy predicted by this fit after five weeks of exposure. Finally, the decreasing nature of fracture energy after one year for both fits can be attributed to the very low value of ultimate slips (Figure 7.9) although the peak shear stress were found to increase significantly (Figure 7.10).

Therefore, from the findings of the experimental fracture energy release rates with exposure duration, it can be understood that the fracture energy of CFRP-concrete bond subjected to cyclic temperature depended on many variables such as maximum peak shear stress which can be related to concrete compressive strength, adhesive properties (softer adhesive means more slips) and CFRP stiffness. Although, the failure occurred in concrete layer and peak shear stress and pull-out strength followed the trend of concrete compressive strength with time, the different behaviour of fracture energy release rate can be attributed to the probable change of epoxy stiffness with time. According to Dai, Ueda & Sato (2005), the effect of adhesive stiffness on the fracture energy of FRP-concrete bond is the most and that of concrete compressive strength is much less but slightly more than the CFRP stiffness. Specially, softer adhesive increases the fracture energy as it possesses higher toughness. As the analytical fracture energy for constant bond width, used in this study, depended mainly on two variables; i.e. maximum pull-out force and CFRP stiffness, the dependence of the experimental fracture energies on many variables stated above could be the possible reason of the discrepancy between analytical and experimental results.

7.3.2.2 Wet-dry series

The shear stress-slip plots (Figures 7.12, 7.13, 7.14 and 7.15) of one month (CH1), six months (CH2), one year (CH3) and 18 months (CH4) wet-dry CFRP-concrete bond systems by rational and Dai, Ueda & Sato (2005) model fit revealed the evolution of the shapes with time of exposure, especially, for CH3 series where the gradual softening branch was evident. The maximum shear stress, corresponding slip values and fracture energies of all four series for both fits, as listed in Table 7.4, show the deviation of the peak shear stress between two fits but the fracture energies for both fits were quite similar as observed for control and cyclic temperature specimens. And the experimental fracture energies were found to be higher than the analytical fracture energies.

The plots of normalised maximum shear stress values and the fracture energies with time of exposure have been illustrated in Figures 7.16 and 7.17, respectively, to understand the effect of wet-dry cycles on these two parameters with the passage of time.

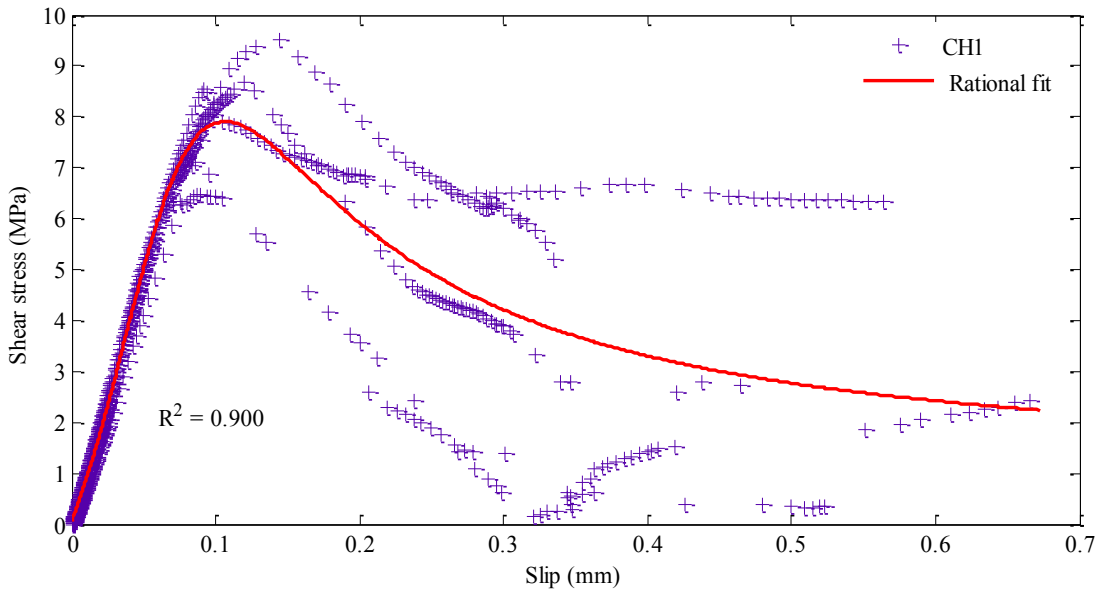

(a) Rational fit

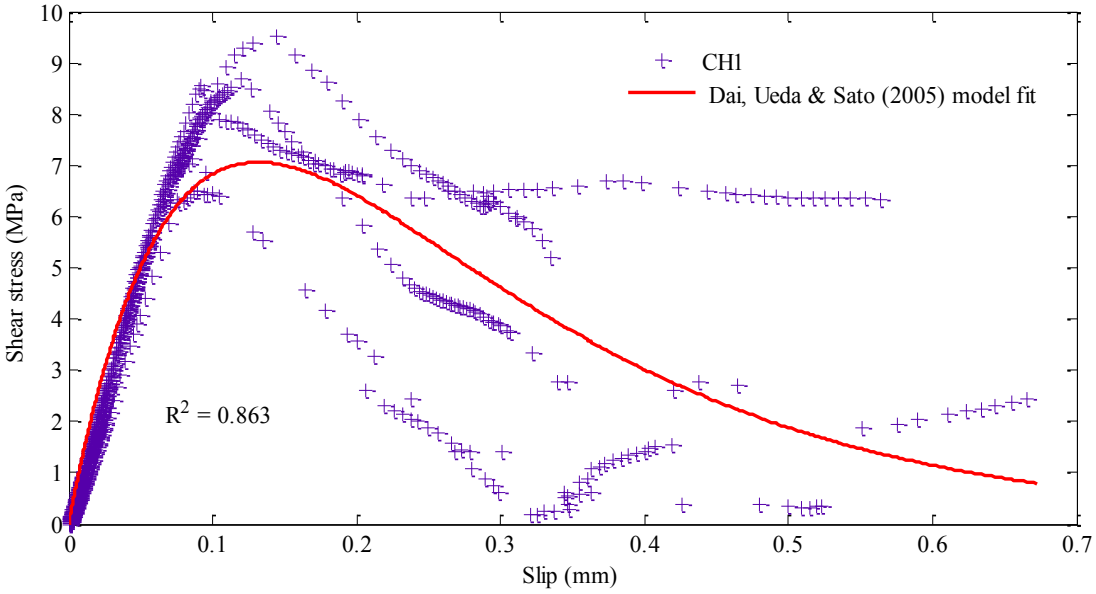

(b) Dai, Ueda & Sato (2005) model fit

Figure 7.12 Fitted curves for CH1 series

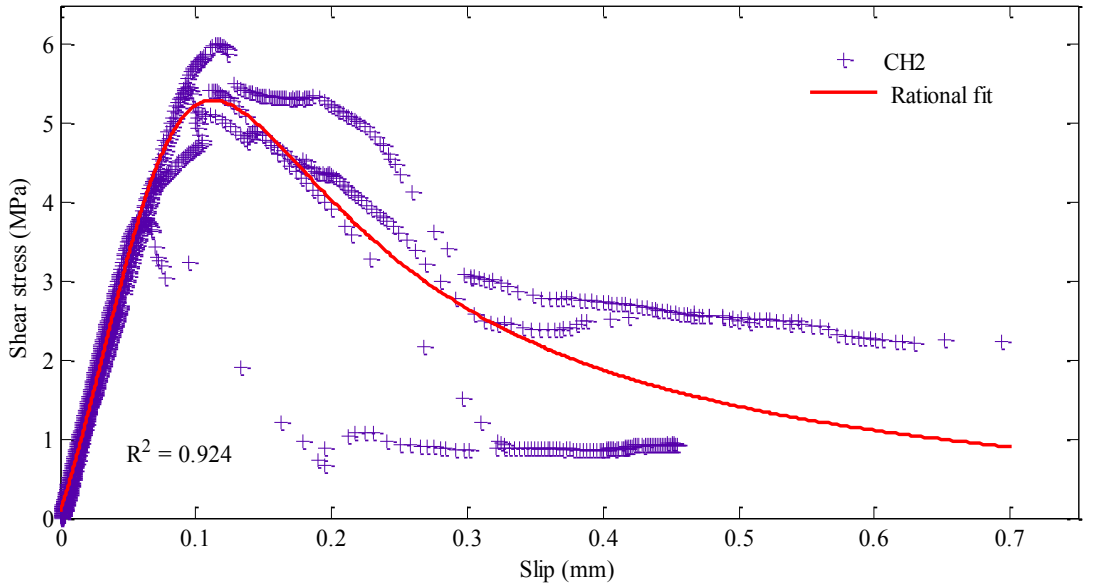

(a) Rational fit

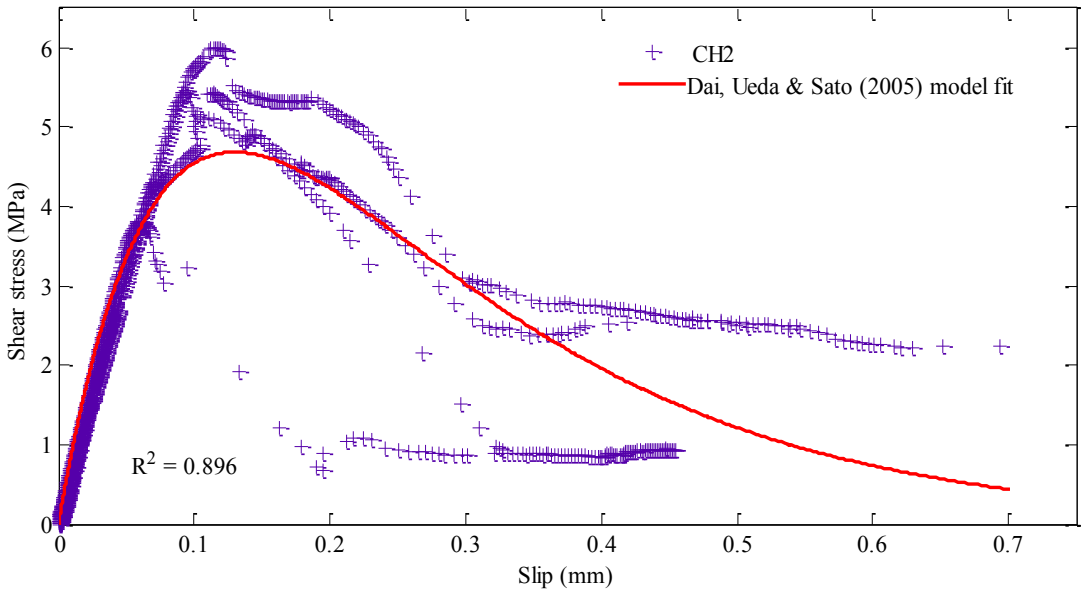

(b) Dai, Ueda & Sato (2005) model fit

Figure 7.13 Fitted curves for CH2 series

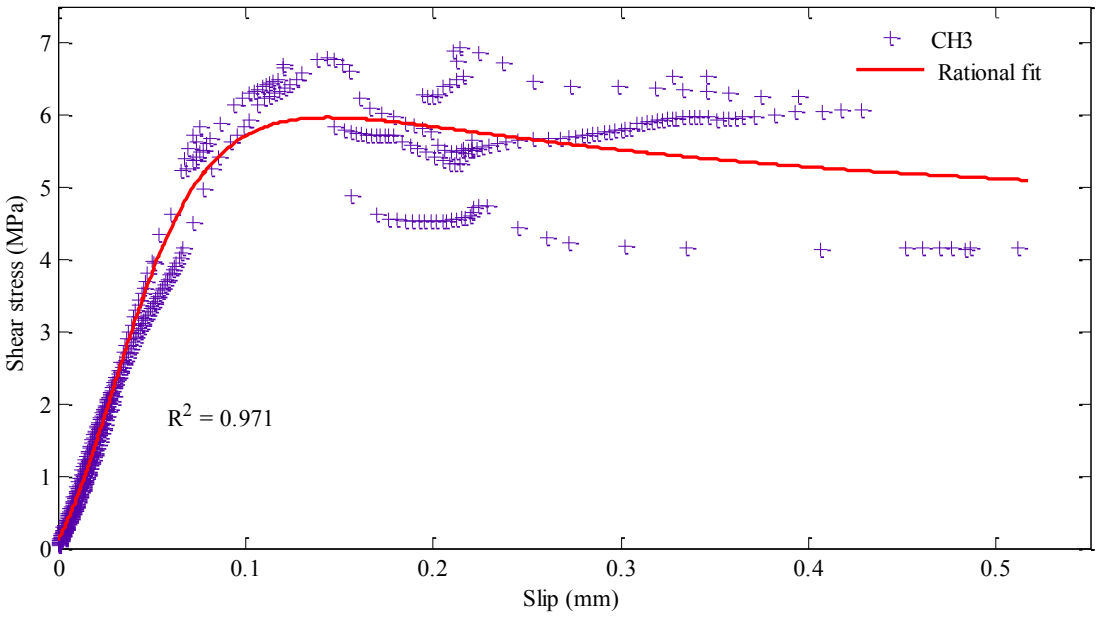

(a) Rational fit

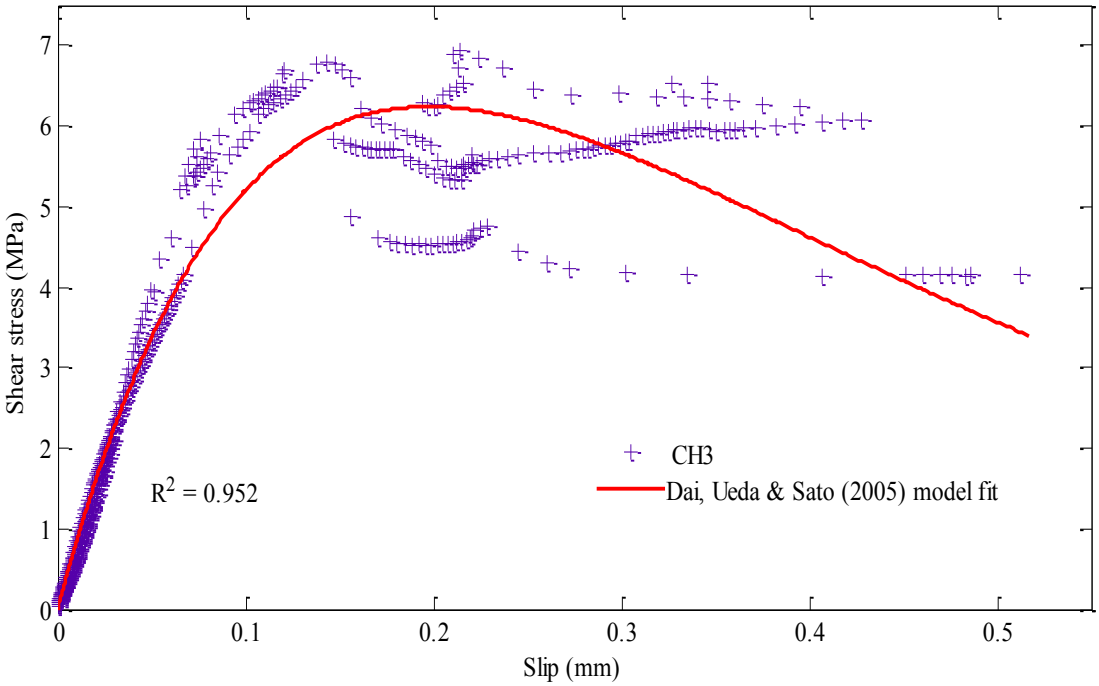

(b) Dai, Ueda & Sato (2005) model fit

Figure 7.14 Fitted curves for CH3 series

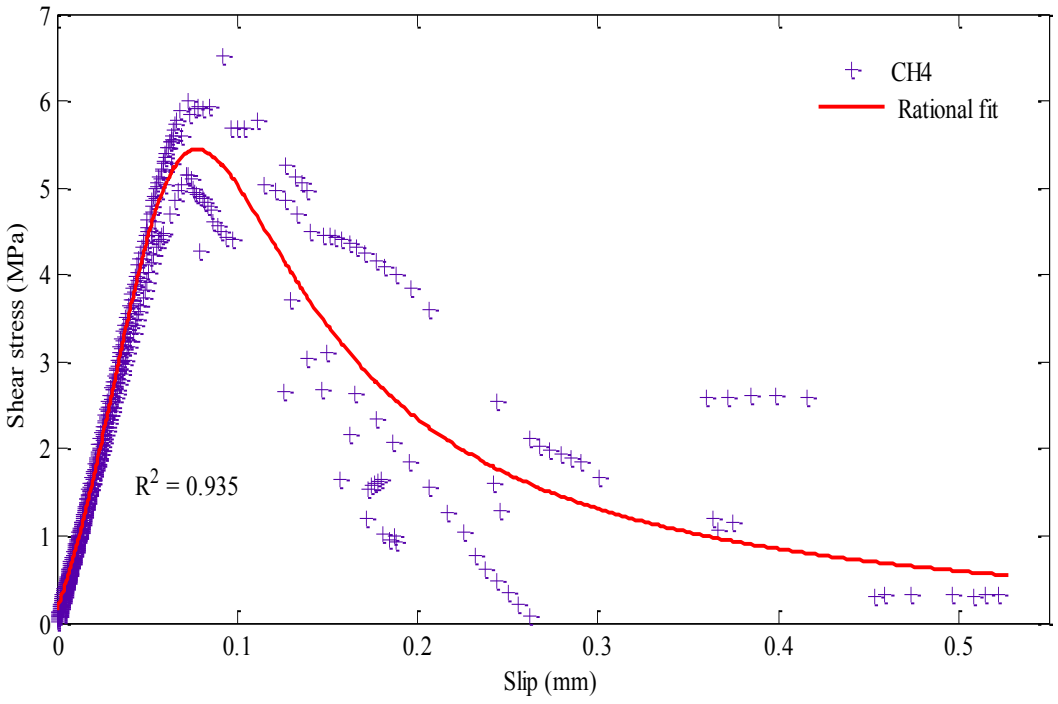

(a) Rational fit

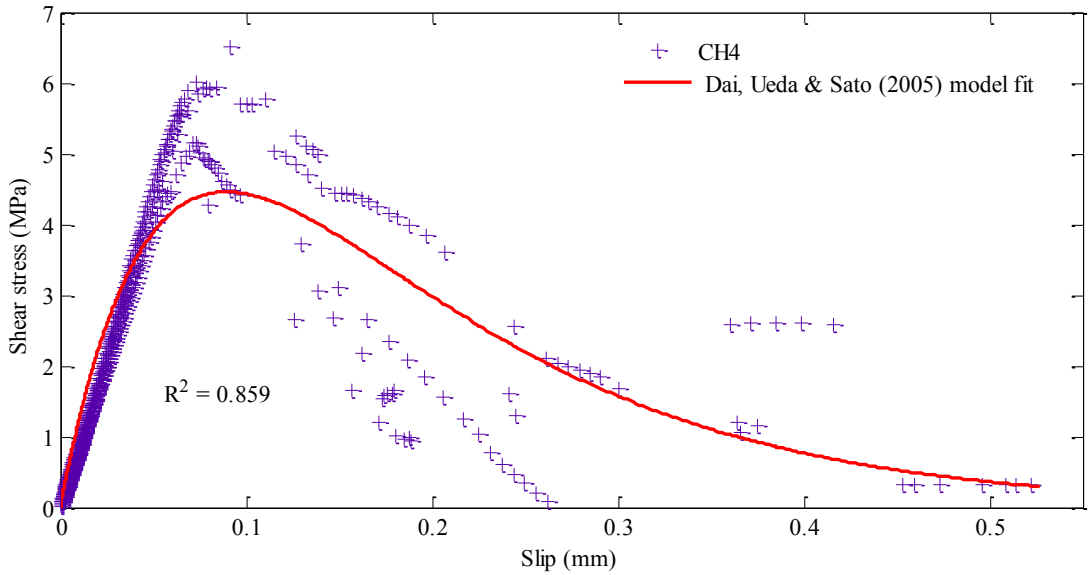

(b) Dai, Ueda & Sato (2005) model fit

Figure 7.15 Fitted curves for CH4 series

Table 7.4 Shear stress-slips and fracture energies of wet-dry specimens

Specimens	Rational fit			Dai, Ueda & Sato (2005) model fit			Analytical G_f (N/mm)
	τ_{max} (MPa)	s_{max} (mm)	G_f (N/mm)	τ_{max} (MPa)	s_{max} (mm)	G_f (N/mm)	
CControl	6.82	0.095	1.570	5.65	0.115	1.656	0.873
CH1	7.90	0.105	2.344	7.06	0.130	2.309	0.774
CH2	5.29	0.115	1.511	4.69	0.130	1.529	1.283
CH3	5.96	0.145	2.196	6.24	0.195	2.157	0.936
CH4	5.43	0.080	0.992	4.46	0.090	1.042	0.852

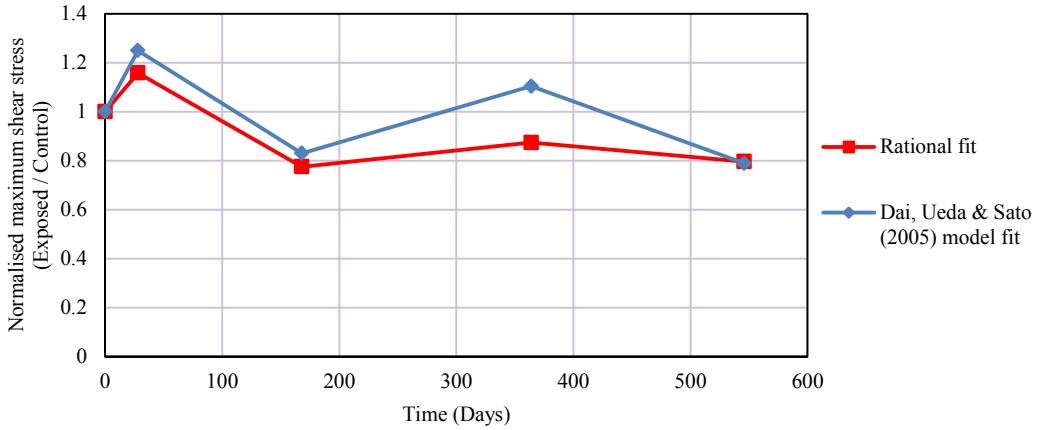

Figure 7.16 Normalised maximum shear stress against days of exposure for wet-dry specimens

From Figure 7.16, it can be observed that the peak shear stress values of wet-dry specimens obtained from both fits showed similar trends and exhibited the cyclic nature of the maximum shear stress with the durations of exposure. The initial increase in maximum shear stress by 15.8% for rational fit and 25.0% for Dai, Ueda & Sato (2005) model fit was observed after one month and a decreasing trend led to degradation by 22.4 % for the former fit and 17.0% for the latter one compared to their corresponding control series after the exposure of six months. The rational fit showed slight improvement of maximum shear stress after one year when the value reached 87.4% of the control value whereas the other fit exhibited significant increase as the peak shear stress reached 10.4% more than the control series. Finally, the maximum shear stress for rational and Dai, Ueda & Sato (2005) model fit approached 79.6% and 78.9% of the corresponding control values, respectively.

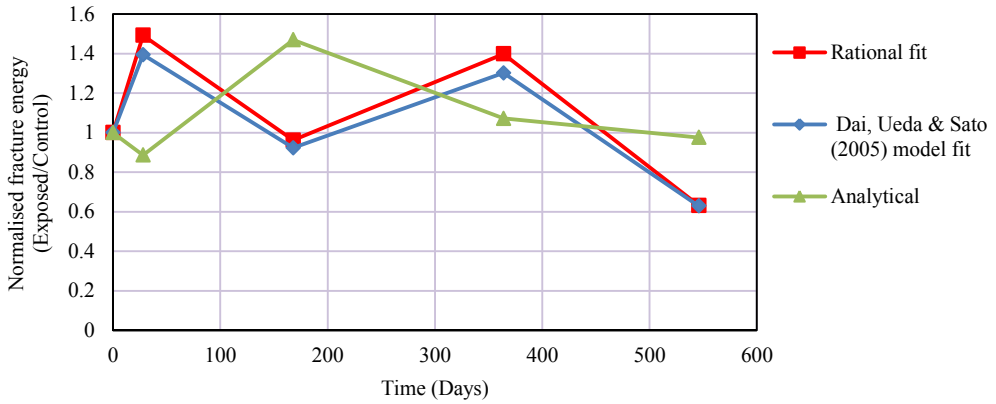

Figure 7.17 Normalised fracture energy against days of exposure for wet-dry specimens

As illustrated in Figure 7.17, the fracture energy for both fits exhibited the similar trend that was observed in the peak shear stress with the time of exposure. The cyclic trend of fracture energy with time can be explained with the peak shear stress values, failure modes and material properties with time. The initial increase in fracture energy (49.3% for rational fit and 39.4% for Dai, Ueda & Sato (2005) model fit) was observed after exposure for one month. This can be attributed to the increase in peak shear stress (Figure 7.16) as well as the softening of adhesive stiffness. The broader area of softening branch of shear stress-slip plot of CH2 series (Figure 7.12) suggests more shear deformation of adhesive than control series, which may lead to the higher fracture energy. Also, the increasing compressive strength (section 3.7.2.2) and thinner layer of concrete attached to debonded CFRP (section 5.2.2) observed in the tests can be interpreted as the degradation of adhesive stiffness. The fracture energy of CH2 (six months wet–dry) series reached close to the control values and can be attributed to the degraded peak shear stress value (Figure 7.16) and narrower softening branch of shear stress-slip plot (Figure 7.13). In addition, the change of failure mode from thinner concrete to relatively thicker concrete attached to debonded CFRP suggests the increase in adhesive stiffness and decrease in adhesive shear deformation leading to lower fracture energy after six months of exposure. After one year of exposure significant increase in fracture energy (39.9% for rational fit and 30.3% for Dai, Ueda & Sato (2005) model compared to the control values) was observed and can be interpreted as the resultant of the higher maximum shear stress and much broader softening branch of

shear stress-slip curve as illustrated in Figure 7.14. The evolution of failure mode from thicker concrete to almost no concrete attached to separated CFRP strip (section 5.2.2) also confirms the softening of adhesive shear stiffness. The maximum degradation of fracture energy was observed after exposure for 18 months. The degradation for rational fit was 36.8% and for Dai, Ueda & Sato (2005) model was 37.1%. The reason for such a significant degradation can be attributed to the decrease in peak shear stress, much narrower softening branch (Figure 7.15); i.e. increased shear stiffness of adhesive and the failure mode associated with thicker concrete layer on debonded CFRP (section 5.2.2).

However, the theoretical fracture energy followed completely the opposite trend to the experimental ones until the exposure duration of 18 months. The explanation for this has already been provided in section 7.3.2.1.

7.3.2.3 Outdoor environment series

The CFRP-concrete bonded prisms exposed to outdoor environment were also analysed in terms of peak shear stress and fracture energy based on the results obtained from curve fitting of experimental shear stress and slip data. The fracture energy was also determined from the analytical formula. Shear stress-slip plots for two months (CE1), six months (CE2), one year (CE3) and 18 months (CE4) outdoor environment specimens are presented in Figures 7.18, 7.19, 7.20 and 7.21, respectively, whereas the maximum shear stress, corresponding slip and fracture energy of all the series have been provided in Table 7.5.

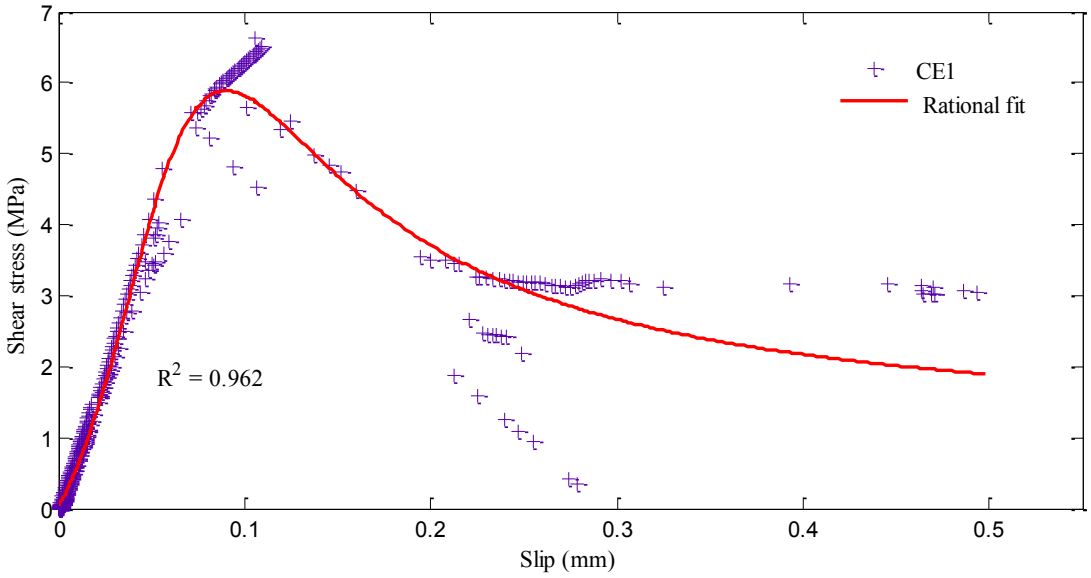

(a) Rational fit

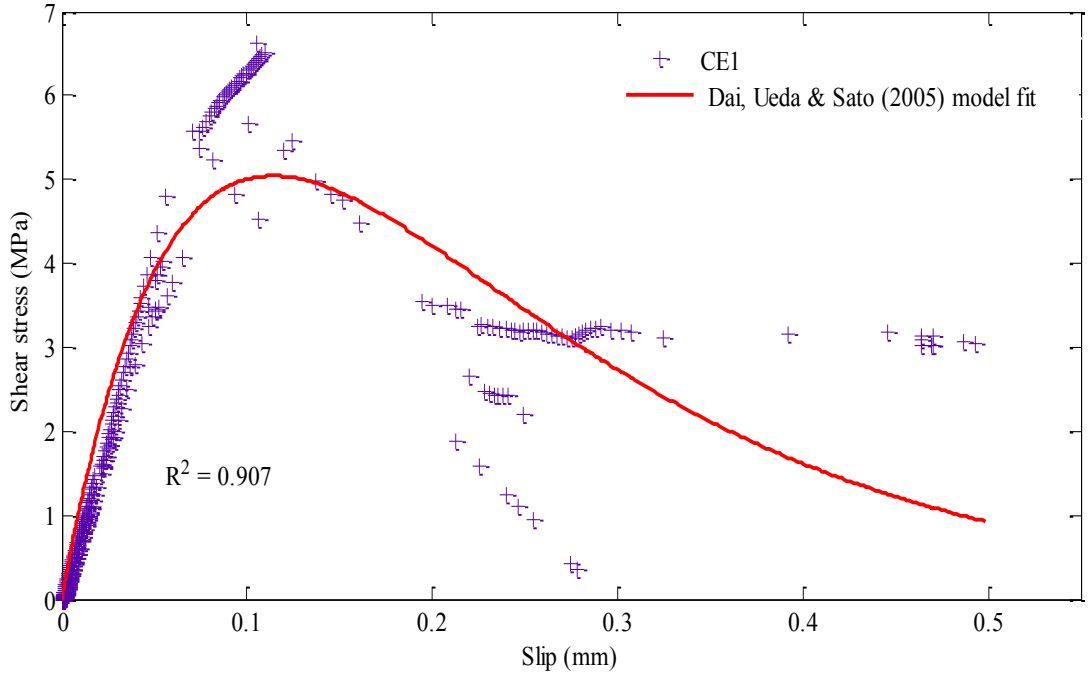

(b) Dai, Ueda & Sato (2005) model fit

Figure 7.18 Fitted curves for CE1

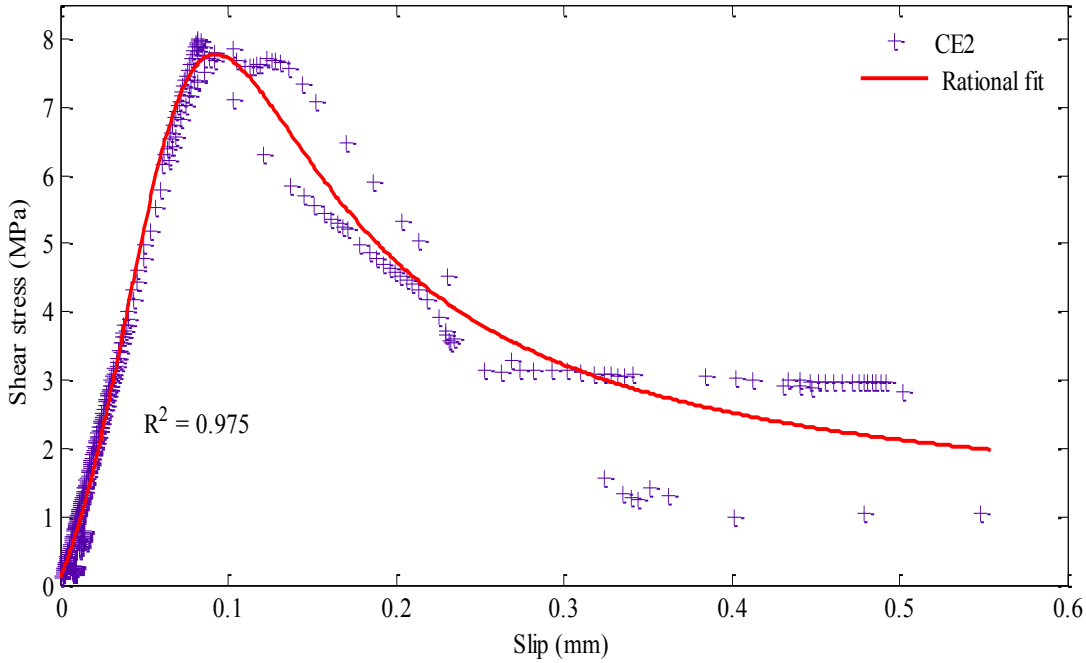

(a) Rational fit

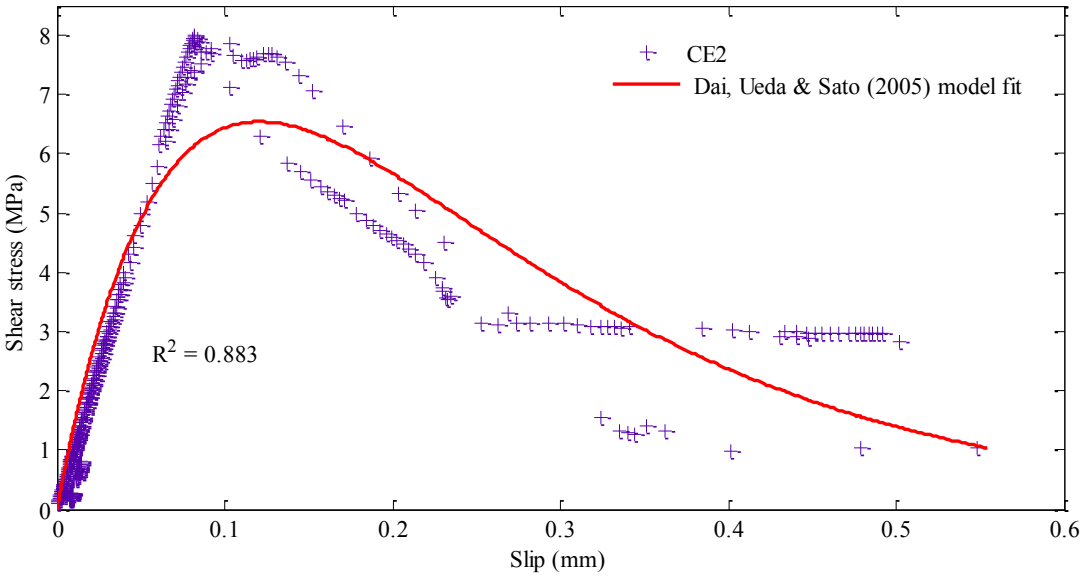

(b) Dai, Ueda & Sato (2005) model fit

Figure 7.19 Fitted curves for CE2

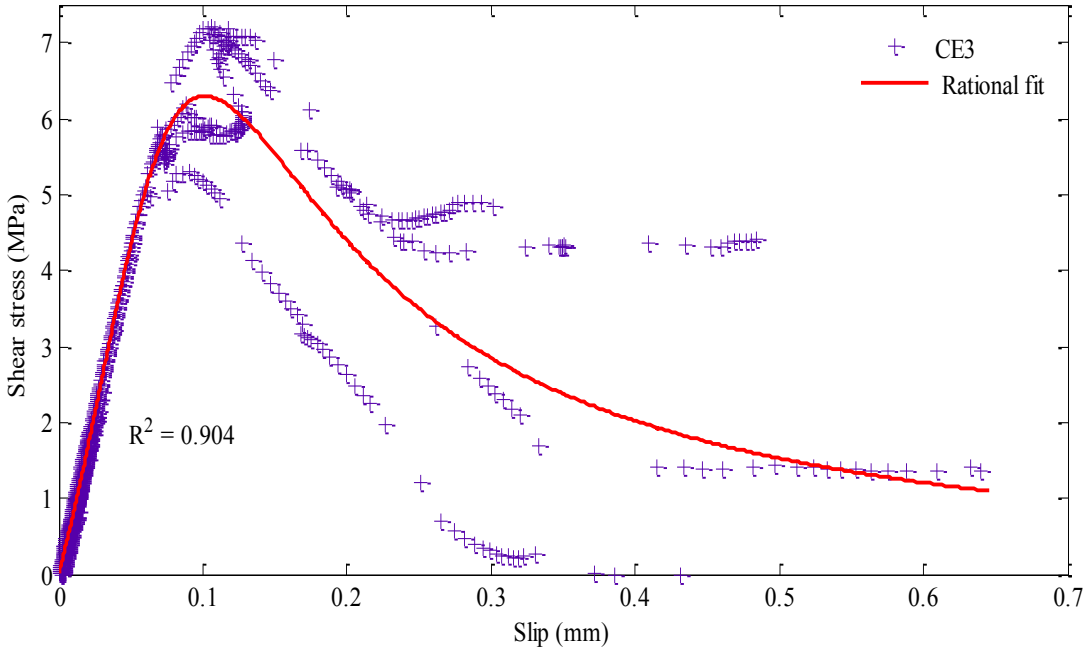

(a) Rational fit

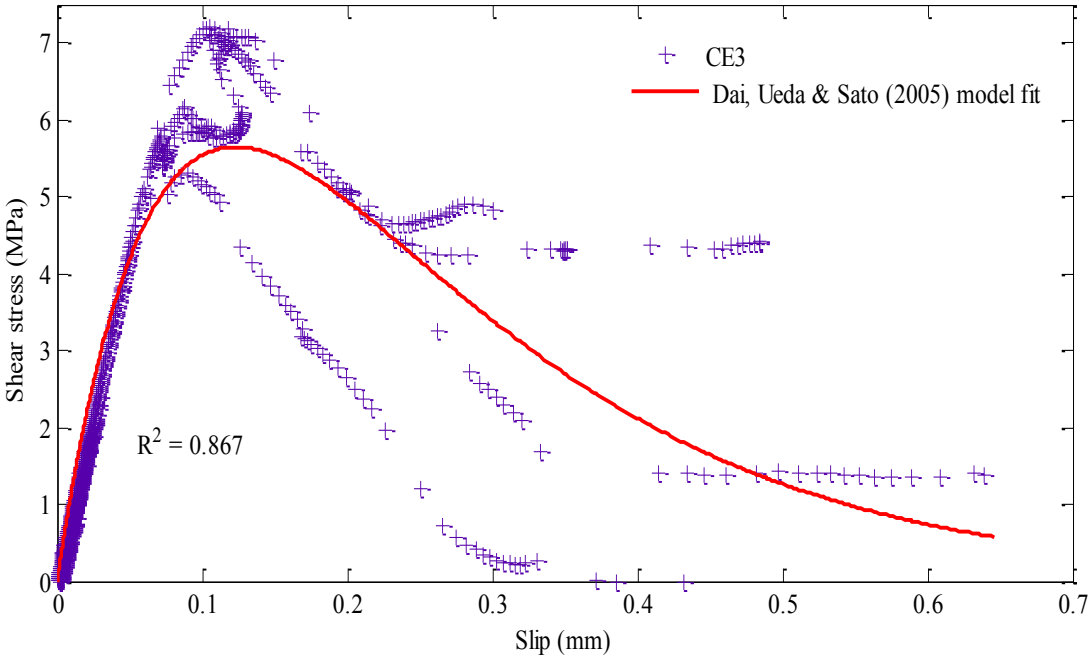

(b) Dai, Ueda & Sato (2005) model fit

Figure 7.20 Fitted curves for CE3

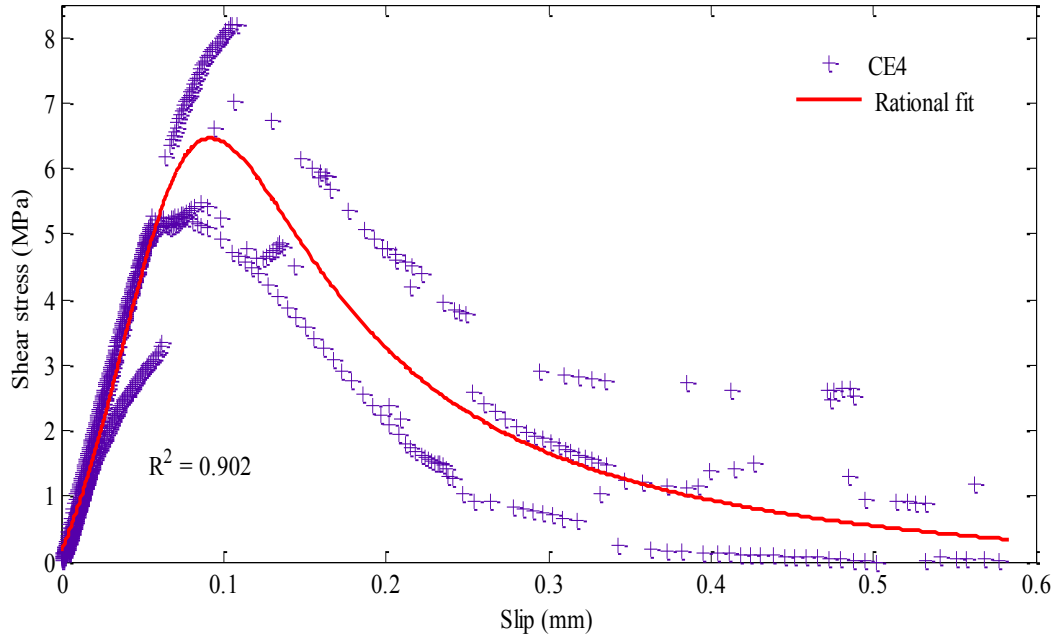

(a) Rational fit

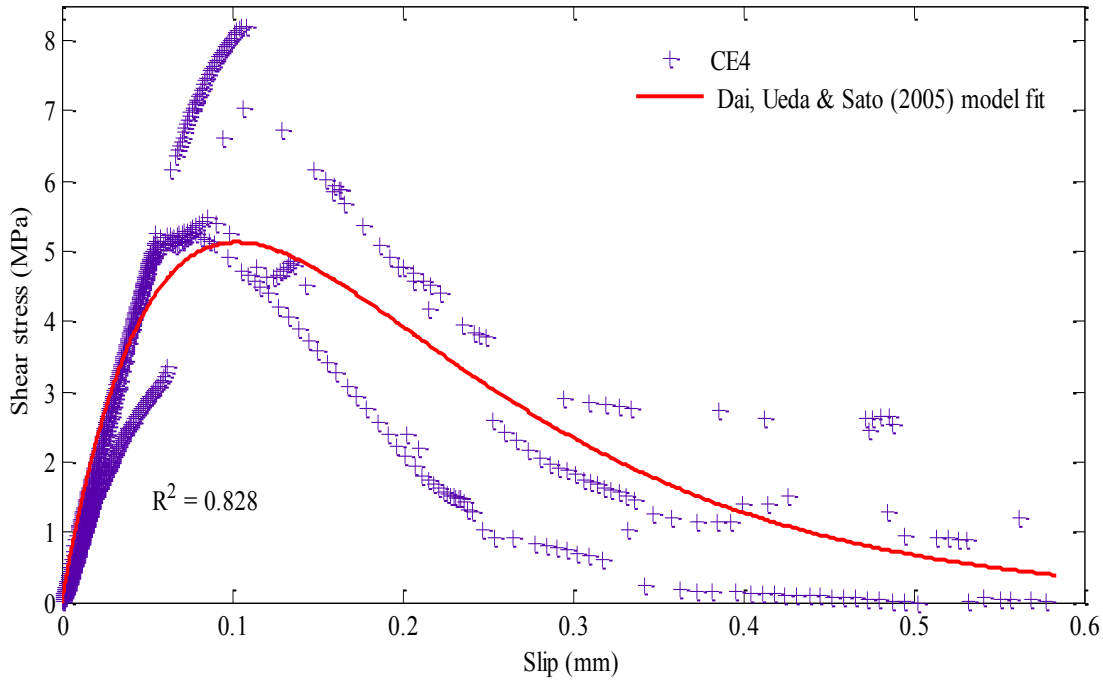

(b) Dai, Ueda & Sato (2005) model fit

Figure 7.21 Fitted curves for CE4 series

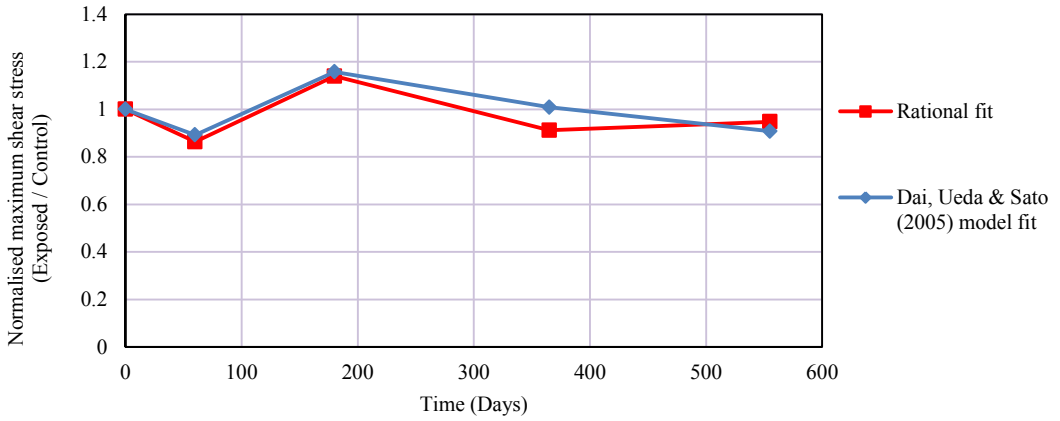

Figure 7.22 Normalised maximum shear stress against days of exposure for outdoor environment specimens

Table 7.5 Shear stress-slips and fracture energies for outdoor environment specimens

Specimens	Rational fit			Dai, Ueda & Sato (2005) model fit			Analytical G_f (N/mm)
	τ_{max} (MPa)	s_{max} (mm)	G_f (N/mm)	τ_{max} (MPa)	s_{max} (mm)	G_f (N/mm)	
CControl	6.82	0.095	1.570	5.65	0.115	1.656	0.873
CE1	5.89	0.090	1.250	5.04	0.115	1.265	0.771
CE2	7.77	0.090	2.047	6.54	0.120	2.060	0.611
CControl (B2)	6.90	0.095	1.489	5.60	0.115	1.584	0.901
CE3	6.29	0.100	1.616	5.65	0.125	1.690	0.890
CE4	6.46	0.090	1.333	5.13	0.105	1.437	0.696

As observed in Figure 7.22, the normalised (expressed as the ratio of exposed value to control value) maximum shear stress decreased by 13.6% for rational fit whereas by 10.8% for Dai, Ueda & Sato (2005) model fit after two months of exposure. Then the maximum shear stress increased by 13.9% for the former and 15.8% for the latter fit after six months compared to the corresponding control value. After one year, the peak shear stress for the rational fit was found to degrade by 8.8 % of the control value and

finally, it increased to reach 94.7% of the control value after 18 months. On the other hand, the peak shear stress predicted by Dai, Ueda & Sato (2005) model fit showed a continuous descending trend after six months and reached 90.8% of the control value after the exposure of 18 months. It should be noted that the one year outdoor environment (CE3) specimens were fabricated from concrete batch 2 and the shear stress and fracture energy of this series were compared to its corresponding control specimens (CControl (B2) series) fabricated from the same concrete batch.

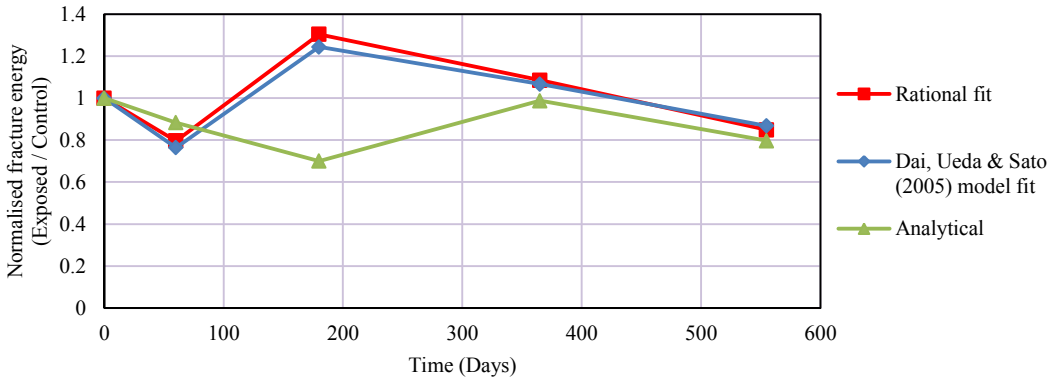

Figure 7.23 Normalised fracture energy against days of exposure for outdoor environment specimens

From Figure 7.23, the change of fracture energy from both fits with time, as well as that from the analytical formula, can be seen. The analytical fracture energy exhibited a similar trend to that of the pull-out strength as explained in section 6.2.1. But the experimental fracture energies determined from curve fitting behaved in a different manner. The maximum degradation for both fits was observed after two months when the rational fit degraded by 20.4% and Dai, Ueda & Sato (2005) model fit by 23.6% compared to their control values. The degradation of fracture energy can be attributed to the reduction of peak shear stress (Figure 7.22) and lower ultimate slip values compared to the control series (Figure 7.18) which resulted in the reduction of area under stress-slip curve. After six months, fracture energy for the former fit increased by 30.4% and that for the latter one by 24.4% of the corresponding control value, which can be attributed to the improvement of peak shear stress and ultimate slip (Figure 7.22). As the failure modes of all outdoor environment series were associated with very thin or

almost no concrete attached to debonded CFRP strip, the increase in fracture energy may also be attributed to the softening of the adhesive shear stiffness (a possible cause of higher slip observed) although the adhesive properties were not evaluated in this study. One year environment specimens (CE3 series) fabricated from the second batch of concrete exhibited decrease in fracture energy to reach 8.5% and 6.7% more than the control (CControl (B2) series) value, which can be due to the reduction of peak shear stress (Figure 7.22) and average ultimate slip (see Figures 7.6 and 7.20). The fracture energy after 18 months continued to decrease and reached 84.9% and 86.8% of the control value for rational fit and Dai model fit, respectively. Although the peak shear stress for the rational fit was very close to the control value (Figure 7.22) the narrower softening branch led to the decrease in fracture energy. On the other hand, the slight reduction of the peak shear stress for Dai model fit can be the possible cause for the deterioration of the fracture energy after 18 months.

As very thin or almost no concrete was attached to the debonded CFRP strips of all environment specimens, fracture energy of the CFRP-concrete bond is likely to be influenced by the ultimate shear strength and the shear stiffness of the adhesive. Hence, the assessment of the adhesive strength and shear stiffness under the outdoor environmental exposure can be an important investigation to properly understand the complex CFRP-concrete bond mechanism.

7.4 Proposed interface laws

Based on the Dai, Ueda & Sato (2005) model fitting to experimental data of this current study, shear stress-slip laws have been proposed for control and exposed conditions. The unknown parameters A and B determined from curve fitting for control and exposed conditions and the FRP stiffness $E_f \times t_f$ are substituted to Equation 7.6 to obtain the stress slip law for FRP-concrete interface.

7.4.1 Interface law for control series

The values of A = 0.008358 and B = 6.083 mm-1 are determined from the averaging the two values obtained for the control specimens from two batches of concrete. Substituting the FRP stiffness value of 52930.8 N/mm and values of A and B into

Equation 7.6, the following stress-slip law is proposed where shear stress τ is in MPa and slip s in mm.

$$\tau = 22.49\exp(-6.083s)(1-\exp(-6.083s)) \quad (7.7)$$

7.4.2 Interface laws for exposed series

Similar to the control series, shear stress-slip laws for temperature cycles, wet-dry cycles and outdoor environment are also proposed.

7.4.2.1 Cyclic temperature series

The interface law for cyclic temperature specimens exposed for five weeks is obtained as follows where the values of A = 0.009311, B = 5.430 mm^{-1} and $E_f \times t_f$ = 56815.2 N/mm are substituted in Equation 7.6.

$$\tau = 26.75\exp(-5.430s)(1-\exp(-5.430s)) \quad (7.8)$$

Similarly, the stress-slip law for three months cyclic temperature specimens can be defined as Equation 7.9 where A = 0.009649, B = 4.945 mm^{-1} and $E_f \times t_f$ = 54849.6 N/mm.

$$\tau = 25.25\exp(-4.945s)(1-\exp(-4.945s)) \quad (7.9)$$

The stress slip law for specimens exposed to temperature cycles for one year is expressed as the following form substituting A = 0.011470, B = 4.055 mm^{-1} and $E_f \times t_f$ = 57692.7 N/mm.

$$\tau = 30.78\exp(-4.055s)(1-\exp(-4.055s)) \quad (7.10)$$

7.4.2.2 Wet-dry series

The interface laws for specimens exposed to wet-dry cycles for one month, six months, 12 months and 18 months, respectively, are listed as follows:

$$\tau = 28.23\exp(-5.267s)(1-\exp(-5.267s)) \quad (7.11)$$

where A = 0.00960, B = 5.267 and $E_f \times t_f$ = 58158.4.

$$\tau = 18.75\exp(-5.328s)(1-\exp(-5.328s)) \quad (7.12)$$

where A = 0.008853, B = 5.328 and $E_f \times t_f$ = 44892.9.

$$\tau = 24.98\exp(-3.514s)(1-\exp(-3.514s)) \quad (7.13)$$

where A = 0.01260, B = 3.514 and $E_f \times t_f$ = 44773.6.

$$\tau = 17.84\exp(-7.749s)(1-\exp(-7.749s)) \quad (7.14)$$

where A = 0.006527, B = 7.749 and $E_f \times t_f$ = 54049.3.

7.4.2.3 Outdoor environment series

The interface laws for specimens exposed to outdoor environment for two months, six months, 12 months and 18 months, respectively, are expressed as following equations.

$$\tau = 20.17\exp(-6.081s)(1-\exp(-6.081s)) \quad (7.15)$$

where A = 0.008189, B = 6.081 and $E_f \times t_f$ = 49458.2.

$$\tau = 26.17\exp(-5.743s)(1-\exp(-5.743s)) \quad (7.16)$$

where A = 0.009153, B = 5.743 and $E_f \times t_f$ = 54386.3.

$$\tau = 22.59\exp(-5.641s)(1-\exp(-5.641s)) \quad (7.17)$$

where A = 0.008726, B = 5.641 and $E_f \times t_f$ = 52589.2.

$$\tau = 20.52\exp(-6.760s)(1-\exp(-6.760s)) \quad (7.18)$$

where A = 0.007405, B = 6.760 and $E_f \times t_f$ = 55350.4.

7.5 Chapter summary

The experimental study on the fracture properties of CFRP-concrete bond revealed the interesting relationship of maximum shear stress and fracture energy with the time of

exposure to three different environmental conditions, namely, temperature cycles, wet-dry cycles and outdoor environment. Also, fracture energies of all environment series determined from the plot of shear stress as a function of the ratio of two quadratic expression of slip were compared to those determined from an existing interface law provided by Dai, Ueda & Sato (2005). Finally, the parameters of Dai, Ueda & Sato (2005) model obtained from curve fitting of experimental data of this study were used to develop interface laws for control specimens and specimens exposed to temperature cycles, wet-dry cycles and outdoor environment. The findings of this study can be summarised as follows:

- Both rational fit and Dai, Ueda & Sato (2005) model fit provided almost similar fracture energy values although the Dai, Ueda & Sato (2005) model predicted relatively lower maximum shear stress than the experimental data.
- The fracture energies from the curve fitting of shear stress-slip relation always showed much higher values than those obtained from the analytical formula. The possible reason can be the conservative nature of the formula as the formula shows the dependence of fracture energy only on the maximum pull-out force and CFRP stiffness when the width of CFRP is constant. But the change of slip values due to the change of deformability of the adhesive properties observed in this study from fitted results may lead to quite different fracture energy from the analytical results. However, the difficulty of the precise computation of shear stress and slip values with very small number of strain gauges along the bond length and the influence of local irregularity of materials on the strain gauge reading may be another reason for higher fracture energy values obtained from the curve fitting. Hence, no conclusion on the conservativeness can be made unless a large number of strain gauges with very close intervals are employed in the study. An alternate way of continuous measurement of surface strains can be conducted by Digital Image Correlation (DIC) as reported by Subramaniam, Ali-Ahmad & Ghosn (2008). Also, the slip at the loaded end of bond can be measured alternatively by attaching Linear Variable Differential Transformer (LVDT) as adopted by Dai, Ueda & Sato (2005) and Imani (2010) in their study.
- The temperature cycles were found to have no negative effect on the fracture energy determined by both fits. However, the descending trend after three months for

rational fit and after five weeks for Dai, Ueda & Sato (2005) model fit implies the necessity of further study for longer durations.

- The wet-dry cycles caused the most significant degradation of fracture energy by about 37% after the exposure for 18 months. However, the cyclic nature of the fracture energy with time suggests the need for future studies for extended durations to find out the time required for the fracture energy to reach a plateau.
- An initial degradation of fracture energy by 20.4% and 23.6% for rational and Dai model fit, respectively, was observed after two months of outdoor environmental exposure. Similar to the other two series, studies for longer periods need to be conducted due to continuous decreasing trend of fracture energy after six months.
- As the change of adhesive properties due to three environmental conditions is likely to influence the fracture energy, thorough investigation of epoxy adhesive under similar conditions applied in this study should be carried out.

CHAPTER 8

EXPERIMENTAL STUDY ON SHORT TERM PERFORMANCE OF REINFORCED CONCRETE STRUCTURES REPAIRED WITH FRP

8 Experimental study on short term performance of reinforced concrete structures repaired with FRP

8.1 Introduction

Local failure of structural members due to extreme loading such as earthquake or blast loading may require retrofitting of the members to maintain partial functionality of the structure. A typical example may be where a bridge girder may have some localised failure because of an extreme load event but partial traffic flow needs to be allowed temporarily. As stated in Chapter 2, strengthening of reinforced concrete beams with FRP is well-established and design standards are also available. But design guidelines for repairing of severely damaged beams considering the residual strength of steel after yielding are not proposed in the available standards. So, the focus of this chapter is to report on research undertaken as part of this PhD project by repairing damaged reinforced concrete beams, fabricated from three different concrete mix designs, with some modifications of typical strengthening schemes and by investigating the performance of the repaired beams experimentally and analytically.

This chapter has been divided into sections and subsections related to different aspects of the study. Section 8.2 mainly deals with the experimental programme which is further divided into subsections explaining the fabrication of control beams, repair schemes for damaged beams and testing procedure of repaired beams. Test results of control and repaired beams have been provided in section 8.3 through comparison of load carrying capacity and load-deflection response of control and repaired beams, failure modes and strain profiles of repaired beams. Finally, analytical results of repaired beams obtained from existing closed form equations for strengthening of reinforced concrete beams with FRP have been compared to the experimental results. In addition, an analytical study on the effect of steel reinforcement on the performance of repaired beams has been reported in section 8.4. Section 8.5 provides a summary based on the observed results.

8.2 Experimental investigation

8.2.1 Fabrication of beams and geometric properties

Three reinforced concrete beams with identical geometry and steel reinforcement had been fabricated as a part of separate research study by Ghosni (2012), Haddad (2012) and Sharifi (2012) from three different concrete mixes. Control Beam 1 was fabricated replacing Portland Cement (PC) partially with 30% Fly Ash (FA) by mass. The fabrication of Control Beam 2 was carried out by the partial replacement of coarse aggregates with 6% - 12 to 15 mm Styrene Butadiene Rubber (SBR) by mass as well as partial replacement of PC with 30% FA by mass. And for Control Beam 3, 1% -19 mm Fibrillated Polypropylene (PP) fibre was incorporated into the mix volume. All beams were 1900 mm in length, 150 mm in width and 200 mm in height. The geometry and reinforcement details of all three beams are identical to the schematic diagram provided in Figure 8.1. The beams were designed as singly reinforced according to Australian standard, AS 3600 (2009). Three N12 steel bars were used as bottom steel reinforcement whereas top steel reinforcement (2-N10 bars) was provided only to hold the shear reinforcement. The shear reinforcement or stirrups used in the fabrication were N10 bars with 150 mm spacing. The material properties of Beams 1, 2 and 3 are listed in Table 8.1.

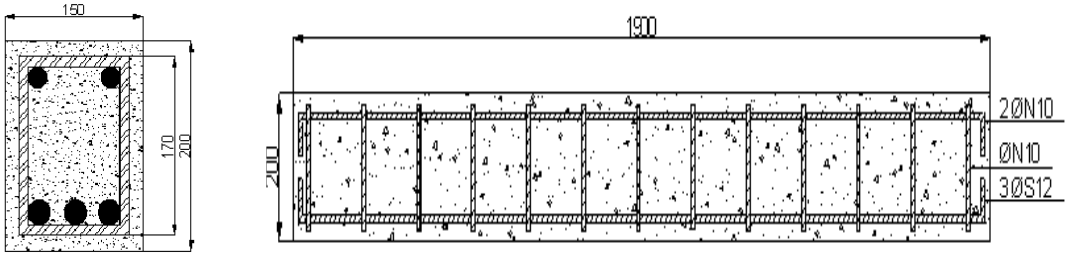

Figure 8.1 Beam geometry and reinforcement details (Ghosni 2012)

Table 8.1 Material properties of control beams

Steel			Concrete		
Steel diameter (mm)	Yield Strength (MPa)	Tensile modulus of elasticity (GPa)	Beam ID	Mix design	Compressive Strength (MPa)
12	500	200	1	30% Fly Ash (partially replacing Portland Cement by mass)	80.0
10	500	200	2	6%-12-15 mm Styrene Butadiene Rubber (partially replacing coarse aggregates by mass) + 30% Fly ash	53.0
			3	1 % -19 mm Fibrillated Polypropylene fibre by volume of the mix+30% Fly ash	71.8

8.2.2 Repair scheme for damaged beams

All control beams were repaired using a typical strengthening scheme after being loaded under four-point bending test to failure. Two layers of CFRP fabric were glued to the beam soffit with epoxy resin to improve the flexural capacity of the damaged beams. In addition, two layers of the same type of FRP were wrapped completely around the beam cross-section at both ends and in the middle of the span to delay the premature debonding failure (Figure 8.2). Same amount of FRP reinforcement was used for all

three beams. As the main focus of the repair work was to investigate the effectiveness of FRP itself, no crack repairing technique, i.e. epoxy injection, was applied in this study but the existing large voids due to cracks were filled with high strength repair mortar to facilitate application of FRP fabric.

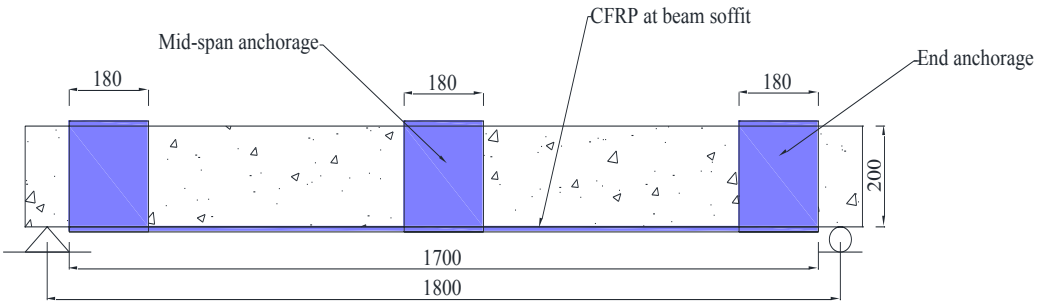

Figure 8.2 Repair scheme for the beams

Repair of the beams was carried out as follows; (i) removal of loose debris from the cracks in the concrete by using compressed air, (ii) application of repair mortar to fill in the voids, (iii) curing the repair mortar with wet rug for one week, (iv) rounding off the corners of beams to avoid the stress concentration on FRP, (v) preparing the concrete substrate on which FRP was to be applied, and (vi) application of FRP to the beam soffit with epoxy resin. Some of these steps have been shown in Figure 8.3. The material properties of the CFRP, epoxy resin and repair mortar have been provided in Table 8.2, and dimensions of the CFRP longitudinal reinforcement and anchorages are listed in Table 8.3.

(a) Loose debris removed from the top

(b) Gaps filled with repair mortar

(c) Exposing the concrete substrate

(d) Gaps filled in after exposing the concrete substrate

(e) Rounding off the corners

(f) applying pressure with a roller

Figure 8.3 Steps involved in beam repairing

Table 8.2 Material properties of CFRP, epoxy resin and high build repair mortar

Material Properties	Material type		
	CFRP	Epoxy Resin	High build repair mortar
Ply thickness, (mm)	0.117	-	-
Tensile strength, (MPa)	2987.4 *	30 **	-
Tensile modulus of elasticity, (GPa)	284.36 *	4.5 **	-
Coefficient of thermal expansion (/ ^{o}C)	-	4.5×10^{-5} ***	-
Heat Distortion temperature (^{o}C)	-	+47 **	-
Water : Powder (by mass)	-	-	1 : 6.7
Compressive strength (MPa)	-	-	32.6 (7 days air cured)
Flexural strength (MPa)	-	-	6.5 (28 days)

*Measured

** 7 days of curing at 23^{o} C

*** Between -10^{o} C to +40^{o} C

Table 8.3 FRP reinforcement details

Longitudinal FRP		FRP complete wrapping	
Dimension in mm	layer	Dimension in mm	Layer
1700 × 140 × 0.117	2	850 × 180 × 0.117	2

8.2.3 Design of repair scheme

The main aim was to design the repair scheme to cause the external CFRP reinforcement reach close to its rupture strain and to prevent the debonding of FRP from concrete at least partially. The minimum amount of FRP reinforcement to be applied in order to preclude FRP rupture before concrete crushing was determined according to Equation 8.1 (El-Mihilmy & Tedesco 2000).

$$A_{f\min} = (\alpha_2 f_c^{'} a_{f\min} b - A_s f_y)/f_{fu} \tag{8.1}$$

where $\alpha_2 = 1.0 - 0.003 f_c^{'}$; but $0.67 \le \alpha_2 \le 0.85$ (according to AS 3600 (2009)) (8.2)

$f_c^{'}$ = concrete compressive strength;

$$a_{f\min} = \gamma \times c_{f\min} \text{ where } c_{f\min} = \frac{\varepsilon_{cu}}{\varepsilon_{cu} + \varepsilon_{fu} + \varepsilon_{f0}} \times h \tag{8.3}$$

and $\gamma = 1.05 - .007 f_c^{'}$; but $0.67 \le \alpha_2 \le 0.85$ (according to AS 3600 (2009)) (8.4)

Here, ε_{cu} = ultimate compressive strain of concrete = 0.003, and ε_{fu} and ε_{f0} are the ultimate tensile strain of FRP and the initial strain of concrete at the level of FRP, respectively. Also, h = height of the beam, b = width of the beam A_s = area of the steel reinforcement, f_y = yield stress of steel reinforcement and f_{fu} = ultimate rupture stress of FRP tensile reinforcement.

The initial strain at the level of FRP reinforcement was collected from the strain gauge reading of the control beams tested for flexure from the research study conducted by

Ghosni (2012), Haddad (2012) and Sharifi (2012). The strain gauge reading after the unloading of the beams has been considered as initial strain. And the initial strain at the level of FRP reinforcements is subtracted from the FRP strain to obtain the effective FRP strain.

The test data of control beams showed that the steel reinforcement of Beams 1 and 2 reached close to yield strain and that of Beam 3 exceeded well above the yield strain. So, the effect of steel reinforcement on the performance of repaired beams can be neglected, although this assumption may be conservative because of the strain hardening of steel reinforcement. Hence, the second term of the numerator of Equation 8.1 can be considered as zero. From the calculated minimum amount of reinforcement to prevent FRP rupture, it was observed that Beams 1, 2 and 3 need 49.2 mm^2, 42 mm^2 and 47.6 mm^2 of CFRP reinforcement, respectively. Due to the varied amount of minimum FRP required for the three beams, two layers of 140 mm wide and 1700 mm long FRP longitudinal reinforcements with thickness of 0.117 mm (32.76 mm^2 of cross-sectional area) were chosen for all beams for better comparison. The reason behind the selection of FRP area being less than the minimum reinforcement required to prevent FRP rupture was to cause the beams to fail by FRP rupture. Considering the failure by rupture of FRP, the nominal moment capacity and load carrying capacity of the three repaired beams under four point bending test set-up can be predicted analytically from the following equations.

$$M_n = A_f f_{fu}(h - \frac{a_f}{2}) \tag{8.5}$$

where M_n = Nominal moment capacity of the repaired beam for given FRP area, A_f,

f_{fu} = ultimate rupture stress of FRP tensile reinforcement and h = height of the beam

$$a_f = \frac{A_f f_{fu}}{\alpha_2 f_c^{'} b} \tag{8.6}$$

$$P = 3 \times \frac{M_n}{L} \tag{8.7}$$

where P = the value of load of one load cell in a four-point bend test set-up

The FRP complete wrapping was designed with the assumption that the strain of complete wraps will reach its effective strain as defined by ACI 440.2R (2008), when the longitudinal FRP reinforcement will reach the rupture strain. So, the area of the end anchorage or mid-span anchorages can be calculated from the following equation:

$$A_{f_{anchor}} = \frac{\left(A_f f_{fu}\right)_{longitudinal}}{\left(E_f \varepsilon_{fe}\right)_{anchor}} \tag{8.8}$$

where $A_{f_{anchor}}$ = area of the FRP anchor $= 2nt_f w_f$, n = number of FRP layers, t_f = thickness of FRP layer, w_f = width of FRP anchor and $\varepsilon_{fe_{anchor}}$ = effective FRP strain of the anchor = $0.004 \le 0.75\varepsilon_{fu}$; ε_{fu} = ultimate strain of FRP

Based on the calculations using Equation 8.8, two layers of CFRP with the dimensions of 850mm × 180 mm × 0.117 mm were wrapped completely around the beam cross section at both ends of the FRP longitudinal reinforcement and in the mid-span.

8.2.4 Four-point-bending test

All repaired beams were loaded monotonically under four-point-bending till failure. During the test, load values and corresponding mid-span deflection were recorded. In addition, one LVDT was attached on the top of the beam at one third distance from the left support to record the deflection under one of the loading points. In order to determine the strain distributions of FRP with the progress of loading, five strain gauges (two at the one third lengths from supports, one at mid-span and two in the middle of load cells and mid-span) were attached on the FRP surface. Also, one strain gauge was attached to concrete on the top of the beam surface close to the middle of the span. During the testing, opening of existing cracks and formation of new cracks were marked at every 5 kN of loading until no new cracks were observed. Figure 8.4 shows the four-point-bending test set-up.

(a) Specimen under loading

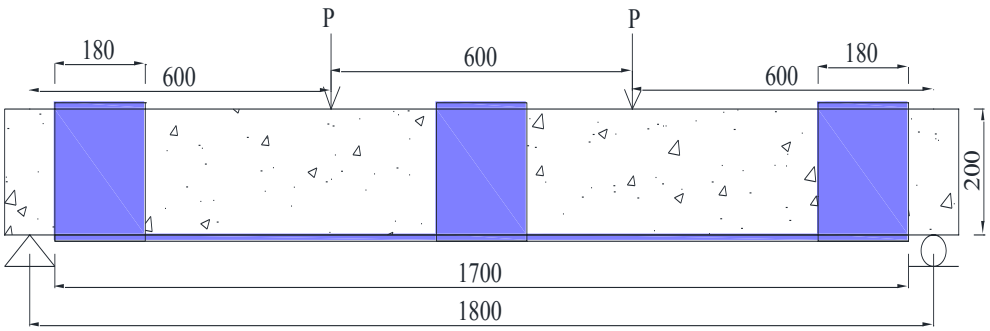

(b) Schematic diagram of four-point-bend test

Figure 8.4 Four-point-bending test set-up

8.3 Test results and discussion

The test results have been presented in terms of ultimate load carrying capacity of repaired and control beams, load-deflection response, failure modes and strain profiles. Also, analytical prediction of ultimate load carrying capacity of the repaired beams has been compared to the experimental results.

8.3.1 Load-deflection response

Figure 8.5 shows the plot of mid-span deflection against the total load (2P) for all three beams. The continuous red line represents the control beam whereas the dashed blue

line represents the repaired beam. The failure was controlled by the debonding of FRP for all three repaired beams but the anchorages helped to prevent complete debonding and caused FRP reinforcement rupture near the anchorage for Beams 1 and 2. Although complete FRP rupture was not observed for Beam 3, FRP ruptured partially near the mid-span anchorage. In terms of ultimate load, it is obvious from Figure 8.5 that the strength of Beams 1 and 2 could be fully restored even though these beams were tested till failure before the FRP application. The initial stiffness of repaired Beams 1 and 2 was almost identical to the control beams which can be attributed to the CFRP repair. The performance of Beam 3, compared to the other two beams, was less effective as the strength could only be restored to 45.6% compared to the control beam. The poor performance of Beam 3 is mainly because of the large amount of deflection and pre-existing wide cracks in the beam before the repair. This is also supported by the strain values of the steel in control Beam 3, observed in a separate study by Ghosni (2012), which exceeded far beyond the yield strain and approached close to the value (0.01) corresponding to that of tensile strength of steel. The wide cracks caused high stress concentration on FRP and further helped the debonding initiation at lower load value (2P = 50 kN) than the other two beams. On the other hand, the control Beams 1 and 2 only exhibited 35 and 30 mm deflections, respectively and the steel strain values just reached close to the yield values. So, these two beams showed large deflections after the initiation of FRP debonding until the complete failure. But the repaired Beam 3 failed immediately after the debonding propagated from one of the loading points to the mid-span anchorage probably because of the complete failure of the steel reinforcement. Although the steel reinforcement was not assessed after the beam failed, the failure of the steel can be assumed due to the muffled sound heard at failure of the beam. Although different concrete mix designs were used for the three beams, no conclusion can be drawn on the effect of mix design on the performance of repaired beams from the load-deflection response and the failure modes. The load carrying capacity of the control beams and repaired beams have been listed in Table 8.4.

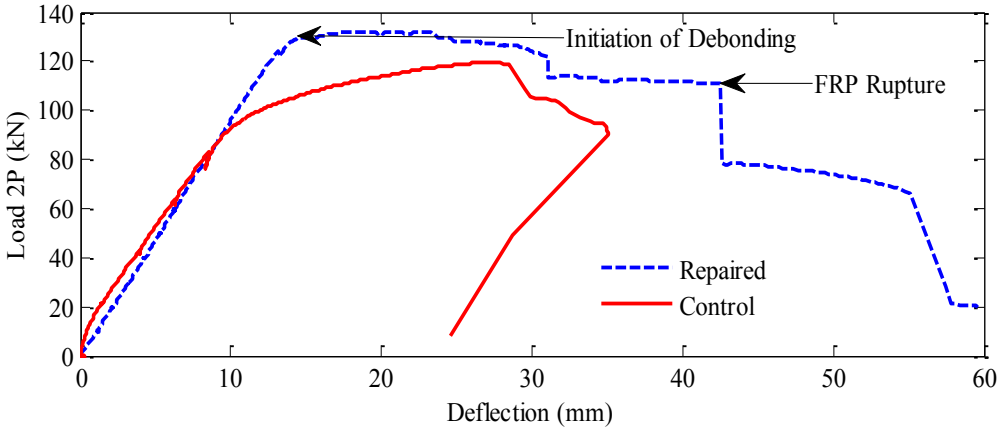

(a) Load deflection plot of Beam 1

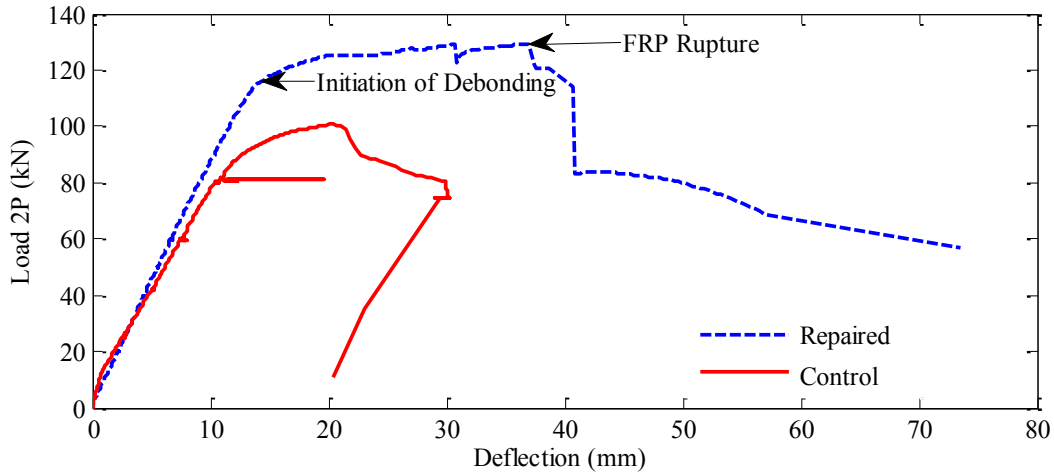

(b) Load-deflection plot of Beam 2

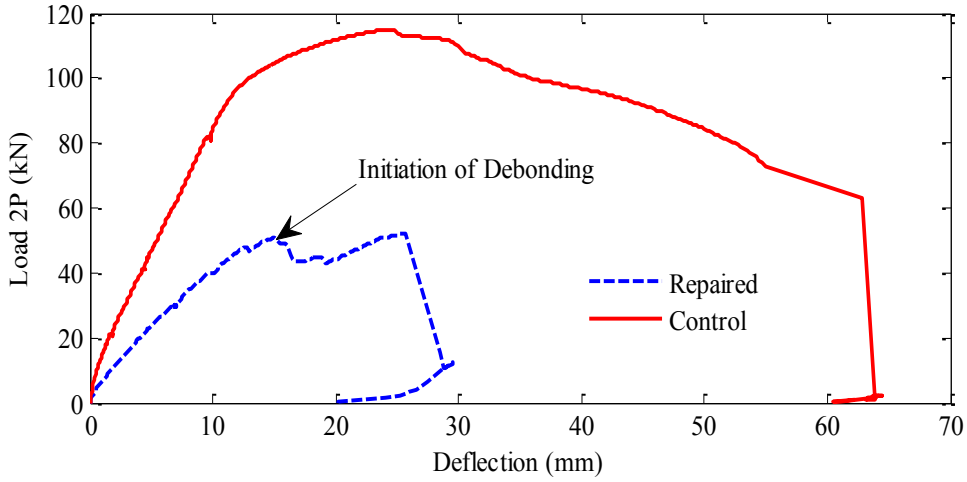

(c) Load-deflection plot of Beam 3

Figure 8.5 Load-deflection plot of control and repaired beams

Table 8.4 Strength and deflection properties of control and repaired beams

Specimen ID	Maximum total load 2P (kN)		Maximum mid-span deflection (mm)		% Strength restored
	Control	Repaired	Control	Repaired	
Beam 1	119.44	132.22	35.05	59.62	110.7
Beam 2	100.64	129.33	30.25	73.47	128.5
Beam 3	114.79	52.30	63.84	29.6	45.6

8.3.2 Failure modes

Failure of Beams 1 and 2 (repaired beams) initiated with FRP debonding from the left loading point and the debonding propagated to the end anchorage and mid-span anchorage. Beam 1 showed FRP rupture near the end and mid-span anchorage, whereas FRP ruptured at the end anchorage for Beam 2 (Figure 8.6). After the rupture of FRP, very rapid crack propagation and crack widening was observed and crack propagated to the compressive zone around the complete wrapping of mid-span. The crushing in the compression zone was also visible mainly in the part repaired with mortar.

On the other hand, Beam 3 exhibited immediate failure with a muffled sound after the debonding propagated from the right loading point to the end and mid-span anchorage. Also, the failure in repair mortar was observed on the top of beam at the middle of the span. Unlike Beam 1 and Beam 2, the rupture of FRP was not noticed except for few cracks on FRP near the mid-span anchorage.

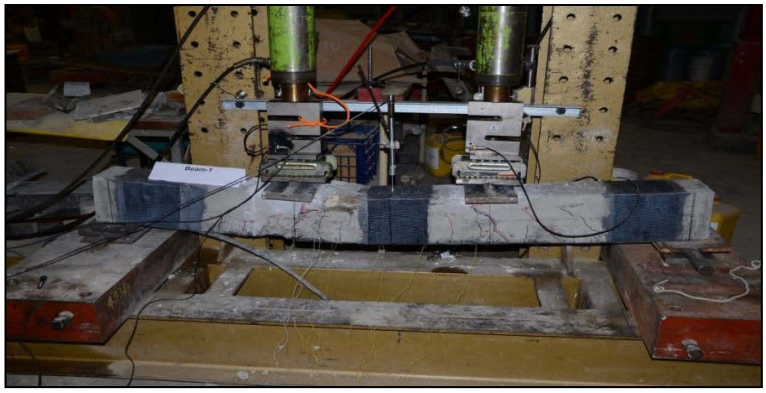

(a) Failed repaired Beam 1

(b) Ruptured FRP strip of Beam 1

(c) Failed repaired Beam 2

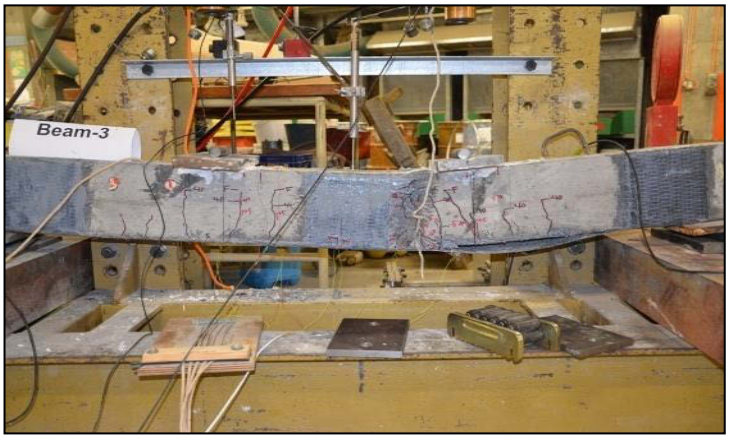

(d) Failed repaired Beam 3

Figure 8.6 Failed repaired beams

8.3.3 Strain profiles

Figure 8.7 shows the strain profiles of FRP attached to beam soffit for all of the three repaired beams. The low value of strain represents good bond between FRP and concrete while sudden increase of strain at any location with increase in load represents the initiation of debonding at that location. The rupture strain for the CFRP was 15000 $\mu\varepsilon$ as specified by the supplier. The strain profiles of the three beams have been explained separately as follows:

Beam 1:

From Figure 8.7 (a), it can be observed that all strain gauge locations showed gradual increase in strain values with the increase in loads. And strain values at each level of load were almost constant at all locations. But at 130 kN of load, the strain values at left load cell (0 mm) and at 150 mm from the left load cell showed sudden increases which represent the initiation of debonding of FRP near the left load cell.

Beam 2:

The strain profiles of Beam 2 (Figure 8.7 (b)) showed similar behaviour as Beam 1. The debonding also started near the left load cell at about 125 kN.

Beam 3:

Beam 3 strain profiles, from Figure 8.7 (c), shows different behaviour than the other two beams and the initiation of debonding occurred near the right load cell and mid-span location. Even at low levels of loads, strain values from the middle of the span to the right load cell were higher than the left part of the beam. This may be attributed to the widening of existing cracks at those locations and crack formation due to interfacial stress at FRP-concrete bond.

From the strain profiles of Beams 1 and 2, it can be understood that the debonding started near the left load cell and the Beam 3 strain profile shows the debonding initiation near the right load cell.

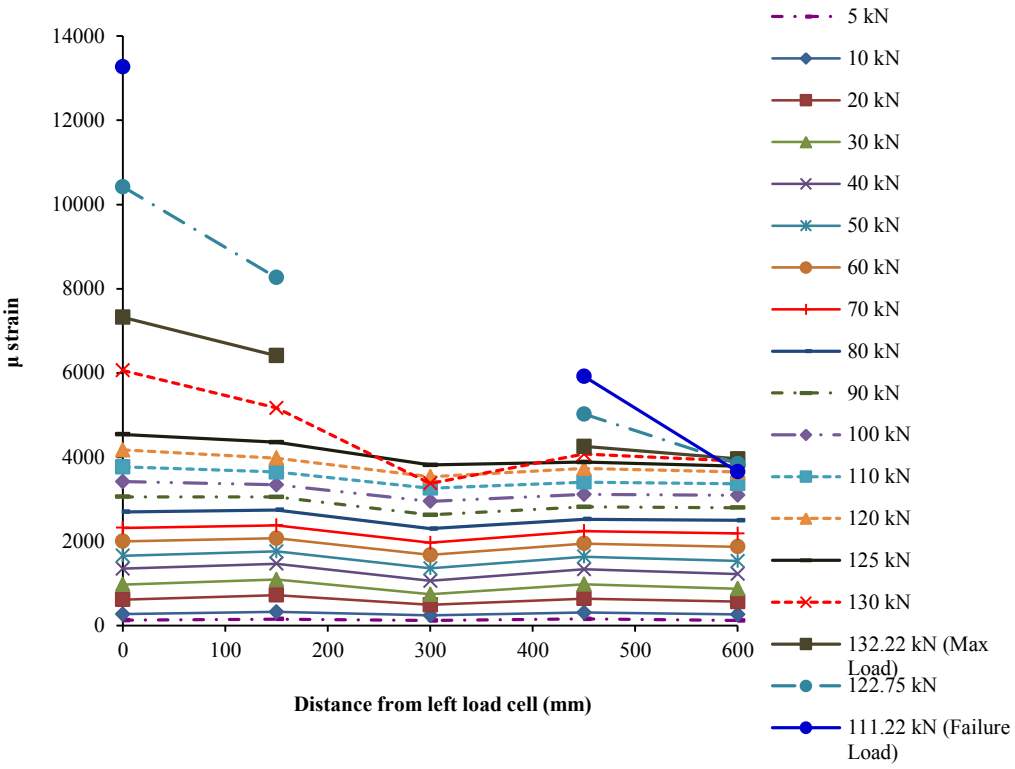

(a) Strain profile of Beam 1

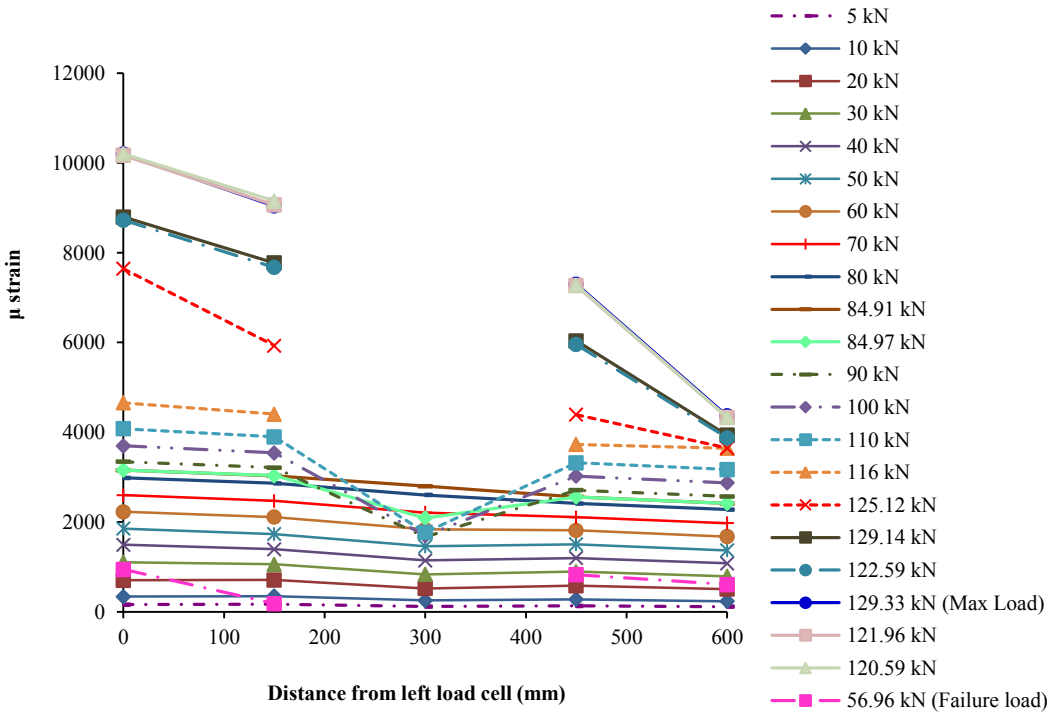

(b) Strain profile of Beam 2

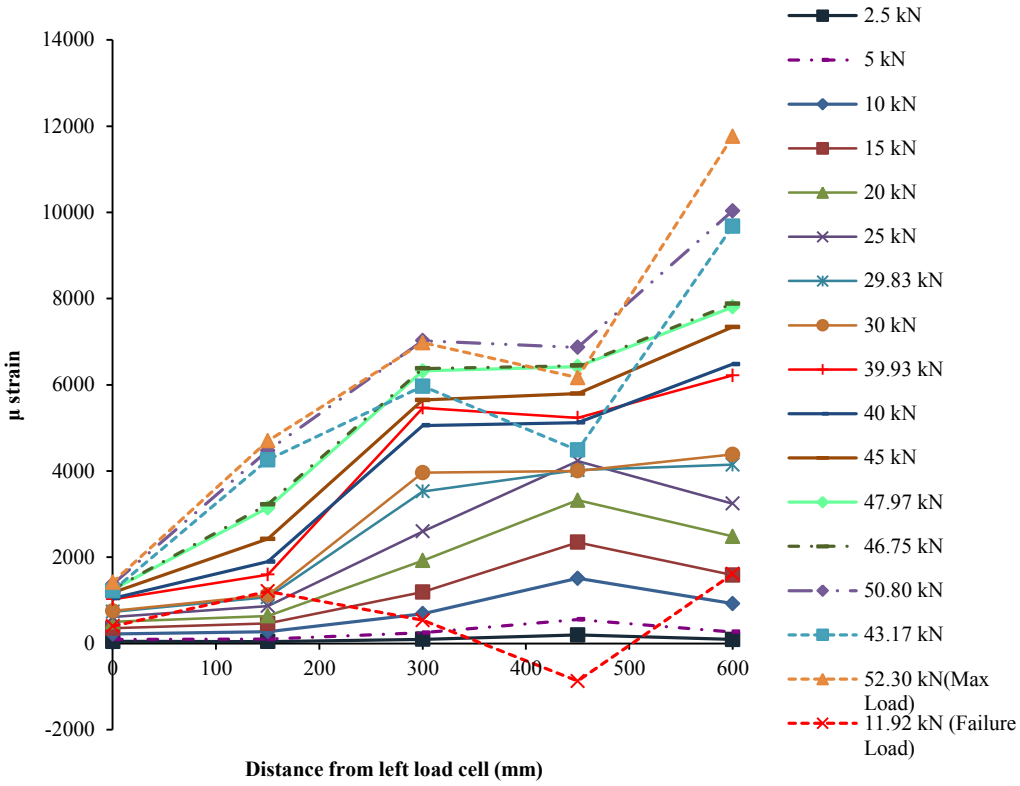

(c) Strain profile of Beam 3

Figure 8.7 Strain profiles of repaired beams

8.3.4 Comparison of experimental with analytical results

The load carrying capacity of the beams calculated based on Equations 8.5 to 8.7 and the experimental load carrying capacity have been provided in Table 8.5 for comparison. The analytical ultimate loads for Beams 1 and 2 have been found to be 48.0 % and 48.6 % of the experimental values, respectively, leading to very conservative predictions. This can be attributed to ignoring the contribution of steel reinforcement to load carrying capacity of the repaired beams (discussed later in Section 8.4). For the design of reinforced concrete beams, a yield plateau is considered for the stress-strain curve of steel reinforcement and the strain hardening part after the yield plateau is usually neglected as the reinforced concrete beams are designed to fail by the yielding of steel and to provide warning by the large amount of deflections after the yield point. From the control beam results provided by a separate research study (Ghosni 2012; Haddad 2012; Sharifi 2012), it was observed that steel reinforcements of Beams1 and 2 reached close to the yield strain but that of Beam 3 was much higher than the yield

strain. So, it may be assumed that mainly the FRP reinforcement carried the tensile stress initially due to the applied load and steel reinforcement had partial contribution for Beams 1 and 2. On the other hand, due to existing large amount of deflection in Beam 3, only FRP contributed to tensile stress and steel reinforcement may only have a negligible contribution. So, the assumption that steel reinforcement has no contribution in the load carrying capacity of the repaired beam is found to be more appropriate for Beam 3, which can further be confirmed by the very close analytical result to the experimental one.

Table 8.5 Analytical and experimental load carrying capacity of repaired beams

Specimen ID	Analytical Maximum load $2P_{analytical}$ (kN)	Experimental maximum load $2P_{experimental}$ (kN)	% (Analytical / Experimental)
Beam 1	63.49	132.22	48.0
Beam 2	62.86	129.33	48.6
Beam 3	63.35	52.30	121.1

8.4 Analytical study on the effect of steel reinforcement on the performance of repaired beams

In order to investigate the effect of steel reinforcement on the repaired beams tested under four-point bending, mid-span deflection, Δ of beams at different load values were calculated analytically from the following equation considering different cases of steel reinforcements and some assumptions:

$$\Delta = \frac{Pa}{24EI}(3L^2 - 4a^2) \tag{8.9}$$

where P = the value of one load cell = the average of two load cell values in a four-point-bending test, a = the distance of load cell from support, L = span length of the beam.

After obtaining the analytical values of mid-span deflection, which are in the elastic range, the experimental deflections plotted against loads were compared to the analytical values for different cases of steel reinforcements.

Assumptions in this study were as follows:

1. Beam sections are cracked
2. Stresses are elastic

The schematic diagram of transformed (all materials were transformed into equivalent concrete) cracked section of repaired beam is shown in Figure 8.8.

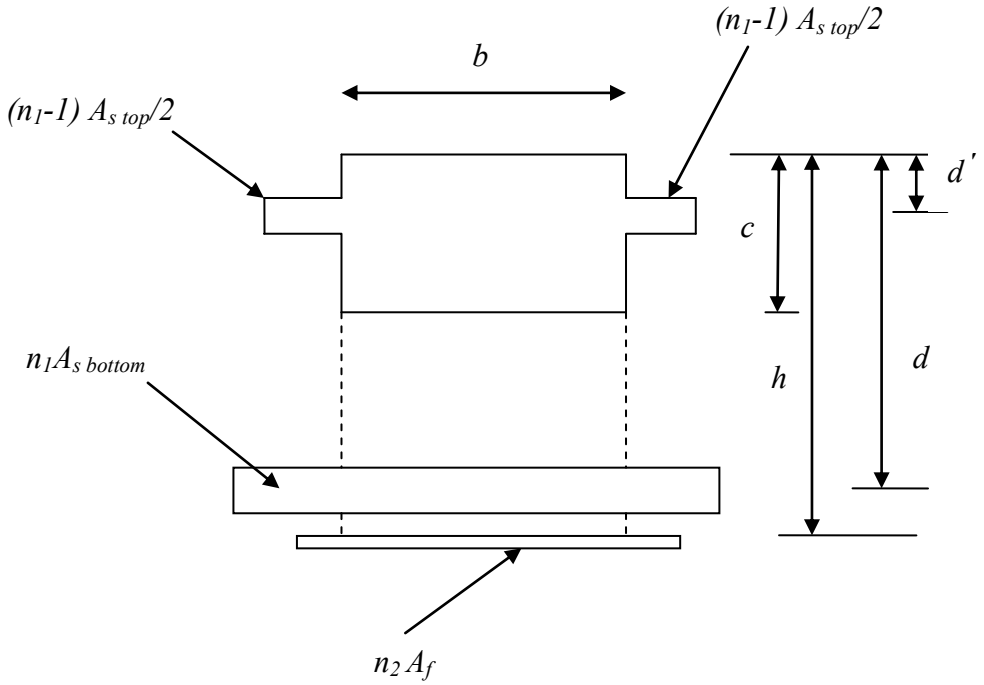

Figure 8.8 Schematic diagram of transformed cracked section of repaired beam

In order to obtain the bending stiffness *EI*, first the depth of neutral axis *c* was calculated for four different cases: 1) top and bottom steel is in elastic range, concrete has cracked and FRP is intact, 2) both top and bottom steel have yielded, concrete has cracked and FRP is intact, 3) bottom steel has yielded, top steel is in elastic range,

concrete has cracked and FRP is intact and 4) top steel has yielded, bottom steel is in elastic range, concrete has cracked and FRP is intact. The moment of inertia *I* for all cases were determined and multiplied by the concrete elastic modulus to get the value of *EI* of the beams.

Case 1:

By equilibrating the moment of area of compression and tension zone,

$$(n_1 - 1)A_{s_{top}}d' + bc \times \frac{c}{2} = n_1 A_{s_{bottom}} d + n_2 A_f h \tag{8.10}$$

where $n_1 = \frac{E_s}{E_c}$, $n_2 = \frac{E_f}{E_c}$, $A_{s_{top}}$ = area of top steel reinforcements, $A_{s_{bottom}}$ = area of bottom steel reinforcement, A_f = area of FRP, d' = depth of top steel axis from the top fibre of the beam, d = depth of bottom steel axis from the top fibre of beam and h = depth of bottom steel axis

Also, E_s = elastic modulus of steel, E_c = elastic modulus of concrete and E_f = elastic modulus of FRP.

The value of *c* can be calculated from the following equation,

$$c = \sqrt{\frac{2\{n_1 A_{s_{bottom}} d + n_2 A_f h - (n_1 - 1)A_{s_{top}} d'\}}{b}} \tag{8.11}$$

and $I = b\frac{c^3}{12} + bc \times \left(\frac{c}{2}\right)^2 + n_1 A_{s_{bottom}} (d - c)^2 + (n_1 - 1)A_{s_{top}} \left(c - d'\right)^2 + n_2 A_f (h - c)^2$ (8.12)

Case 2:

As the reinforced concrete beams are designed to fail by initiation of yielding of steel reinforcements, the contribution of steel reinforcement can be neglected after yielding. Therefore, $A_{s_{bottom}}$ and $A_{s_{top}}$ in Equation 8.10 can be considered as '0' which leads to the following equation:

$$c = \sqrt{\frac{2n_2 A_f h}{b}} \tag{8.13}$$

$$\text{and } I = b\frac{c^3}{12} + bc \times \left(\frac{c}{2}\right)^2 + n_2 A_f (h-c)^2 \tag{8.14}$$

Case 3:

Considering $A_{s_{bottom}} = 0$, Equation 8.10 turns into the following equation:

$$c = \sqrt{\frac{2\{n_2 A_f h - (n_1 - 1)A_{s_{top}} d'\}}{b}} \tag{8.15}$$

$$\text{and } I = b\frac{c^3}{12} + bc \times \left(\frac{c}{2}\right)^2 + (n_1 - 1)A_{s_{top}} (c - d')^2 + n_2 A_f (h-c)^2 \tag{8.16}$$

Case 4:

Considering $A_{s_{top}} = 0$, Equation 8.10 can be re-written as:

$$c = \sqrt{\frac{2(n_1 A_{s_{bottom}} d + n_2 A_f h)}{b}} \tag{8.17}$$

$$\text{and } I = b\frac{c^3}{12} + bc \times \left(\frac{c}{2}\right)^2 + n_1 A_{s_{bottom}} (d-c)^2 + n_2 A_f (h-c)^2 \tag{8.18}$$

Applying the above equations for cases 1-4, *EI* values and mid-span deflections *Δ* for arbitrary values of *P* can be calculated and a linear plot of the total load (*2P*) in a four-point bending set-up against the mid-span deflection (*Δ*) can be obtained and this plot has been referred as *2P-Δ* plot or relationship in the rest of this chapter. The experimental *2P-Δ* for three repaired beams can then be compared to the analytical ones

to understand the proximity of the experimental initial stiffness with any of the four cases of analytical stiffness.

8.4.1 Results of the analytical study on the effect of steel reinforcement

Repaired Beam 1:

The analytical 2P-Δ relationship of Repaired Beam 1 for four cases stated in the previous section and the experimental 2P-Δ have been plotted in Figure 8.9. It is obvious that the analytical stiffness considering the effect of top and bottom steel, cracked concrete and FRP are almost the same as the stiffness neglecting the effect of top steel. Even for the other two analytical stiffness, the effect of top steel is negligible although the stiffness neglecting top and bottom steel is slightly lower than the one neglecting only the bottom steel. Comparison of the experimental initial slope to the analytical ones clearly shows that the steel reinforcements are effective in the repaired beams to provide sufficient stiffness which is very close to the analytical stiffness considering the effect of steel reinforcements. Therefore, both steel reinforcements and FRP contributed to the load carrying capacity of Repaired Beam 1, although the steel of Control Beam 1 just exceeded the yield strain before unloading was carried out. This can be attributed to the strain hardening of steel reinforcement after it reaches plastic range. Hence, considering the steel as ineffective after yielding may severely underestimate the stiffness of the repaired beam.

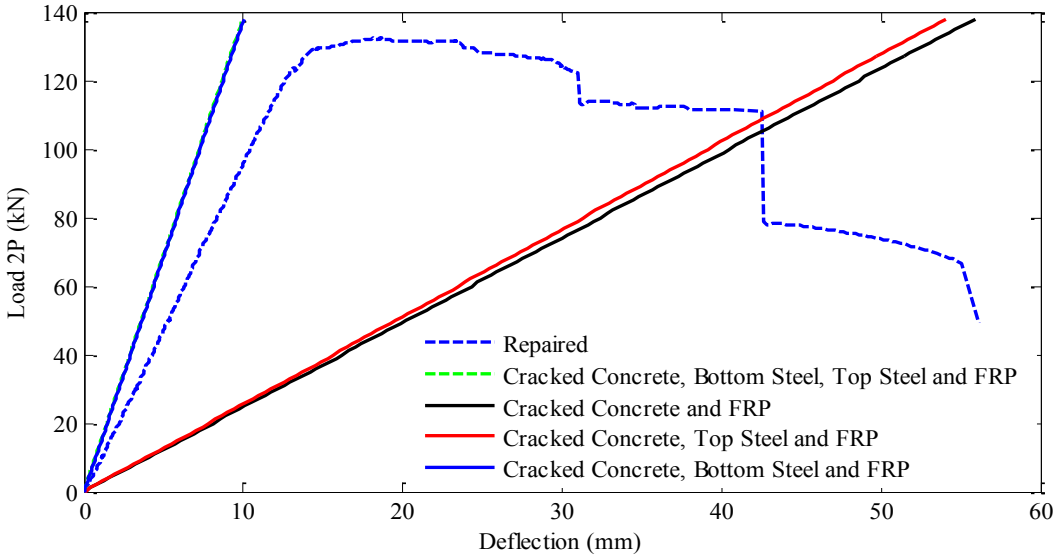

Figure 8.9 Load-deflection plot of Repaired Beam 1 considering the effects of steel reinforcement

Repaired Beam 2:

Similar to Beam 1, Beam 2 exhibited an initial slope of the load-deflection response (Figure 8.10) quite close to the analytical load-deflection plot considering steel reinforcement is effective in load carrying capacity. This behaviour represents the considerable contribution of steel reinforcement in the load carrying capacity of Beam 2 even though the strain of bottom steel reinforcement of control beam approached the yield strain before unloading. Therefore, considering the strain hardening part after steel yielding may lead to prediction of the stiffness of the repaired beam close to the experimental stiffness.

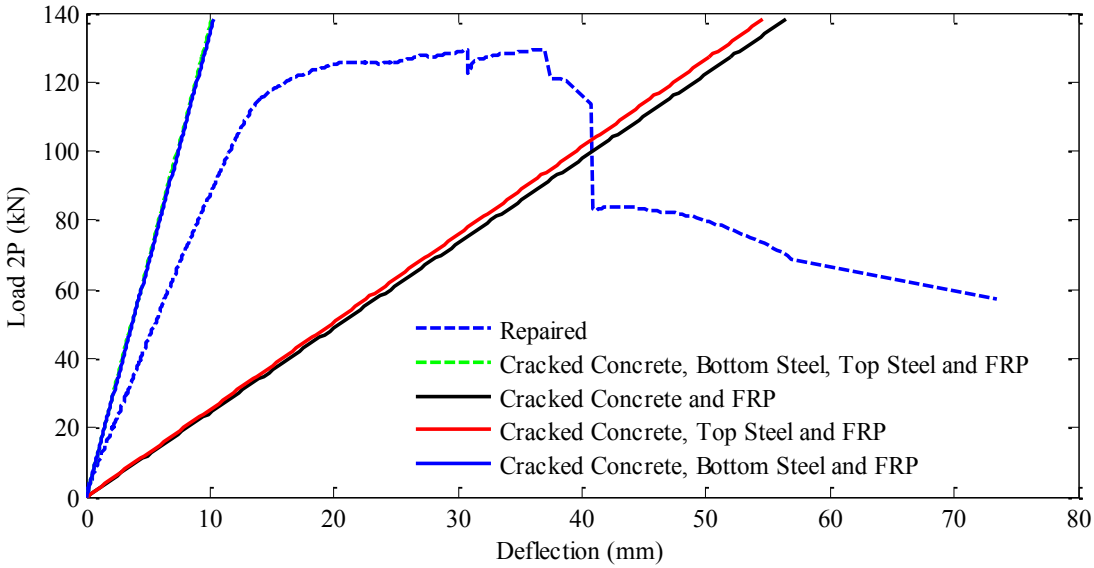

Figure 8.10 Load-deflection plot of Repaired Beam 2 considering the effects of steel reinforcement

Repaired Beam 3:

Unlike Beams 1 and 2, Beam 3 had lower initial stiffness that can be observed from Figure 8.11. Also, the experimental stiffness was close enough to the analytical stiffness ignoring the effect of steel. The better prediction for Beam 3 stiffness could be possible due to the fact that the steel of Control Beam 3 exceeded far beyond the yield strain and almost reached the value corresponding to its tensile strength. So, the strain hardening part was absent in case of repaired Beam 3. As a result, the maximum deflection reached for this beam was only about 30 mm, which was much lower than the other two beams. And the beam failed immediately after the FRP debonding.

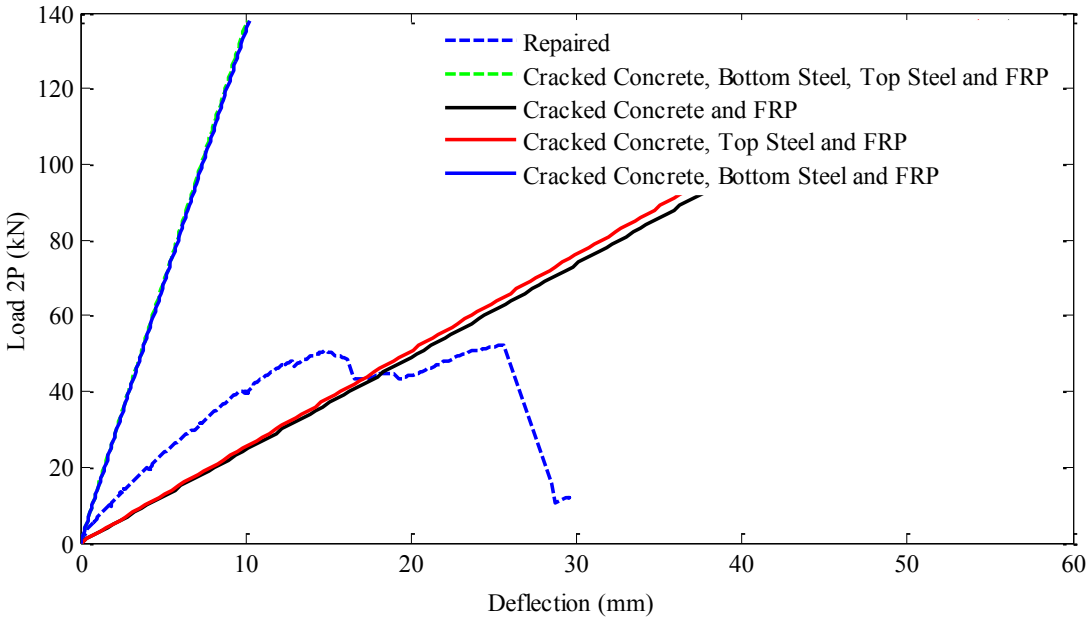

Figure 8.11 Load-deflection plot of Repaired Beam 3 considering the effects of steel reinforcements

From the observations stated above, it is worth mentioning that the modification of Equations 8.5 and 8.6 by considering the residual strength of the steel reinforcement instead of neglecting the strength completely is likely to improve the prediction of ultimate moment and load carrying capacity of repaired beams. The analytical equations considering this fact and the corresponding results have been presented in the following section.

8.4.2 Prediction of load-carrying capacity of repaired beams considering steel strain hardening

The inclusion of strain hardening of steel reinforcements after the steel yielding to predict the ultimate moment and load carrying capacity of FRP repaired beams has been adopted from an analytical investigation by Quantrill, Hollaway & Thorne (1996). In this study, Quantrill, Hollaway & Thorne (1996) replaced the yield plateau of steel stress strain curve with the strain hardening part as shown in Figure 8.12 to predict the response of FRP strengthened beams. Unlike their study where uncracked beams were strengthened with FRP, considering the residual steel strength is necessary to predict the

response of the damaged beams repaired with FRP. And the residual tensile strength of steel considering strain hardening instead of perfect plasticity after yield point can be calculated by Equation 8.19.

$$f_{s\,Res} = E_s(\varepsilon_y - \varepsilon_{s0}) + (f_u - f_y);\ \text{if}\ \varepsilon_{s0} \le \varepsilon_y \tag{8.19}$$

where $f_{s\,Res}$ = residual tensile strength of steel, E_s = modulus of elasticity of steel, ε_{s0} = strain in steel reinforcement at the failure of control beam, ε_y = yield strain of steel, f_u = ultimate tensile stress of steel and f_y = yield stress of steel.

Equation 8.19 turns into the following equation if $\varepsilon_y < \varepsilon_{s0} \le \varepsilon_u$.

$$f_{s\,Res} = \left(\frac{f_u - f_y}{\varepsilon_u - \varepsilon_y}\right) \times (\varepsilon_u - \varepsilon_{s0}) \tag{8.20}$$

where ε_u = strain of steel at ultimate tensile strength and ε_y = yield strain of steel.

As the steel reinforcement reaches the necking stage after it reaches the ultimate stress, it is no longer able to contribute to load carrying or stiffness of the beam. Therefore, the residual strength of steel is considered as zero when the steel reinforcement reaches or exceeds the value of ε_u at the failure of control beam.

Finally, the nominal moment capacity and load capacity of the repaired beams can be determined from Equations 8.21 - 8.23 .

$$M_n = A_f f_{fu}\left(h - \frac{a_f}{2}\right) + A_s f_{s\,Res}\left(d - \frac{a_f}{2}\right) \tag{8.21}$$

where $a_f = \dfrac{A_f f_{fu} + A_s f_{s\,Res}}{\alpha_2 f_c' b}$ (8.22)

and the load carrying capacity for four point bending test set-up,

$$P = 3 \times \frac{M_n}{L} \tag{8.23}$$

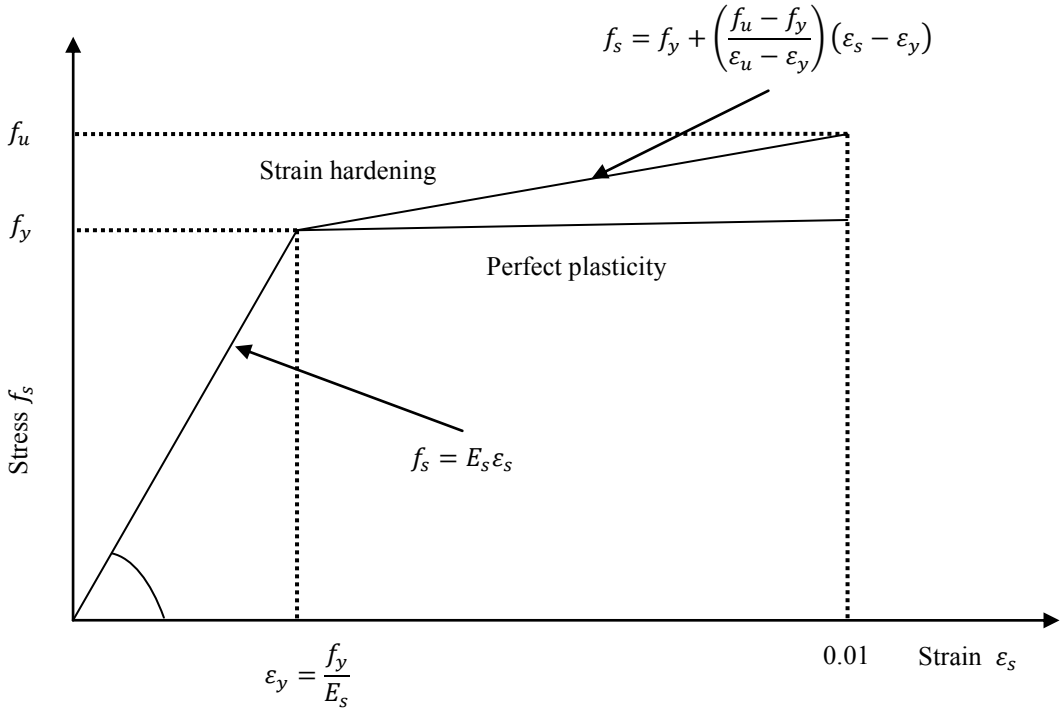

Figure 8.12 Stress-strain curve of mild steel (Quantrill, Hollaway & Thorne 1996)

The results obtained by the analytical prediction considering the residual strength of steel reinforcement have been summarised in Table 8.6. In addition, a comparison of analytical predictions to the experimental ones has been shown. It is evident that taking the strain hardening of steel into account has led to significant improvement in the analytical prediction of ultimate loads of Beams 1 and 2. The analytical loads were 93.6 % and 81.0% of the experimental values for Beams 1 and 2, respectively, whereas neglecting the steel reinforcement showed very conservative prediction for these beams before.

Table 8.6 Analytical and experimental load carrying capacity of repaired beams considering the residual steel strength

Specimen ID	Analytical maximum load $2P_{analytical}$ (kN)	Experimental maximum load $2P_{experimental}$ (kN)	% (Analytical / Experimental)
Beam 1	123.74	132.22	93.6
Beam 2	104.77	129.33	81.0
Beam 3	63.35	52.30	121.1

8.5 Conclusions

The purpose of the study was to investigate the appropriateness of typical FRP strengthening scheme applied to repair severely damaged reinforced concrete beams. Although, most of the repair works are usually conducted to structural members loaded within the serviceable limit, this study was mainly carried out considering the local failures of members due to extreme loading and to provide temporary solutions in the case where immediate retrofitting is necessary. All beams were designed with some modifications of the existing closed form equations and neglecting the effect of existing steel reinforcement which had already yielded before the repair works. Moreover, an analytical study was conducted considering the effect of residual strength of steel reinforcement. The findings of the study are listed as follows:

- Beams 1, 2 and 3, regardless of the concrete mix design used for their fabrication, showed reasonable amount of strength recovery after being repaired with CFRP. The percentage of strength recovery for Beams 1, 2 and 3 was 110.7, 128.5 and 45.6, respectively.
- The failure of all beams was controlled by the debonding of CFRP from concrete, although the beams were designed with minimum amount of CFRP. This failure mode is typical of FRP strengthened structural members and is initiated by the new or existing cracks in concrete.
- CFRP complete wrapping applied at both ends of CFRP longitudinal reinforcement and middle of the beam span improved the performance of the beams by preventing

the propagation of delamination of FRP. Even, partial fracture of FRP in strips was observed in Beams 1 and 2.

- In prediction of ultimate load carrying capacity, the analytical approach neglecting the steel reinforcement was found to be too conservative for Beams 1 and 2 but reasonable for Beam 3. This is mainly because of the conservative assumption on the steel reinforcement performance after yielding. In reality, yielding of the steel reinforcement and subsequent unloading will result in strain hardening and not loss of strength. However, this assumption is valid where the beam has been subjected to large deflections and steel strain has exceeded well beyond the yield strain.
- The analytical approach with consideration of strain hardening of steel after yielding can provide better prediction of ultimate loads and can be used especially for the retrofitting of severely damaged beams with FRP where the steel reinforcement has already yielded.
- The use of non-conventional concrete had no visible effect on the effectiveness of the FRP repair technique applied in this study. Hence, the repair technique is equally applicable to conventional and non-conventional concrete.

From the findings stated above, it can be concluded that a suitable strengthening scheme with FRP can provide considerable strength recovery even to severely damaged reinforced concrete beams loaded beyond their ultimate loads and subjected to large deflections and significant cracking. As a result, this repairing technique can be applied to repair structural members failed by extreme loading conditions to provide quick and temporary solutions. However, the strain in the steel reinforcement at the time of failure of the control beams should be assessed and any residual contribution of steel reinforcement should be included for better analytical or numerical prediction of response of the FRP-repaired beams. Although crack repairing technique was not applied in this study and the strengthening scheme mainly depended on the effectiveness of FRP itself, the effect of crack repairing technique on the obtained results specially the initiation of debonding and shear strength of bond cannot be overlooked in real applications and should be considered in future studies.

CHAPTER 9

CONCLUSIONS AND RECOMMENDATIONS FOR FUTURE RESEARCH

9 Conclusions and recommendations for future research

9.1 Introduction

Based on the identified gaps in the available literature on long term performance of FRP-concrete bond, the main aim of this research project was to investigate long term performance of FRP (CFRP and GFRP)-concrete bond subjected to temperature cycles, wet-dry cycles and outdoor environment for extended durations. The three environmental conditions used for the study were mainly selected to overcome some limitations found in the previous research in the literature. Especially, separating two variables, namely, temperature and humidity from the hydro-thermal ageing was the main reason to investigate the effect of temperature cycles and wet-dry cycles separately. Using high temperature for acceleration of any ageing condition such as wet-dry cycles was found to be a very common practice in the available literature. But the conservativeness of this acceleration technique was also reported by researchers. Hence, in wet-dry cycles, the range of temperature was kept close to the ambient temperature (although constant temperature could not be maintained), and in temperature cycles, dry environment was chosen. The outdoor environmental ageing was also chosen as only limited data for long term natural ageing of FRP-concrete bond could be found in the literature. The effects of the three exposure conditions on concrete and CFRP were also studied separately to understand the dependence of the bond strength on the change in material properties with exposure time. The secondary objective of this project was to conduct an experimental study to investigate the efficacy of well-established FRP-strengthening scheme in the repair of three severely damaged RC beams fabricated from conventional and non-conventional concrete. All three damaged beams were repaired with CFRP and same repairing schemes were used for all beams. In addition, a short analytical study on the CFRP-repaired beams was conducted to understand the effect of residual strength of steel reinforcement on the repaired beams by comparison of analytical and experimental results and modified equations were proposed for the prediction of load carrying capacity for such repaired beams considering the strain hardening of steel reinforcement after yielding.

In this chapter, a summary of research findings as well as some recommendations for future research have been provided.

9.2 Material properties due to exposure

The experimental material characterisation, namely, CFRP tensile strength and modulus of elasticity, and concrete compressive strength were investigated after being exposed to temperature cycles (up to five weeks, three months and one year), wet-dry cycles (up to one month, six months, one year and 18 months), and outdoor environment (up to two months, six months, one year and 18 months). The observations of the study are summarised for CFRP tensile properties and concrete compressive strength as follows:

- **<u>CFRP tensile properties</u>:**

- Direct exposure to outdoor environment and wet-dry cycles were found to cause the most degradation in the tensile strength of CFRP (about 20% over the period of 18 months compared to 14.3% due to temperature cycles over one year period).
- Modulus of elasticity of CFRP was observed to reduce due to exposure to wet-dry cycles and maximum reduction was by 15.2%, whereas for specimens exposed to outdoor environment, there was only an initial reduction (by 6.6%) but an increase of 9% after 18 months was observed. Temperature cycles resulted in an increase in MOE by 11% over the period of one year.

The increase in MOE, despite the reduction in tensile strength for cyclic temperature exposure, can be attributed to the possible increase in the MOE of carbon fibres (Fitzer 1988; Sauder, Lamon & Pailler 2004) and the softening of epoxy matrix which was also noticed in some of the previous research (Cao, Zhis & Wang 2009). The possible softening of epoxy can lead to the uneven stress distribution among fibres in CFRP coupons which would have caused the failure at lower loads even though the fibre stiffness increased.

- **Concrete compressive strength:**

Temperature cycles, wet-dry cycles and outdoor environment were found to cause significant improvement of compressive strengths of two batches of concrete during almost the whole exposure period and the most prominent increase was due to outdoor environmental exposure. Only an initial reduction in strength (by 9%) for batch 1 was observed due to cyclic temperature. The possible reason for the development of concrete strength due to exposure conditions can be explained from the concept of maturity and concrete curing temperature. As the concrete was cured at lab temperature (about 20-23^{o} C), the initial strength gain during the curing was slower than the other curing techniques associated with relatively higher temperatures. Although the curing process at low temperature causes slower rate of strength development at the earlier stages such as up to 28 days, it helps to improve the strength at a later stage (Neville 1963). From the maturity rule, the higher temperature applied after the initial setting and hardening period leads to higher compressive strength of concrete (Neville 1963), and the temperature cycles applied in this study therefore improved the concrete strength with the exposure time. Also, the increase in compressive strength due to wet-dry cycles can be attributed to the suitable humid condition for the development of concrete strength. Similarly, the increase in compressive strength of concrete exposed to outdoor environment can be attributed to the combined effect of components of outdoor environmental exposure such temperature and moisture.

Increases in compressive strength due to temperature cycles were 32% and 28% for batch 1 and 2, respectively, whereas those for wet-dry cycles were 32% and 40.7%, respectively. Outdoor environment caused the increase of about 59-66% compared to the compressive strength of control series.

9.3 Long term performance of FRP-concrete bond

The experimental investigation on the CFRP and GFRP-concrete bond exposed to cyclic temperature, wet-dry cycles and outdoor environment revealed some interesting findings based on the analysis of pull-out strength, failure modes, strain profiles and fracture properties. The findings of CFRP and GFRP-concrete bond are highlighted separately for temperature cycles, wet-dry cycles and outdoor environment:

- **Temperature cycles:**

- The temperature cycles were found to have no negative effect on the pull-out strength of CFRP and GFRP-concrete bond with the exception of initial degradation by 1% for CFRP-concrete bond. In fact, temperature cycles improved pull-out strength by 10% for CFRP-concrete bond and 8% for GFRP-concrete bond. These improvements of pull-out strength can be attributed to the increased concrete compressive strength as the failure of both types of bond occurred within the concrete substrate with minimal reduction in concrete thickness.
- Strain profiles did not show any changes with the exception of longer effective bond length observed in some exposed series. The longer effective bond lengths of exposed specimens, compared to the unexposed specimens, suggests that the bond length longer than the theoretical effective bond length of unexposed specimens can be helpful to proper attainment of bond capacity in the long term.
- Experimental fracture energy of CFRP-concrete bond increased due to temperature cycles. The two methods used for fitting the experimental shear stress-slip curves, namely, rational fit and Dai, Ueda & Sato (2005) model, gave an increment of 23.1% and 19.9%, respectively.
- Discrepancies between the analytical and experimental fracture energies were attributed to the possible conservativeness of the analytical approach which mainly depends on the maximum pull-out force and FRP stiffness. Trends in the fracture energy from the experimental results imply possible dependence of fracture energy on the adhesive stiffness (deformability of adhesive) as well as the concrete compressive strength, although adhesive properties were not investigated in the study. Difficulty in obtaining the shear stress and slip precisely from a small number of strain gauges used in this study and the likelihood of the strain gauge reading being biased by any local material non-uniformity could also have led to the observed discrepancies.
- Shear stress-slip laws were proposed for CFRP-concrete bond specimens exposed to temperature cycles based on the identification of unknown parameters of Dai, Ueda & Sato (2005) model fitted to experimental data of this current study.

- **Wet-dry cycles:**

- Cyclic nature of the pull-out strength and failure patterns of CFRP-concrete bond with exposure durations was observed, where only 5% reduction in pull-out strength occurred and was attributed to the degraded epoxy strength based on the change in failure mode from thick concrete layer to almost no concrete attached to debonded CFRP. Performance of GFRP-concrete bond under wet-dry cycles was marginally poor (strength reduction by 6.4%) compared to that of CFRP-concrete bond. The degradation was attributed to the epoxy degradation and the most series failed with almost no concrete attached to the debonded GFRP.
- Strain profiles of CFRP-concrete bond also revealed a cyclic nature in terms of the load at the shifting of initial stress transfer length similar to that of pull-out strength. For GFRP-concrete bond, the trend of the loads at the change of initial stress transfer length also changed with time (no cyclic nature) and followed almost a similar trend to the pull-out strength. Effective bond lengths for most of CFRP and GFRP exposed specimens were longer than that of unexposed specimens for most exposure durations.
- The cyclic nature of the experimental fracture energy of CFRP-concrete bond was also observed. Wet-dry cycles were found to cause the highest degradation of fracture energy among all exposure conditions (by about 37 % for both fits after 18 months of exposure). The deterioration was related to the brittle failure mode in concrete layer observed after 18 months. Discrepancy between the analytical and experimental fracture energies were observed for wet-dry cycles too and analytical fracture energies were always lower than the experimental values similar to the observation made for temperature cycle.
- Shear stress-slip laws were proposed for CFRP-concrete bond specimens exposed to wet-dry series by fitting Dai, Ueda & Sato (2005) model to experimental data of this current study.

- **Outdoor environment:**

- Exposure to outdoor environment caused the most serious deterioration of pull-out strength for both CFRP and GFRP concrete-bond. The effect was more prominent for CFRP specimens (15.2 % reduction in strength compared to 9.3% for GFRP specimens). Deterioration of bond strength due to outdoor environment can also be

attributed to the degraded epoxy strength as unlike the control specimens, very thin or almost no concrete layer was found to be attached to debonded FRP for exposed specimens.

- The change in strain profiles, in terms of the loads at the shifting of initial stress transfer length, and increase in effective bond lengths for both FRP types was identified.
- Only initial degradation of fracture energy of CFRP-concrete bond by 20.4% and 23.6% for rational and Dai, Ueda & Sato (2005) model fit, respectively, was observed. Similar to other two environmental conditions, discrepancies between analytical and experimental fracture energies were observed.
- Similar to other two exposure conditions, shear stress-slip laws were also proposed for outdoor environment series.

9.4 Strength reduction factors for long term performance of FRP-concrete bond

The strength reductions observed for CFRP and GFRP-concrete bond subjected to outdoor environment were the highest among all three exposures applied in this study. This is attributed to the various environmental variables such as temperature, moisture/humidity, solar exposure (UV), salinity and other chemical substances present in the air. Hence, the degradation of FRP-concrete bond due to outdoor environment can be considered as the combined effect of all the variables. Assuming $k_{outdoor}$ as the bond strength reduction factor for outdoor environmental exposure, the following relationship between $k_{outdoor}$ and reduction factors (k) due to individual components of the environmental exposure can be assumed:

$$k_{outdoor} = k_{temperatre} \times k_{wet-dry} \times k_{UV} \times ..... \times k_z \quad (9.1)$$

where $k_{temperature}$, $k_{wet\text{-}dry}$, k_{UV} represent reduction factors due to individual components of environmental exposure such as temperature, wetting and drying and UV light, respectively.

Based on the observations of this research study, the reduction factors for temperature cycles, wet-dry cycles and outdoor environment are proposed as listed in Table 9.1. For each exposed condition, reduction factor was obtained from the maximum percentage of

pull-out strength degradation observed in this study. It should be noted that the reduction factor proposed for outdoor environmental exposure is applicable to the climatic conditions similar to Sydney, Australia. According to the map of climate zones of Australia based on temperature and humidity (Australian Government Bureau of Meteorology 2012), Sydney is in warm summer, cold winter zone but the winter has no freezing and thawing. Melbourne, Adelaide, Port Lincoln, Perth, Albany and few other cities in Australia are in the same climate zone. The proposed factor, therefore, may not be applicable to extreme climatic conditions such as in areas where freezing and thawing or too high temperatures are expected. From the proposed factors, it can be observed that the reduction factors for both FRP types due to outdoor environment are lower than the product of the factors due to temperature and wet-dry cycles, which follows the relationship shown in Equation 9.1. The reason can be attributed to the large number of variables (temperature, humidity, UV, salinity, other chemical substances) involved in the real outdoor environmental exposure. Hence, the proposed reduction factor for outdoor environmental exposure represents the products of the factors for all exposure components and has a lower value than the product of the factors for temperature cycles and wet-dry cycles. It should be noted that the temperature cycles and wet-dry cycles applied in this study do not represent the true components of outdoor environment as these were applied mainly to simulate severe exposure conditions. The proposed factors for these two exposure conditions, especially for wet-dry cycles, therefore, represent strength reductions due to severe conditions.

Table 9.1 Strength reduction factors for CFRP and GFRP-concrete bond

Bond type	$k_{outdoor}$	$k_{temperature}$	$k_{wet\text{-}dry}$	$k_{temperature} \times k_{wet\text{-}dry}$
CFRP-concrete	0.84	0.99	0.95	0.94
GFRP-concrete	0.90	1	0.93	0.93

9.5 Short term performance of CFRP repaired beams

Experimental study on the repair of three severely damaged RC beams demonstrated the effectiveness of typical FRP strengthening schemes in the repair of damaged RC beams. Load carrying capacity of two beams could be fully restored and that of the third one with pre-existing wide cracks could be restored to up to 45 % of its original strength. Also, the effectiveness of FRP anchorage provided by wrapping at the both ends and in the mid span of the beam was demonstrated by the partial rupture of external FRP flexural reinforcement. Although debonding of FRP could not be prevented completely, the anchorage restricted the propagation of debonding. It should be noted that no crack repairing technique, except filling of voids with repair mortar, was adopted and the repairing technique solely depended on the FRP itself. The suitability of the applied FRP repairing technique to conventional and non-conventional concrete could also be understood as no visible effect of concrete type was observed in the study. The analytical prediction of ultimate load and moment carrying capacity by neglecting the contribution of steel reinforcement was found to be too conservative for the strain level of steel reinforcement which is very close to the yield point. But this prediction method can be reasonable for the case where the steel strain has exceeded far beyond the yield point and reached almost close to the ultimate strain value. Analytical prediction considering the steel strain hardening part showed much better prediction of load carrying capacity for all repaired beams. Although the concept of considering the residual strength of steel was adopted from the study of Quantrill, Hollaway & Thorne (1996), modifications of their equations are proposed in order to use for repairing of damaged beams for three conditions of steel reinforcement: i) strain lower than the yield strain, ii) strain exceeding the yield strain but lower than ultimate tensile strain and iii) strain at ultimate tensile strain. The importance of assessment of the condition of steel reinforcement before repairing is, therefore, stressed.

9.6 Recommendations for future research

Based on the findings and limitations of the current study a number of recommendations can be made as future studies as follows:

1. As the trend of pull-out strength and fracture energy observed in this study revealed the possible dependence of these parameters on the adhesive strength and shear

stiffness, adhesive properties can be determined for similar environmental conditions.

2. The lower boundary of the temperature cycles could not be reached below 30^{o} C due to the limitation of the drying oven used in this study. Hence, FRP-concrete bond system can be studied by reducing the minimum temperature, for example, to 5^{o} C as a wider temperature range is likely to result in more significant bond-strength deterioration. In addition, the coupled effect of temperature cycles and wet-dry cycles can be a possible investigation in future studies.
3. Cyclic nature of pull-out strength of CFRP-concrete bond under wet-dry cycles observed in this study suggests the need for investigation for extended durations.
4. As the conservativeness of the analytical fracture energy could not be conclusive due to very small number of strain gauges attached to the FRP in this study, using a large number of strain gauges with close intervals is suggested to capture the strain profile, slip, average local shear stress, and stress transfer lengths, precisely. An alternate to using large number of strain gauges is by using digital image correlation (DIC) as reported by Subramaniam, Ali-Ahmad & Ghosn (2008). In addition, for measurement of slip at the loaded end of FRP-concrete bond, attachment of LVDT instead of the installation of large number strain gauges can also be conducted.
5. Study of the effect of sustained load on the FRP-concrete bond subjected to environmental conditions can be conducted.
6. A numerical model can be developed for the prediction of long term performance of FRP-concrete bond subjected to environmental conditions using the information and data obtained from this research.

   Results from this study could not be extended for the prediction of service life for two types of FRP-concrete bond by developing an empirical relationship such as the one based on the Arrhenius principle (Litherland, Oakley & Proctor 1981) due to the discontinuous trend of the bond strength with duration of exposure. Empirical relationship based on Arrhenius principle has been used in some previous research by Litherland, Oakley & Proctor (1981), Dejke & Tepfers (2001) and Chen, Davalos & Ray (2006), mostly for durability evaluation of FRP reinforcement exposed to simulated concrete environment. However, there is a scope for using the information from this study to predict long term performance of FRP-concrete bond exposed to environment for evaluation of numerical models.

7. As the proposed equations for the repair of damaged RC beams have been verified only with the data from three beams and a single type of FRP, further experimental studies incorporating different degrees of damage and other FRP types can be conducted.
8. No crack repairing technique before the application of FRP was applied in this study. But acknowledging the effect of this on the results obtained, it is recommended to include this technique in future studies.

References

ACI 440.2R 2008, *Guide for the design and construction of externally bonded FRP systems for strengthening concrete structures*, American Concrete Institute, Farmington Mills, Michigan, USA.

Al-Amery, R. & Al-Mahaidi, R. 2006, 'Coupled flexural–shear retrofitting of RC beams using CFRP straps', *Composite Structures*, vol. 75, no. 1, pp. 457-464.

Ali-Ahmad, M. 2006, *Debonding of FRP from concrete in strengthening applications| Experimental investigation and theoretical validation*, City University of New York.

Ali-Ahmad, M.K., Subramaniam, K.V. & Ghosn, M. 2007, 'Analysis of scaling and instability in FRP-concrete shear debonding for beam-strengthening applications', *Journal of engineering mechanics*, vol. 133, no. 1, pp. 58-65.

An, W., Saadatmanesh, H. & Ehsani, M.R. 1991, 'RC Beams Strengthened with FRP Plates. II: Analysis and Parametric Study', *Journal of Structural Engineering*, vol. 117, no. 11, pp. 3434-3455.

Arduini, M. & Nanni, A. 1997, 'Behavior of Precracked RC Beams Strengthened with Carbon FRP Sheets', *Journal of Composites for Construction*, vol. 1, no. 2, pp. 63-70.

AS 1012.9 1999, *Method of testing concrete, Determination of the compressive strength of concrete specimens*, Standards Australia, Sydney, Australia.

AS 1012.17 1997, *Method of testing concrete, Determination of the static chord modulus of elasticity and Poisson's ratio of concrete specimens*, Standards Australia, Sydney, Australia.

AS 3600 2009, *Concrete Structures*, Standards Australia, Sydney, Australia.

ASTM D3039/D3039M 2008, *Standard test method for tensile properties of polymer matrix composite materials*, American Society for Testing and Materials (ASTM), Pennsylvania, USA.

Australian Government Bureau of Meteorology 2012, *Climate Classification Maps*, viewed 11 October 2014

<http://www.bom.gov.au/jsp/ncc/climate_averages/climate-classifications/index.jsp?maptype=tmp_zones#maps>.

Bank, L.C. 2006, *Composites for construction: structural design with FRP materials*, Wiley.

Barenblatt, G. 1962, 'The mathematical theory of equilibrium cracks in brittle fracture', *Advances in applied mechanics*, vol. 7, no. 55-129, p. 104.

Bazant, Z.P., Daniel, I.M. & Li, Z. 1996, 'Size effect and fracture characteristics of composite laminates', *Journal of Engineering Materials and Technology(Transactions of the ASME)(USA)*, vol. 118, no. 3, pp. 317-324.

Benjeddou, O., Ouezdou, M.B. & Bedday, A. 2007, 'Damaged RC beams repaired by bonding of CFRP laminates', *Construction and Building Materials*, vol. 21, no. 6, pp. 1301-1310.

Benzarti, K., Chataigner, S., Quiertant, M., Marty, C. & Aubagnac, C. 2011, 'Accelerated ageing behaviour of the adhesive bond between concrete specimens and CFRP overlays', *Construction and Building Materials*, vol. 25, no. 2, pp. 523-538.

Biscaia, H.C., Chastre, C. & Silva, M.A.G. 2013, 'Linear and nonlinear analysis of bond-slip models for interfaces between FRP composites and concrete', *Composites Part B: Engineering*, vol. 45, no. 1, pp. 1554-1568.

Bizindavyi, L. & Neale, K. 1999, 'Transfer Lengths and Bond Strengths for Composites Bonded to Concrete', *Journal of Composites for Construction*, vol. 3, no. 4, pp. 153-160.

Boyajian, D.M. 2002, 'Mode I fracture and durability of the CFRP-concrete interface bond', Ph.D. thesis, West Virginia University, Ann Arbor.

Boyajian, D.M., Ray, I. & Davalos, J.F. 2007, 'Freeze-thaw cycling under a calcium chloride environment: effects on CFRP strengthened concrete structures', *International Journal of Materials and Product Technology*, vol. 28, no. 1, pp. 89-102.

Camanho, P.P. & Davila, C.G. 2002, 'Mixed-mode decohesion finite elements for the simulation of delamination in composite materials', *NASA-Technical Paper*, vol. 211737.

Cao, S., Zhis, W. & Wang, X. 2009, 'Tensile properties of CFRP and hybrid FRP composites at elevated temperatures', *Journal of Composite Materials*, vol. 43, no. 4, pp. 315-330.

Chaallal, O., Nollet, M.-J. & Perraton, D. 1998, 'Strengthening of reinforced concrete beams with externally bonded fiber-reinforced-plastic plates: Design guidelines for shear and flexure', *Canadian Journal of Civil Engineering*, vol. 25, no. 4, pp. 692-704.

Chajes, M.J., Finch Jr, W.W., Januszka, T.F. & Thomson Jr, T.A. 1996, 'Bond and force transfer of composite-material plates bonded to concrete', *ACI structural journal*, vol. 93, no. 2.

Chajes, M.J., Thomson Jr, T.A., Januszka, T.F. & Finch Jr, W.W. 1994, 'Flexural strengthening of concrete beams using externally bonded composite materials', *Construction and Building Materials*, vol. 8, no. 3, pp. 191-201.

Chajes, M.J., Thomson, T.A. & Farschman, C.A. 1995, 'Durability of concrete beams externally reinforced with composite fabrics', *Construction and Building Materials*, vol. 9, no. 3, pp. 141-148.

Chen, J. & Teng, J. 2001, 'Anchorage Strength Models for FRP and Steel Plates Bonded to Concrete', *Journal of Structural Engineering*, vol. 127, no. 7, pp. 784-791.

Chen, Y., Davalos, J.F. & Ray, I. 2006, 'Durability prediction for GFRP reinforcing bars using short-term data of accelerated aging tests', *Journal of Composites for Construction*, vol. 10, no. 4, pp. 279-286.

Coronado, C.A. & Lopez, M.M. 2006, 'Sensitivity analysis of reinforced concrete beams strengthened with FRP laminates', *Cement and Concrete Composites*, vol. 28, no. 1, pp. 102-114.

Cousins, T., Lesko, J. & Carlin, B. 1998, 'Tailored Performance and Durability of Reinforced Concrete Beams Strengthened with FRP Plates', *Second International Conference on Composites in Infrastructure*, vol. 2.

Cromwell, J., Harries, K. & Shahrooz, B. 2011, 'Environmental durability of externally bonded FRP materials intended for repair of concrete structures', *Construction and Building Materials*, vol. 25, no. 5, pp. 2528-2539.

Dai, J., Ueda, T. & Sato, Y. 2005, 'Development of the Nonlinear Bond Stress–Slip Model of Fiber Reinforced Plastics Sheet–Concrete Interfaces with a Simple Method', *Journal of Composites for Construction*, vol. 9, no. 1, pp. 52-62.

Dai, J.G., Yokota, H., Iwanami, M. & Kato, E. 2010, 'Experimental Investigation of the Influence of Moisture on the Bond Behavior of FRP to Concrete Interfaces', *Journal of Composites for Construction*, vol. 14, p. 834.

De Lorenzis, L., Miller, B. & Nanni, A. 2001, 'Bond of FRP laminates to concrete', *ACI Materials Journal*, vol. 98, no. 3, pp. 256-264.

Dejke, V. & Tepfers, R. 2001, 'Durability and service life prediction of GFRP for concrete reinforcement', *Proc., 5th Int. Conf. on Fiber-Reinforced Plastics for Reinforced Concrete Structures (FRPRCS-5)*, vol. 1, Thomas Telford London, pp. 505-516.

Dong, J., Wang, Q. & Guan, Z. 2013, 'Structural behaviour of RC beams with external flexural and flexural–shear strengthening by FRP sheets', *Composites Part B: Engineering*, vol. 44, no. 1, pp. 604-612.

El-Mihilmy, M.T. & Tedesco, J.W. 2000, 'Analysis of reinforced concrete beams strengthened with FRP laminates', *Journal of Structural Engineering*, vol. 126, no. 6, pp. 684-691.

El-Sayed, A.K. 2014, 'Effect of longitudinal CFRP strengthening on the shear resistance of reinforced concrete beams', *Composites Part B: Engineering*, vol. 58, no. 0, pp. 422-429.

Ferracuti, B., Savoia, M. & Mazzotti, C. 2006, 'A numerical model for FRP–concrete delamination', *Composites Part B: Engineering*, vol. 37, no. 4–5, pp. 356-364.

Ferracuti, B., Savoia, M. & Mazzotti, C. 2007, 'Interface law for FRP–concrete delamination', *Composite structures*, vol. 80, no. 4, pp. 523-531.

Fitzer, E. 1988, 'Composites for high temperatures', *Pure Appl. Chem*, vol. 60, no. 3, pp. 287-302.

Gamage, K., Al-Mahaidi, R. & Wong, B. 2010, 'Fe modelling of CFRP-concrete interface subjected to cyclic temperature, humidity and mechanical stress', *Composite Structures*, vol. 92, no. 4, pp. 826-834.

GangaRao, H.V., Taly, N. & Vijay, P. 2006, *Reinforced concrete design with FRP composites*, CRC.

Ghosni, N. 2012, 'Evaluation of Static and Dynamic Behaviour of Fibre reinforced Concrete Incorporating Polypropylene Fibres', ME thesis, University of Technology Sydney, Sydney, Australia.

Grace, N.F. 2004, 'Concrete repair with CFRP', *Concrete international*, vol. 26, no. 5, pp. 45-52.

Green, M.F., Bisby, L.A., Beaudoin, Y. & Labossière, P. 2000, 'Effect of freeze-thaw cycles on the bond durability between fibre reinforced polymer plate reinforcement and concrete', *Canadian journal of civil engineering*, vol. 27, no. 5, pp. 949-959.

Haber, Z.B., Mackie, K.R. & Zhao, L. 2012, 'Mechanical and environmental loading of concrete beams strengthened with epoxy and polyurethane matrix carbon fiber laminates', *Construction and Building Materials*, vol. 26, no. 1, pp. 604-612.

Haddad, R. 2012, 'Structural Properties of Control and Special Concrete Specimens and Beams', ME thesis, University of Technology Sydney, Sydney, Australia.

Head, P. 1996, 'Advanced composites in civil engineering–A critical overview at this high interest, low use stage of development', *Proceedings of ACMBS*, pp. 3-15.

Hiroyuki, Y. & Wu, Z. 1997, 'Analysis of debonding fracture properties of CFS strengthened member subject to tension', *Non-Metallic (FRP) Reinforcement for Concrete Structures, Proceedings of the Third International Symposium*, vol. 1, pp. 287-294.

Högberg, J. 2006, 'Mixed mode cohesive law', *International journal of fracture*, vol. 141, no. 3, pp. 549-559.

Homam, S., Sheikh, S. & Mukherjee, P. 2001, 'Durability of fibre reinforced polymers (FRP) wraps and external FRP–concrete bond', pp. 18–20.

Imani, F.S., Chen, A., Davalos, J.F. & Ray, I. 2010, 'Temperature and Water-Immersion Effect on Mode II Fracture Behavior of CFRP-Concrete Interface', *CICE 2010 - The 5th International Conference on FRP Composites in Civil Engineering*, eds L. Ye, P. Feng & Q. Yue, Springer Berlin Heidelberg, Beijing, China, pp. 557-561.

Imani, S. 2010, 'Traction-separation law for CFRP-concrete interface fracture under mode II loading', West Virginia University, Morgantown, West Virginia.

JCI TC952 1998, *Technical Report on Continuous Fiber Reinforced Concrete*, Tokyo, Japan.

Karbhari, V., Chin, J., Hunston, D., Benmokrane, B., Juska, T., Morgan, R., Lesko, J., Sorathia, U. & Reynaud, D. 2003, 'Durability gap analysis for fiber-reinforced

polymer composites in civil infrastructure', *Journal of Composites for Construction*, vol. 7, no. 3, p. 238.

Karbhari, V.M. 2003, 'Durability of FRP composites for civil infrastructure myth, mystery or reality', *Advances in Structural Engineering*, vol. 6, no. 3, pp. 243-255.

Karbhari, V.M. & Abanilla, M.A. 2007, 'Design factors, reliability, and durability prediction of wet layup carbon/epoxy used in external strengthening', *Composites Part B: Engineering*, vol. 38, no. 1, pp. 10-23.

Lai, W.L., Kou, S.C., Poon, C.S., Tsang, W.F. & Lai, C.C. 2009, 'Effects of elevated water temperatures on interfacial delaminations, failure modes and shear strength in externally-bonded CFRP-concrete beams using infrared thermography, gray-scale images and direct shear test', *Construction and Building Materials*, vol. 23, no. 10, pp. 3152-3160.

Lai, W.L., Kou, S.C., Poon, C.S., Tsang, W.F. & Lai, C.C. 2010, 'Characterization of the deterioration of externally bonded CFRP-concrete composites using quantitative infrared thermography', *Cement and Concrete Composites*, vol. 32, no. 9, pp. 740-746.

Leone, M., Matthys, S. & Aiello, M.A. 2009, 'Effect of elevated service temperature on bond between FRP EBR systems and concrete', *Composites Part B: Engineering*, vol. 40, no. 1, pp. 85-93.

Li, G., Pang, S., Helms, J., Mukai, D., Ibekwe, S. & Alaywan, W. 2002, 'Stiffness degradation of FRP strengthened RC beams subjected to hygrothermal and aging attacks', *Journal of Composite Materials*, vol. 36, no. 7, p. 795.

Litherland, K.L., Oakley, D.R. & Proctor, B.A. 1981, 'The use of accelerated ageing procedures to predict the long term strength of GRC composites', *Cement and Concrete Research*, vol. 11, no. 3, pp. 455-466.

Lu, X.Z., Teng, J.G., Ye, L.P. & Jiang, J.J. 2005, 'Bond-slip models for FRP sheets/plates bonded to concrete', *Engineering Structures*, vol. 27, no. 6, pp. 920-937.

Maeda, T., Asano, Y., Sato, Y., Ueda, T. & Kakuta, Y. 1997, 'A study on bond mechanism of carbon fiber sheet', *Non-Metallic (FRP) Reinforcement for Concrete Structures, Proceedings of the Third Symposium*, vol. 1, pp. 279-286.

Mahini, S.S. & Ronagh, H.R. 2010, 'Strength and ductility of FRP web-bonded RC beams for the assessment of retrofitted beam–column joints', *Composite Structures*, vol. 92, no. 6, pp. 1325-1332.

Mazzotti, C., Ferracuti, B. & Savoia, M. 2004, 'An experimental study on FRP–concrete delamination', *Proc. FraMCoS, Vail USA*, vol. 2, pp. 795-802.

Mazzotti, C., Savoia, M. & Ferracuti, B. 2008, 'An experimental study on delamination of FRP plates bonded to concrete', *Construction and Building Materials*, vol. 22, no. 7, pp. 1409-1421.

Mazzotti, C., Savoia, M. & Ferracuti, B. 2009, 'A new single-shear set-up for stable debonding of FRP–concrete joints', *Construction and Building Materials*, vol. 23, no. 4, pp. 1529-1537.

Myers, J., Murthy, S. & Micelli, F. 2001, 'Effect of combined environmental cycles on the bond of FRP sheets to concrete'.

Nakaba, K., Kanakubo, T., Furuta, T. & Yoshizawa, H. 2001, 'Bond behavior between fiber-reinforced polymer laminates and concrete', *ACI structural journal*, vol. 98, no. 3.

Neubauer, U. & Rostasy, F. 1997, 'Design aspects of concrete structures strengthened with externally bonded CFRP-plates', *Proceedings of the Seventh International Conference on Structural Faults and Repair, 8 July 1997. Volume 2: Concrete and Composites*.

Neville, A.M. 1963, *Properties Of Concrete, 4/E*, Pearson Education.

Norris, T., Saadatmanesh, H. & Ehsani, M.R. 1997, 'Shear and Flexural Strengthening of R/C Beams with Carbon Fiber Sheets', *Journal of Structural Engineering*, vol. 123, no. 7, pp. 903-911.

Ouyang, Z. & Wan, B. 2008a, 'Experimental and Numerical Study of Moisture Effects on the Bond Fracture Energy of FRP/Concrete Joints', *Journal of Reinforced Plastics and Composites*, vol. 27, no. 2, pp. 205-223.

Ouyang, Z. & Wan, B. 2008b, 'Modeling of Moisture Diffusion in FRP Strengthened Concrete Specimens', *Journal of Composites for Construction*, vol. 12, no. 4, pp. 425-434.

Park, R. & Paulay, T. 1975, *Reinforced concrete structures*, John Wiley & Sons Inc.

Pham, H.B. & Al-Mahaidi, R. 2007, 'Modelling of CFRP-concrete shear-lap tests', *Construction and Building Materials*, vol. 21, no. 4, pp. 727-735.

Phani, K.K. & Bose, N.R. 1987, 'Temperature dependence of hydrothermal ageing of CSM-laminate during water immersion', *Composites Science and Technology*, vol. 29, no. 2, pp. 79-87.

Picard, A., Massicotte, B. & Boucher, E. 1995, 'Strengthening of reinforced concrete beams with composite materials: theoretical study', *Composite Structures*, vol. 33, no. 2, pp. 63-75.

Popovics, S. 1973, 'A numerical approach to the complete stress-strain curve of concrete', *Cement and Concrete Research*, vol. 3, no. 5, pp. 583-599.

Qiao, P. & Chen, Y. 2008, 'Cohesive fracture simulation and failure modes of FRP–concrete bonded interfaces', *Theoretical and Applied Fracture Mechanics*, vol. 49, no. 2, pp. 213-225.

Quantrill, R., Hollaway, L. & Thorne, A. 1996, 'Experimental and analytical investigation of FRP strengthened beam response: Part I', *Magazine of Concrete Research*, vol. 48, no. 177.

Rasheed, H.A. & Pervaiz, S. 2003, 'Closed form equations for FRP flexural strengthening design of RC beams', *Composites Part B: Engineering*, vol. 34, no. 6, pp. 539-550.

Robert, M., Wang, P., Cousin, P. & Benmokrane, B. 2010, 'Temperature as an Accelerating Factor for Long-Term Durability Testing of FRPs: Should There Be Any Limitations?', *J. Compos. Constr.*, vol. 14, no. 4, p. 361.

Saadatmanesh, H. & Ehsani, M.R. 1991, 'RC Beams Strengthened with GFRP Plates. I: Experimental Study', *Journal of Structural Engineering*, vol. 117, no. 11, pp. 3417-3433.

Saadatmanesh, H. & Malek, A.M. 1998, 'Design Guidelines for Flexural Strengthening of RC Beams with FRP Plates', *Journal of Composites for Construction*, vol. 2, no. 4, pp. 158-164.

Sauder, C., Lamon, J. & Pailler, R. 2004, 'The tensile behavior of carbon fibers at high temperatures up to 2400 °C', *Carbon*, vol. 42, no. 4, pp. 715-725.

Sharifi, N. 2012, 'Investigation into the Ductile and Damping Behaviour of Concrete Incorporating Waste Tyre Rubber', ME thesis, University of Technology Sydney, Sydney, Australia.

Shrestha, R. 2009, 'Behaviour of RC Beam-Column Connections Retrofitted with FRP Strips', PhD thesis, University of Technology Sydney, Sydney, Australia.

Silva, M.A. & Biscaia, H.C. 2010, 'Effects of exposure to saline humidity on bond between GFRP and concrete', *Composite Structures*, vol. 93, no. 1, pp. 216-224.

Silva, M.A.G. & Biscaia, H. 2008, 'Degradation of bond between FRP and RC beams', *Composite Structures*, vol. 85, no. 2, pp. 164-174.

Su, K. 2012, 'Repair of Reinforced Concrete Beams with Fibre Reinforced Polymer (FRP)', Capstone thesis, University of Technology Sydney, Sydney, Australia.

Subramaniam, K.V., Ali-Ahmad, M. & Ghosn, M. 2008, 'Freeze–thaw degradation of FRP–concrete interface: Impact on cohesive fracture response', *Engineering Fracture Mechanics*, vol. 75, no. 13, pp. 3924-3940.

Subramaniam, K.V., Carloni, C. & Nobile, L. 2007, 'Width effect in the interface fracture during shear debonding of FRP sheets from concrete', *Engineering Fracture Mechanics*, vol. 74, no. 4, pp. 578-594.

Täljsten, B. 1996, 'Strengthening of concrete prisms using the plate-bonding technique', *International journal of fracture*, vol. 82, no. 3, pp. 253-266.

Täljsten, B. 1997, 'Defining anchor lengths of steel and CFRP plates bonded to concrete', *International Journal of adhesion and adhesives*, vol. 17, no. 4, pp. 319-327.

Tanaka, T. 1996, 'Shear resisting mechanism of reinforced concrete beams with CFS as shear reinforcement', *Graduation Thesis, Hokkaido University, Japan*.

Teng, J.G. 2002, *FRP-strengthened RC structures*, John Wiley & Sons Inc.

Toutanji, H.A. & Gómez, W. 1997, 'Durability characteristics of concrete beams externally bonded with FRP composite sheets', *Cement and Concrete Composites*, vol. 19, no. 4, pp. 351-358.

Tuakta, C. & Büyüköztürk, O. 2011a, 'Conceptual Model for Prediction of FRP-Concrete Bond Strength under Moisture Cycles', *Journal of Composites for Construction*, vol. 15, no. 5, pp. 743-756.

Tuakta, C. & Büyüköztürk, O. 2011b, 'Deterioration of FRP/concrete bond system under variable moisture conditions quantified by fracture mechanics', *Composites Part B: Engineering*, vol. 42, no. 2, pp. 145-154.

Ulaga, T. & Meier, U. 2001, 'Long-term Behaviour of CFRP-laminate-strengthened Concrete Beams at Elevated Temperatures', *Proceedings of the Fifth International Symposium on Fiber Reinforced Polymer Reinforcement for Reinforced Concrete Structures (FRPRCS-5)*, vol. 1, p. 147.

Woo, S.-K. & Lee, Y. 2010, 'Experimental study on interfacial behavior of CFRP-bonded concrete', *KSCE Journal of Civil Engineering*, vol. 14, no. 3, pp. 385-393.

Wu, Z., Yuan, H. & Niu, H. 2002, 'Stress transfer and fracture propagation in different kinds of adhesive joints', *Journal of engineering mechanics*, vol. 128, no. 5, pp. 562-573.

Yao, J., Teng, J.G. & Chen, J.F. 2005, 'Experimental study on FRP-to-concrete bonded joints', *Composites Part B: Engineering*, vol. 36, no. 2, pp. 99-113.

Yuan, H., Lu, X., Hui, D. & Feo, L. 2012, 'Studies on FRP-concrete interface with hardening and softening bond-slip law', *Composite Structures*, vol. 94, no. 12, pp. 3781-3792.

Yuan, H., Teng, J.G., Seracino, R., Wu, Z.S. & Yao, J. 2004, 'Full-range behavior of FRP-to-concrete bonded joints', *Engineering Structures*, vol. 26, no. 5, pp. 553-565.

Yuan, H., Wu, Z. & Yoshizawa, H. 2001, 'Theoretical solutions on interfacial stress transfer of externally bonded steel/composite laminates', *Structural Engineering Earthquake Engineering*, vol. 18, no. 1, pp. 27-40.

Yun, Y. & Wu, Y.-F. 2011, 'Durability of CFRP-concrete joints under freeze-thaw cycling', *Cold Regions Science and Technology*, vol. 65, no. 3, pp. 401-412.

Zhou, Y.-W., Wu, Y.-F. & Yun, Y. 2010, 'Analytical modeling of the bond–slip relationship at FRP-concrete interfaces for adhesively-bonded joints', *Composites Part B: Engineering*, vol. 41, no. 6, pp. 423-433.

APPENDICES

A. Appendix A: Material test results for long term performance of FRP-concrete bond

A.1 Concrete compressive strength

Table A.1 Compressive strength of concrete for CFRP cyclic temperature pull-out specimens

Series	Mean compressive strength (MPa)
Control	31.2
CT2	36.3
CT3	28.6
CT4	41.2

Table A.2 Compressive strength of concrete for GFRP cyclic temperature pull-out specimens

Series	Mean compressive strength (MPa)
Control	35.9
GT2	42.3
GT3	39.4
GT4	46.0

Table A.3 Compressive strength of concrete for CFRP cyclic wet-dry pull-out specimens

Series	Mean compressive strength (MPa)
Control	31.2
CH1	35.5
CH2	35.1
CH3	37.9
CH4	41.4

Table A.4 Compressive strength of concrete for GFRP cyclic wet-dry pull-out specimens

Series	Mean compressive strength (MPa)
Control	35.9
GH1	39.0
GH2	42.7
GH3	50.5
GH4	49.9

Table A.5 Compressive strength of concrete for CFRP outdoor environment pull-out specimens

Series	Mean compressive strength (MPa)
Control	31.2
CE1	38.9
CE2	43.3
CE4	41.1
Fabricated from concrete batch two	
Control	35.9
CE3	59.7

Table A.6 Compressive strength of concrete for GFRP outdoor environment pull-out specimens

Series	Mean compressive strength (MPa)
Control	35.9
GE1	44.2
GE2	48.4
GE3	54.9
GE4	57.1

A.2 Tensile stress-strain curves of FRP coupons

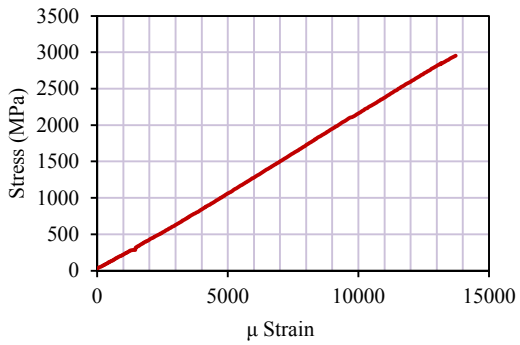

(a) CTControl-6

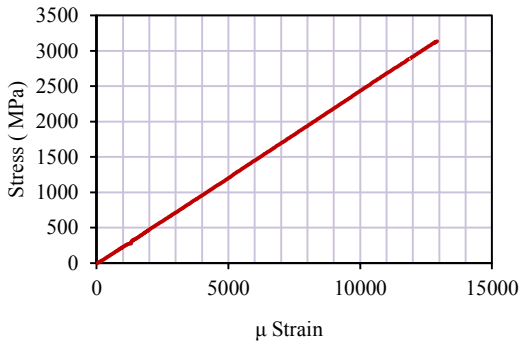

(b) CTControl-7

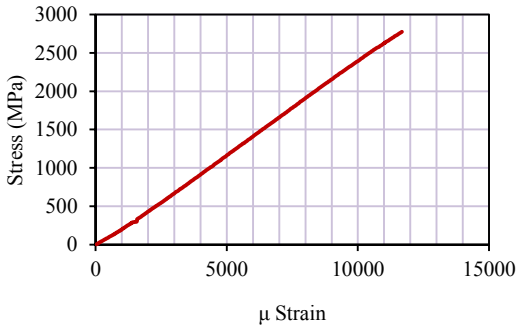

(c) CTControl-8

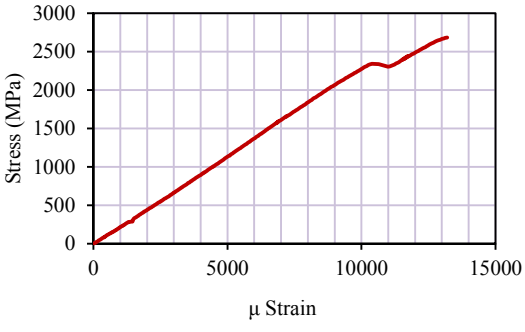

(d) CTControl-9

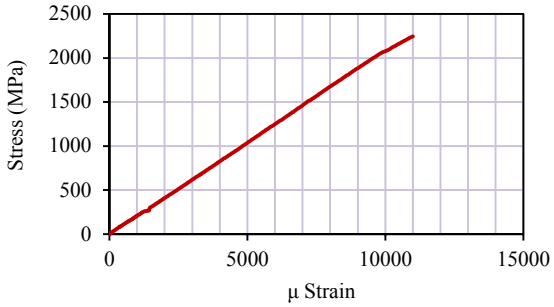

(e) CTControl-10

Figure A.1 Stress-strain curves of CFRP control coupons

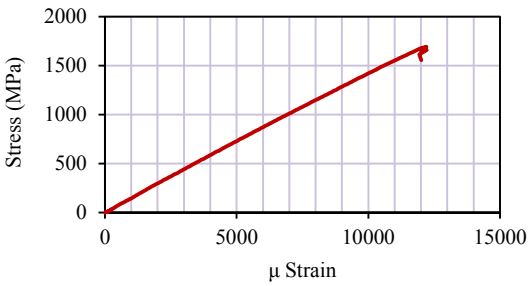

(a) GTControl-1

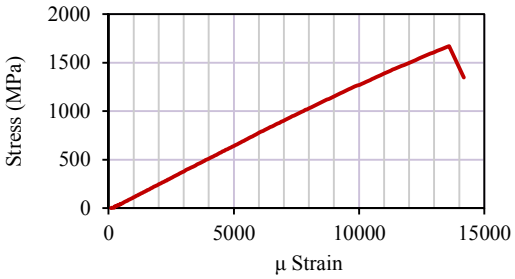

(b) GTControl-2

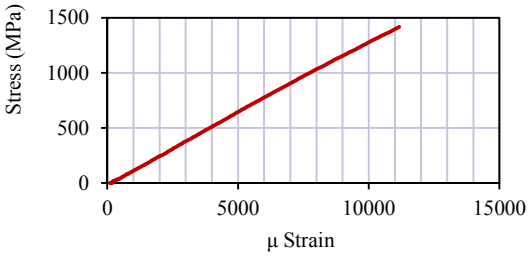

(c) GTControl-3

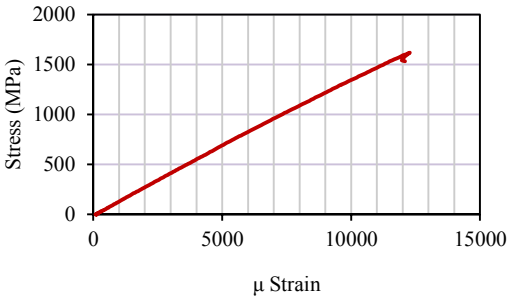

Figure A.2 Stress-strain curves of GFRP control coupons

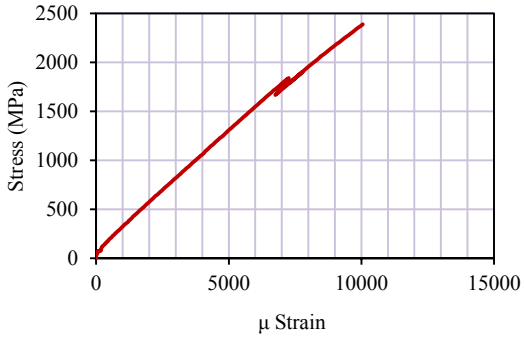

(a) CTT2-6

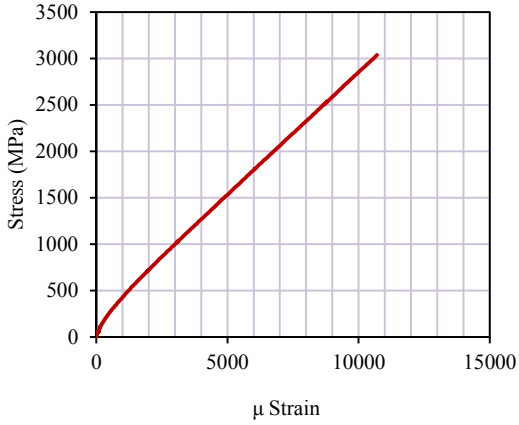

(b) CTT2-7

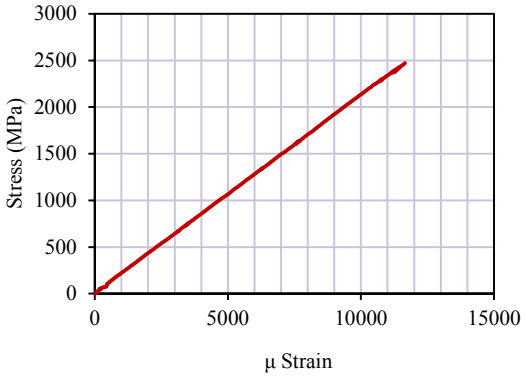

(c) CTT2-8

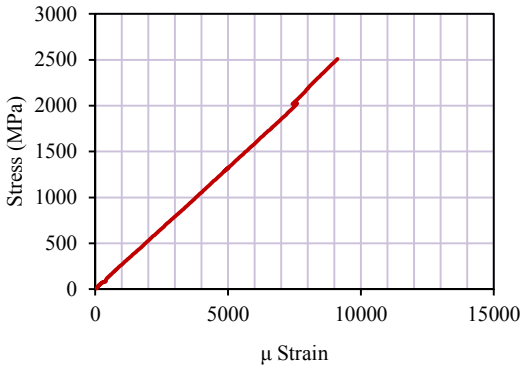

(d) CTT2-9

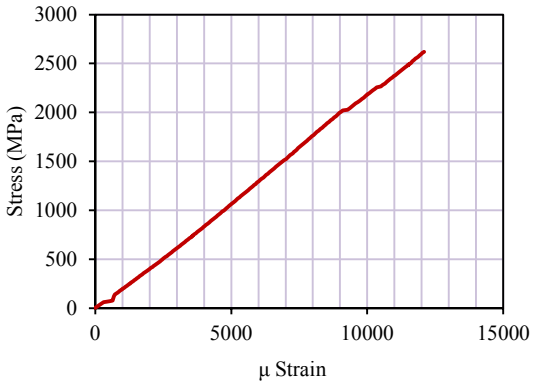

(e) CTT2-10

Figure A.3 Stress-strain curves of CFRP five week cyclic temperature coupons

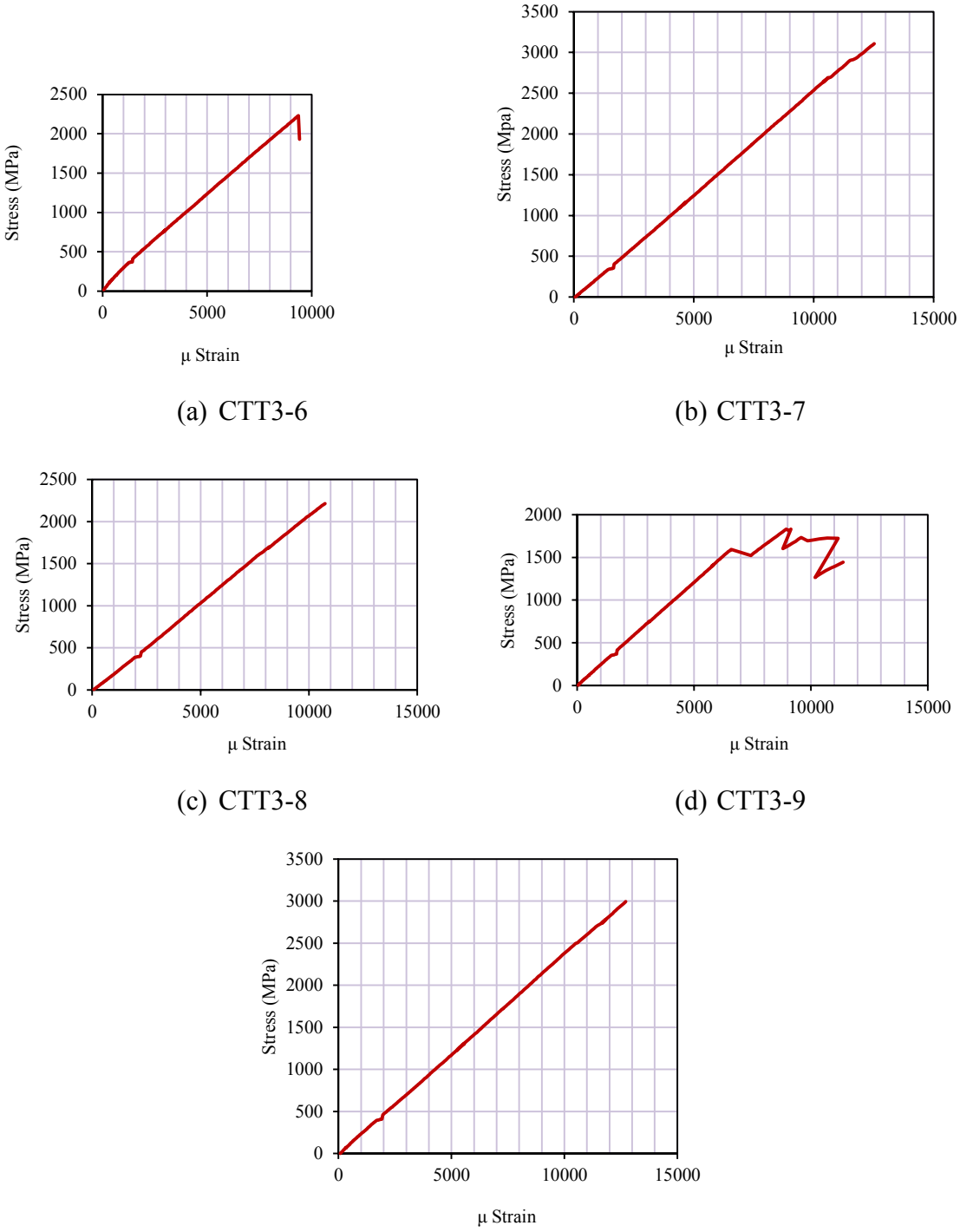

Figure A.4 Stress-strain curves of CFRP three month cyclic temperature coupons

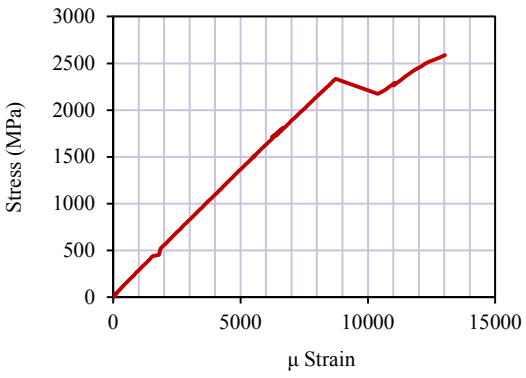

(a) CTT4-6

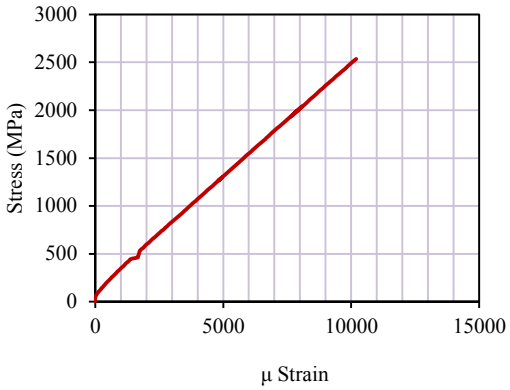

(b) CTT4-7

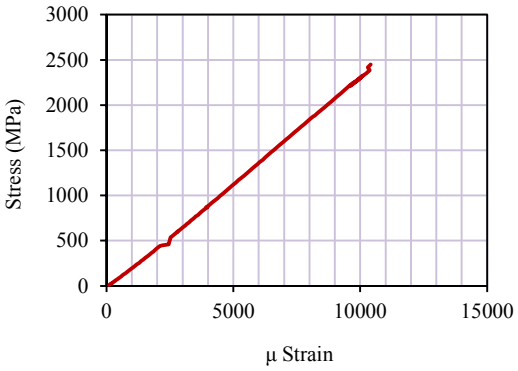

(c) CTT4-9

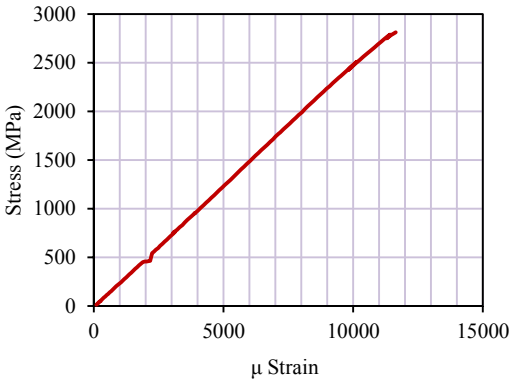

(d) CTT4-10

Figure A.5 Stress-strain curves of CFRP one year cyclic temperature coupons

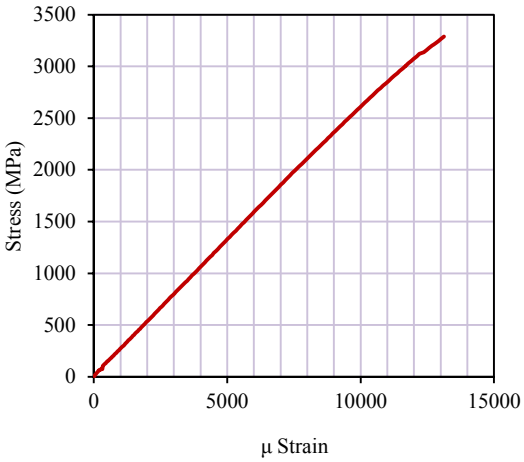

(a) CTH1-6

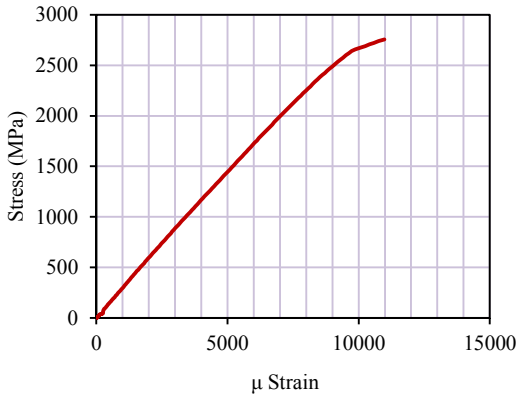

(b) CTH1-7

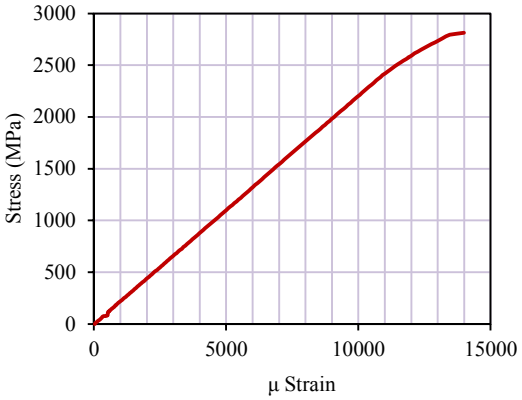

(c) CTH1-8

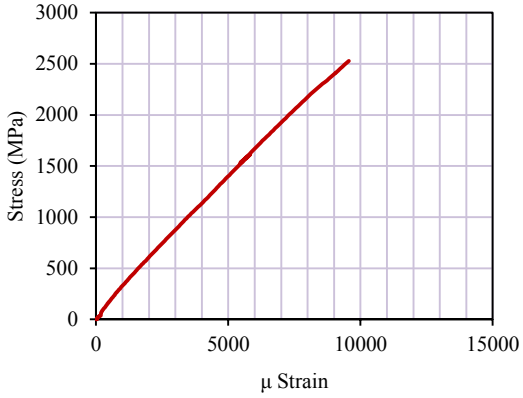

(d) CTH1-9

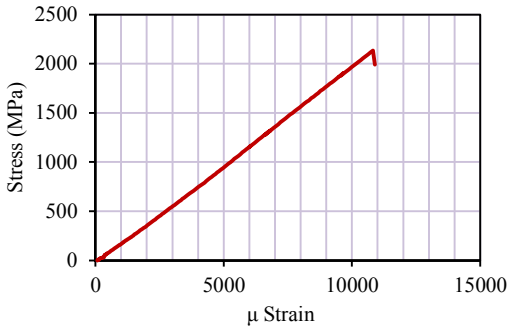

(e) CTH1-10

Figure A.6 Stress-strain curves of CFRP one month cyclic wet-dry coupons

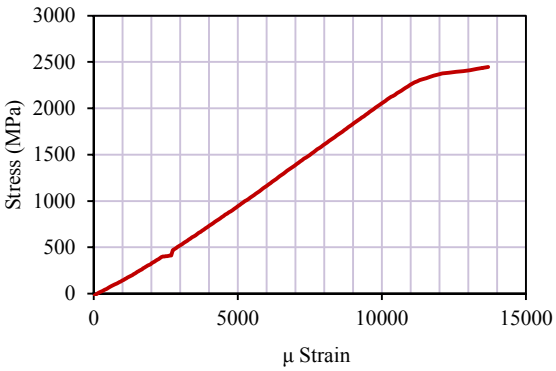

(a) CTH2-6

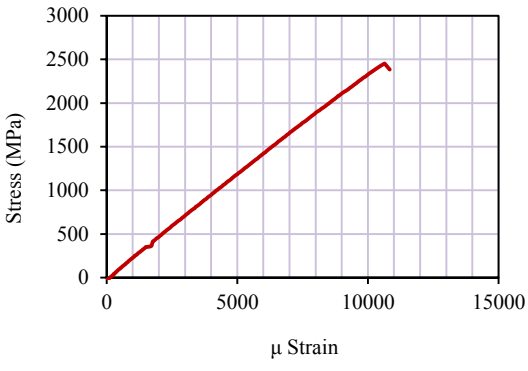

(b) CTH2-7

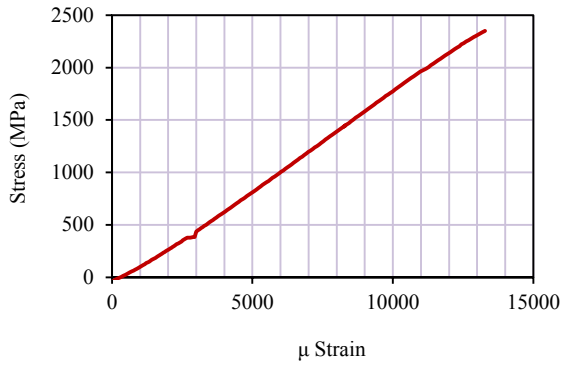

(c) CTH2-9

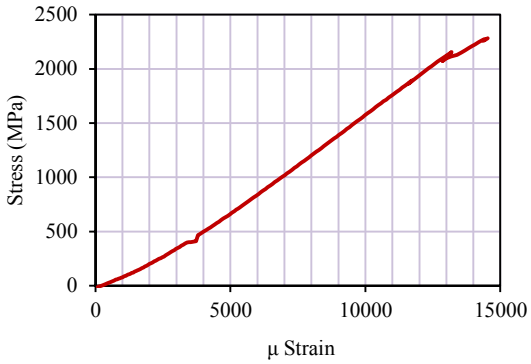

(d) CTH2-10

Figure A.7 Stress-strain curves of CFRP six month cyclic wet-dry coupons

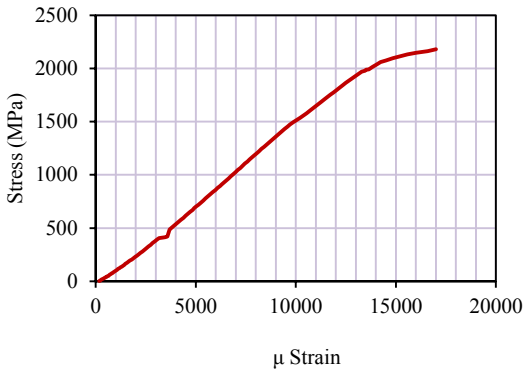

(a) CTH3-6

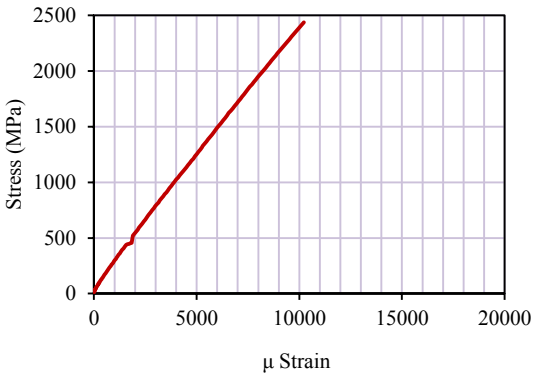

(b) CTH3-7

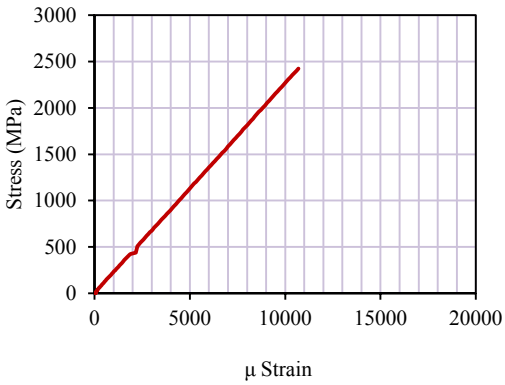

(c) CTH3-8

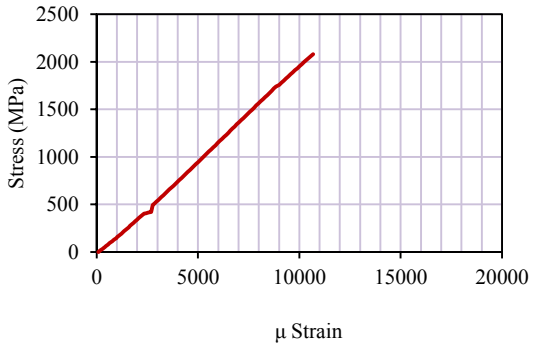

(d) CTH3-9

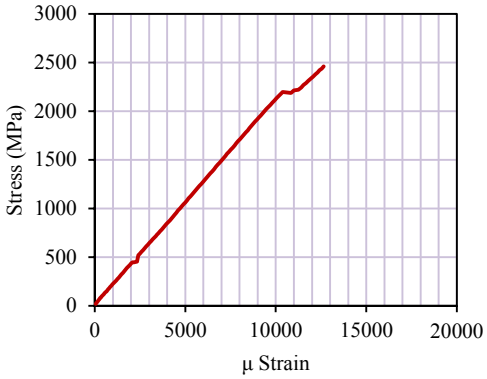

CTH3-10

Figure A.8 Stress-strain curves of CFRP one year cyclic wet-dry coupons

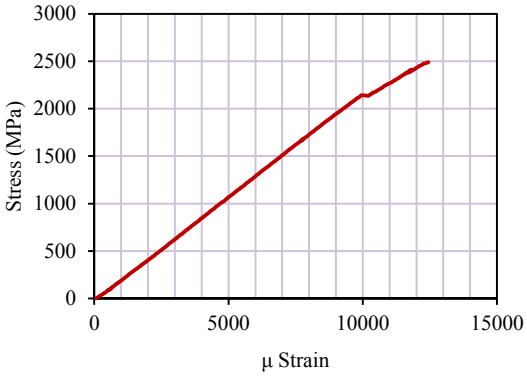

(a) CTH4-6

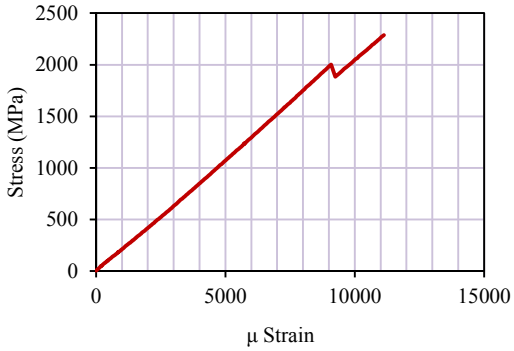

(b) CTH4-7

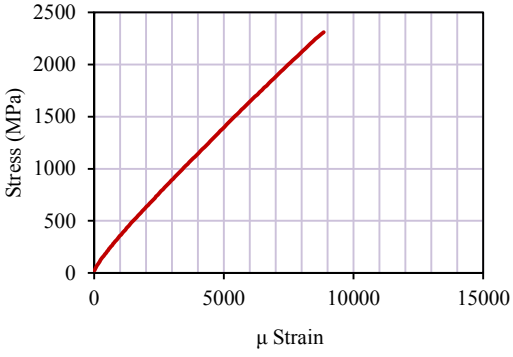

(c) CTH4-8

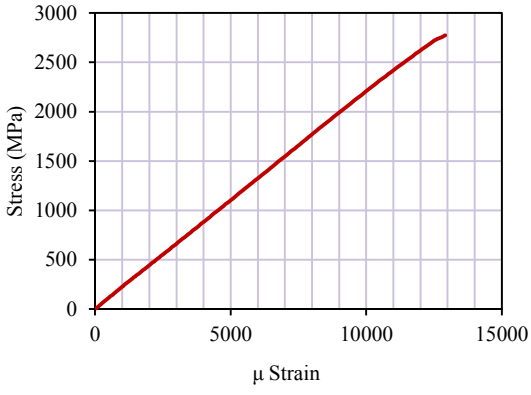

(d) CTH4-9

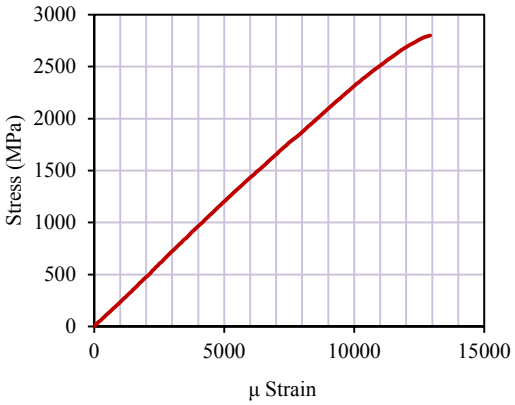

(e) CTH4-10

Figure A.9 Stress-strain curves of CFRP 18 month cyclic wet-dry coupons

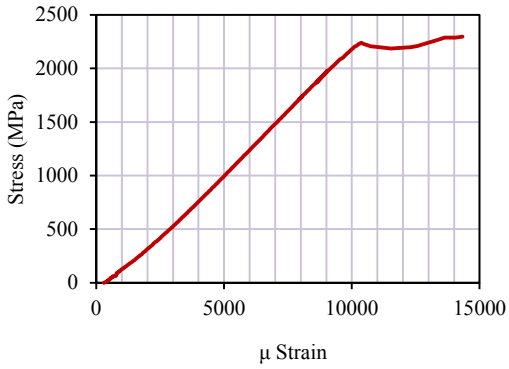

(a) CTE1-6

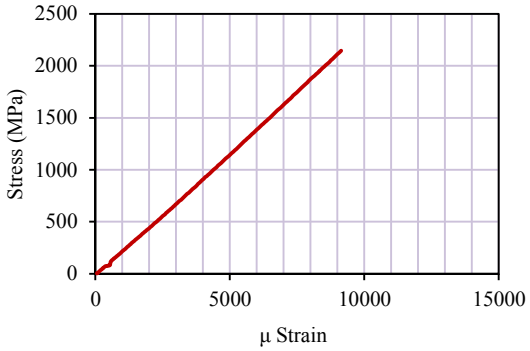

(b) CTE1-7

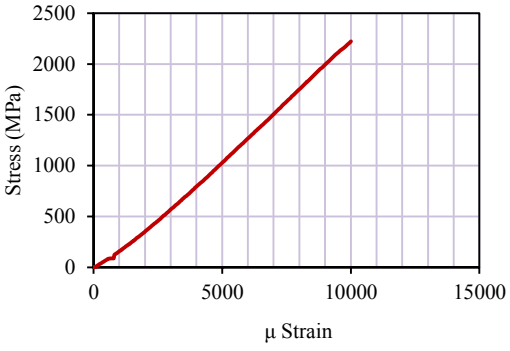

(c) CTE1-8

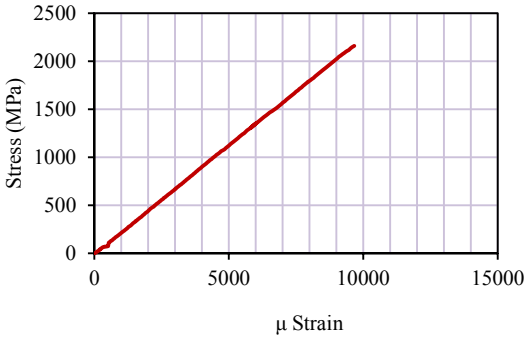

(d) CTE1-9

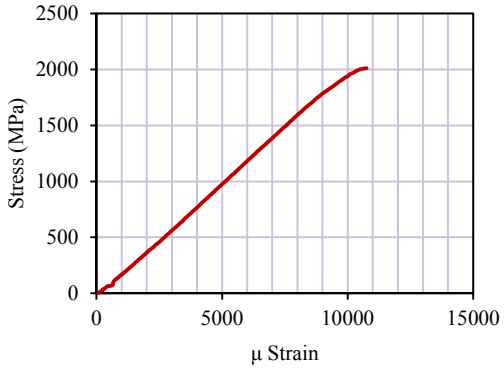

(e) CTE1-10

Figure A.10 Stress-strain curves of CFRP two month outdoor environment coupons

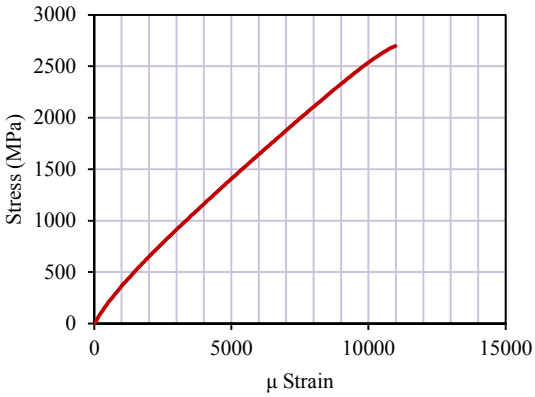

(a) CTE2-6

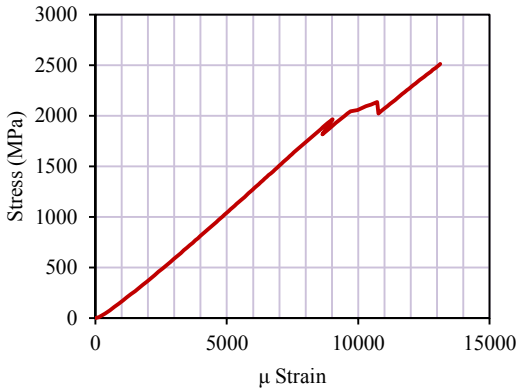

(b) CTE2-7

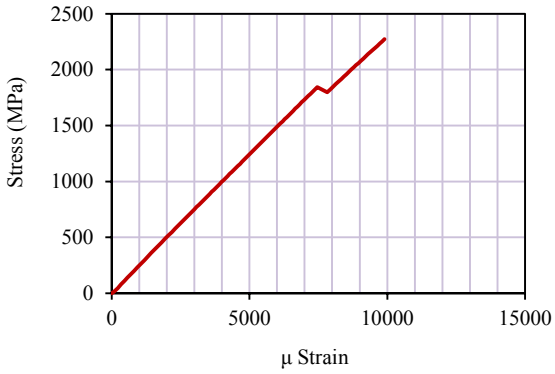

(c) CTE2-8

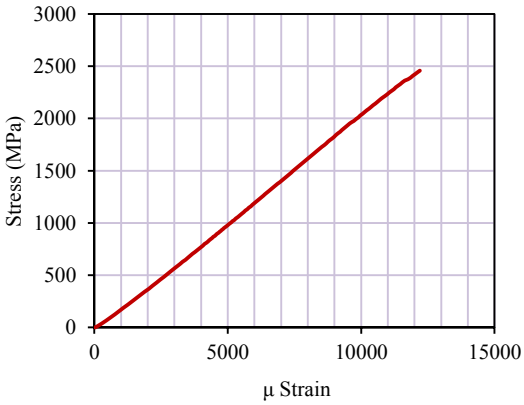

(d) CTE2-9

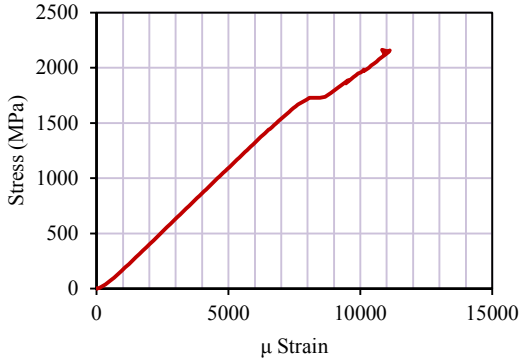

(e) CTE2-10

Figure A.11 Stress-strain curves of CFRP six month outdoor environment coupons

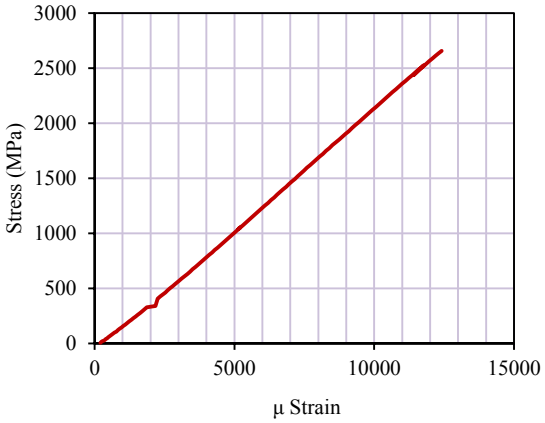

(a) CTE3-6

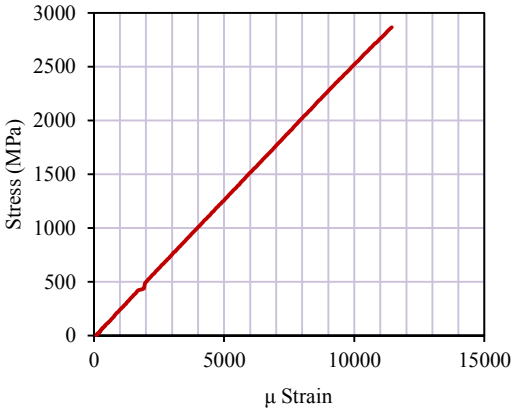

(b) CTE3-7

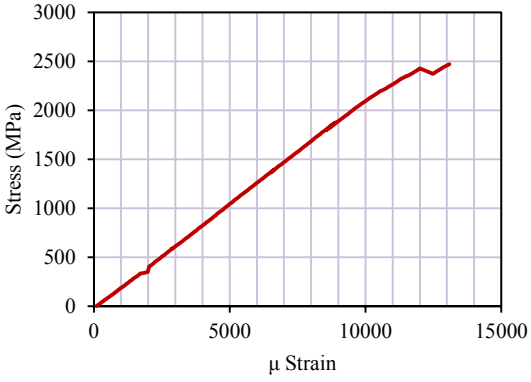

(c) CTE3-8

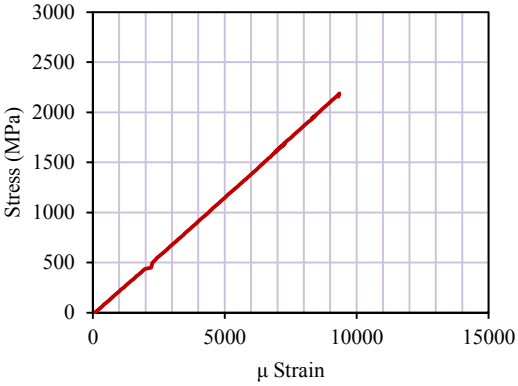

(d) CTE3-9

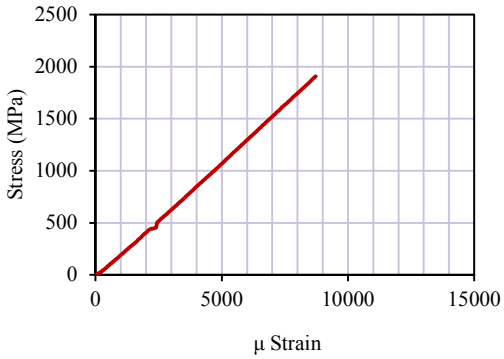

(e) CTE3-10

Figure A.12 Stress-strain curves of CFRP one year outdoor environment coupons

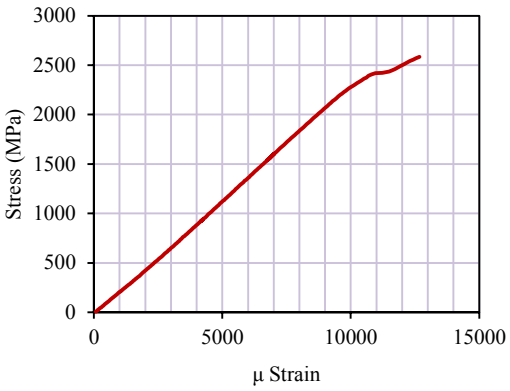

(a) CTE4-6

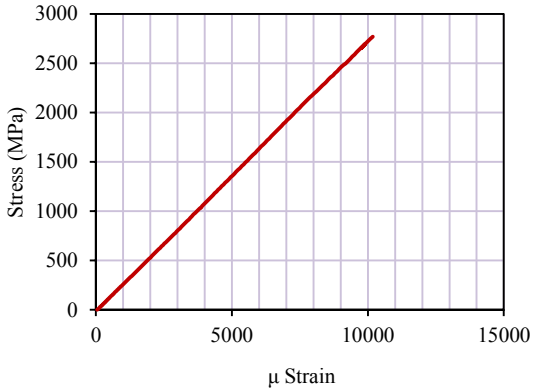

(b) CTE4-7

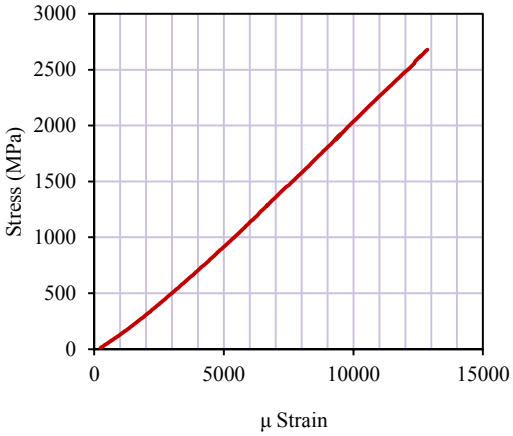

(c) CTE4-8

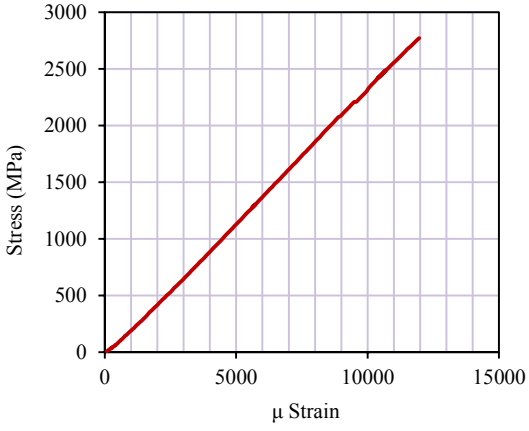

(d) CTE4-9

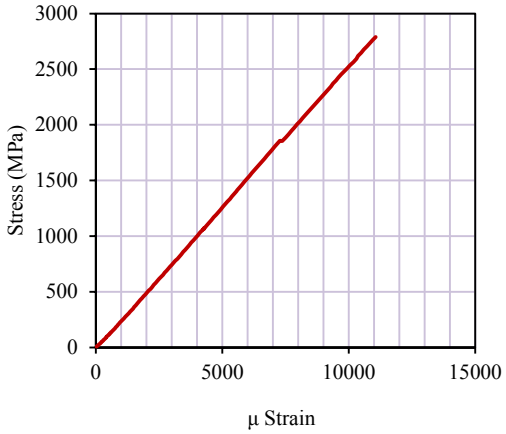

(e) CTE4-10

Figure A.13 Stress-strain curves of CFRP 18 month outdoor environment coupons

A.3 Tensile strength and modulus of elasticity (MOE) of FRP

Table A.7 Tensile properties of CFRP five week cyclic temperature coupons

Specimen ID	Tensile strength (MPa)	Mean (MPa)	CoV (%)	Tensile MOE (MPa)	Mean (GPa)	CoV (%)
CTT2-6	2389.0	2613.6	9.6	247.2	242.8	13.8
CTT2-7	3035.8			286.5		
CTT2-8	2470.1			209.9		
CTT2-9	2554.8			261.4		
CTT2-10	2618.2			209.0		

Table A.8 Tensile properties of CFRP three month cyclic temperature coupons

Specimen ID	Tensile strength (MPa)	Mean (MPa)	CoV (%)	Tensile MOE (MPa)	Mean (GPa)	CoV (%)
CTT3-6	2230.2	2474.8	22.2	238.3	234.4	7.2
CTT3-7	3105.2			251.8		
CTT3-8	2213.3			207.5		
CTT3-9	1831.2			243.4		
CTT3-10	2993.9			231.0		

Table A.9 Tensile properties of CFRP one year cyclic temperature coupons

Specimen ID	Tensile strength (MPa)	Mean (MPa)	CoV (%)	Tensile MOE (MPa)	Mean (GPa)	CoV (%)
CTT4-6	2589.1	2595.9	6.0	270.4	246.6	7.5
CTT4-7	2535.2			242.3		
CTT4-8	-			-		
CTT4-9	2447.8			225.9		
CTT4-10	2811.6			247.6		

Table A.10 Tensile properties of CFRP one month cyclic wet-dry coupons

Specimen ID	Tensile strength (MPa)	Mean (MPa)	CoV (%)	Tensile MOE (MPa)	Mean (GPa)	CoV (%)
CTH1-6	3288.2	2703.9	15.6	263.6	248.5	17.0
CTH1-7	2754.7			295.1		
CTH1-8	2812.5			220.2		
CTH1-9	2528.6			273.3		
CTH1-10	2135.5			190.5		

Table A.11 Tensile properties of CFRP six month cyclic wet-dry coupons

Specimen ID	Tensile strength (MPa)	Mean (MPa)	CoV (%)	Tensile MOE (MPa)	Mean (GPa)	CoV (%)
CTH2-6	2447.8	2383.9	18.3	189.2	191.9	16.3
CTH2-7	2452.9			240.9		
CTH2-8	-			-		
CTH2-9	2350.9			183.1		
CTH2-10	2284.1			154.2		

Table A.12 Tensile properties of CFRP one year cyclic wet-dry coupons

Specimen ID	Tensile strength (MPa)	Mean (MPa)	CoV (%)	Tensile MOE (MPa)	Mean (GPa)	CoV (%)
CTH3-6	2180.7	2316.5	7.5	140.7	191.3	25.8
CTH3-7	2436.4			245.4		
CTH3-8	2423.8			223.9		
CTH3-9	2080.8			137.5		
CTH3-10	2460.8			209.2		

Table A.13 Tensile properties of CFRP 18 month cyclic wet-dry coupons

Specimen ID	Tensile strength (MPa)	Mean (MPa)	CoV (%)	Tensile MOE (MPa)	Mean (GPa)	CoV (%)
CTH4-6	2489.7	2629.0	8.8	216.2	231.0	10.6
CTH4-7	2288.4			209.5		
CTH4-8	2795.0			267.4		
CTH4-9	2773.4			217		
CTH4-10	2798.4			244.8		

Table A.14 Tensile properties of CFRP two month outdoor environment coupons

Specimen ID	Tensile strength (MPa)	Mean (MPa)	CoV (%)	Tensile MOE (MPa)	Mean (GPa)	CoV (%)
CTE1-6	2295.0	2301.4	13.1	198.6	211.4	7.3
CTE1-7	2144.4			228.0		
CTE1-8	2222.3			205.8		
CTE1-9	2810.8			227.8		
CTE1-10	2034.4			196.6		

Table A.15 Tensile properties of CFRP six month outdoor environment coupons

Specimen ID	Tensile strength (MPa)	Mean (MPa)	CoV (%)	Tensile MOE (MPa)	Mean (GPa)	CoV (%)
CTE2-6	2697.6	2420.5	8.6	273.7	232.4	13.1
CTE2-7	2511.7			211.0		
CTE2-8	2271.9			250.1		
CTE2-9	2458.0			197.2		
CTE2-10	2163.2			230.1		

Table A.16 Tensile properties of CFRP one year outdoor environment coupons

Specimen ID	Tensile strength (MPa)	Mean (MPa)	CoV (%)	Tensile MOE (MPa)	Mean (GPa)	CoV (%)
CTE3-6	2658.3	2472.3	12.1	206.0	224.7	9.0
CTE3-7	2866.0			256.7		
CTE3-8	2470.0			212.1		
CTE3-9	2188.8			231.1		
CTE3-10	2178.2			217.8		

Table A.17 Tensile properties of CFRP 18 month outdoor environment coupons

Specimen ID	Tensile strength (MPa)	Mean (MPa)	CoV (%)	Tensile MOE (MPa)	Mean (GPa)	CoV (%)
CTE4-6	2584.5	2737.2	3.1	222.4	236.5	11.1
CTE4-7	2769.7			272.4		
CTE4-8	2769.7			206.4		
CTE4-9	2772.9			227.5		
CTE4-10	2789.0			254		

A.4 FRP failure modes

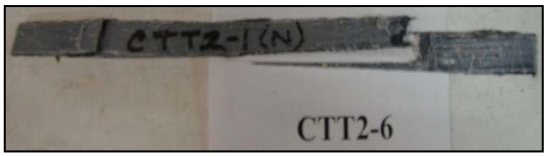

(a) CTT2-6

(b) CTT2-7

(c) CTT2-8

(d) CTT2-9

(e) CTT2-10

Figure A.14 Failed coupons of CFRP five week cyclic temperature series

(a) CTT3-6

(b) CTT3-7

(c) CTT3-8

(d) CTT3-9

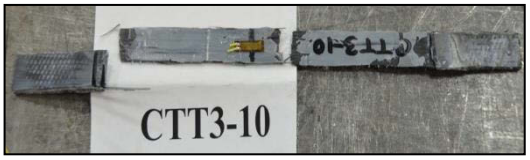

(e) CTT3-10

Figure A.15 Failed coupons of CFRP three month cyclic temperature series

(a) CTT4-6

(b) CTT4-7

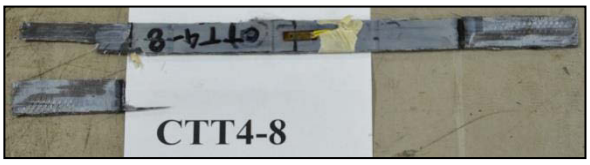

(c) CTT4-8

(d) CTT4-9

(e) CTT4-10

Figure A.16 Failed coupons of CFRP one year cyclic temperature series

(a) CTH1-7

(b) CTH1-8

(c) CTH1-9

(d) CTH1-10

Figure A.17 Failed coupons of CFRP one month cyclic wet-dry series

(a) CTH2-6

(b) CTH2-7

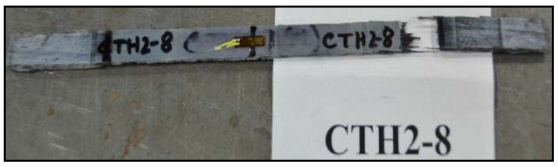

(c) CTH2-8

(d) CTH2-9

(e) CTH2-10

Figure A.18 Failed coupons of CFRP six month cyclic wet-dry series

(a) CTH3-6

(b) CTH3-7

(c) CTH3-8

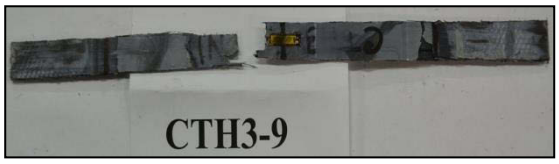

(d) CTH3-9

(e) CTH3-10

Figure A.19 Failed coupons of CFRP one year cyclic wet-dry series

(a) CTH4-6

(b) CTH4-7

(c) CTH4-8

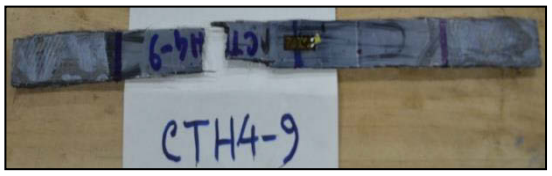

(d) CTH4-9

(e) CTH4-10

Figure A.20 Failed coupons of CFRP 18 month cyclic wet-dry series

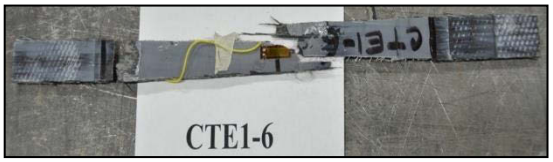

(a) CTE1-6

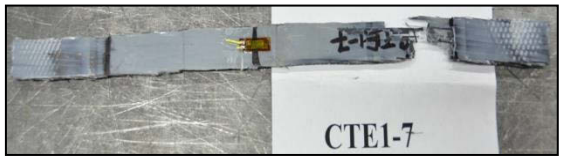

(b) CTE1-7

(c) CTE1-8

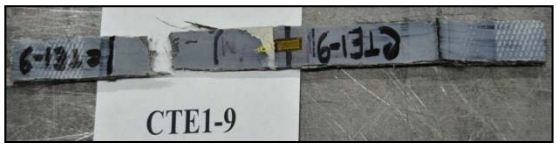

(d) CTE1-9

(e) CTE1-10

Figure A.21 Failed coupons of CFRP two month outdoor environment series

(a) CTE2-7

(b) CTE2-8

(c) CTE2-9

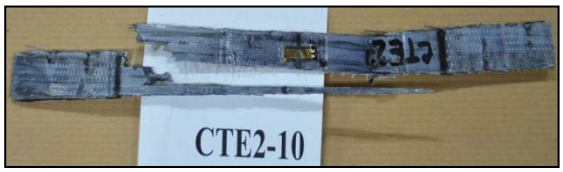

(d) CTE2-10

Figure A.22 Failed coupons of CFRP six month outdoor environment series

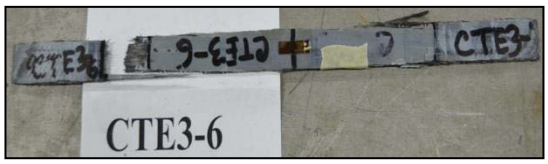

(a) CTE3-6

(b) CTE3-7

(c) CTE3-8

(d) CTE3-9

(e) CTE3-10

Figure A.23 Failed coupons of CFRP one year outdoor environment series

(a) CTE4-6

(b) CTE4-7

(c) CTE4-8

(d) CTE4-9

(e) CTE4-10

Figure A.24 Failed coupons of CFRP 18 month outdoor environment series

A.5 Material data sheets for FRP

BASF
The Chemical Company

MBRACE ™ FIBER

Carbon, aramid and glass fibre sheeting used for structural strengthening

Description of Product
MBRACE FIBRE sheet reinforcement materials are envelopd in MBRACE SATURANT resin to yeild a range of high performance composites with many features.

The MBRACE FIBRE reinforcement systems include:

- MBRACE CF 130,120 & Sheet 140 similar) and MBRACE CF 530 uni-directional tow sheet carbon fibres.
- MBRACE AF129 & AF 142 uni-directional aramid fibres.
- MBRACE EG & ARG (50/50 & 90/10 A&B) bi-directional glass fibres.

Each type of fibre used within the finished MBRACE Fibre Reinforced Polyer (FRP) System permits high strength to cross section ratio and structural integrity as an alternative to bonding steel plates to concrete, masonry, timber and steel surfaces.

Fields of Application

- Walls, beams and slabs
- Columns and chimneys
- Silos and tanks
- Pipes and tunnels

Features and Benefits
MBRACE Fibres (in general)

- Light weight
- Durable
- Control of crack propagation
- High strength to thickness ratio
- Colours
  - Carbon Fibre – Black
  - Aramid Fibre – Yellow
  - Glass Fibre - White

MBRACE Carbon Fibre

- Increased strength particularly for
  - Flexure
  - Shear
  - Confinement
  - Fatigue enhancement
  - End anchoring of MBRACE LAMINATES

MBRACE Aramid fibre

- Increased strength particularly for
  - Impact resistance
  - Blast (explosion) resistance

MBRACE Glass Fibre

- Seismic (Earthquake) Retrofitting
- Retrofit of masonry structures or low strength substrates
- "AR" type for alkali resistant requirements

Typical Physical Properties
MBRACE CF 530 (Carbon Fibre (CF) Reinforcement – (High Modulus CF)

Fibre Reinforcement:	Carbon – High modulus
Fibre density:	2.1gm/cm^3
Fibre modulus:	640 GPa
Fibre weight (CF):	400gm/m^2
Thickness(1):	0.19mm
Tensile strength(2):	2,650 MPa
Tensile elongation, ultimate	0.4%
Design tensile force(3): at 0.2% strain/m width:	200 kN
Roll length:	50m
Sheet width:	300mm

MBRACE CF 120,130 & 140
MBRACE CF 120 and CF 140
Carbon Fibre (CF) Reinforcement – (High tensile CF)

Fibre Reinforcement:	Carbon – High tensile
Fibre density:	1.7gm/cm^3
Fibre modulus:	240 GPa
Fibre weight (CF):	
CF 120	200gm/m^2
CF 130	300gm/m^2
CF 140	400gm/m^2

BASF
The Chemical Company

MBRACE ™ FIBER

Thickness[1]:	
CF 120	0.117mm
CF 130	0.176mm
CF 140	0.235mm
Tensile strength[2]:	3,800 MPa
Tensile elongation, ultimate	1.55%
Design tensile force[3]: at 0.6% strain/m width:	140, 211, 280 kN
Roll length:	150m
Sheet width:	300mm

MBRACE AF129 & AF 142 Aramid Fibre (AF) Reinforcement System

Fibre Reinforcement:	Aramid
Fibre density:	1.45gm/cm^3
Fibre modulus:	120 GPa
Fibre weight:	
AF 129	290gm/m^2
AF 142	420gm/m^2
Thickness[1]:	
AF 129	0.200mm
AF 142	0.290mm
Tensile strength[2]:	2,900 MPa
Tensile elongation, ultimate	2.5%
Tensile force[3]: at ult. strain/m width (in kN):	AF 129:446 kN AF 142:647 kN
Roll length:	150m
Sheet width:	300mm

MBRAC EG & ARG (50/50 & 90/10 A&B) E-Glass (EG) & AR-Glass (ARG) Reinforcement

Fibre Reinforcement:	E-Glass or (AR-Glass)
Fibre density:	2.6 (2.68) gm/cm^3
Fibre modulus:	73 (65) GPa
Fibre weight:	
EG & ARG 50/50	(both directions) 175 gm/cm^2
EG & ARG 90/10A	(main directions) 400gm/cm^2
EG & ARG 90/10B	(main directions) 800gm/cm^2
Thickness[1]:	
EG & ARG 50/50	0.067 (0.065) mm
EG & ARG 90/10A	0.154 (0.149) mm
EG & ARG 90/10B	0.308 (0.299) mm
Tensile strength fibre[2]:	3,400 (3,000) MPa
Tensile strength impregnated fibre[4]:	2,400 (1,700) MPa
Tensile elongation, ultimate	4.5 (4.3)%
EG & ARG 90/10B	(main directions) 528 (362)
Roll length:	50m
Sheet width:	670mm
Tensile force[3]: at ult. strain/m width (in kN):	AF 129:446 kN AF 142:647 kN
EG & ARG 50/50	(both directions) 115 (79)
EG & ARG 90/10A	(main directions) 264 (181)

Notes:

[1] Design thickness (mm/ply) is based on the total thickness of fibres (only)in a unit width. It is calculated by dividing the fibre weight by the density. From experience, the actual cured thickness of sheet on averae is 0.6 to 1.0mm/ply.

[2] Fibre tensile strengths (MPa) and tensile modulus (Gpa) are derived from the strength or modulus per sheet width divided by the design thickness.

Figure A.25 Material data sheet for MBRACE carbon and glass fibre

Construction

Technical Data Sheet
Version: 20/01/2010

Sikadur®-330

2-part epoxy impregnation resin

Product Description	Sikadur®-330 is a two part, thixotropic epoxy based impregnating resin / adhesive.
Uses	■ Impregnation resin for SikaWrap® fabric reinforcement for the dry application method ■ Primer resin for the wet application system ■ Structural adhesive for bonding Sika® CarboDur® plates to even surfaces
Characteristics / Advantages	■ Easy mix and application by trowel and impregnation roller ■ Manufactured for manual saturation methods ■ Excellent application behaviour to vertical and overhead surfaces ■ Good adhesion to many substrates ■ High mechanical properties ■ No separate primer required

Tests

Approval / Standards	Conforms to the requirements of: - SOCOTEC (France): Cahier des charges Sika® CarboDur, SikaWrap®. - Road and Bridges Research Institute (Poland): IBDiM No AT/2003-04-336. Testing according to EN 1504-4

Product Data

Form

Appearance / Colours	Resin part. A: Hardener part B:	paste paste
	Colour: Part A: Part B: Part A+B mixed:	 white grey light grey
Packaging	Standard: 5 kg (A+B) pre-dosed units	

Storage

Storage Conditions / Shelf life	24 months from date of production if stored properly in original unopened, sealed and undamaged packaging in dry conditions at temperatures between +5°C and +25°C. Protect from direct sunlight.

Technical Data

Chemical Base	Epoxy resin.
Density	1.30 kg/l ± 0.1 kg/l (parts A+B mixed) (at +23°C)
Viscosity	Shear rate: 50 /s

Temperature	Viscosity
+10°C	~ 10'000 mPas
+23°C	~ 6'000 mPas
+35°C	~ 5'000 mPas

Thermal Expansion Coefficient	4.5 x 10^{-5} per °C (-10°C to +40°C)
Thermal Stability	Heat Distortion Temperature (HDT) (ASTM D648)

Curing	Temperature	HDT
7 days	+10°C	+36°C
7 days	+23°C	+47°C
7 days	+35°C	+53°C
7 days, +10°C plus 7 days, +23°C	-	+43°C

Service Temperature	-40°C to +45°C

Mechanical / Physical Properties

Tensile Strength	30 N/mm^2 (7 days at +23°C)	(DIN 53455)
Bond Strength	Concrete fracture (> 4 N/mm^2) on sandblasted substrate: > 1 day	(EN 24624)
E-Modulus	Flexural: 3800 N/mm^2 (7 days at +23°C)	(DIN 53452)
	Tensile: 4500 N/mm^2 (7 days at +23°C)	(DIN 53455)
Elongation at Break	0.9% (7 days at +23°C)	(DIN 53455)

Resistance

Chemical Resistance	The product is not suitable for chemical exposure.
Thermal Resistance	Continuous exposure +45°C.

System Information

System Structure	Substrate primer - Sikadur®-330. Impregnating / laminating resin - Sikadur®-330. Structural strengthening fabric - SikaWrap® type to suit requirements.

Figure A.26 Material data sheet for Sikadur 330 epoxy resin

B. Appendix B: Pull-out test results

B.1 Failure modes of CFRP pull-out specimens

(a) CT2-2

(b) CT4-2

Figure B.1 Failure modes of CFRP cyclic temperature pull-out specimens

(a) CH1-3

(b) CH1-4

(c) CH2-4

(d) CH2-5

(e) CH3-1

(f) CH3-3

(g) CH4-3

(h) CH4-5

Figure B.2 Failure modes of CFRP cyclic wet-dry pull-out specimens

(a) CE1-2

(b) CE1-3

(c) CE1-4

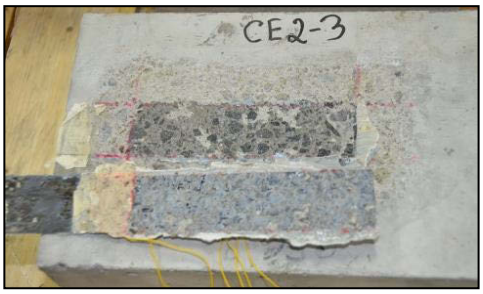

(d) CE2-3

(e) CE2-4

(f) CE3-2

(g) CE3-3

(h) CE3-4

(i) CE3-5

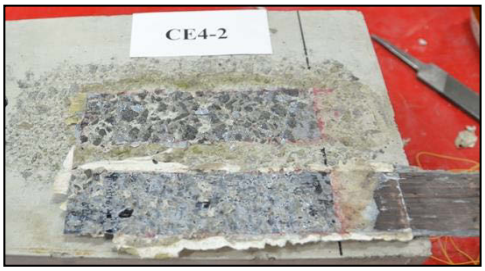

(j) CE4-2

(k) CE4-5

Figure B.3 Failure modes of CFRP outdoor environment pull-out specimens

B.2 Failure modes of GFRP pull-out specimens

(a) GControl-2

(b) GControl-3

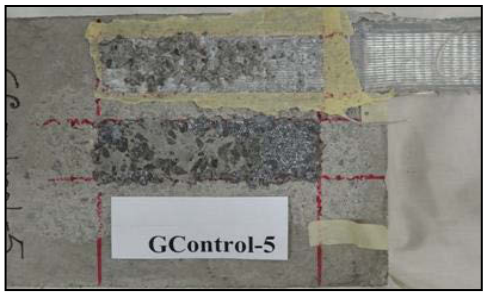

(c) GControl-5

Figure B.4 Failure modes of GFRP control pull-out specimens

(a) GT2-2

(b) GT3-3

(c) GT4-1

Figure B.5 Failure modes of GFRP cyclic temperature pull-out specimens

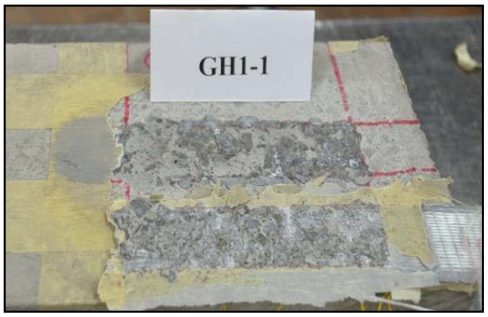

(a) GH1-1

(b) GH1-3

(c) GH1-4

(d) GH2-1

(e) GH2-2

(f) GH2-4

(g) GH3-1

(h) GH3-2

(i) GH3-5

(j) GH4-4

(k) GH4-5

Figure B.6 Failure modes of GFRP cyclic wet-dry pull-out specimens

(a) GE1-2

(b) GE1-3

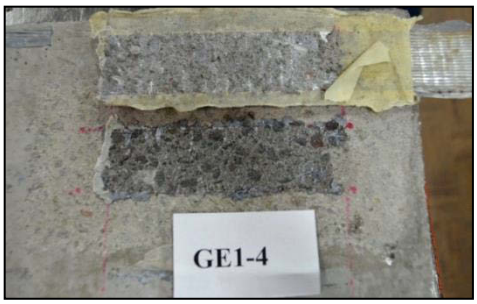

(c) GE1-4

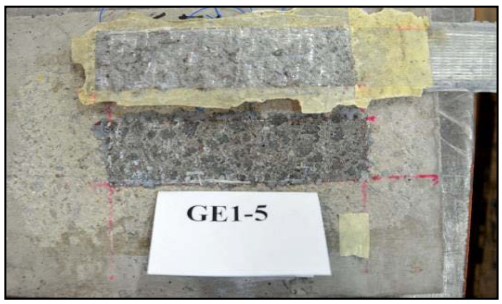

(d) GE1-5

(e) GE2-1

(f) GE2-2

(g) GE2-4

(h) GE2-5

(i) GE3-2

(j) GE3-3

(k) GE3-4

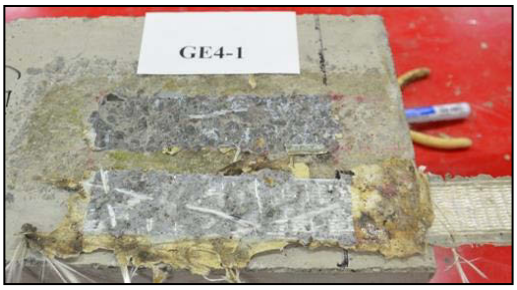

(l) GE4-1

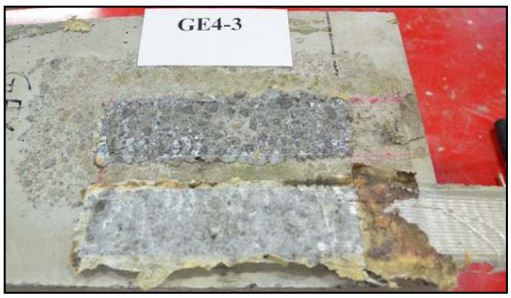

(m) GE4-3

(n) GE4-4

(o) GE4-5

Figure B.7 Failure modes of GFRP outdoor environment pull-out specimens

C. Appendix C: Fracture properties of CFRP-concrete bond

C.1 Shear stress-slip curve fitting for individual control specimens

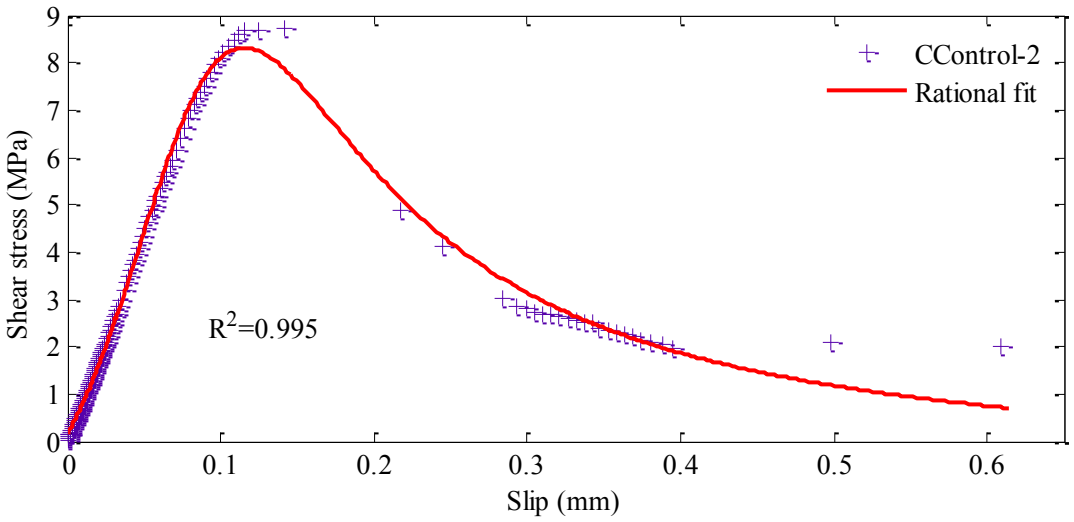

(a) CControl-2

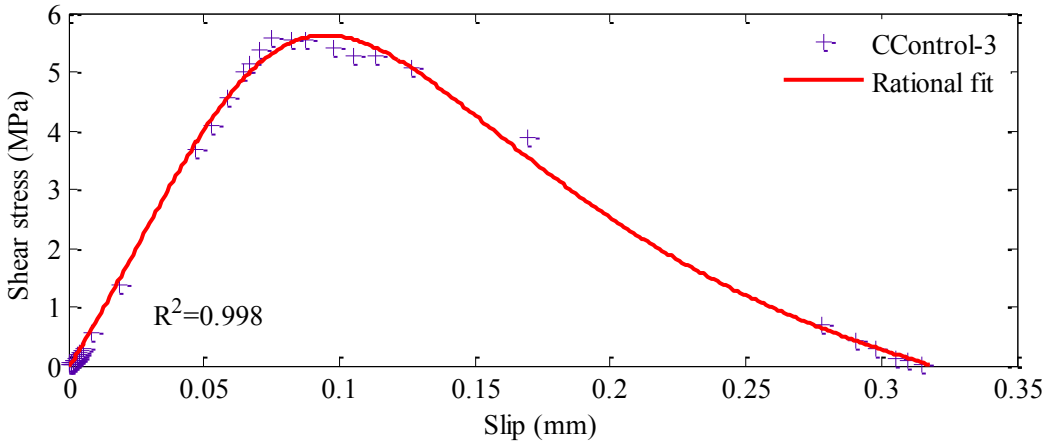

(b) CControl-3

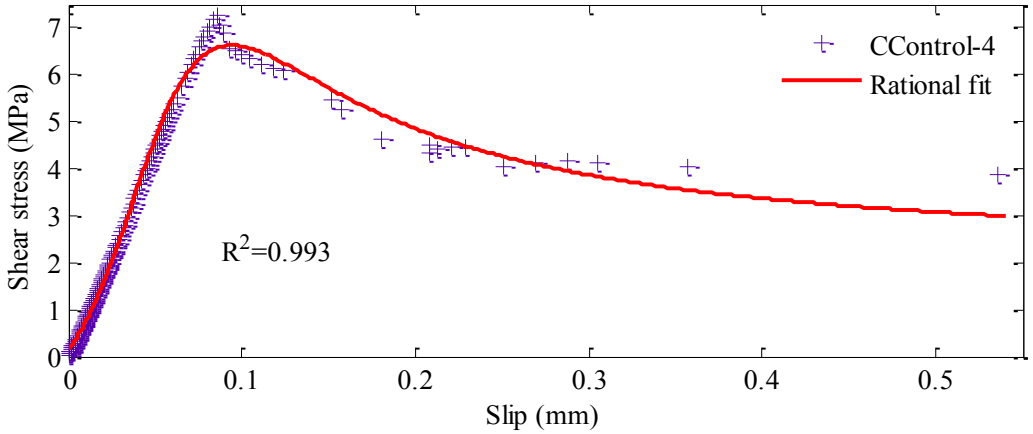

(c) CControl-4

Figure C.1 Rational fits of control specimens

Table C.1 Fitting parameters for rational fits of control specimens

Specimens	p_1	p_2	p_3	q_1	q_2
CControl-1	-0.03927	0.3661	0.0003473	-0.07945	0.005984
CControl-2	-0.9049	0.8979	0.002142	-0.1479	0.01501
CControl-3	-3.38	1.081	-0.0006209	-0.1118	0.01432
CControl-4	2.032	0.2969	0.0009538	-0.08545	0.006261

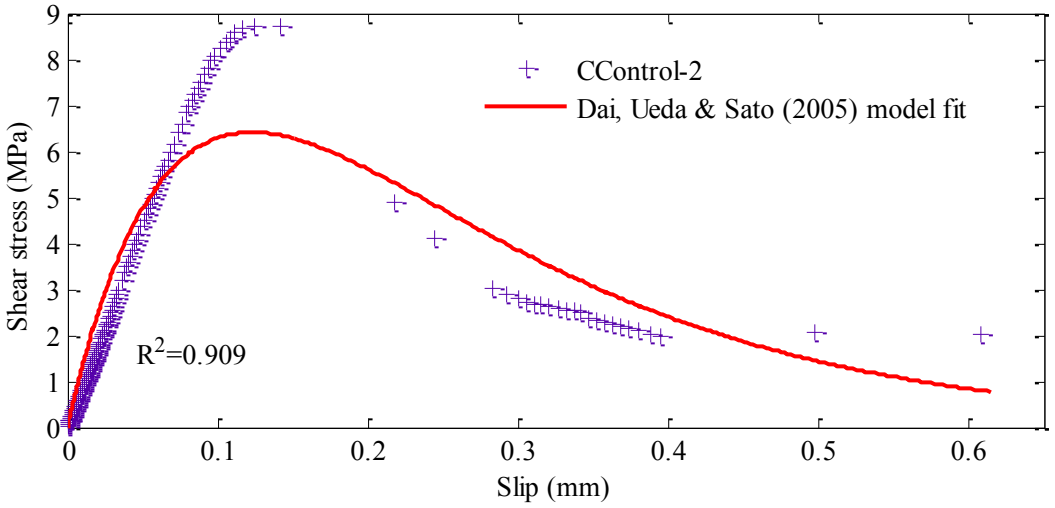

(a) CControl-2

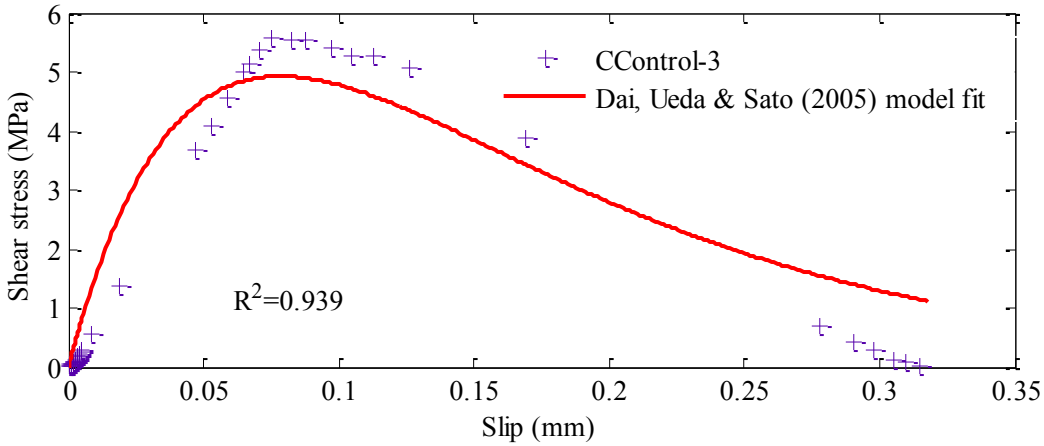

(b) CControl-3

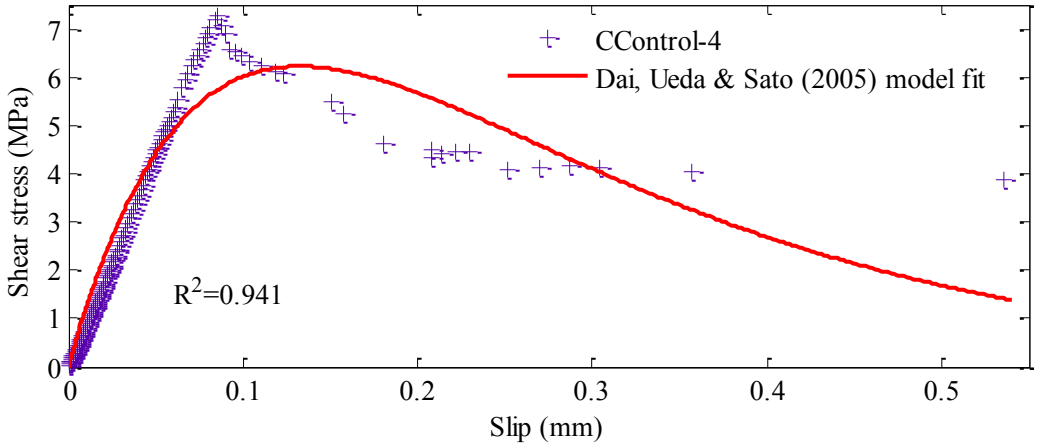

(c) CControl-4

Figure C.2 Dai, Ueda & Sato (2005) model fits for control specimens

Table C.2 Fitting parameters for Dai, Ueda & Sato (2005) model fits for control specimens

Specimens	A (ε)	B (mm^{-1})
CControl-1	0.006608	7.033
CControl-2	0.009267	5.643
CControl-3	0.006493	8.836
CControl-4	0.00948	5.234

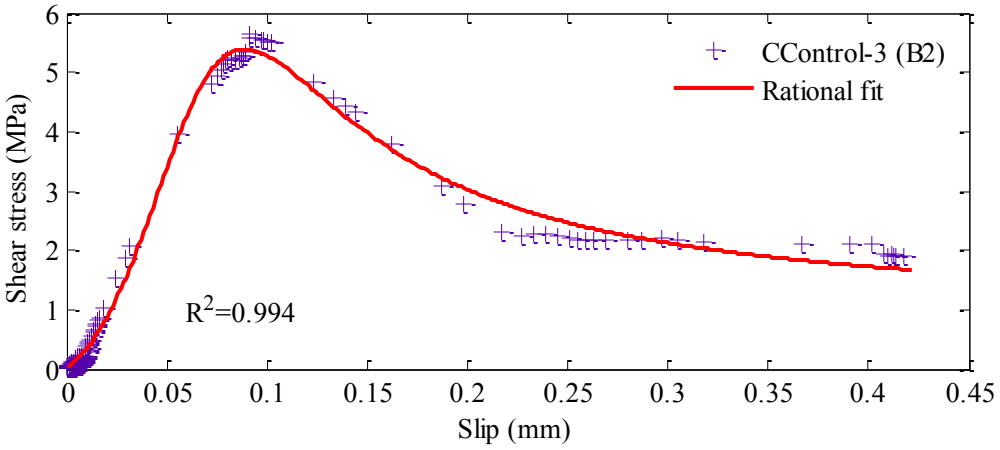

(a) CControl-3 (B2)

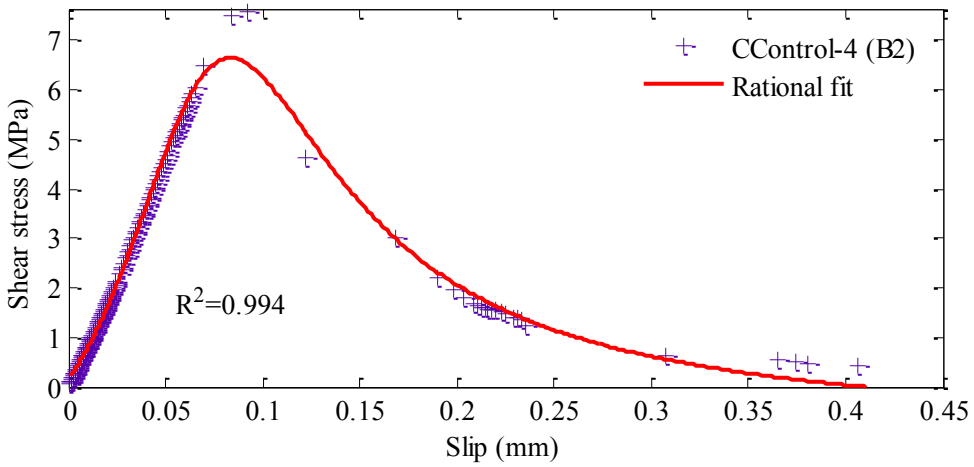

(b) CControl-4 (B2)

Figure C.3 Rational fits for control specimens from concrete batch 2

Table C.3 Fitting parameters for rational fits for control specimens from concrete batch 2

Specimens	p_1	p_2	p_3	q_1	q_2
CControl-2 (B2)	-0.4803	0.9346	0.003071	-0.1248	0.01434
CControl-3 (B2)	0.812	0.1981	-9.699e-005	-0.1144	0.006708
CControl-4 (B2)	-1.114	0.4532	0.001341	-0.1261	0.008278

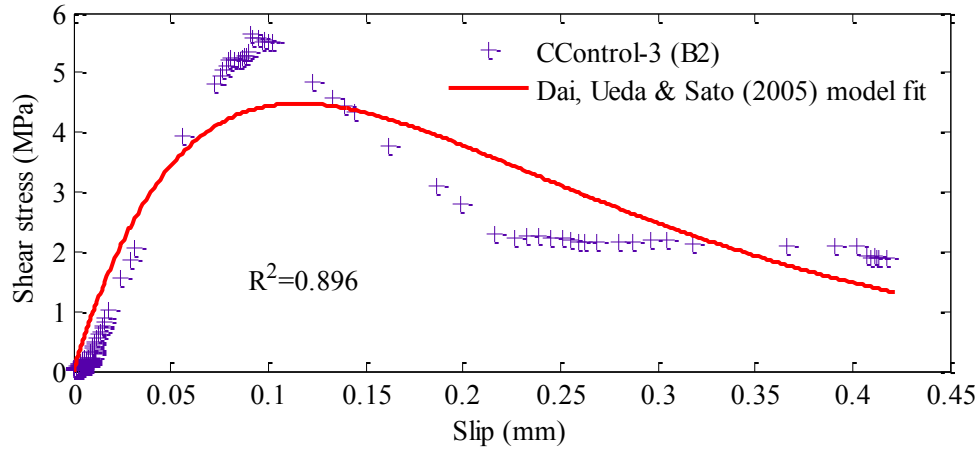

(a) CControl-3 (B2)

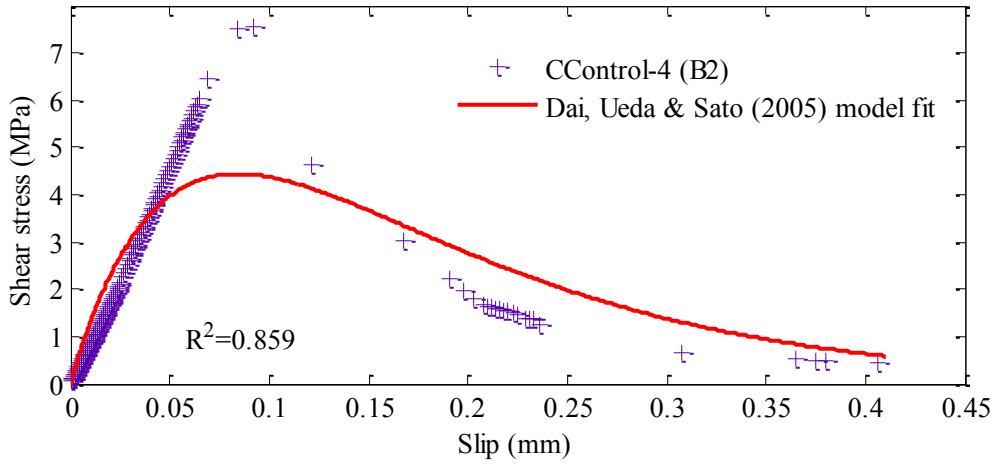

(b) CControl-4 (B2)

Figure C.4 Dai, Ueda & Sato (2005) model fits for control specimens from concrete batch 2

Table C.4 Fitting parameters for Dai, Ueda & Sato (2005) model fits for control specimens from concrete batch 2

Specimens	A (ε)	B (mm^{-1})
CControl-2 (B2)	0.0102	5.034
CControl-3 (B2)	0.00752	5.993
CControl-4 (B2)	0.006387	8.227

C.2 Shear stress-slip curve fitting for control and exposed specimens with a single curve for each series

Table C.5 Fitting parameters for rational fits for control series

Series	p_1	p_2	p_3	q_1	q_2
CControl	-0.1715	0.5723	0.0007071	-0.1142	0.009668
CControl (B2)	-0.5939	0.6707	9.425e-005	-0.1111	0.009998

Table C.6 Fitting parameters for Dai, Ueda & Sato (2005) model fits for control series

Series	A (ε)	B (mm^{-1})
CControl	0.008399	6.049
CControl (B2)	0.008317	6.116

Table C.7 Fitting parameters for rational fits for cyclic temperature series

Series	p_1	p_2	p_3	q_1	q_2
CT2	-6.209	2.635	0.001346	-0.1325	0.02993
CT3	1.809	0.5422	0.0002803	-0.07097	0.007917
CT4	4.329	0.2815	0.000723	-0.06674	0.00613

Table C.8 Fitting parameters for Dai, Ueda & Sato (2005) model fits for cyclic temperature series

Series	A (ε)	B (mm^{-1})
CT2	0.009311	5.430
CT3	0.009649	4.945
CT4	0.01147	4.055

Table C.9 Fitting parameters for rational fits for cyclic wet-dry series

Series	p_1	p_2	p_3	q_1	q_2
CH1	0.8735	0.7358	0.0005899	-0.09648	0.01018
CH2	-0.2247	0.713	0.0009257	-0.09997	0.01338
CH3	4.363	0.2699	0.0006211	-0.03224	0.005702
CH4	-0.2301	0.3626	0.0009844	-0.09532	0.006473

Table C.10 Fitting parameters for Dai, Ueda & Sato (2005) model fits for cyclic wet-dry series

Series	A (ε)	B (mm^{-1})
CH1	0.0096	5.267
CH2	0.008853	5.328
CH3	0.0126	3.514
CH4	0.006527	7.749

Table C.11 Fitting parameters for rational fits for outdoor environment series

Series	p_1	p_2	p_3	q_1	q_2
CE1	0.9336	0.3204	0.0002327	-0.09732	0.006882
CE2	0.8173	0.4606	0.0007427	-0.1062	0.007745
CE3	-0.2251	0.7759	4.719e-005	-0.08688	0.01066
CE4	-0.668	0.5504	0.001499	-0.1176	0.009553

Table C.12 Fitting parameters for Dai, Ueda & Sato (2005) model fits for outdoor environment series

Series	A (ε)	B (mm^{-1})
CE1	0.008189	6.081
CE2	0.009153	5.743
CE3	0.008726	5.641
CE4	0.007405	6.760

D. Appendix D: Short term performance of FRP-repaired beams

D.1 Prediction of load-carrying capacity of repaired beams considering strain hardening and residual strength of steel

- **Beam 1 example:**

An example of the prediction of load carrying capacity of a damaged RC beam repaired with FRP is given in this section where all calculations are for Beam 1 which was used for the experimental study.

Concrete compressive strength $f_c^{'}$ = 80 MPa

Tensile modulus of elasticity of steel E_s =200 GPa = 200,000 MPa

Yield strength of steel f_y = 500 MPa

Yield strain of steel $\varepsilon_y = \frac{f_y}{E_s} = 0.0025$

Strain at the ultimate tensile strength of steel, ε_u = 0.01

Ultimate tensile strength of steel f_u = 560 MPa

The strain of steel reinforcement at the failure of control beam ε_{s0} = 0.00102

Steel area A_s = 330 mm^2

Tensile modulus of elasticity of FRP E_f = 284.436 GPa = 284,436 MPa

Ultimate tensile strength (rupture strength) of FRP f_{fu} = 2987.4 MPa

and FRP area A_f = 32.76 mm^2

As $\varepsilon_{s0} < \varepsilon_y$ the residual strength of steel reinforcement can be calculated considering the strain hardening after yielding of the steel as follows:

$$f_{s\,\mathrm{Res}} = E_s(\varepsilon_y - \varepsilon_{s0}) + (f_u - f_y)$$

$$\Rightarrow f_{s\,\mathrm{Res}} = 360.96$$

Now, height of beam $h = 200$ mm, depth of the bottom steel reinforcement from the top of the beam $d = 169$ mm and width of the beam, $b = 150$ mm. Hence, the depth of equivalent rectangular stress block of the FRP-repaired beam, a_f can be calculated as follows:

$$a_f = \frac{A_f f_{fu} + A_s f_{s\,\mathrm{Res}}}{\alpha_2 f_c^{'} b} = 23.79 \text{ mm}$$

where $\alpha_2 = 1.0 - 0.003 f_c^{'}$ but $0.67 \le \alpha_2 \le 0.85$ (according to AS 3600 (2009))

After calculating a_f, the moment carrying capacity was calculated as follows:

$$M_n = A_f f_{fu}\left(h - \frac{a_f}{2}\right) + A_s f_{s\,\mathrm{Res}}\left(d - \frac{a_f}{2}\right) = 37.12 \text{ kNm}$$

and the load carrying capacity of the beam for four-point bending set-up is

$$P = 3 \times \frac{M_n}{L} = 61.87 \text{ kN}$$

Hence, the total load from two loading points $= 2 \times P = 123.74$ kN.

D.2 Material data sheets

The technical data sheets for the high build repair mortar applied for filling the voids of the damaged beams is shown in Figure D.1.

Construction

Technical Data Sheet
07/2009

Sika MonoTop®-615 HB

High build repair mortar

Description	Sika MonoTop-615 HB is a cementitious polymer and Silica Fume modified, one-component repair and patching mortar.
Uses	As a repair mortar on concrete structures affected by spalling due to corroding reinforcement. As a concrete patching and reprofiling mortar for the treatment of: ▪ Honeycombing and voids caused by faulty formwork. ▪ Broken upstands, ribs, edges, etc. on architectural units. ▪ Break outs for service entrances in walls and slabs etc. For use in conjunction with the Sika concrete repair system: ▪ **SikaTop-110 EpoCem** Bonding Mortar and Reinforcement Protection. ▪ **Sika MonoTop-615 HB** Patching Mortar. ▪ **Sika MonoTop-620** Fairing Coat.
Advantages	▪ One-component system requires only the addition of clean water. ▪ Easily applied and worked. ▪ Adjustable consistency to suit application. ▪ Non-sagging in vertical and overhead work. ▪ Layers of up to 80 mm in one application are possible on vertical surfaces. ▪ Compatible with the thermal expansion properties of concrete. ▪ Contains shrinkage compensating admixture. ▪ Free from chlorides. ▪ Non-corrosive to reinforcing steel. ▪ Non-toxic. ▪ Applicable by trowel or suitable wet-mix process spray equipment. ▪ Approved for use in potable water (AS4020-1999)
Storage and Shelf Life	Stored in the original sealed packaging in dry conditions, this product will keep for at least nine (9) months.
Instructions for Use	
Surface Preparation	Correct and thorough surface preparation is essential to achieve the high adhesive qualities of Sika MonoTop mortars. All surfaces must be clean, sound and free from dust, ice, oils, grease or other surface contaminants such as curing membranes and form release agents etc. *Concrete, Mortar, Stone:* Mechanically abrade the surface with a needle gun, mechanical wire brush, grind, grit or water blast. All surface laitance must be removed. The strength of the concrete or mortar substrate should be at least 20MPa. The prepared substrate should be thoroughly soaked with clean water until uniformly saturated, leaving no standing water, ie. Saturated Surface Dry (SSD) condition.
Bonding Bridge	To the prepared substrate apply Sika MonoTop-610 or SikaTop-110 EpoCem as a bonding bridge in accordance with the instructions on the Technical Data Sheet.

Construction

Technical Data Sheet
07/2009

Bonding Bridge ***(continued)***	In some circumstances alternate bonding bridge material may be preferable eg. Sikadur-32; please consult Sika's Technical Department for further information. In all cases the bonding bridge must be tacky at the time of applying Sika MonoTop-615 HB, ie. wet on wet application.
Mixing	Sika MonoTop-615 HB should be mechanically mixed in a forced action mixer or in a clean drum using a low speed drill and spiral mixer (max. 500rpm). Pour 90% of the recommended water content into the mixing vessel, slowly add the powder while continuing to mix. Continue mixing until a uniform homogenous consistency is achieved (minimum 3 minutes) then add the remaining water until the desired application consistency is obtained. If Sika MonoTop-615 HB begins to stiffen within a few minutes of mixing, it may be necessary to remix the mortar to regain a smooth, workable mix. Note that the recommended water addition of 3 litres per 20kg bag can be adjusted by plus or minus 10% to achieve the desired application necessary.
Application	Sika MonoTop-615 HB must be applied wet on wet to the substrate previously primed with Sika MonoTop-610, SikaTop-110 EpoCem or Sikadur-32. Work the mortar well into the substrate, using a placing rather than a rendering technique to fill all pores and voids. Compact well. Force material against the edge of the repair, working towards the centre. For repairs in excess of 80mm deep, apply in layers ensuring previous layers are well keyed and hardened. Application of a bonding bridge between layers is recommended to ensure optimum bond.
Finishing	When the applied mortar has stiffened, but no dried, various methods may be employed to obtain the desired surface finish, eg. steel trowel, wooded float, styrofoam block or sponge. The addition of water to the surface to obtain the desired finish is not recommended as this may cause colour variations and surface cracking. Where Sika MonoTop-615 HB is to be overcoated with a fairing mortar (eg. Sika MonoTop-620) or protective coating (eg. Sikagard-680S) the surface should be finished to provide a fine gripping texture.
Cleaning	Remove soft Sika MonoTop-615 HB from tools and equipment with water. Hardened material can only be removed mechanically.
Additional Protective and Decorative Coatings	The remaining areas of the structure can be coated with Sika FerroGard-903 to fully protect the steel reinforcement from potential corrosion. Sika MonoTop-620 is recommended as a final fairing coat and additional protective anti-carbonation coating to the patched area and also to the remaining areas of the structure, not yet showing the effects of, but susceptible to spalling due to corroding reinforcement. Sikagard-680 S and Sikagard-670 W are also recommended as further decorative and protective coatings. Consult Sika's Technical Department for further information on this range of coating products.
Curing	Suitable curing methods as per the Concrete Institute's recommended practice, such as plastic sheet, wet hessian, liquid membrane (eg. Sikagard-680 S (Finish), Sikagard-551 S Primer or Antisol curing compounds) must be used to protect the freshly applied mortar from the drying effects of sun and wind.

Sika®

Construction

Technical Data Sheet
07/2009

Technical and Physical Data

Form	Lightweight, smooth mortar
Granulometry	0-1.5 mm
Density	1.65 kg/litre approx. (fresh wet density)
Yield	14 litres of mixed mortar per 20kg bag (approx.)
Mixing ratio	Water : Powder 1 : 6.7 by mass 3 litres : 20kg *Note that the water addition rate can be adjusted by a ±10% to achieve the desired application consistency.*
Potlife @ 20°C	50 minutes approximately
Application Thickness	Minimum 5 mm Maximum 80 mm
Application Temperature	+5 °C - +35°C (substrate and ambient temperature) +5°C - 25°C(mortar temperature)
Compressive strength (AS 1012)	24 hours 15 MPa approx. 7 days 30 MPa approx. 28 days 40 MPa approx.
Flexural Strength (AS 1012)	6.5 MPa approx. at 28 days
Bond Strength	1.0 – 1.3 MPa approx. (cohesive failure of mortar) (using Sika MonoTop-610 bonding bridge on concrete substrate)
Chloride Ion Diffusion Resistance (Taywood Method)	4.0 x 10^{-13} m^2/sec

Determined Diffusion Coefficient: 4.0 x 10^{-13} m^2sec^{-1}

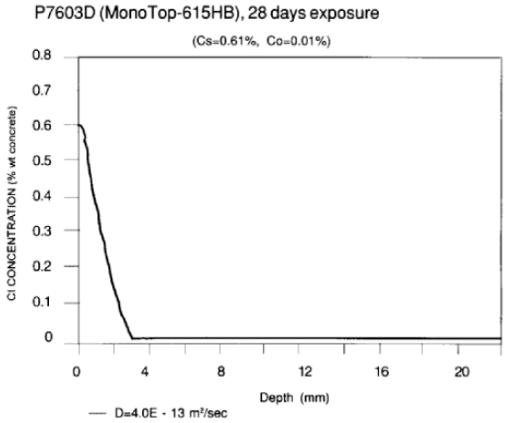

Construction

Technical Data Sheet
07/2009

Technical and Physical Data (cont'd)

Modulus of Elasticity (AS 1012)	15 GPa approx.	
Coefficient of thermal expansion	11 x 10^{-6} per °C	
Water vapour diffusion resistance (μH_2O)	130	
Carbon Dioxide Diffusion Resistance (Taywood Method)	CO_2 Diffusion Coefficient Diffusion Resistance Coefficient (μ): Equivalent Air Layer Thickness (R): Equivalent Thickness of Concrete (Sc):	1.4 x 10^{-4} cm^2/sec 1143 57m @ 50mm thickness 140mm @ 50mm thickness
Oxygen Diffusion Resistance (Taywood Certificate No. 833)	8.2 x 10^{-4} cm^2/sec	
Colour	Light Grey	
Packaging	20kg bag	
Important Notes	• Apply only to clean sound substrates. • Never apply to dry substrates. • In warm, hot or windy conditions ensure adequate curing of freshly applied mortar. • Sika MonoTop-615 HB mortar will not bridge live cracks. • Sika MonoTop-615 HB has various uses which may necessitate adjusting the consistency slightly to better suit the particular application. A reduction of up to 10% of either the powder or water is permissible to either stiffen or increase workability of the mixed mortar. • Not suitable as an adhesive for ceramic wall tiles. • Refer to Sika's Technical Department for a full concrete repair and protection system.	
Handling Precautions	• Avoid contact with the skin. • Protective gloves and clothing are recommended when mixing or using this product. • A full Material Safety Data Sheet is available from Sika on request.	
Important Notification	The information, and, in particular, the recommendations relating to the application and end-use of Sika's products, are given in good faith based on Sika's current knowledge and experience of the products when properly stored, handled and applied under normal conditions. In practice, the differences in materials, substrates and actual site conditions are such that no warranty in respect of merchantability or of fitness for a particular purpose, nor any liability arising out of any legal relationship whatsoever, can be inferred either from this information, or from any written recommendations, or from any other advice offered. The proprietary rights of third parties must be observed. All orders are accepted subject of our terms and conditions of sale. Users should always refer to the most recent issue of the Australian version of the Technical Data Sheet for the product concerned, copies of which will be supplied on request. PLEASE CONSULT OUR TECHNICAL DEPARTMENT FOR FURTHER INFORMATION.	

Sika®

Sika Australia Pty Limited
ABN 12 001 342 329

www.sika.com.au
Tel: 1300 22 33 48

Sika MonoTop®-615 HB
Page 4 of 4

Figure D.1 Data sheets for repair mortar Sika Mono Top-615HB